

AD-A134579

AFWAL-TR-82-3112

MACH 0.6 TO 3.0 FLOWS OVER RECTANGULAR CAVITIES

Louis G. Kaufman II  
Algirdas Maciulaitis  
Research and Development Center  
Grumman Aerospace Corporation  
Bethpage, New York 11714

and

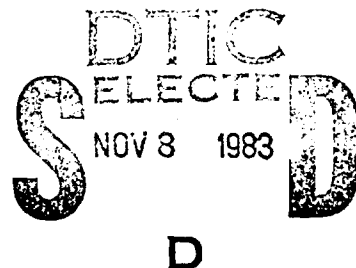
Rodney L. Clark  
Aeromechanics Division  
Air Force Wright Aeronautical Laboratories  
Wright Patterson AFB, Ohio 45433



MAY 1983

FINAL REPORT FOR PERIOD JUNE 1978 - JUNE 1980

Approved for public release; distribution unlimited



FLIGHT DYNAMICS LABORATORY  
AIR FORCE WRIGHT AERONAUTICAL LABORATORIES  
AIR FORCE SYSTEMS COMMAND  
WRIGHT-PATTERSON AIR FORCE BASE, OHIO, 45433

83 11 08 120


DTIC FILE COPY

NOTICE


When Government drawings, specifications, or other data are used for any purpose other than in connection with a definitely related Government procurement operation, the United States Government thereby incurs no responsibility nor any obligation whatsoever; and the fact that the government may have formulated, furnished, or in any way supplied the said drawings, specifications, or other data, is not to be regarded by implication or otherwise as in any manner licensing the holder or any other person or corporation, or conveying any rights or permission to manufacture use, or sell any patented invention that may in any way be related thereto.

This report has been reviewed by the Office of Public Affairs (ASD/PA) and is releasable to the National Technical Information Service (NTIS). At NTIS, it will be available to the general public, including foreign nations.

This technical report has been reviewed and is approved for publication.




RODNEY L. CLARK  
Project Engineer



TOMMY J. KENT, Maj, USAF  
Chief, Aerodynamics & Airframe Br  
Aeromechanics Division

FOR THE COMMANDER:



RALPH W. HOLM, Colonel, USAF  
Chief, Aeromechanics Division  
Flight Dynamics Laboratory

"If your address has changed, if you wish to be removed from our mailing list, or if the addressee is no longer employed by your organization please notify AEWAL/FIMM W-PAFB, OH 45433 to help us maintain a current mailing list".

Copies of this report should not be returned unless return is required by security considerations, contractual obligations, or notice on a specific document.

UNCLASSIFIED

SECURITY CLASSIFICATION OF THIS PAGE (When Data Entered)

REPORT DOCUMENTATION PAGE		READ INSTRUCTIONS BEFORE COMPLETING FORM
1. REPORT NUMBER AFWAL-TR-82-3112	2. GOVT ACCESSION NO. AD A134579	3. RECIPIENT'S CATALOG NUMBER
4. TITLE (and Subtitle)  MACH 0.6 TO 3.0 FLOWS OVER RECTANGULAR CAVITIES		5. TYPE OF REPORT & PERIOD COVERED Final Report June 1978-June 1980
7. AUTHOR(s) Louis G. Kaufman II Algirdas Maciulaitis Rodney L. Clark		6. PERFORMING ORG. REPORT NUMBER RE-
9. PERFORMING ORGANIZATION NAME AND ADDRESS Grumman Aerospace Corp, Bethpage, NY and AFWAL, Wright-Patterson, Ohio		8. CONTRACT OR GRANT NUMBER(s)
11. CONTROLLING OFFICE NAME AND ADDRESS Flight Dynamics Laboratory (AFWAL/FIMM) Air Force Wright Aeronautical Laboratories Wright-Patterson AFB, Ohio 45433		10. PROGRAM ELEMENT, PROJECT, TASK AREA & WORK UNIT NUMBERS  24041045
14. MONITORING AGENCY NAME & ADDRESS (if different from Controlling Office)		12. REPORT DATE May 1983
		13. NUMBER OF PAGES 292
		15. SECURITY CLASS. (of this report)  UNCLASSIFIED
		15a. DECLASSIFICATION/DOWNGRADING SCHEDULE
16. DISTRIBUTION STATEMENT (of this Report)  Approved for public release, distribution unlimited		
17. DISTRIBUTION STATEMENT (of the abstract entered in Block 20, if different from Report)		
18. SUPPLEMENTARY NOTES		
19. KEY WORDS (Continue on reverse side if necessary and identify by block number)  aeroacoustics, cavity flow, subsonic, supersonic, bomb bays, noise suppression, oil flow, prediction methods, wind tunnel		
20. ABSTRACT (Continue on reverse side if necessary and identify by block number) → Internal weapons carriage in high performance aircraft is often adversely affected by the severe aeroacoustic environment produced with the weapons bay doors open. To obtain a better understanding of this fluid dynamic problem, basic static and oscillatory pressure data were obtained for Mach 0.6 to 3.0 flows over shallow rectangular cavities in a generic flat plate model. Cavity length to depth ratios were varied from approximately 5 to 10. Static pressure data characteristic of both open and closed cavity flows were obtained. An improved Rossiter method is presented that satisfactorily predicts the		

DD FORM 1 JAN 73 1473

EDITION OF 1 NOV 65 IS OBSOLETE

UNCLASSIFIED

SECURITY CLASSIFICATION OF THIS PAGE (When Data Entered)

7 possible frequency modes within the cavity. Highest fluctuating pressure occurs on the aft bulkhead, peaking near Mach 1.5 for the conditions tested. Aeroacoustic levels are substantially reduced by installing suppression fences (spoilers) at subsonic and low supersonic conditions. Acoustic levels generally drop rapidly above Mach 1.5.



## FOREWORD

The work described herein was accomplished jointly by personnel at the Flight Dynamics Laboratory, Aeromechanics Division, Air Force Wright Aeronautical Laboratories (AFWAL), Wright Patterson AFB, Ohio 45433 and Grumman Aerospace Corporation, Research and Development Center, Bethpage, New York 11714. The experiments were conducted in the AFWAL Trisonic Gas Dynamics Facility (Wright Patterson AFB) using an Air Force model that was refurbished and reinstrumented by Grumman. This AFWAL project No. 2404, Work Unit 24041045 "Advanced Weapons Carriage/Separation" was managed by Rodney L. Clark (AFWAL/FIMM).

Phyllis Bolds (AFWAL/FIBG) accomplished the spectral analysis of the aeroacoustic data. Her substantial aid was instrumental in accomplishing this work.

Ray Haynes, Kermit Knisley, Randy Mainquist, Howard White and Glenn Williams (AFWAL) were instrumental in the successful completion of the experiments.

Accession For	
NTIS	<b>X</b>
DTIC	
U	
Summary	
By _____	
Distribution _____	
Availability _____	
Dist	Availability Special
<b>A/1</b>	



BLIND

# CONTENTS

<u>Section</u>	<u>Page</u>
I INTRODUCTION.....	1
II EXPERIMENTAL PROGRAM.....	2
Model & Instrumentation.....	2
Tunnel & Test Conditions.....	4
III EXPERIMENTAL RESULTS.....	6
Static Experimental Results.....	8
Subsonic.....	8
$M_\infty = 1.5$ .....	11
$M_\infty = 2.3$ .....	13
$M_\infty = 3.0$ .....	14
Acoustic Experimental Results.....	15
Overall Acoustic Pressure Distributions.....	15
Subsonic.....	15
$M_\infty = 1.5$ .....	17
$M_\infty = 2.3$ .....	17
$M_\infty = 3.0$ .....	18
Survey of Suppressor Fence Effects on Acoustic Pressures.....	19
Subsonic Data for the L/D = 5.6 Cavity.....	19
$M_\infty = 1.5$ for All Four Cavities.....	20
$M_\infty = 2.3$ .....	20
$M_\infty = 3.0$ .....	20
Acoustic Modal Pressure Distributions.....	20
$M_\infty = 0.7$ .....	21
$M_\infty = 1.5$ .....	21
$M_\infty = 2.3$ .....	21
Summary of Maximum Acoustic Pressure Variations with $M_\infty$ .....	21
Effect of the Total Head Tube on the Acoustic Pressure Distributions.....	23
Subsonic.....	23
Supersonic.....	23
Cross correlations.....	23

## CONTENTS (contd)

<u>Section</u>	<u>Page</u>
IV ANALYSES & COMPARISONS.....	25
Aerodynamic Data.....	25
Prediction of Frequency Modes for Oscillatory Pressures.....	25
Comparison of Measured and Predicted Oscillatory Pressure Frequencies.....	28
V CONCLUSIONS.....	31
REFERENCES.....	33

# ILLUSTRATIONS

<u>Figure</u>		<u>Page</u>
1	Typical Fighter-Bomber Airplane Profile and Orientation of Weapon Bay Cavity Flow Model.....	34
2	Sketch of Cavity Flow Model.....	35
3	Cavity Lengths and Depths.....	36
4	Photographs of Cavity Flow Model Configurations.....	37
5	Forward View of Sawtooth & Perforated Fences.....	38
6	Model Instrumentation Locations.....	39
7	Schematic of Aeroacoustic Data Acquisition and Reduction System.....	40
8	Forward-Facing Total Pressure Probe Attached to Ceiling of L/D = 5.6 Cavity.....	41
9	Photographs of Cavity Flow Model in Test Section of AFWAL Trisonic Gasdynamics Facility with Mach 3.0 Nozzle Blocks Installed.....	42
10	Rectangular Coordinate System.....	44
11	Pressure Coefficient Distributions for L/D = 5.1 Cavity with Boundary Layer Trip, $M_\infty = 0.60$ .....	45
12	" $M_\infty = 0.61$ .....	46
13	" $M_\infty = 0.64$ .....	47
14	" $M_\infty = 0.71$ .....	48
15	" $M_\infty = 0.74$ .....	49
16	" $M_\infty = 0.76$ .....	50
17	Schlieren Flow Photograph; L/D = 5.1 Cavity with Boundary Layer Trip, $M_\infty = 0.60$ .....	51
18	Pressure Coefficient Distributions for L/D = 5.6 Cavity, $M_\infty = 0.60$	52
19	" $M_\infty = 0.61$	53
20	" $M_\infty = 0.64$	54

# ILLUSTRATIONS (Contd)

<u>Figure</u>		<u>Page</u>
21	Pressure Coefficient Distributions for L/D = 5.6 Cavity, $M_\infty = 0.66$	55
22	" $M_\infty = 0.70$	56
23	" $M_\infty = 0.72$	57
24	" $M_\infty = 0.74$	58
25	Schlieren Flow Photograph, L/D = 5.6 Cavity, $M_\infty = 0.60$ .....	59
26	" $M_\infty = 0.61$ .....	60
27	" $M_\infty = 0.64$ .....	61
28	Oil Drop Pattern Prior to Test Run, L/D = 5.6 Cavity.....	62
29	Oil Flow in L/D = 5.6 Cavity at $M_\infty = 0.75$ , Ceiling.....	62
30	" Port Side.....	63
31	" Starboard Side.....	63
32	Pressure Coefficient Distributions for L/D = 5.6 Cavity with Sawtooth Fence, $M_\infty = 0.60$ .....	64
33	" $M_\infty = 0.70$ .....	65
34	" $M_\infty = 0.74$ .....	66
35	Oil Drop Pattern Prior to Test Run, L/D = 5.6 Cavity with Sawtooth Fence.....	67
36	Oil Flow in L/D = 5.6 Cavity with Saw-Tooth Fence, $M_\infty = 0.70$ , Ceiling.....	67
37	" Port Side.....	68
38	Oil Drop Pattern Prior to Test Run, L/D = 5.6 Cavity with Perforated Fence.....	68
39	Oil Flow in L/D = 5.6 Cavity with Perforated Fence, $M_\infty = 0.70$ , Ceiling.....	69
40	" Port Side.....	69
41	Pressure Coefficient Distributions for L/D = 5.6 Cavity with Forward-Facing Total Pressure Probe, $M_\infty = 0.60$ .....	70

# ILLUSTRATIONS (Contd)

Figure		Page
42	Pressure Coefficient Distributions for $L/D = 5.6$ Cavity with Forward-Facing Total Pressure Probe, $M_\infty = 0.70$ .....	71
43	" $M_\infty = 0.74$ .....	72
44	Pressure Coefficient Distributions for $L/D = 5.6$ Cavity with Sawtooth Fence and Forward-Facing Total Pressure Probe, $M_\infty = 0.60$	73
45	" $M_\infty = 0.70$ ....	74
46	" $M_\infty = 0.74$ ....	75
47	Pressure Coefficient Distributions for $L/D = 5.6$ Cavity with Aft-Facing Total Pressure Probe, $M_\infty = 0.61$ .....	76
48	" $M_\infty = 0.64$ .....	77
49	" $M_\infty = 0.72$ .....	78
50	" $M_\infty = 0.75$ .....	79
51	Pressure Coefficient Distributions for $L/D = 5.6$ Cavity with Sawtooth Fence and Aft-Facing Total Pressure Probe, $M_\infty = 0.60$ ....	80
52	" $M_\infty = 0.70$ .....	81
53	" $M_\infty = 0.71$ .....	82
54	" $M_\infty = 0.74$ .....	83
55	" $M_\infty = 0.74$ , Model Pitched Nose Down $3/4^\circ$ .....	84
56	" $M_\infty = 0.74$ , Model Pitched Nose Up $3/4^\circ$ .....	85
57	" $M_\infty = 0.80$ .....	86
58	Pressure Coefficient Distributions for $L/D = 6.2$ Cavity, $M_\infty = 0.60$	87
59	" $M_\infty = 0.70$	88
60	" $M_\infty = 0.74$	89
61	Schlieren Flow Photograph, $L/D = 6.2$ Cavity, $M_\infty = 0.70$ .....	90
62	Pressure Coefficient Distributions for $L/D = 9.9$ Cavity with Boundary Layer Trip, $M_\infty = 0.60$ .....	91
63	" $M_\infty = 0.61$ .....	92

# ILLUSTRATION (Contd)

<u>Figure</u>		<u>Page</u>
64	Pressure Coefficient Distributions for L/D = 9.9 Cavity with Boundary Layer Trip, $M_\infty = 0.71$ .....	93
65	" $M_\infty = 0.74$ .....	94
66	Oil Pattern Prior to Test Run, L/D = 9.9 Cavity.....	95
67	Oil Flow in L/D = 9.9 Cavity at $M_\infty = 0.70$ , Ceiling.....	96
68	" Starboard Side.....	96
69	Schlieren Flow Photograph, L/D = 9.9 Cavity, $M_\infty = 0.61$ .....	97
70	Pressure Coefficient Distributions for L/D = 9.9 Cavity with Boundary Layer Trip and Perforated Fence, $M_\infty = 0.58$ .....	98
71	" Perforated Fence, $M_\infty = 0.60$ .....	99
72	" Sawtooth Fence, $M_\infty = 0.60$ .....	100
73	" Perforated Fence, $M_\infty = 0.70$ .....	101
74	" Sawtooth Fence, $M_\infty = 0.70$ .....	102
75	" Perforated Fence, $M_\infty = 0.74$ .....	103
76	" Sawtooth Fence, $M_\infty = 0.74$ .....	104
77	Schlieren Flow Photograph, L/D = 9.9 Cavity with Boundary Layer Trip and Perforated Fence, $M_\infty = 0.70$ .....	105
78	" Sawtooth Fence, $M_\infty = 0.70$ .....	105
79	Oil Drop Pattern Prior to Test Run, L/D = 9.9 Cavity with Boundary Layer Trip and Perforated Fence.....	106
80	Oil Flow in L/D = 9.9 Cavity with Boundary Layer Trip and Perforated Fence, $M_\infty = 0.70$ , Ceiling View 1.....	106
81	" Ceiling View 2.....	107
82	" Starboard Side.....	107
83	Pressure Coefficient Distributions for L/D = 5.1 Cavity, $M_\infty = 1.5$	108
84	Pressure Coefficient Distributions for L/D = 5.1 Cavity with Sawtooth Fence, $M_\infty = 1.5$ .....	109



# ILLUSTRATIONS (Contd)

Figure		Page
85	Schlieren Flow Photograph, L/D = 5.1 Cavity, $M_\infty = 1.5$ .....	110
86	Schlieren Flow Photograph, L/D = 5.1 Cavity, Sawtooth Fence, $M_\infty = 1.5$ .....	110
87	Pressure Coefficient Distributions for L/D = 5.6 Cavity, $M_\infty = 1.5$	111
88	Pressure Coefficient Distributions for L/D = 5.6 Cavity with Sawtooth Fence, $M_\infty = 1.5$ .....	112
89	Schlieren Flow Photograph, L/D = 5.6 Cavity, $M_\infty = 1.5$ .....	113
90	Schlieren Flow Photograph, L/D = 5.6 Cavity, Sawtooth Fence, $M_\infty = 1.5$ .....	113
91	Oil Drop Pattern Prior to Test Run, L/D = 5.6 Cavity.....	114
92	Oil Flow in L/D = 5.6 Cavity at $M_\infty = 1.5$ , Forward Portion.....	114
93	" Aft Portion.....	115
94	" Port Side.....	115
95	Oil Drop Pattern Prior to Test Run, L/D = 5.6 Cavity with Perforated Fence.....	116
96	Oil Flow in L/D = 5.6 Cavity, Perforated Fence Attached, $M_\infty = 1.5$ , Ceiling.....	116
97	" Starboard Side.....	117
98	" Port Side.....	117
99	Oil Pattern Prior to Test Run, L/D = 5.6 Cavity with Sawtooth Fence.....	118
100	Oil Flow in L/D = 5.6 Cavity, Sawtooth Fence Attached, $M_\infty = 1.5$ , Ceiling.....	118
101	" Port Side.....	118
102	Pressure Coefficient Distributions for L/D = 5.6 Cavity with Forward Facing Total Pressure Probe, $M_\infty = 1.5$ .....	119
103	Pressure Coefficient Distributions for L/D = 5.6 Cavity with Sawtooth Fence and Forward Facing Total Pressure Probe, $M_\infty = 1.5$ ..	120

### ILLUSTRATIONS (Contd)

Figure		Page
104	Schlieren Flow Photograph, L/D = 5.6 Cavity, Forward-Facing Total Pressure Probe, $M_\infty = 1.5$ .....	121
105	Schlieren Flow Photograph, L/D = 5.6 Cavity, Sawtooth Fence and Forward-Facing Total Pressure Probe, $M_\infty = 1.5$ .....	121
106	Pressure Coefficient Distributions for L/D = 5.6 Cavity with Aft-Facing Total Pressure Probe, $M_\infty = 1.5$ , Run 1.....	122
107	" Run 2.....	123
108	Pressure Coefficient Distributions for L/D = 5.6 Cavity with Sawtooth Fence and Aft-Facing Total Pressure Probe, $M_\infty = 1.5$ .....	124
109	Schlieren Flow Photograph; L/D = 5.6 Cavity with Sawtooth Fence and Aft-Facing Total Pressure Probe, $M_\infty = 1.5$ .....	125
110	Schlieren Flow Photograph, L/D = 5.6 Cavity with Aft-Facing Total Pressure Probe, $M_\infty = 1.5$ .....	125
111	Pressure Coefficient Distributions for L/D = 6.2 Cavity, $M_\infty = 1.5$	126
112	Pressure Coefficient Distributions for L/D = 6.2 Cavity with Sawtooth Fence, $M_\infty = 1.5$ .....	127
113	Schlieren Flow Photograph, L/D = 6.2 Cavity, $M_\infty = 1.5$ .....	128
114	Schlieren Flow Photograph, L/D = 6.2 Cavity with Sawtooth Fence, $M_\infty = 1.5$ .....	128
115	Pressure Coefficient Distributions for L/D = 9.9 Cavity, $M_\infty = 1.5$	129
116	Pressure Coefficient Distributions for L/D = 9.9 Cavity, Model Pitched Nose Up $3/4^\circ$ , $M_\infty = 1.5$ .....	130
117	Pressure Coefficient Distributions for L/D = 9.9 Cavity with Sawtooth Fence, $M_\infty = 1.5$ .....	131
118	Schlieren Flow Photograph, L/D = 9.9 Cavity, $M_\infty = 1.5$ .....	132
119	Schlieren Flow Photograph, L/D = 9.9 Cavity, Model Pitched Nose Up $3/4^\circ$ , $M_\infty = 1.5$ .....	132
120	Schlieren Flow Photograph, L/D = 9.9 Cavity with Sawtooth Fence, $M_\infty = 1.5$ .....	132
121	Oil Drop Pattern Prior to Test Run, L/D = 9.9 Cavity.....	133

# ILLUSTRATIONS (Contd)

Figure		Page
122	Oil Flow in L/D = 9.9 Cavity, $M_\infty = 1.5$ , Ceiling.....	133
123	" Port Side.....	134
124	" Starboard Side.....	134
125	Oil Drop Pattern Prior to Test Run, L/D = 9.9 Cavity, Perforated Fence Attached.....	135
126	Oil Flow in L/D = 9.9 Cavity, Perforated Fence Attached, $M_\infty = 1.5$ , Ceiling.....	136
127	" Starboard Side.....	136
128	Oil Drop Pattern Prior to Test Run, L/D = 8.9 Cavity, Perforated Fence Attached.....	137
129	Oil Flow in L/D = 8.9 Cavity, Perforated Fence Attached, $M_\infty = 1.5$ , Ceiling.....	137
130	" Starboard Side.....	138
131	Oil Flow in L/D = 8.9 Cavity, Perforated Fence Attached, $M_\infty = 1.5$ , Port Side.....	138
132	Oil Drop Pattern Prior to Test Run, L/D = 9.9 Cavity, Sawtooth Fence Attached.....	139
133	Oil Flow in L/D = 9.9 Cavity, Sawtooth Fence Attached, $M_\infty = 1.5$ , Ceiling.....	140
134	" Port Side.....	140
135	Pressure Coefficient Distributions for L/D = 5.1 Cavity, $M_\infty = 2.3$ , $Re/10^6 = 2.9$ .....	141
136	" $Re/10^6 = 3.9$ .....	142
137	Pressure Coefficient Distributions for L/D = 5.1 Cavity with Sawtooth Fence, $M_\infty = 2.3$ , $Re/10^6 = 3.0$ .....	143
138	" $Re/10^6 = 3.6$ .....	144
139	Schlieren Flow Photograph, L/D = 5.1 Cavity, $M_\infty = 2.3$ , $Re/10^6 = 2.9$	145
140	" $Re/10^6 = 3.9$	145

### ILLUSTRATIONS (Contd)

<u><b>Figure</b></u>	<u><b>Page</b></u>
141 Schlieren Flow Photograph, L/D = 5.1 Cavity with Sawtooth Fence, $M_\infty = 2.3$ , $Re/10^6 = 3.0$ .....	146
142 Schlieren Flow Photograph, L/D = 5.1 Cavity with Sawtooth Fence, $M_\infty = 2.3$ , $Re/10^6 = 3.6$ .....	146
143 Pressure Coefficient Distributions for L/D = 5.6 Cavity, $M_\infty = 2.3$	147
144 Pressure Coefficient Distributions for L/D = 5.6 Cavity with Boundary Layer Trip, $M_\infty = 2.3$ .....	148
145 Pressure Coefficient Distributions for L/D = 5.6 Cavity with Boundary Layer Trip and Perforated Fence, $M_\infty = 2.3$ , Run 1.....	149
146                                "                                Run 2.....	150
147 Pressure Coefficient Distributions for L/D = 5.6 Cavity with Boundary Layer Trip and Sawtooth Fence; $M_\infty = 2.3$ .....	151
148 Schlieren Flow Photograph, L/D = 5.6 Cavity, $M_\infty = 2.3$ .....	152
149 Schlieren Flow Photograph, L/D = 5.6 Cavity with Boundary Layer Trip, $M_\infty = 2.3$ .....	152
150 Schlieren Flow Photograph, L/D = 5.6 Cavity with Boundary Layer Trip and Perforated Fence, $M_\infty = 2.3$ , Run 1.....	153
151 Schlieren Flow Photograph, L/D = 5.6 Cavity with Boundary Layer Trip and Perforated Fence, $M_\infty = 2.3$ , Run 2.....	153
152 Schlieren Flow Photograph, L/D = 5.6 Cavity with Boundary Layer Trip and Sawtooth Fence, $M_\infty = 2.3$ .....	153
153 Pressure Coefficient Distributions for L/D = 5.6 Cavity with Boundary Layer Trip and Forward Facing Probe, $M_\infty = 2.3$ .....	154
154 Schlieren Flow Photograph, L/D = 5.6 Cavity with Boundary Layer Trip and Forward-Facing Probe, $M_\infty = 2.3$ .....	155
155 Pressure Coefficient Distributions for L/D = 6.2 Cavity, $M_\infty = 2.3$	156
156 Pressure Coefficient Distributions for L/D = 6.2 Cavity with Boundary Layer Trip, $M_\infty = 2.3$ .....	157
157 Schlieren Flow Photograph, L/D = 6.2 Cavity, $M_\infty = 2.3$ .....	158
158 Schlieren Flow Photograph, L/D = 6.2 Cavity with Boundary Layer Trip, $M_\infty = 2.3$ .....	158

# ILLUSTRATIONS (Contd)

<u>Figure</u>		<u>Page</u>
159	Pressure Coefficient Distributions for L/D = 6.2 Cavity with Boundary Layer Trip and Perforated Fence, $M_\infty = 2.3$ , $Re/10^6 = 2.9..$	159
160	Pressure Coefficient Distributions for L/D = 6.2 Cavity with Boundary Layer Trip and Perforated Fence, $M_\infty = 2.3$ , $Re/10^6 = 3.9..$	160
161	Pressure Coefficient Distributions for L/D = 6.2 Cavity with Boundary Layer Trip and Sawtooth Fence, $M_\infty = 2.3.....$	161
162	Schlieren Flow Photograph, L/D = 6.2 Cavity with Boundary Layer Trip and Perforated Fence, $M_\infty = 2.3$ , $Re/10^6 = 2.9.....$	162
163	" $Re/10^6 = 3.9.....$	162
164	Pressure Coefficient Distributions for L/D = 9.9 Cavity, $M_\infty = 2.3$	163
165	Pressure Coefficient Distributions for L/D = 9.9 Cavity with Boundary Layer Trip, $M_\infty = 2.3.....$	164
166	Schlieren Flow Photograph, L/D = 9.9 Cavity, $M_\infty = 2.3.....$	165
167	Schlieren Flow Photograph, L/D = 9.9 Cavity with Boundary Layer Trip, $M_\infty = 2.3.....$	165
168	Pressure Coefficient Distributions for L/D = 9.9 Cavity with Boundary Layer Trip and Perforated Fence, $M_\infty = 2.3.....$	166
169	Schlieren Flow Photograph, L/D = 9.9 Cavity with Boundary Layer Trip and Perforated Fence, $M_\infty = 2.3.....$	167
170	Pressure Coefficient Distributions for L/D = 9.9 Cavity with Boundary Layer Trip and Sawtooth Fence, $M_\infty = 2.3$ , Run 1.....	168
171	" Run 2.....	169
172	Schlieren Flow Photograph, L/D = 9.9 Cavity with Boundary Layer Trip and Sawtooth Fence, $M_\infty = 2.3$ , Time T1.....	170
173	" Time T2.....	170
174	" Time T3.....	171
175	" Time T4.....	171
176	Pressure Coefficient Distributions for L/D = 5.1 Cavity with Boundary Layer Trip, $M_\infty = 3.0$ , Run 1.....	172
177	" Run 2.....	173

# ILLUSTRATIONS (Contd)

Figure		Page
178	" Run 3.....	174
179	Oil Flow on Ceiling of L/D = 5.1 Cavity, $M_\infty = 3.0$ .....	175
180	Oil Flow on Port Side of L/D = 5.1 Cavity, $M_\infty = 3.0$ .....	175
181	Pressure Coefficient Distributions for L/D = 5.1 Cavity with Boundary Layer Trip and Perforated Fence, $M_\infty = 3.0$ , Run 1.....	176
182	" Run 2.....	177
183	Oil Flow on Ceiling and Port Side of L/D = 5.1 Cavity, Perforated Fence Attached, $M_\infty = 3.0$ , Photograph 1.....	178
184	" Photograph 2.....	178
185	Pressure Coefficient Distributions for L/D = 5.1 Cavity with Boundary Layer Trip and Sawtooth Fence, $M_\infty = 3.0$ .....	179
186	Schlieren Flow Photograph, L/D = 5.1 Cavity with Boundary Layer Trip, $M_\infty = 3.0$ .....	180
187	Schlieren Flow Photograph, L/D = 5.1 Cavity with Boundary Layer Trip and Perforated Fence, $M_\infty = 3.0$ .....	180
188	Schlieren Flow Photograph, L/D = 5.1 Cavity with Boundary Layer Trip and Sawtooth Fence, $M_\infty = 3.0$ .....	180
189	Pressure Coefficient Distributions for L/D = 5.6 Cavity with Boundary Layer Trip, $M_\infty = 3.0$ , Run 1.....	181
190	" Run 2.....	182
191	Oil Flow on Ceiling and Port Side of L/D = 5.6 Cavity, $M_\infty = 3.0$ ...	183
192	Oil Flow on Ceiling, Port Side and Aft Bulkhead of L/D = 5.6 Cavity, $M_\infty = 3.0$ .....	183
193	Pressure Coefficient Distributions for L/D = 5.6 Cavity with Boundary Layer Trip and Perforated Fence, $M_\infty = 3.0$ , Run 1.....	184
194	" Run 2.....	185
195	Schlieren Flow Photograph; L/D = 5.6 Cavity with Boundary Layer Trip, $M_\infty = 3.0$ .....	186
196	Schlieren Flow Photograph, L/D = 5.6 Cavity with Boundary Layer Trip and Perforated Fence, $M_\infty = 3.0$ .....	186

# ILLUSTRATIONS (Contd)

<u>Figure</u>		<u>Page</u>
197	Pressure Coefficient Distributions for $L/D = 5.6$ Cavity with Boundary Layer Trip and Sawtooth Fence, $M_\infty = 3.0$ .....	187
198	Schlieren Flow Photograph, $L/D = 5.6$ Cavity with Boundary Layer Trip and Sawtooth Fence, $M_\infty = 3.0$ .....	188
199	Pressure Coefficient Distributions for $L/D = 5.6$ Cavity with Boundary Layer Trip and Forward Facing Probe, $M_\infty = 3.0$ .....	189
200	Schlieren Flow Photograph, $L/D = 5.6$ Cavity with Boundary Layer Trip and Forward Facing Probe, $M_\infty = 3.0$ .....	190
201	" Probe Model Pitched 5 Degrees Nose Up.....	190
202	Pressure Coefficient Distributions for $L/D = 6.2$ Cavity with Boundary Layer Trip, $M_\infty = 3.0$ .....	191
203	Pressure Coefficient Distributions for $L/D = 6.2$ Cavity with Boundary Layer Trip and Perforated Fence, $M_\infty = 3.0$ , Run 1.....	192
204	" Run 2.....	193
205	" Run 3.....	194
206	Schlieren Flow Photograph, $L/D = 6.2$ Cavity with Boundary Layer Trip, $M_\infty = 3.0$ .....	195
207	Schlieren Flow Photograph, $L/D = 6.2$ Cavity with Boundary Layer Trip and Perforated Fence, $M_\infty = 3.0$ .....	195
208	Pressure Coefficient Distributions for $L/D = 9.9$ Cavity with Boundary Layer Trip, $M_\infty = 3.0$ , Run 1.....	196
209	" Run 2.....	197
210	Oil Flow on Ceiling and Port Side of $L/D = 9.9$ Cavity, $M_\infty = 3.0$ ...	198
211	Oil Flow on Ceiling and Starboard Side of $L/D = 9.9$ Cavity, $M_\infty = 3.0$ .....	198
212	Pressure Coefficient Distributions for $L/D = 9.9$ Cavity with Boundary Layer Trip and Perforated Fence, $M_\infty = 3.0$ , Run 1.....	199
213	" Run 2.....	200
214	Schlieren Flow Photograph, $L/D = 9.9$ Cavity with Boundary Layer Trip, $M_\infty = 3.0$ .....	201

# ILLUSTRATIONS (Contd)

Figure		Page
215	Schlieren Flow Photograph, $L/D = 9.9$ Cavity with Boundary Layer Trip and Perforated Fence, $M_\infty = 3.0$ .....	201
216	Pressure Coefficient Distributions for $L/D = 9.9$ Cavity with Boundary Layer Trip and Sawtooth Fence, $M_\infty = 3.0$ .....	202
217	Schlieren Flow Photograph, $L/D = 9.9$ Cavity with Boundary Layer Trip and Sawtooth Fence, $M_\infty = 3.0$ .....	203
218	Acoustic Pressure Distributions in $L/D = 5.1$ Cavity at $M_\infty = 0.60$ ..	204
219	" $M_\infty = 0.71$ ..	205
220	" $M_\infty = 0.76$ ..	206
221	Acoustic Pressure Distributions in $L/D = 5.6$ Cavity at $M_\infty = 0.60$ ..	207
222	" $M_\infty = 0.64$ ..	208
223	" $M_\infty = 0.66$ ..	209
224	" $M_\infty = 0.70$ ..	210
225	" $M_\infty = 0.74$ ..	211
226	Acoustic Pressure Distributions in $L/D = 6.2$ Cavity at $M_\infty = 0.60$ ..	212
227	" $M_\infty = 0.70$ ..	213
228	" $M_\infty = 0.74$ ..	214
229	Acoustic Pressure Distributions in $L/D = 9.9$ Cavity at $M_\infty = 0.60$ ..	215
230	" $M_\infty = 0.70$ ..	216
231	" $M_\infty = 0.74$ ..	217
232	" $M_\infty = 0.75$ ..	218
233	Acoustic Pressure Distributions at $M_\infty = 1.5$ in $L/D = 5.1$ Cavity...	219
234	Acoustic Pressure Distributions at $M_\infty = 1.5$ in $L/D = 5.6$ Cavity...	220
235	" $L/D = 6.2$ Cavity...	221
236	" $L/D = 9.9$ Cavity...	222



# ILLUSTRATIONS (Contd)

Figure		Page
237	Acoustic Pressure Distributions at $M_\infty = 2.3$ in $L/D = 5.1$ Cavity, Two Re Numbers, Without Suppressors.....	223
238	Acoustic Pressure Distributions at $M_\infty = 2.3$ in $L/D = 5.1$ Cavity With and Without Sawtooth Fence.....	224
239	Acoustic Pressure Distributions at $M_\infty = 2.3$ in $L/D = 5.6$ Cavity With and Without B.L. Trip, Without Suppressors.....	225
240	" With B.L. Trip, With and Without Sawtooth Suppressor.....	226
241	" With B.L. Trip, Both Suppressor Types.....	227
242	Acoustic Pressure Distributions at $M_\infty = 2.3$ in $L/D = 6.2$ Cavity With and Without B.L. Trip, Without Suppressors.....	228
243	" With B.L. Trip, With and Without Perforated Suppressor.....	229
244	" With B.L. Trip, Both Suppressor Types.....	230
245	" With B.L. Trip, Perforated Suppressor at Two Re.....	231
246	Acoustic Pressure Distributions at $M_\infty = 2.3$ in $L/D = 9.9$ Cavity With and Without B.L. Trip, Without Suppressors.....	232
247	" With B.L. Trip, With and Without Perforated Suppressor.....	233
248	" With B.L. Trip, Both Suppressor Types.....	234
249	Acoustic Pressure Distributions at $M_\infty = 3.0$ in $L/D = 5.1$ Cavity...	235
250	" $L/D = 5.6$ Cavity...	236
251	" $L/D = 6.2$ Cavity...	237
252	" $L/D = 9.9$ Cavity...	238
253	Effects of Cavity Oscillation Suppressor Fence on Frequency Spectra at 3 Locations in $L/D = 5.6$ Cavity at $M_\infty = 0.60$ .....	239
254	" $M_\infty = 0.70$ .....	240
255	" $M_\infty = 0.74$ .....	241
256	" $M_\infty = 1.5$ .....	242

# ILLUSTRATIONS (Contd)

Figure		Page
257	Effects of Cavity Oscillation Suppressor Fence on Frequency Spectra at 3 Locations in L/D = 5.6 Cavity at $M_\infty = 2.3$ .....	243
258	Effects of Cavity Oscillation Suppressor Fence on Frequency Spectra at 3 Locations in L/D = 5.6 Cavity at $M_\infty = 3.0$ .....	244
259	" L/D = 5.1 Cavity at $M_\infty = 1.5$ .....	245
260	" L/D = 6.2 Cavity at $M_\infty = 1.5$ .....	246
261	" L/D = 9.9 Cavity at $M_\infty = 1.5$ .....	247
262	Acoustic Modal Pressure Distributions in the L/D = 5.6 Cavity at $M_\infty = 0.70$ .....	248
263	" $M_\infty = 1.5$ .....	249
264	" $M_\infty = 2.3$ .....	250
265	Maximum Acoustic Pressure Variations with Mach Number for Four L/D Values: a) = 5.1, b) = 5.6, c) = 6.2, d) = 9.9.....	251
266	Pressure Spectrum on the Rear Bulkhead of L/D = 5.1 Cavity for $M_\infty = 2.3$ at $Re = 2.9 \times 10^6$ /ft.....	252
267	" $Re = 3.9 \times 10^6$ /ft.....	253
268	Mach Number Dependence of the Normalized Maximum Acoustic Pressure in the L/D = 5.1 Cavity.....	254
269	" L/D = 5.6 Cavity.....	255
270	" L/D = 6.2 Cavity.....	256
271	" L/D = 9.9 Cavity.....	257
272	Effect of Total Head Tube on the Acoustic Pressure Distributions in L/D = 5.6 Cavity for $M_\infty = 0.60$ , Without Suppression Fence.....	258
273	" $M_\infty = 0.60$ , With Suppression Fence.....	259
274	" $M_\infty = 0.70$ , Without Suppression Fence.....	260
275	" $M_\infty = 0.74$ , Without Suppression Fence.....	261
276	" $M_\infty = 0.74$ , With Suppression Fence.....	262

# ILLUSTRATIONS (Contd)

<u>Figure</u>		<u>Page</u>
277	Effect of Total Head Tube on the Acoustic Pressure Distributions in $L/D = 5.6$ Cavity for $M_\infty = 1.5$ , Without Suppression Fence.....	263
278	" $M_\infty = 1.5$ , With Suppression Fence.....	264
279	Effect of Total Head Tube on the Acoustic Pressure Distributions in $L/D = 5.6$ Cavity for $M_\infty = 2.3$ , Without Suppression Fence.....	265
280	Comparison of Measured vs Predicted Oscillatory Mode Frequencies for Rectangular Cavities, $L/D = 5.1$ .....	266
281	" $L/D = 5.6$ .....	267
282	" $L/D = 6.2$ .....	268
283	" $L/D = 9.9$ .....	269

## LIST OF SYMBOLS

a	speed of sound
$C_p$	pressure coefficient [ $C_p = (p - p_\infty)/Q_\infty$ ]
D	cavity depth, in.
f	frequency, Hz
$K(M_\infty)$	shear layer to free stream velocity ratio function in Equation (3)
L	cavity length, in.
m	mode number in Equation (3)
M	Mach number
p	pressure
$Q_\infty$	free stream dynamic pressure; $Q_\infty = \frac{1}{2} \rho_\infty U_\infty^2$
Re	unit Reynolds number, Reynolds number/ft
rms	root-mean-square
SPL	sound pressure level, rms, dB with regard to $2.90075 \times 10^{-9}$ psi ( $2 \times 10^{-5}$ Pa)
T	temperature, °R
U	velocity
W	cavity width, in.
X, Y, Z	rectangular coordinate system (Figure 10)
$\gamma(L/D)$	phase shift function between vortex train and cavity acoustic waves in Equation (3)
$\lambda$	spacing between vortices
$\rho$	density

### Subscripts

m	frequency mode number
s	static
o	total
$\infty$	free stream value

### Superscript

'	condition behind the oblique shock at model's leading edge
---	--

## Section I

### INTRODUCTION

Carrying weapons internally in high performance fighter-bomber aircraft offers many potential benefits; such as: increased combat range, greater maneuverability, higher target penetration speed (less time over the target), elimination of weapon aerothermal heating problems during transit to the target site, and reduced detection signatures. However, opening weapon bay doors at high aircraft speeds can result in extreme flow instabilities within the open weapon bay cavity. The internal flow instability and associated severe aeroacoustic phenomena can compromise the aircraft structure and crew, the weapon sensing devices and structure, and the stable release of the weapon.

During specific flight conditions and with some current weapons, aircraft speed reductions are required prior to opening weapon bay doors, thereby increasing time (and vulnerability) over the target. Weapon bay cavities and aeroacoustic suppression devices should be designed to overcome this loss in aircraft capability. To accomplish this, one must understand well the internal flow in open weapon bay cavities. The current work is directed to this problem.

The experiments described herein were designed to provide fundamental aerodynamic and aeroacoustic data for a generic set of rectangular cavities for both subsonic and supersonic flows. These experiments supplement earlier experiments conducted using the same model for transonic flows (Reference 1).

---

<sup>1</sup>Clark, R.L., "Weapons Bay Turbulence Reduction Techniques," Flight Dynamics Laboratory, Wright-Patterson AFB, AFFDL TM 75-147 FPM, Dec 1975.

## Section II

### EXPERIMENTAL PROGRAM

#### MODEL & INSTRUMENTATION

In lieu of testing a particular airplane configuration, a "flat plate" cavity flow model (Figure 1) was fabricated and tested. The flat plate model is representative of the lower surface of typical fighter-bomber aircraft capable of carrying stores internally (Figure 2). The flat plate model can accommodate a generic group of several, interchangeable, rectangular cavities (Figures 1 and 3) having various length to depth ratios.

The opening of all cavities tested is 7.25 in. downstream of the sharp leading edge of the flat plate model. By using various insert blocks, the length to depth ratios of the cavities are variable from approximately 5 to 10 (Figures 1 and 3, and Reference 2). All cavities have a width of 2.5 in. (Figure 1).

Photographs of some of the cavities tested are shown in Figure 4. Shown in the photographs is the yoke support system for the model. This suspension system was designed to minimize the propagation of base flow effects into the cavity, while maintaining a small model cross section (particularly important for the transonic tests, Reference 1). The model yoke support system is attachable to the AFWAL Trisonic Tunnel sting.

Aeroacoustic suppression fences (spoilers) are attachable to the flat plate surface just upstream of the cavity opening. Both the "saw-tooth" and the "perforated" fence (Figure 5) are about 0.2 in. high, which is the approximate thickness of a turbulent boundary layer on the flat plate surface at the start of the cavity (References 1 and 3).

<sup>2</sup>Kaufman, L.G.II, Maciulaitis, A., Foreman, K.M. and Danos, S.J., "Pretest Report for Joint AFFDL/GAC Program on Flows Past Weapons Cavities," Grumman Aerospace Corporation, Research Department Memorandum RM-656, July 1978.

<sup>3</sup>Clark, R.L., Kaufman, L.G.II and Maciulaitis, A., "Aeroacoustic Measurements for Mach 0.6 to 3.0 Flows Past Rectangular Cavities," AIAA Paper 80-0036 presented at 18th Aerospace Sciences Meeting in Pasadena, CA, Jan 1980.

The model instrumentation includes 35 surface static pressure taps, 21 silicon diaphragm transducers (to measure transient pressures), and three thermocouples. Locations of the instrumentation on the cavity ceiling, sidewalls and bulkheads, as well as on the surrounding flat plate surface, are shown in Figure 6.

Scanning valves and pressure transducers are used to measure the static pressures (Reference 4). The transient pressure (acoustic) data are measured using miniature differential pressure transducers\*. Screens over the transducers prevent damage from extraneous particles in the tunnel flow and greatly increase the life expectancy of the transducers. The transducers have a resonant frequency at 125 kHz and can measure transient pressure differences up to 25 psi. They are well suited for these experiments (Reference 2).

The AC-coupled amplified voltage signal from each transducer is processed "on-line" and recorded on tape recorders for later narrow band frequency analysis (approximately 8 Hz bandwidth) "off-line" (Figure 7). On-line, the signals are reduced to rms voltages and converted to rms pressures in psi. The pressures are nondimensionalized by Q and converted to SPL (db) using:

$$\text{SPL (dB)} = 20 \log \left[ \frac{p_{\text{rms}} (\text{psi})}{2.90075 (\text{psi})} \right] 10^9 \quad (1)$$

$$\text{SPL (dB)} = 180 + 20 \log (p_{\text{rms}} / 2.90075)$$

Selected transducers are also processed on-line using a Fourier analyzer. All of the acoustic and static pressure data are stored in the mini computer for off-line reduction, listing and plotting.

In addition to the surface instrumentation, forward- and rearward- facing total pressure probes are attachable to the cavity ceiling (Figure 8). The total pressure measurements are used in determining the velocity of the shear flow over the center of the L/D = 5.583 cavity in the plane of the flat plate surface. The opening of the total pressure probe is directly beneath static

<sup>4</sup>White, H.L., "Trisonic Gasdynamic Facility User Manual," AFFDL TM 73-82 FM, June 1973.

\*Kulite Model XCQ-093-25 with "B" screens.

pressure tap No. 15 (Fig. 6). A secondary function of the total pressure probes is to establish the extent to which its presence affects the acoustic and static pressure measurements.

#### TUNNEL & TEST CONDITIONS

The Trisonic Gasdynamics Facility of the Air Force Wright Aeronautical Laboratories is located at Wright-Patterson AFB, Ohio. As described by White (Reference 4), the Trisonic Gasdynamics Facility is a closed-circuit, variable density, continuous-flow wind tunnel capable of providing subsonic, transonic and supersonic flows through a range of Mach numbers from 0.23 to 3.0. Subsonic nozzle blocks can provide flows in a 2-ft-square test section for Mach numbers varying from 0.23 up to 0.85. There is a replaceable 15 in. square transonic test section with slotted walls. Replaceable supersonic nozzle blocks are available for Mach 1.5, 1.9, 2.3, and 3.0 flows in a 2-ft-square test section. The maximum attainable stagnation pressure is: 19.8 psi for the subsonic nozzle blocks, 27.8 psi for the transonic nozzle blocks, and 29.2 psi for the supersonic nozzle blocks. The stagnation temperature of the tunnel flow is 560°R for all nozzle blocks (Reference 4).

Photographs of the cavity flow model mounted in the tunnel test section are shown in Figure 9. The Mach 3.0 nozzle blocks are installed in the tunnel, and a boundary layer trip is attached to the model to make sure there is a turbulent boundary flow upstream of the cavity. The boundary layer trip consists of fine grit glued to the flat plate surface at a location 1 in. downstream of the leading edge of the model.

Results of transonic flow experiments on the model are described by Clark (Reference 1). The cavity flow results presented here were obtained using the variable Mach number subsonic nozzle blocks and selected supersonic nozzle blocks. The tunnel flow test conditions for the results presented herein are indicated in Table I.

TABLE I - TUNNEL FLOW TEST CONDITIONS

$M_\infty$	$Re_\infty/10^6 \text{ft}$
0.58 - 0.80	2.06 - 2.40
1.5	2.7
2.3	2.9 & 3.9
3.0	2.8



The boundary layer was naturally turbulent at the cavity leading edge for most cases, but the model was tested both with and without the trip in several instances to ascertain firmly turbulent boundary layer effects. The boundary layer trip is evident in Figure 9.

Several profile schlieren flow photographs, taken during many tunnel runs, are useful in ascertaining the stability of the cavity flow.

The movement of oil drops applied to the surface of the model is helpful in determining locations of flow separation and the symmetry of the surface flow. These photographic data are given along with corresponding pressure data.

The flat plate portion of the model is aligned with the free stream flow direction in all except three test cases mentioned in Section III, when the model is slightly pitched.

Particular tunnel flow conditions and model configurations are listed in Section III.

### Section III

#### EXPERIMENTAL RESULTS

Data are presented for the tunnel flow conditions and model configurations listed in Table II. The subsonic flow static data are presented first. Following these are the static data for the supersonic tunnel flows (Mach 1.5, 2.3 and 3.0). For each of the tunnel Mach number flow regimes, data are presented first for the  $L/D = 5.1$  cavity and then for the  $L/D = 5.6$ , 6.2, and 9.9 cavities. Static pressure data (and total pressure probe data when available) are presented first for each Mach number regime and cavity length-to-depth ratio. Accompanying profile schlieren photographs are then shown for the same flow conditions. Observations of oil drop flow experiments are described for the configurations indicated in Table II.

Three types of aeroacoustic data are presented in this report. Measurement results are given as overall (covering the entire sound pressure frequency range between 0.1 and 5 kHz) levels (SPL), as intensity spectra in the frequency domain for particular pressure transducers and, lastly, as spatial intensity distributions of various oscillatory pressure modes. Since earlier analysis had established the existence of high-intensity noise at very low frequencies, which probably was tunnel-related, it was decided to filter out all signals below 0.1 kHz. Unfortunately, this decision made it impossible to use the overall SPL values directly either from the on-line computer memory, or from the test printout. Although the acoustic recording instrumentation had a flat response up to 10 kHz, in order to gain better resolution data were frequency analyzed up to 5 kHz. Comparisons with sample results analyzed to 10 kHz showed that in a few instances there were oscillatory frequency modes above 5 kHz which, naturally were not picked up in our frequency analysis. However, this is of little importance, inasmuch as the intensities above 5 kHz were significantly lower than those below 5 kHz. Overall acoustic data distributions are shown for the same test configurations as for the static pressure distributions shown.

The cavity was instrumented with 21 Kulite pressure transducers. Each transducer yields a pressure-time history for every tunnel run. It was necessary to limit the number of transducer data frequency analyses presented

TABLE II TEST CONDITIONS AND CONFIGURATIONS

$M_\infty$	0.58 - 0.80		1.5	2.3		3.0	
$Re_\infty/10^6$ ft	2.2 - 2.4		2.5 - 2.8	2.9 - 3.9		2.7 - 2.9	
Boundary Lyr Trip	off	on	off	off	on	on	
<u>L/D = 5.1</u>							
No fence		P	P	P		0	P
Perforated fence						0	P
Sawtooth fence			P	P			P
<u>L/D = 5.6</u>							
No fence	P		0 P	P	P	0	P
Total pres. probe	P		P		P		P
Perforated fence	0		0		P		P
Sawtooth fence	A 0 P		0 P		P		P
<u>L/D = 6.2</u>							
No fence	P		P	P	P		P
Perforated fence					P		P
Sawtooth fence			P		P		
<u>L/D = 8.9</u>							
Perforated fence			0				
<u>L/D = 9.9</u>							
No fence		P	A P	P	P	0	P
Perforated fence		P			P		P
Sawtooth fence		P	P		P		P
A Also includes data for small angles of attack $\neq 0$ 0 Oil drop flow experiments P Static and transient (acoustic) pressure data and profile schlieren flow photographs							

to a reasonable research effort. Therefore, the acoustic data presented herein does not constitute a complete set of all the data obtained. Instead, the limited acoustic data presented are intended to document the important dependences and trends by a judicious selection of the experimental results.

Unless otherwise stated, the SPL values are computed using  $2.90074 \times 10^{-9}$  psi (20  $\mu$ Pa) as the reference pressure.

Detailed acoustic (transient) pressure spectrum data are shown for selected transient pressure gauges and configurations. (Several hundred plots would be required to show all of the transient pressure data).

A right-hand rectangular coordinate system is used (Figure 10). The origin is in the central plane at the leading edge of the cavity;  $x$  is streamwise,  $y$  is spanwise, and  $z$  is vertical (positive upwards, towards the cavity ceiling).

#### STATIC EXPERIMENTAL RESULTS

Static and total pressure data are shown in dimensionless coefficient form:

$$C_p = \frac{p - p_\infty}{0.7 \rho_\infty M_\infty^2} \quad (2)$$

Pressure coefficient values are plotted versus distances nondimensionalized using the cavity length, width and depth. Acoustic data are shown in sound pressure levels (dB) (see Equation 1).

#### Subsonic

Static pressure coefficient distributions obtained on the shortest cavity model ( $L/D = 5.067$ ) are essentially invariant for  $0.60 < M_\infty < 0.76$  (Figures 11 - 16). The pressures are nearly the same as the free stream static pressure except in the aft portion of the cavity, where there is a small increase in pressure. On the surface downstream of the cavity ( $x > L$ ) there is a separated flow bubble (evidenced by negative pressure coefficients). The only discernable change in the pressure coefficient distributions, for  $0.60 < M_\infty < 0.76$ , is that for the pressure on the surface immediately downstream of the cavity:  $C_p = -0.46$  for  $M_\infty = 0.60$  and  $C_p = -0.52$  for  $M_\infty = 0.74$ . Profile schlieren flow photographs were investigated and revealed no anomalies for these subsonic flows (Figure 17).

Results obtained for a longer and deeper cavity ( $L/D = 5.583$ ) reveal more pronounced Mach number effects through the subsonic flow regime, although the  $L/D$  ratio is just 10 percent larger than for the shortest cavity. Pressure coefficient distributions are shown for  $0.60 < M_\infty < 0.74$  (Figures 18 - 24); distributions at the intermediate Mach numbers change smoothly and continuously from the lowest to the highest subsonic Mach number. The most pronounced distribution, at Mach 0.74, indicates: 1) a local thinning of the boundary layer just upstream of the cavity, 2) separated flow over the forward portion of the cavity, 3) reattachment on the aft portion of the cavity ceiling, and 4) separated flow on the surface downstream of the cavity.

Profile schlieren flow photographs for this cavity configuration reveal no evidence of either compression or expansion waves. A small region of separated flow is noticeable at the aft shoulder of the cavity (Figures 25 - 27).

Oil drop flow photographs support the observation of separated flow in the forward portion of the cavity, and vortices of reversed flow after reattachment on the after portion of the cavity (Figures 28 - 31). These photographs indicate the complex, three-dimensional nature of the surface flow, which appears to be symmetric about the centerline of the cavity.

Adding the sawtooth fence (referred to as "large" fence in plots) to this model configuration results in substantially different pressure distribution (Figures 32 - 34). The flow bridges the cavity and reattaches near the aft corner, with no separation on the surface downstream of the cavity. There are no significant changes in the pressure distributions for  $0.60 < M_\infty < 0.74$ .

Oil flow photographs indicate two vortices within the cavity; the aft reverse flow vortex having a stronger surface shear flow than the forward, shorter, vortex. Sample oil drop flow photographs for the sawtooth and perforated fence configurations are shown in Figures 35 - 37 and in Figures 38-40.

The forward facing probe has negligible effect on the pressure distributions either without or with the sawtooth fence attached (Figures 41 - 46). However, the sawtooth fence strongly affects the total pressure probe measurements. Without the fence the probe measures pressure values typical of those within a shear layer. With the fence, the forward facing total pressure probe measures pressures very nearly equal to the static pressure on the

cavity ceiling; this suggests that the probe was in the separated flow region caused by the sawtooth fence.

The aft-facing total pressure probe does not change the static pressure distributions with or without the sawtooth fence (Figures 47 - 57). In all cases the aft-facing probe recorded smaller pressures than the static pressure on the cavity ceiling. The model was pitched at  $+ 3/4^\circ$  and at  $- 3/4^\circ$  for two test runs; the plotted results were indistinguishable from those obtained at zero angle of attack.

A somewhat longer cavity ( $L/D = 6.167$ ) exhibits similar static pressure distributions to those obtained for the  $L/D = 5.583$  cavity (Figures 58 - 60). Profile schlieren flow photographs indicate little more than a small disturbance at the aft end of the cavity (Figure 61).

Pressure coefficient distributions for the long shallow cavity ( $L/D = 9.867$ ) indicate: 1) separation from the forward shoulder of the cavity, 2) reattachment on the cavity ceiling, and 3) a separated flow bubble downstream of the cavity (Figures 62 - 65). There is very little difference in the distributions for  $0.60 < M_\infty < 0.74$ . These data were obtained with a boundary layer trip strip located 1 in. downstream of the flat plate leading edge.

Oil flow photographs (Figures 66 - 68) indicate reverse flow in the forward portion of the cavity, attached flow on the middle portion of the cavity ceiling, and a separated flow region in the aft portion of the cavity. There are symmetric vortices in the after portion of the cavity and also on the plate surface downstream of the cavity. Profile schlieren flow photographs indicate a small separation bubble at the aft shoulder of the cavity (Figure 69).

The addition of either the perforated or sawtooth fence reduces the pressures in the aft portion of the cavity and reduces the extent of the separated flow bubble downstream of the cavity (Figures 70 - 76). Profile schlieren flow photographs indicate a substantial increase in the thickness of the shear layer when either fence is added to the model (Figures 77 and 78). Oil flow photographs indicate separated, reverse flow throughout the entire cavity (Figures 79 - 82), with nearly "dead" air in the forward portion of the cavity.

$$M_{\infty} = 1.5$$

The pressure coefficient distributions for the smallest cavity, (Figures 83 and 84) have small positive values instead of the small negative values recorded for subsonic Mach numbers. The sawtooth fence causes a larger region of separated flow, resulting in very small pressure coefficients on the cavity ceiling, and reduces the pressures on the aft bulkhead. Profile schlieren flow photographs give further evidence of the increased depth of the shear layer with the fence (Figures 85 and 86).

The pressure coefficient distributions for the longer and deeper cavity ( $L/D = 5.583$ ) are positive for  $M_{\infty} = 1.5$ , whereas they are negative for subsonic Mach numbers (Figure 87). The sawtooth fence reduces the pressures on the cavity ceiling, (Figure 88), similarly to the effects of adding the fence in subsonic free stream flows, (Figures 18 and 32). The distributions are similar to those for the smaller cavity ( $L/D = 5.067$ ).

Profile schlieren flow photographs again indicate an increased shear layer thickness when the saw-tooth fence is attached to the model (Figures 89 and 90).

Oil flow photographs indicate reverse flow in the aft portion of the cavity and very little shear in the forward portion of the cavity (Figures 91 - 94). When the perforated fence is attached upstream of the cavity, there results a marked asymmetry in the forward portion of the cavity (Figures 95 - 98). The saw-tooth fence also results in an asymmetric flow on the cavity ceiling (Figures 99 - 101).

The problem of flow asymmetry deserves some elaboration, especially since it was observed not only in oil flow photographs but also was established in terms of the static pressure distributions. The observed pressure and oil flow asymmetries are not always compatible. In some instances the oil flow indicated a clockwise asymmetry whereas the static pressure distribution for the same configuration indicated a counterclockwise asymmetry. These anomalies can be explained only by speculation at the present time. The oil flow work was done at the end of the entire test series, and the possibility exists that some of the flows are bistable, requiring the slightest changes (such as the presence of oil itself, or a minute asymmetry in cavity shape) to form an asymmetry of one type, or another. This remains to be explored in the future.

The forward facing probe has essentially no effect on the pressure distribution on the model, either with or without the sawtooth fence attached. No shock wave emanates from the probe, which is in a shear layer. The fence thickens the shear layer and results in a considerably lower pressure read by the forward-facing probe, (Figures 102 and 103). Profile schlierens, without and with the sawtooth fence, are shown in Figures 104 and 105.

Similarly, the aft-facing probe has no effect on the pressure distributions, either without (Figures 106 and 107) or with (Figure 108) the sawtooth fence attached to the model. Again, the fence increases considerably the thickness of the shear layer (profile schlieren flow photographs, Figures 109 and 110).

The somewhat longer cavity ( $L/D = 6.167$ ) results in pressure distributions very similar to those for the  $L/D = 5.583$  cavity (Figures 111 and 112). The sawtooth fence increases the thickness of the shear layer (Figures 113 and 114).

The long shallow cavity ( $L/D = 9.867$ ) was tested at a small ( $0.75^\circ$ ) angle of attack as well as at zero angle of attack. The small angle of attack had essentially no effect on the pressure coefficient distribution. The pressure distributions indicate flow reattachment to the cavity ceiling near the middle of the cavity. The pressure rise in the aft portion of the cavity is more pronounced when the sawtooth fence is attached to the model (Figures 115 - 117).

Profile schlieren flow photographs (Figures 118 - 120) reveal similar shear layer thicknesses for zero and  $0.75^\circ$  angles of attack, and whether or not the fence was attached to the model.

With no fence, oil flow experiments indicate reverse flow with two vortices in the aft portion of the cavity, symmetric about the center plane (Figures 121 - 124). With the perforated fence, oil flows indicate an increased trend to flow from the sides of the cavity to the center plane (Figures 125 - 127). A slightly shorter cavity ( $L/D = 8.933$ ) exhibits a non-symmetric oil pattern on the cavity ceiling (Figures 128 - 131). Oil flows with the sawtooth fence again exhibit a symmetric reverse flow (Figures 132 - 134).



$M_\infty = 2.3$

Pressure distributions in the smallest cavity ( $L/D = 5.067$ ) are shown in Figures 135 - 138) for different Reynolds numbers and without and with the sawtooth fence attached to the model. Except for the higher density, profile schlieren flow photographs indicate no noticeable changes in the flow pattern or shear layer thickness at either Reynolds number, without or with the sawtooth fence attached to the model (Figures 139 - 142).

Pressure coefficient distributions on the cavity ceiling for the  $L/D = 5.583$  cavity are similar at  $M_\infty = 2.3$  to those for  $M_\infty = 1.5$ , (Figure 143). However, the pressures, particularly those on the aft bulkhead, are reduced when a boundary layer trip is applied to the model (Figure 144). Both the perforated and sawtooth fences reduce the pressure levels (Figures 145 - 147).

Without a fence, profile schlieren flow photographs indicate boundary layer transition near the cavity forward bulkhead when there is no trip. The addition of the grit strip causes boundary layer transition near the leading edge of the flat plate model (Figures 148 and 149). The fences increase the thickness of the shear layer over the forward portion of the cavity (Figures 150 - 152).

The forward facing probe does not significantly change the pressure coefficient distributions on the cavity ceiling and sidewalls. A small change is evident on the aft bulkhead, (Figure 153). Faint waves emanating from the probe are visible in the original, glossy, schlieren photographs (Figure 154).

The boundary layer trip does not affect the pressure coefficient distributions in the larger ( $L/D = 6.167$ ) cavity (Figures 155 and 156). However, as evidenced by profile schlieren photographs (Figures 157 and 158), it is effective in causing earlier transition of the boundary layer.

The perforated fence reduces the pressure coefficients on the aft bulkhead (Figure 159). Reynolds number effects are negligible on the pressure distributions (Figures 159 and 160). The sawtooth fence (Figure 161), has essentially the same effect on the pressure coefficient distributions as the perforated fence. Except for the higher density, Reynolds number effects on the flow pattern are not noticeable in profile schlieren flow photographs (Figures 162 and 163).

Pressure coefficients over the long shallow cavity ( $L/D = 9.867$ ) are nearly constant (Figures 164 and 165). The boundary layer trip slightly reduces the pressures on the cavity ceiling. Again, the boundary layer trip is effective in causing earlier transition, but does not result in a significantly thicker shear layer over the aft portion of the cavity (Figures 166 and 167). Similarly, the perforated fence has little effect on the pressure coefficient distributions, (Figure 168). It does increase the shear layer thickness over the cavity (Figure 169).

The sawtooth fence strongly effects the pressure distributions (Figures 170 and 171). The flow is separated in the forward portion of the cavity, reattaches on the cavity ceiling, and results in large pressure coefficient values on the aft bulkhead. Repeat runs indicate consistency in these pressure distributions. The schlieren flow pattern was observed to be slightly unsteady during these test runs (Figures 172 - 175).

$$M_{\infty} = 3.0$$

Pressure coefficient distributions over the smallest cavity ( $L/D = 5.067$ ) are repeatable and have small positive values over the cavity ceiling (Figures 176 - 178). Oil flow patterns for this configuration are shown in Figures 179 and 180. The perforated fence has very little effect on the pressure distributions (Figures 181 and 182). Oil flow photographs for this configuration are shown in Figures 183 and 184. The sawtooth fence also has little effect on the pressure distribution (Figure 185). Schlieren photographs (Figures 186 - 188) show the increase in the shear layer thickness caused by the fences.

The larger ( $L/D = 5.583$ ) cavity has very similar static pressure coefficient distributions (Figures 189 and 190). Oil flow photographs for this configuration are shown in Figures 191 and 192. The perforated small fence does not significantly affect the pressure distributions (Figures 193 and 194), but does thicken the shear layer (Figures 195 and 196). The sawtooth fence effects on the pressure distribution and on the flow field are also small, similar to those caused by the perforated fence (Figures 197 and 198). The total pressure measured using the forward facing probe is indicated in Figure 199. Schlieren photographs, with the probe installed in the  $L/D = 5.583$  cavity, are shown in Figures 200 and 201. In Figure 201, the model is pitched 5 degrees nose up.

The larger ( $L/D = 6.167$ ) cavity has very similar pressure distributions, (Figures 202 - 205). Except for the thickening of the shear layer (Figures 206 and 207), the static flow does not appear to be affected by the perforated fence.

The long shallow cavity ( $L/D = 9.867$ ) has pressure coefficient distributions similar to the other (smaller  $L/D$  ratio) cavities at Mach 3.0. No flow reattachment is evident on the cavity ceiling, (Figures 208 and 209). The data are repeatable. Oil flow photographs for this configuration are shown in Figures 210 and 211. The perforated fence does not affect the pressure distributions, but results in a thicker shear layer (Figures 212 - 215). Also, the sawtooth fence has little effect on the flow (Figures 216 and 217).

#### ACOUSTIC EXPERIMENTAL RESULTS

##### Overall Acoustic Pressure Level Distributions

###### Subsonic

An examination of the overall acoustic pressure distributions in and around the  $L/D = 5.1$  cavity at the subsonic Mach numbers (0.6 to 0.76) at which data are available (Figures 218 - 220) leads to the following observations: The highest acoustic pressure invariably was measured at the mid-height point of the rear bulkhead. Its value peaked at  $M_\infty = 0.71$ , at a value of about 158 dB. The distributions within the cavity are not quite symmetrical, the values in the central longitudinal plane developing a distinct dip in the forward cavity portion with increasing Mach number, while the corresponding values on the side walls differ by as much as 5 dB in the forward section of the cavity. This difference is practically Mach number independent and decreases toward the rear of the cavity. Pressures on the side walls are usually higher than those in the central plane, except at the rear of the cavity.

Similar trends are also observable from the overall acoustic pressure distributions for the somewhat shallower,  $L/D = 5.6$ , cavity (Figures 221 - 225), however, for this cavity the peak value on the rear bulkhead continued to rise with Mach number, reaching 164 dB at  $M_\infty = 0.74$ . With the generally rising pressure levels, the nonsymmetry has also increased, exceeding 7 dB. Center plane pressures are lower than the port wall values by as much as 10 dB.

Figures 221 - 225 also illustrate the beneficial effect of the sawtooth suppression fence in lowering the acoustic pressure level distributions. The amount of reduction is Mach number dependent, reaching a maximum of over 10 dB at  $M_\infty = 0.7$ . Figures 224 and 225 show that the presence of the fence reduced the pressure asymmetry to within experimental error ( $< 2$  dB); however, note that the "depression" of the central plane values practically remained unaltered, being uniformly displaced downward (see e.g., Figures 224 and 225).

Figures 226 - 228 for a slightly shallower cavity ( $L/D = 6.2$ ) show no new phenomena, except that the maximum acoustic pressure values on the rear bulkhead are the same (160 dB) for  $M_\infty = 0.6$  and 0.7, decreasing for  $M_\infty = 0.74$ . The asymmetry is still there but is slightly weaker than for  $L/D = 5.6$  cavity. Also, note that the pressure on the forward bulkhead is relatively lower than for deeper cavities.

Figures 229 - 232 show subsonic acoustic data for the shallowest cavity investigated,  $L/D = 9.9$ . All results were obtained using a boundary layer trip. Both types of suppression fences were used. The general trends are similar to those already described for the deeper cavities, however, the maximum acoustic pressures on the rear bulkhead and the general pressure level are lower than for the deeper cavities, indicating that there must be a  $L/D$  value for the highest maximum pressure values. The extremely low value on the port wall at  $X/L = 0.4$  for  $M_\infty = 0.6$  is somewhat in doubt. The frequency spectrum of that particular signal is singularly free of any modal peaks, such that it is impossible to say whether it is real, or represents the output of a defective pressure transducer. The effectiveness of both suppressor fences was very similar and much smaller than for the deeper cavities (2 - 3 dB on the rear bulkhead).

An attempt was made to correlate the asymmetries in the acoustic pressure level distributions with those of the static pressure. A few sample calculations proved beyond doubt that the latter could not be the same or be caused by the acoustic pressures, since the orders of magnitude involved are greatly different; in other words, the largest acoustic asymmetries represent negligibly small differences in terms of the corresponding pressure coefficients,  $C_p$ . As an illustration, we can compare the corresponding values at about  $X/L = 0.9$  in Figures 58 and 226. The 5dB difference between the centerline and starboard wall values in Figure 226 corresponds to a pressure

difference of  $5.22 \times 10^{-9}$  psi. The 0.12 difference in  $C_p$  in Figure 58 is equivalent to 8.48 psi for  $p_\infty = 8.236$  psi which is many orders of magnitude higher. Similar results could be shown from Figures 62 and 229 and others.

#### $M_\infty = 1.5$

Acoustic pressure level distributions for all four different cavities at  $M_\infty = 1.5$  are shown in Figures 233 - 236. As at subsonic flow velocities, the maximum acoustic pressure always is found on the rear bulkhead. It peaks at 165 dB for  $L/D = 5.6$ , just 1 dB above the highest subsonic value. The point for the  $L/D = 5.6$  cavity at  $Z/D = 0.5$  on the rear bulkhead is of doubtful validity, since its frequency spectrum is uncharacteristically flat; besides, it is difficult to visualize an acoustic field where points 0.375 in. apart would have such difference in sound pressure level. The effectiveness of the sawtooth fence as an acoustic pressure suppressor is highest in the  $L/D = 5.6$  cavity, diminishing noticeably as the cavity becomes shallower.

#### $M_\infty = 2.3$

Figures 237 and 238 show the acoustic pressure distribution for the  $L/D = 5.1$  cavity at  $M_\infty = 2.3$ . Compared to data at  $M_\infty = 1.5$ , apparently both the general levels and the maximum values on the rear bulkhead have decreased. Otherwise the figures illustrate the familiar trends: the asymmetry inside the cavity, the dip in the central plane and the beneficial effect of the sawtooth suppression fence. In addition, Figure 237 shows a distinct Reynolds number effect, i.e., the sound pressure rises by a few dB, when the Reynolds number is increased from below 3 to 3.9 ( $10^6$ /ft).

The acoustic pressure level distributions for the  $L/D = 5.6$  cavity are illustrated in Figures 239 - 241 for a variety of operating conditions, including the utilization of a boundary layer trip and both suppression fences. Compared to the deepest cavity, the maximum values on the rear bulkhead have increased by about 6 dB to a value of 159 dB. The boundary layer trip accounts for about 2 to 3 dB reduction in SPL. A reduction of similar magnitude has been achieved with either of the suppressor fences, the perforated fence being more effective by about 2 dB.

Acoustic pressure level distributions covering the same set of variables plus a higher Reynolds number for the  $L/D = 6.2$  cavity are shown in Figures 242 - 245. At this Mach number the installation of a boundary layer trip is

more beneficial as the cavity becomes shallower. As for  $L/D = 5.6$ , the perforated fence is superior to the sawtooth in effecting further acoustic pressure reductions. The maximum reduction attributable to the boundary layer trip and the perforated fence amounts to about 10 dB, with the contributions about evenly divided. With boundary layer trip and perforated suppressor fence installed, raising the Reynolds number from 3 to  $3.9 \times 10^6/\text{ft}$  increased the acoustic pressure by about 3 dB (Figure 245). No significance should be attached to the point at  $X/L = 0.85$  on the starboard side with boundary layer trip and perforated fence in Figures 243 - 245, since a closer scrutiny of its frequency spectrum strongly suggests a defective signal. The same statement applies also to the Figures 247 and 248 for the shallowest ( $L/D = 9.9$  cavity).

The beneficial effect of the boundary layer trip in the  $L/D = 9.9$  cavity is similar to that in the deeper cavities; however, this is not true for the suppression fences. Interestingly, in this shallow cavity even the perforated fence has mostly a marginally detrimental effect on SPL, whereas the sawtooth fence increases the acoustic pressure significantly, as shown in Figure 248. Finally, note that the SPL in this cavity is about 5 dB lower than in the  $L/D = 6.2$  cavity.

#### $M_\infty = 3.0$

All tests at  $M_\infty = 3$  were conducted with the boundary layer trip installed. Only the perforated suppressor fence was used during the acoustic pressure measurements test phase. It is clear from the results shown in Figures 249 - 252 that both the general SPL levels and their maximum values were lower at  $M_\infty = 3$  than at  $M_\infty = 2.3$ . In most instances the presence of the perforated fence resulted in negligible changes in SPL. In some cases the effect of the suppressor was to increase the acoustic pressure. No explanation can be offered as to why the data point with the fence at  $X/L = 0.45$  in Figure 250 is so high. Its frequency spectrum looks normal but could hide a spurious dc component. In contrast to data at lower Mach numbers, at  $M_\infty = 3$  the maximum acoustic pressures sometimes are at the rear of the cavity ceiling and not on the rear bulkhead.

## Survey of the Suppressor Fence Effects on Acoustic Pressures

Having just completed a discussion of overall acoustic pressures as a function of test conditions, it is now expedient to examine some of those results in greater detail, i.e., on the basis of the frequency spectra. As mentioned earlier, practical space considerations restrict the number of spectra that can be presented. The spectral analysis was carried out for a  $\Delta f = 8.14$  Hz. Because it exhibited the highest acoustic pressures, we have selected the  $L/D = 5.6$  cavity at  $M_\infty = 1.5$  as the basic reference case, and in this section shall present spectra for this cavity at various Mach numbers and for various cavities at the  $M_\infty = 1.5$  number. In each instance, spectra at three spatial locations are shown with and without a suppression fence. In general, the acoustic pressure reaches its maximum value at the  $X/L = 1$ ,  $Z/D = 0.25$  location corresponding to the rear bulkhead. Also shown in the figures are the theoretically predicted mode frequencies calculated using the method presented in Reference 10 and summarized herein (Equation (3)). These analytical prediction methods and comparisons of the calculated results with experimental data are described in the following section.

### Subsonic Data for the $L/D = 5.6$ Cavity

In practically all cases, the signal consists of the superposition of a broadband "noise" which falls off with frequency and a certain number of well-defined, or sufficiently well-defined peaks which correspond to the different oscillatory modes. As expected, the signals always peak on the rear bulkhead. Within the Mach number range covered by Figures 253 - 255 ( $M_\infty = 0.6$  to  $0.74$ ) the number of modes contributing to the signal strength did not exceed 5; in most cases the number was even smaller. Mode 1 is usually ill-defined and is rather weak when tests are run without any suppressor fence. The general tendency is for one of the lower modes, the second, or third, to predominate at all three spatial positions at a given Mach number; however, there are exceptions to this rule.

The installation of a sawtooth suppression fence has a twofold effect: it lowers both the broadband acoustic pressure level and the magnitudes of the modal peaks. The lowering of the modal peaks is selective; e.g., Figure 253 shows that relative to the broadband background the fence was only marginally efficient in reducing the second mode but that it was very effective in suppressing the higher modes. In fact, this observation is valid for all

three subsonic Mach numbers at which tests were run.

$M_\infty = 1.5$  for All Four Cavities

The effect of varying the cavity length-to-depth ratio on the pressure spectral distributions is shown in Figures 256 and 259 - 261. The suppression fence was extremely effective in lowering the modal peaks for the deepest ( $L/D = 5.1$ , Figure 259) and shallowest ( $L/D = 9.9$ , Figure 261) cavities. The effect of the fence on broadband noise was only marginal for the deepest cavity and practically nonexistent for the shallowest cavity. The situation in the  $L/D = 6.2$  cavity is similar to that of the  $L/D = 5.6$  cavity to be discussed next.

As Figure 256 illustrates for the  $L/D = 5.6$  cavity, the spatial distribution of the modal peaks can be rather complicated. This problem has been treated in considerable detail in Reference 5, including an empirical equation for the longitudinal variation in the mode shapes. Although the second mode predominates at all three locations, note that at  $X/L = 0.02$  there are six well defined modal peaks. Five of these are still clearly discernible on the rear bulkhead; however, just  $0.05 L/D$  upstream of the bulkhead, on the cavity ceiling only three modes stand out. The effect of the suppressor fence is similar to that in the subsonic case, except that the suppression of the modal peaks is much more effective.

$M_\infty = 2.3$

Figure 257 illustrates the relevance of the higher modes for some flow conditions. This fact has been overlooked by many cavity flow investigators. More will be said about this later. At  $M_\infty = 2.3$  the suppression fence is only marginally efficient in lowering the broadband noise; however, it is extremely effective in suppressing the modal peaks, especially towards the rear of the cavity, where they are most important.

$M_\infty = 3.0$

At this Mach number the acoustic pressures are rather low, in general, containing very few modal peaks, and the effect of the perforated fence suppressor is beneficial but only marginally so. This is clearly shown in Figure 258.

#### Acoustic Modal Pressure Distributions



Figures 262 - 264 were prepared to show the distribution of modal intensities throughout the interior and around the  $L/D = 5.6$  cavity at three Mach numbers: 0.7, 1.5 and 2.3 without any suppression fence. The modal SPL values were simply read off from the SPL frequency spectra with no attempt made to separate out the broadband contribution.

$M_\infty = 0.7$

Figure 262 indicates that at  $M_\infty = 0.7$  the cavity noise was dominated by the third mode throughout most of the cavity, with the exception of the  $X/L = 0.75$  region. The order of importance of the higher modes depends on the location within and in front and behind the cavity. Note that at  $X/L = 0.45$  the fourth mode predominates both on the starboard and port walls and that this is true for  $X/L = 0.75$  in the central plane. Figure 262 presents a rather complex picture of the mode distribution strongly suggesting that the cavity oscillation is truly a three-dimensional phenomenon.

$M_\infty = 1.5$

The acoustic pressures at  $M_\infty = 1.5$  are mostly dominated by the second mode but not without some exceptions (Figure 263,  $X/L = 0.25$ ). Since more modes could be identified at this Mach number, the picture is even more complicated than for the subsonic case.

$M_\infty = 2.3$

As seen from Figure 264, at  $M_\infty = 2.3$ , depending on the location, the oscillatory pressures are dominated by modes two and four. The ordering of the lesser modes is also irregular, again strongly suggesting a complicated three-dimensional oscillatory phenomenon. The higher modes are by no means unimportant.

#### Summary of the Maximum Acoustic Pressure Variations with $M_\infty$

In many applications, the maximum acoustic pressure within the cavity is of primary interest, since it sets the ceiling of acoustic field. Figure 265 summarizes for all four cavity  $L/D$ 's the maximum acoustic pressure variations for various operating conditions as a function of Mach number. The highest SPL was measured in the  $L/D = 5.6$  cavity at  $M_\infty = 1.5$ . The results for the  $L/D = 6.2$  cavity were quite similar. Apparently the maximum SPL values always peaked at  $M_\infty = 1.5$ , decreasing rapidly toward higher Mach numbers. A properly

selected suppression fence can be very effective in reducing the maximum SPL values, however, as Figure 265 (d) illustrates, a wrong suppressor can, in fact, raise the acoustic pressure. Increasing the Reynolds number at  $M_\infty = 2.3$  also increases the SPL. Figure 265 (b) proves the extreme sensitivity of the maximum pressure to Mach number variation in the subsonic velocity range.

The experimental data plotted in Figure 265 show that the maximum rms pressure on the rear bulkhead can be strongly dependent on the test Reynolds number. For example, for the  $L/D = 5.1$  cavity at  $M_\infty = 2.3$  the maximum SPL rose by over 4 dB, when the Reynolds number was raised from  $2.9 \times 10^6/\text{ft}$  to  $3.9 \times 10^6/\text{ft}$ , while holding the Mach number and total temperature constant. A comparison of the frequency spectra for these two data points, shown in Figures 266 and 267, clearly shows that the increase in the SPL was brought about not by amplification of modal peaks but by raising the broadband background level.\* The latter is primarily due to anisotropically oriented dipoles at the leading and trailing edges of the cavity. Previous research (e.g., in Reference 6) show that the sound pressure produced at cavity edges is proportional to the density of the flow medium. It is self evident that a variation in Reynolds number, while holding the Mach number and total temperatures constant is tantamount to a variation in density, or pressure. With the velocity kept invariant, a change in Reynolds number is directly proportional to a change in  $Q$ . The latter therefore constitutes a natural parameter for nondimensionalization. That this indeed is the case is proven in Figures 268 - 271 where the two data points were moved within 1.5 dB from each other, which can be considered to be within the range of experimental error and repeatability.

The results shown in Figure 265 have been replotted in Figures 268 - 271 for  $Q$  as the reference pressure. Plotted in this manner, the data have a tendency to collapse better than with the standard acoustic reference pressure. The fall-off with Mach number above  $M_\infty = 1.5$  appears to be more gradual. Figures 268 - 271 (b) contain one data point corresponding to test conditions involving the saw-tooth fence and the placement of a total head tube in the cavity. From these figures, the presence of the total head tube obviously had no effect on the maximum acoustic pressure. This question is discussed in detail in Section V.

---

\*This was found to be true also for other  $L/D$  cavities.

McLardin, J.C., "Airframe Self Noise-Four Years of Research," in AGARD Lecture Series No. 80, Aerodynamic Noise, AGARD-LS-80, 1977.

Plotted as circles in Figure 269 are also three points from Reference 1. Since the data in that reference were not subjected to a 100 Hz highpass filter, they were adjusted to the present ordinate scale by reducing the fluctuating pressure values by the same amount, as was found to be attributable to the filter at  $M_\infty = 0.7$  in the present experiments. As expected, the Reference 1 data agree well with the new measurements.

#### Effect of the Total Head Tube on the Acoustic Pressure Distributions

The placement of a total head tube into the cavity shear layer, or more precisely into the plane of the  $L/D = 5.6$  cavity opening at its center, had dual purposes. First, it was emplaced to see if its presence would distort acoustic and static pressure measurements; second, its purpose was to take some preliminary total head data in the shear layer.

##### Subsonic

At subsonic tunnel Mach numbers (Figures 272 - 276) the effect of the total head tube was to lower the SPL readings by less than about 1.5 dB, which is considered to be within the range of reproducibility of the test results and experimental error. This small difference was found both with and without the sawtooth suppression fence, the difference being smaller without the fence.

##### Supersonic

At supersonic tunnel Mach numbers ( $M_\infty = 1.5$  and  $M_\infty = 2.3$ ) the effect of the total head tube was less than 1 dB (Figures 277 - 279); there is no discernable effect for  $M_\infty = 1.5$ . This finding applies to tests with and without suppression fence and the boundary layer trip. No acoustic data were taken with the total head tube installed at  $M_\infty = 3$ .

#### Cross-correlations

Since up to 12 oscillating pressure signals were tape-recorded on a single analogue tape recorder, cross-correlations were carried out between a reference signal from a pressure transducer in the forward portion of the cavity and other transducer signals. Although after a lengthy learning period we were able to obtain many well defined cross-correlations between narrowly filtered modal frequency peaks, the findings did not produce a clear picture of the pressure wave pattern within the cavity. There were numerous

inconsistencies in the derived wave propagation speed and their direction. Having reached no definite conclusions based on the cross-correlation work, we present no results from this phase of our work.

A likely reason for our difficulties is that we did not precalibrate the transducers with the respective signal amplification and recording channels using a simple source driver at different frequencies.

## Section IV

### ANALYSES & COMPARISONS

#### AERODYNAMIC DATA

All of the flows discussed here are for relatively shallow cavities ( $L > 5D$ ). However, there are both "open" and "closed" shallow cavity flows (Reference 7). A closed cavity flow is one for which the shear layer flow reattaches to the cavity ceiling prior to separating ahead of the downstream corner of the cavity. An open cavity flow is one for which the shear layer flow bridges the cavity; the free shear layer does not reattach to the cavity ceiling in this case. Charwat et al (Reference 7) established criteria for open and closed flows over shallow cavities for supersonic flows. Using their criteria, only the  $L/D = 9.9$  cavity should experience closed flow for Mach 1.5 and 2.3 free stream flows. Data shown in Figures 87, 88, 115 - 117, 143, 144, 164, and 165 support their conclusions.

#### PREDICTION OF FREQUENCY MODES FOR OSCILLATORY PRESSURES

The available prediction method for the possible frequencies at which oscillatory pressure peak modes can occur is based mainly on References 8 and 9. A review of this method showed that the method could be improved by incorporating an empirical dependence of the cavity shear layer velocity on the Mach number. An estimate of this relationship was available from the total head tube measurements taken during the course of the experiments reported herein. As shown in Table V, the inclusion of this refinement noticeably improved the predictability of mode frequencies, especially for the higher modes. Since the background of the method and its details are fully described in Reference 10, its essential features will be only sketched out here.

---

<sup>7</sup>Charwat, A.F., Roos, J.N., Dewey, F.C. and Hitz, J.A., "An Investigation of Separated Flows, Parts I and II," J. Aero. Sci., Vol 28, Nos. 6 and 7, June and July 1961.

<sup>8</sup>Rossiter, J.E., "Wind Tunnel Experiments on the Flow Over Rectangular Cavities at Subsonic and Transonic Speeds," RAE TR 64037, October 1964.

<sup>9</sup>Heller, H.H., Holmes, G., and Covert, E.E., "Flow Induced Pressure Oscillations in Shallow Cavities," AFFDL-TR-70-104, December 1970.

Our method for oscillatory mode frequency prediction can be viewed as a fairly straightforward refinement of the Rossiter (Reference 8) prediction model based on his original feedback loop idea. Rossiter envisioned a vortex train leaving the cavity leading edge and travelling towards the rear edge at the shear layer velocity. Once these vortices hit the rear edge, they produce upstream propagating acoustic waves travelling at the local speed of sound. When these sound waves hit the forward edge, they immediately trigger the release of new vortices, thus completing the feedback loop. The finer points (or the missing links) in this formulation are at least three: what is the shear layer velocity for a given set of flow conditions, what is the static temperature inside the cavity and what phase shift is to be allowed between the vortex hitting the rear cavity edge and the generation of the acoustic wave? The last question was answered experimentally by Rossiter himself. Although his Mach number range did not extend above 1.2, his cavity L/D ratios did cover our cavities, as shown in Table III, taken from Rossiter's paper.

TABLE III

L/D	$\gamma(L/D)$
4	0.25
6	0.38
8	0.54
10	0.58

To impart some physical meaning to the phase shift parameter  $\gamma(L/D)$ , we simply recall that in Rossiter's model a vortex is located  $\gamma(L/D)\lambda$  downstream of the cavity trailing edge at the instant when the reference acoustic wave leaves the source at the rear edge.  $\lambda$  is the spacing of the vortices.

Heller et al. (Reference 9) showed that the cavity static temperature was approximately equal to the free stream total temperature. We have substantiated this experimentally in the experiments reported herein. Two thermocouples were flush-mounted in the cavity ceiling at the locations indicated in Figure 6. The following tabulation lists the various measured temperatures and the computed  $T_s'/T_s$  ratios for the L/D = 5.6 cavity over the Mach number range covered in the experiments:

TABLE IV

$M_\infty$	Temperature, °R				$T_s'/T_s$
	$T_s$	$T_0$	$T_1$	$T_2$	
0.6	525	562	560	548	-
0.7	512	562	552	547	-
0.74	507	563	551	547	-
1.5	392	568	539	545	1.013
2.3	269	557	528	543	1.014
3.0	198	567	526	535	1.024

In Table IV,  $T_s$  and  $T_0$  are the tunnel static and total temperatures,  $T_1$  and  $T_2$  are the cavity wall temperatures, and  $T_s'$  is the static temperature behind the oblique shock emanating from the leading edge of the model. Keeping in mind that the model represents a heat sink and that the Mach number inside the cavity is always low, Table IV shows that the assumption that the cavity static temperature is  $T_0$  is reasonably good for the computation of the local speed of sound, which is proportional to its square root. Our contribution to the prediction method is in using an experimentally determined shear layer vs Mach number dependence. Previous investigators used an empirical constant for that value. We also retained Rossiter's experimentally determined variation of the phase shift factor. In the modified Rossiter method a constant number serves that purpose.

As derived in detail in Reference 10, our formula for the possible oscillatory frequency modes is:

$$f = \frac{U[m - \gamma(L/D)]}{L \left[ \frac{M_\infty}{\sqrt{1 + 0.2M_\infty^2}} + \frac{1}{K(M_\infty)} \right]} \quad (3)$$

where  $U$  is the free stream velocity,  $m$  is the mode number,  $\gamma(L/D)$  is the phase shift function,  $L$  is the cavity length and  $K(M_\infty)$  is the ratio of the shear layer to the free stream velocities. The experimentally determined  $K(M_\infty)$  values were:

<sup>10</sup> Maciulaitis, A., "Improved Prediction of Frequency Modes for Peak Amplitude Pressures in Simulated Bomb Bays at Mach 0.6 to 3.0," Grumman Aerospace Corporation, Research Department Memorandum RM-708, June 1980.

<u>M<sub>∞</sub></u>	<u>K(M<sub>∞</sub>)</u>
0.60	0.617
0.70	0.681
0.74	0.681
1.50	0.7285
2.30	0.622

Since no  $K(M_\infty)$  values were measured at  $M_\infty = 3$ , we used the  $K(2.3)$  value for this case. Note that although the  $K(M_\infty)$  values were determined in the  $L/D = 5.6$  cavity, the same values were used to predict the modal frequencies in cavities having  $L/D$  ratios from 5.1 to 9.9. Equation (3) was used to predict the frequency modes throughout the present report.

#### COMPARISON OF MEASURED AND PREDICTED OSCILLATORY PRESSURE FREQUENCIES

As explained in the preceding section, using the experimentally determined total heads in the cavity shear layer, we have improved on the existing method for predicting at which frequencies modal peaks are possible. These predictions were already indicated in Figures 253 - 261. A cursory examination of figures shows that in most instances the agreement between predicted and measured acoustic pressure modal peaks is good-to-excellent. We have carried out such comparisons for all our acoustic data and compared our predictions with those using two older prediction schemes. Figures 280 - 283, which includes data for all four  $L/D$  cavities tested, show our prediction method to yield the best agreement with experimental data, especially for the higher modes.

To provide a ready overview over the findings we have prepared a summary table (Table V). Note that for each mode two columns are provided, one for the best agreement with test data, the other for an agreement within  $\pm 5\%$  of the respective frequency. Letter H identifies the so-called "Modified Rossiter" prediction, as proposed by Heller et al., Reference 8. The totals and grand totals in this table show that our prediction method is the best and that its relative merits increase for the higher frequency modes. The importance of the latter finding has been demonstrated by our experimental results, which clearly indicated the importance of the higher modes for some test conditions. For instance, Figures 253, 254 and 261 illustrate the predominance of the third mode on the rear cavity bulk head, while Figure 257 shows the importance of the fourth mode. Clearly any empirical amplitude prediction method that considers the second mode as the dominant one could not



TABLE V  
SUMMARY OF RELATIVE ACCURACIES OF THE VARIOUS  
METHODS FOR PREDICTING CAVITY OSCILLATION MODE  
FREQUENCIES

[illegible]

M = "ACULAITIS H = HELLER et al, R = ROSSITER

yield accurate results in these cases. More importantly, in trying to understand the phenomena present in a cavity flow it is misleading to start out a priori with the assumption that the two lowest modes are the only ones worth considering. Careful test results prove that this is simply not always so. This point has been missed by some previous investigators who maintain that only the lowest modes are of any importance.

## Section V

### CONCLUSIONS

Basic static and oscillatory pressure data were obtained for flows over rectangular cavities in a flat plate model for  $0.6 < M_\infty < 3.0$ . Effects of acoustic suppression devices (fences) and the presence of total pressure probes were ascertained.

Static pressure distributions characteristic of both open and closed cavity flows, depending upon Mach number and cavity geometry, were observed. Further work is required to improve methods for estimating the pressure distributions in cavities. At supersonic flight speeds the pressures on the aft bulkhead are increased above static free-stream values, indicative of an increase in aircraft drag.

Asymmetric flows were observed for some flow conditions and cavity geometries. The effects of asymmetric flows on the cavity side wall static pressures require further investigation.

The aeroacoustic environment represents a complicated, three-dimensional situation even for the case of simple shallow rectangular cavities. Whereas the frequencies at which oscillatory cavity pressure modes are possible can now be predicted with improved precision, it is still not possible to predict which of these modes will actually occur, and how each will vary within the cavity. Improved techniques are also needed for prediction of SPL levels of modal peaks and of broadband background noise. At supersonic speeds our test data indicate that increasing the Reynolds number increases the sound pressure level by increasing the broadband noise level, while the modal peaks remain essentially unaffected.

If a trial and error approach is to be avoided in the development of effective and aerodynamically acceptable aeroacoustic suppression devices for real weapons bays, the fundamental aeroacoustics phenomena of cavities must be better understood (Reference 11). Detailed surveys of the shear layer flow and of the phase relationships of the acoustic waves are two areas of

---

<sup>11</sup>Clark, R.L., "Evaluation of F-111 Weapon Bay Aeroacoustic and Weapons Separation Improvement Techniques," AFFDL-TR-79-3003, February 1979.

particular interest. The present work has established the feasibility of using a total head tube right in the shear layer; therefore, complete velocity traverses at several axial positions in the bomb bay cavity could be performed. Cross-correlations between modal frequencies at different cavity positions may provide valuable insights into the acoustic wave behavior. Such cross-correlation work should be preceded by a proper calibration of all recording channels starting from the pressure transducers.

## REFERENCES

1. Clark, R. L., "Weapons Bay Turbulence Reduction Techniques," Flight Dynamics Laboratory, Wright-Patterson AFB, AFFDL TM 75-147 FXM, December 1975.
2. Kaufman, L.G.II, Maciulaitis, A., Foreman, K.M. and Danos, S.J., "Pretest Report for Joint AFFDL/GAC Program on Flows Past Weapons Cavities," Grumman Aerospace Corp., Research Memorandum RM-656, July 1978.
3. Clark, R.L., Kaufman, L.G.II and Maciulaitis, A., "Aeroacoustic Measurements for Mach 0.6 to 3.0 Flows Past Rectangular Cavities," AIAA Paper 80-0036 presented at 18th Aerospace sciences Meeting in Pasadena, January 1980.
4. White, H.L., "Trisomic Gasdynamic Facility User Manual", AFFLD TM 73-82 FXM, June 1973.
5. Smith, D.L., and Shaw, L.L., "Prediction of the Pressure Oscillations in Cavities Exposed to Aerodynamic Flow," AFFDL-TR-75-34, October 1975.
6. Hardin, J.C., "Airframe Self Noise-Four Years of Research," in AGARD Lecture Series No. 80, Aerodynamic Noise, AGARD-LS-80, 1977.
7. Charwat, A.F., Roos, J.N., Dewey, F.C. and Hitz, J.A., "An Investigation of Separated Flows, Parts I and II," J. Aero. Sci., Vol. 28, Nos. 6 and 7, June and July 1961.
8. Rossiter, J. E., "Wind Tunnel Experiments on the Flow Over Rectangular Cavities at Subsonic and Transonic Speeds," RAE TR 64037, October 1964.
9. Heller, H. H., Holmes, G., and Covert, E.E., "Flow Induced Pressure Oscillations in Shallow Cavities," AFFDL-TR-70-104, December 1970.
10. Maciulaitis, A., "Improved Prediction of Frequency Modes for Peak Amplitude Pressures in Simulated Bomb Bays at Mach 0.6 to 3.0," Grumman Aerospace Corporation, Research Memorandum RM-708, June 1980.
11. Clark, R.L., "Evaluation of F-111 Weapon Bay Aero-Acoustic and Weapons Separation Improvement Techniques," AFFDL-TR-79-3003, February 1979.

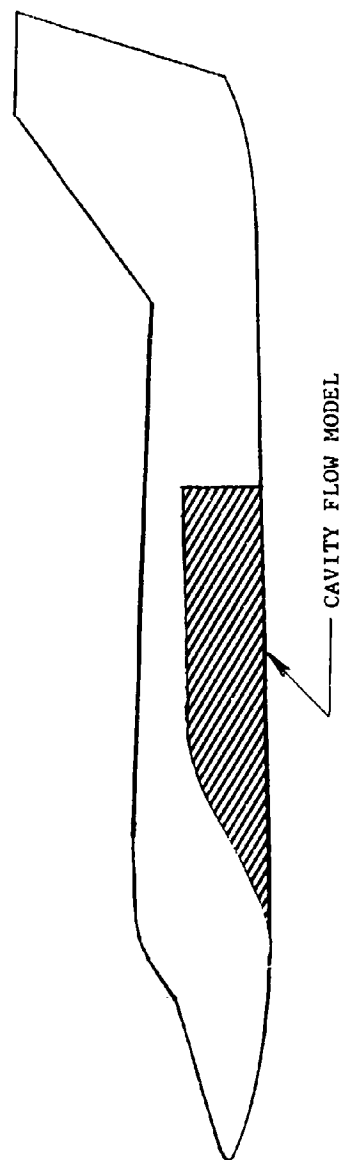
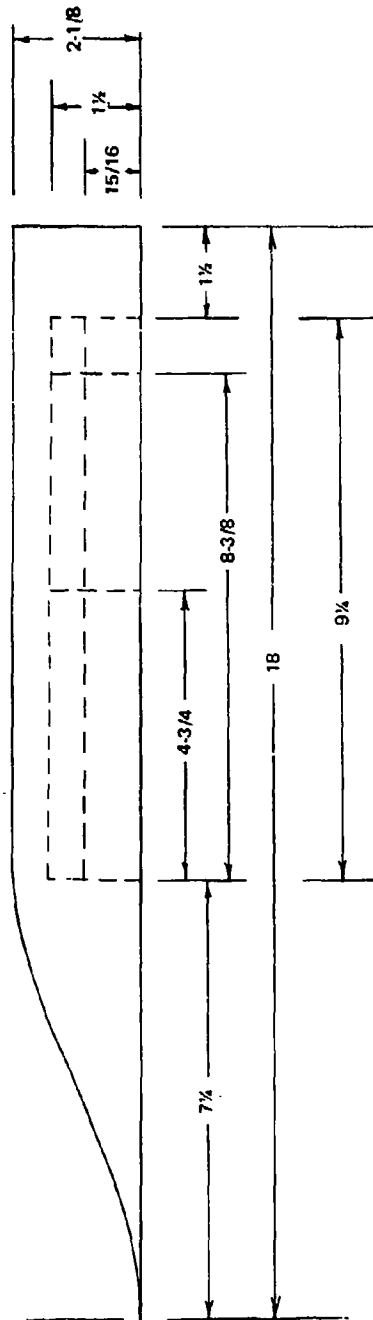
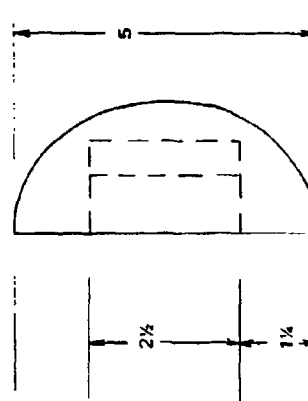


Figure 1 Typical Fighter-Bomber Airplane Profile and Orientation of Weapon Bay Cavity Flow Model

PORT SIDE PROFILE



PORT



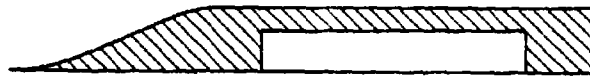
STARBOARD

BOTTOM VIEW

Figure 2 Sketch of Cavity Flow Model  
(all dimensions in inches)



a)  $L/D = 6.067$   
 $D = 0.9375 \text{ IN.}$   
 $L = 4.750 \text{ IN.}$



b)  $L/D = 5.583$   
 $D = 1.50 \text{ IN.}$   
 $L = 8.375 \text{ IN.}$



c)  $L/D = 6.167$   
 $D = 1.50 \text{ IN.}$   
 $L = 9.25 \text{ IN.}$



d)  $L/D = 8.933$   
 $D = 0.9375 \text{ IN.}$   
 $L = 8.375 \text{ IN.}$

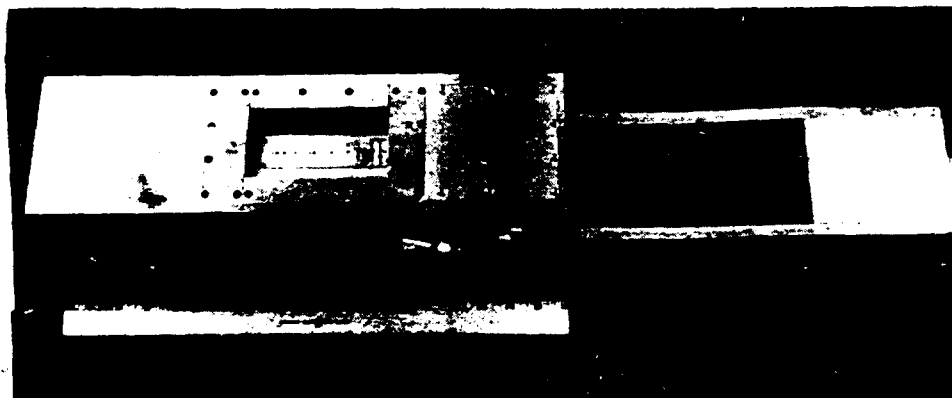


e)  $L/D = 9.867$   
 $D = 0.9375 \text{ IN.}$   
 $L = 9.25 \text{ IN.}$

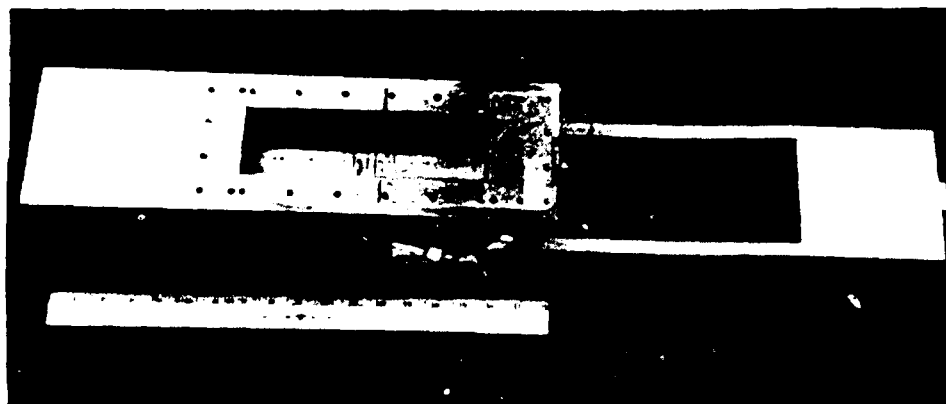
0934-001(T)

Figure 3 Cavity Lengths and Depths

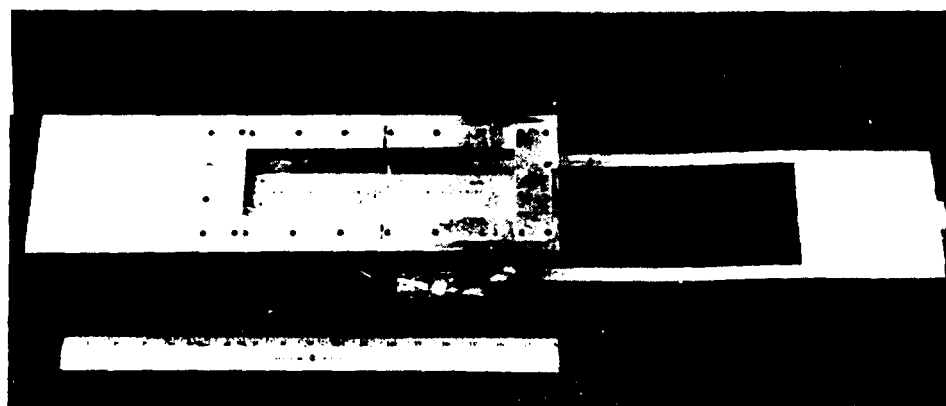




a)  $D = 0.9375$  in.,  $L = 4.750$  in.



b)  $D = 1.50$  in.,  $L = 8.375$  in.



c)  $D = 0.9375$  in.,  $L = 9.250$  in.

Figure 4 Photographs of Cavity Flow Model Configurations

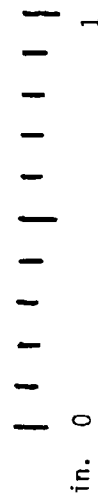


Figure 5 Forward View of Saw-Tooth and Perforated Fences

Note: Total pressure probe openings, either aft or forward facing, are in the plane of the flat plate surface at the streamwise location of static tap number 14.

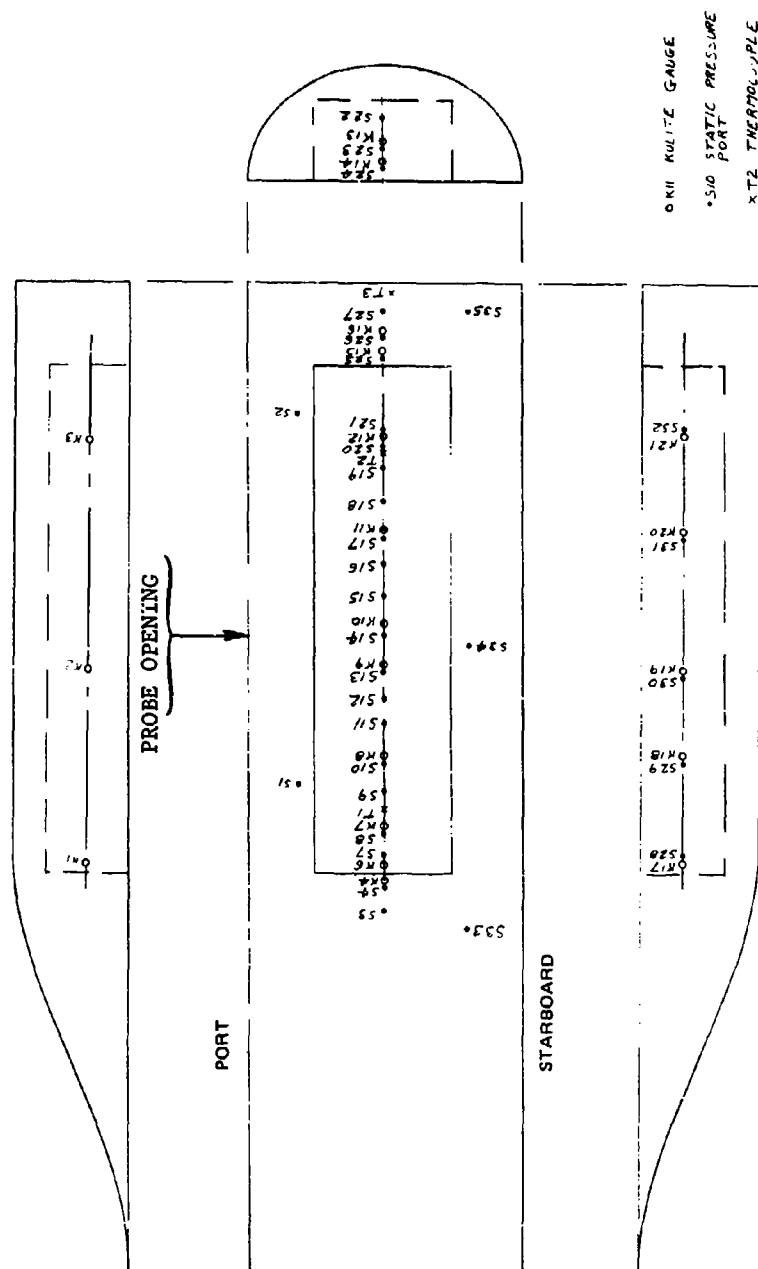


Figure 6 Model Instrumentation Locations

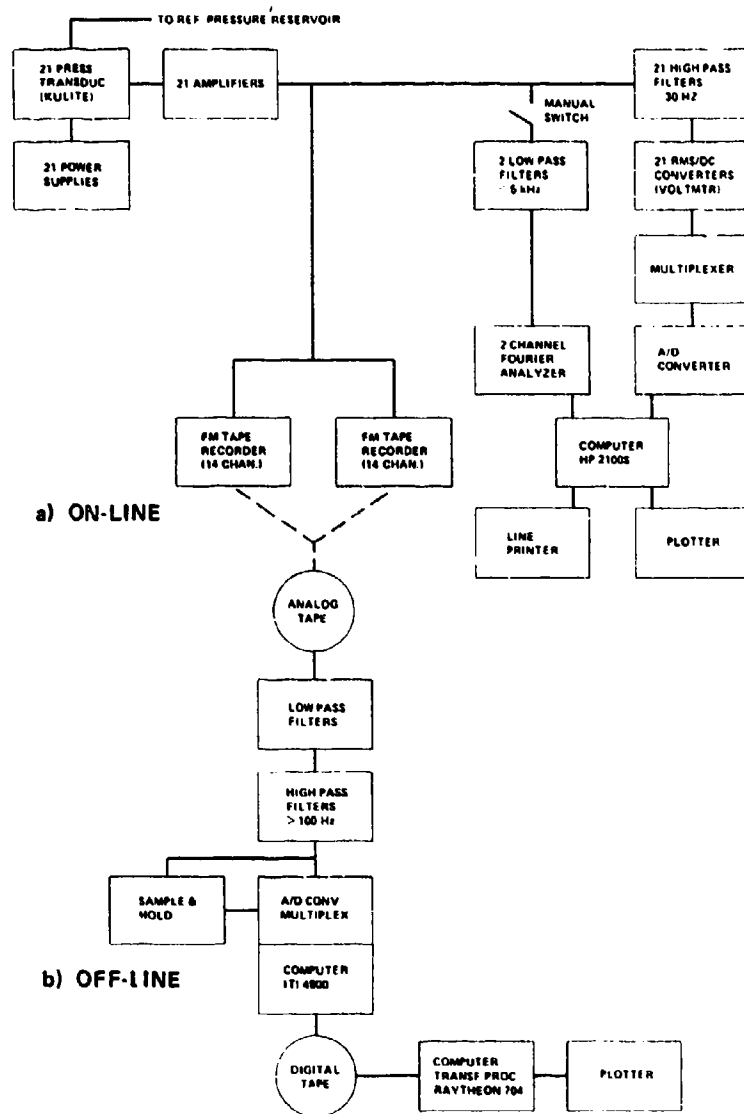


Figure 7 Schematic of Aeroacoustic Data Acquisition and Reduction System

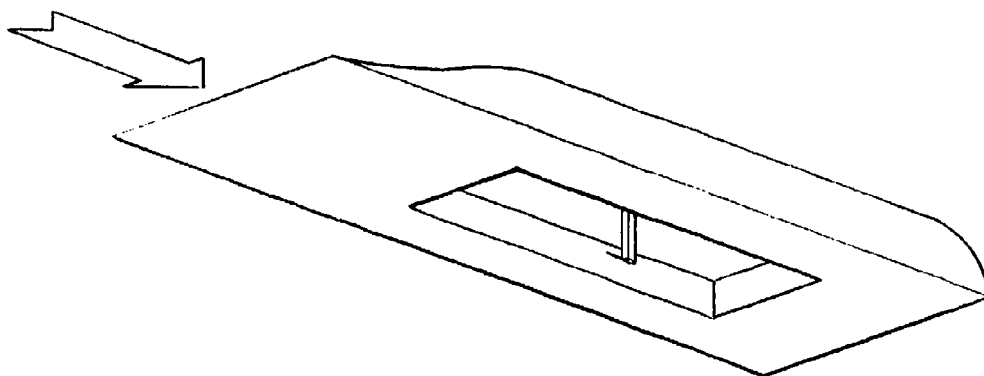


Figure 8 Forward-Facing Total Pressure Probe attached to Ceiling  
of  $L/D = 5.6$  Cavity

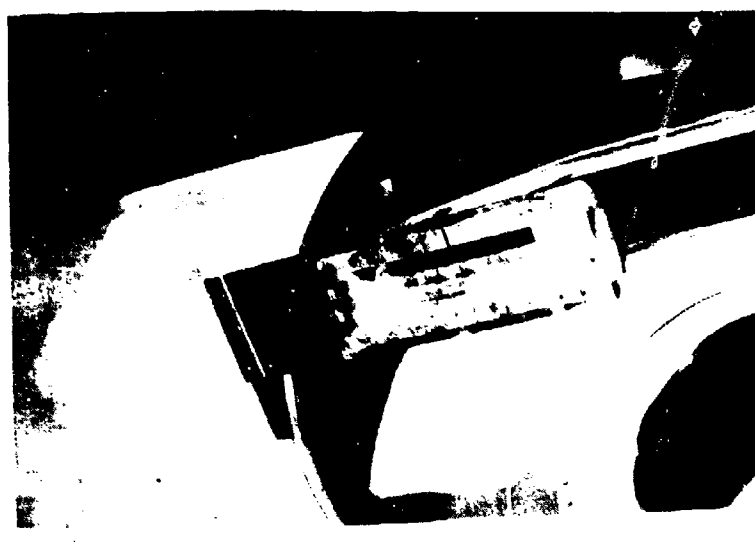
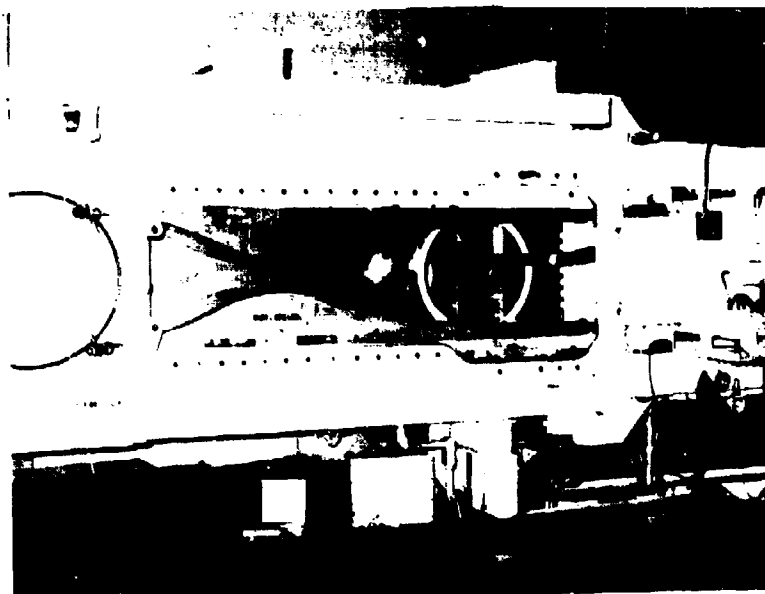


Figure 9 Photographs of Cavity Flow Model in Test Section of AFFDL  
Trisonic Gasdynamics Facility with Mach 3.0 Nozzle Blocks  
Installed (page 1 of 2)



Figure 9 Photographs of Cavity Flow Model in Test Section of AFFDL  
Trisonic Gasdynamics Facility with Mach 3.0 Nozzle Blocks  
Installed (page 2 of 2)

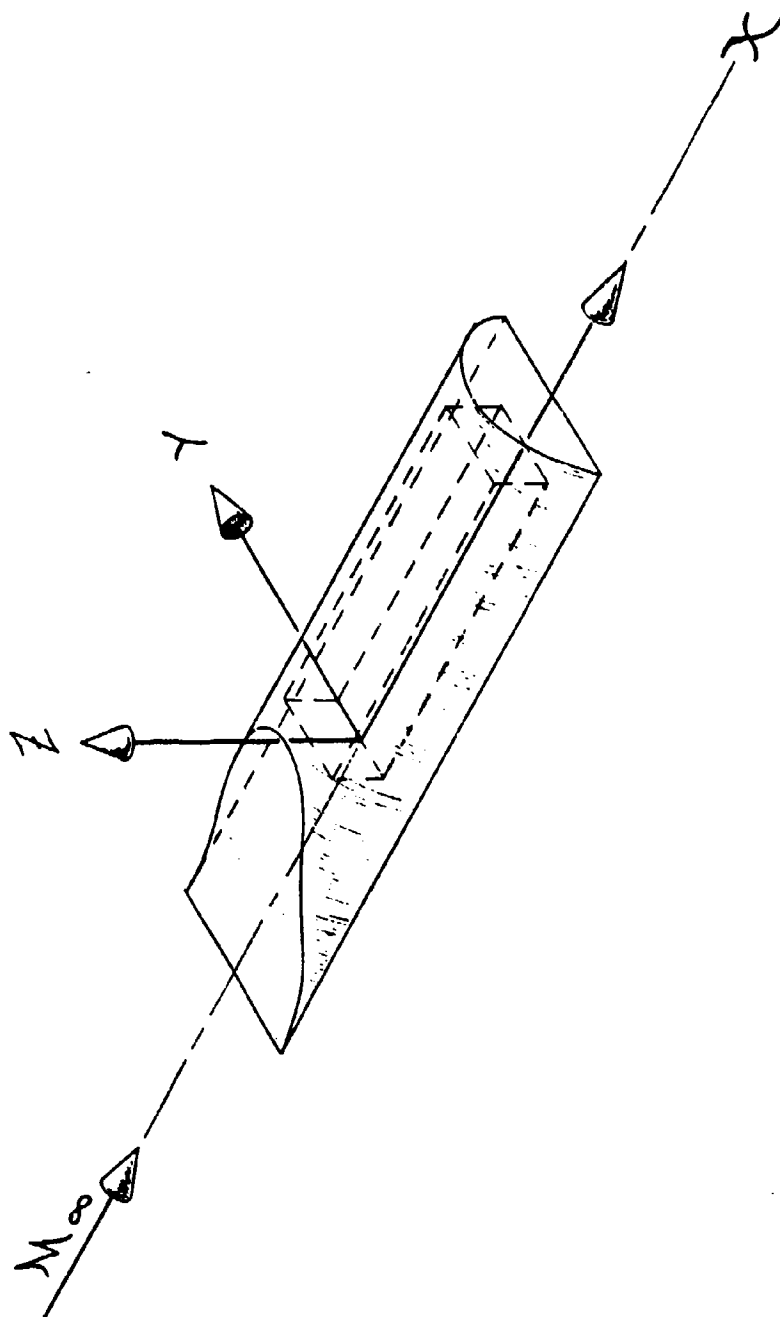


Figure 10 Rectangular Coordinate System



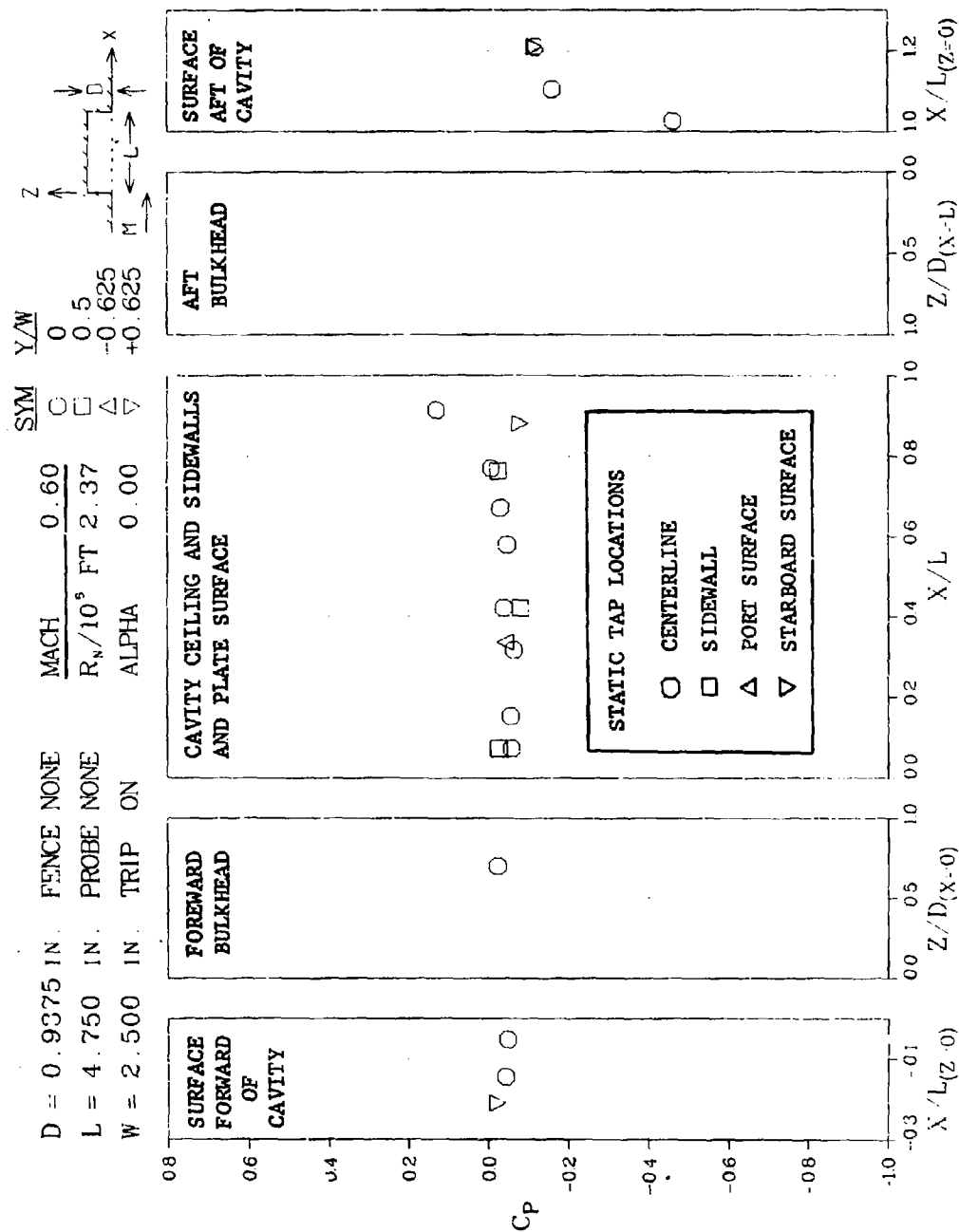


Figure 11 Pressure Coefficient Distributions for  $L/D = 5.1$  Cavity with Boundary Layer Trip,  $M_\infty = 0.60$

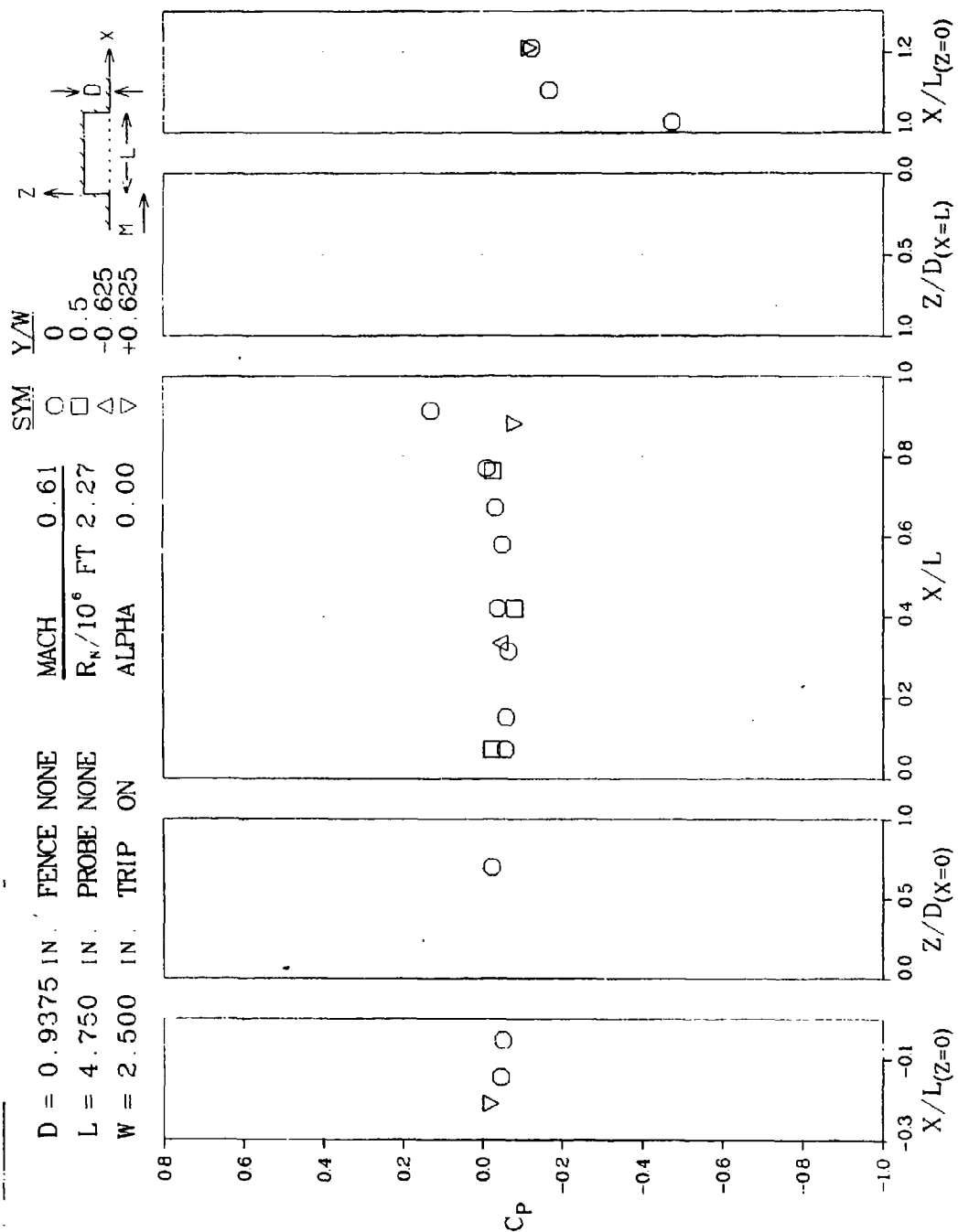


Figure 12 Pressure Coefficient Distributions for  $L/D = 5.1$  Cavity with Boundary Layer Trip,  $M_\infty = 0.61$

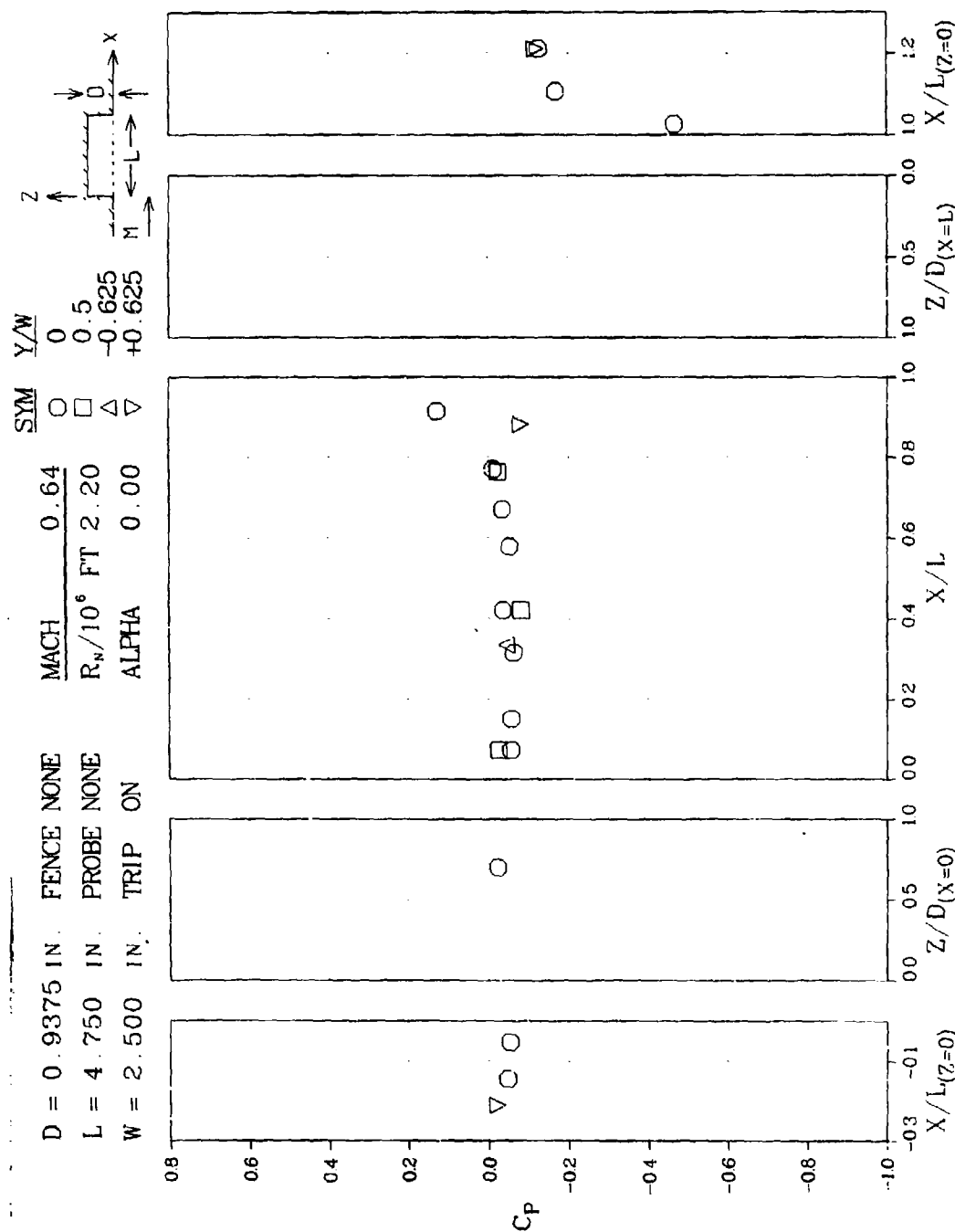


Figure 13 Pressure Coefficient Distributions for  $L/D = 5.1$  Cavity with Boundary Layer Trip,  $M_\infty = 0.64$

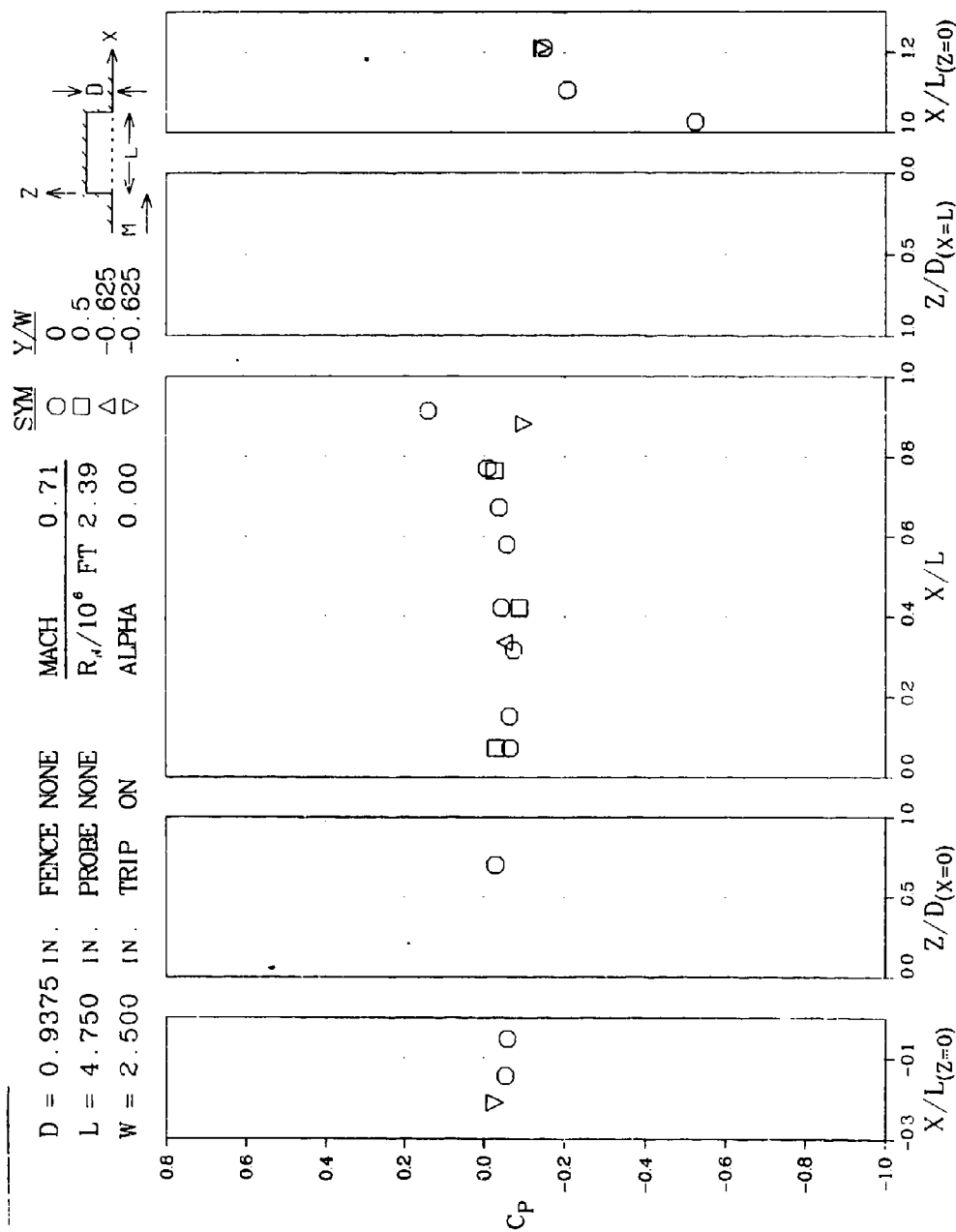


Figure 14 Pressure Coefficient Distributions for  $L/D = 5.1$  Cavity with Boundary Layer  
 Trip,  $M_\infty = 0.71$

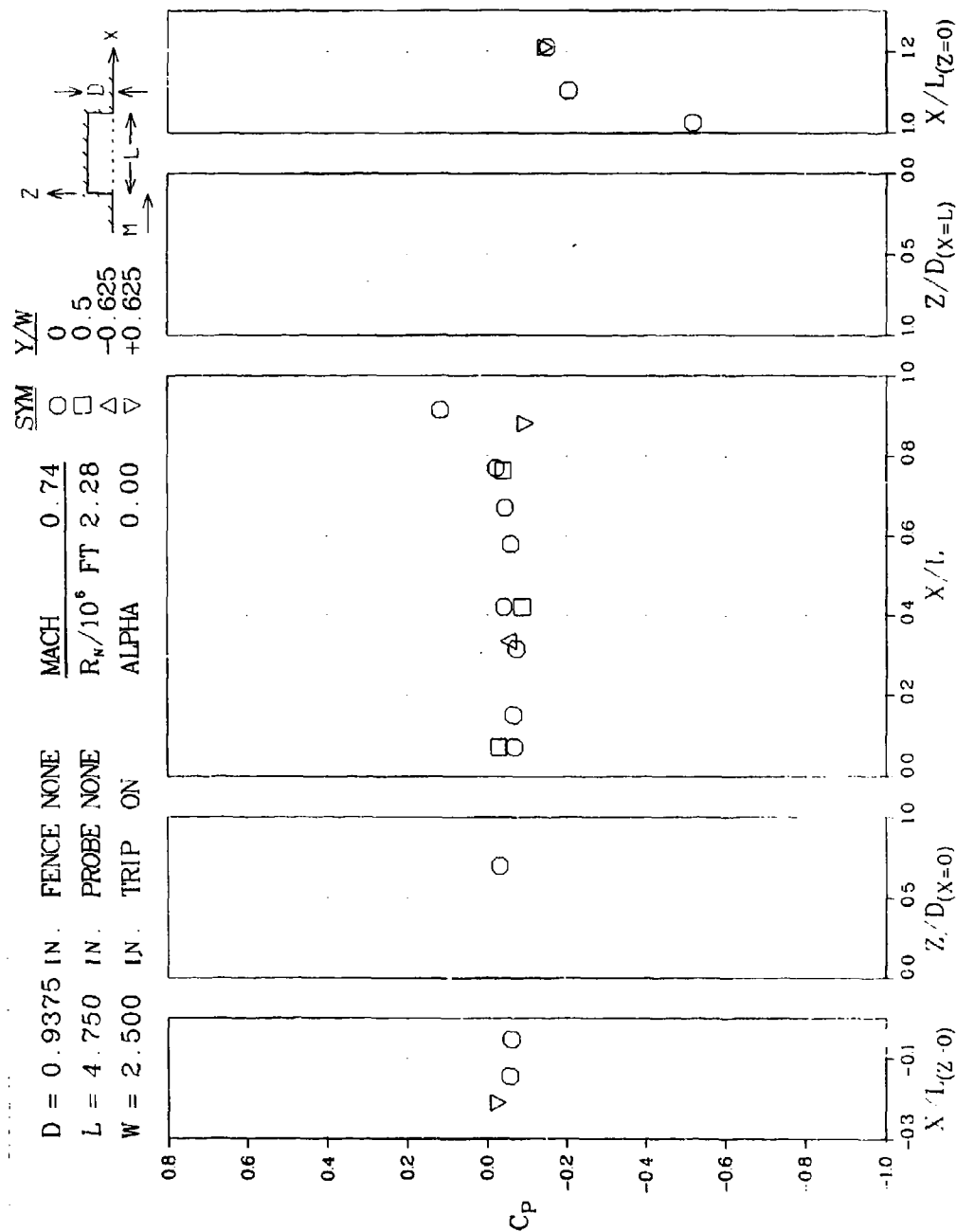


Figure 15 Pressure Coefficient Distributions for  $L/D = 5.1$  Cavity with Boundary Layer  
 Trip,  $M_\infty = 0.74$

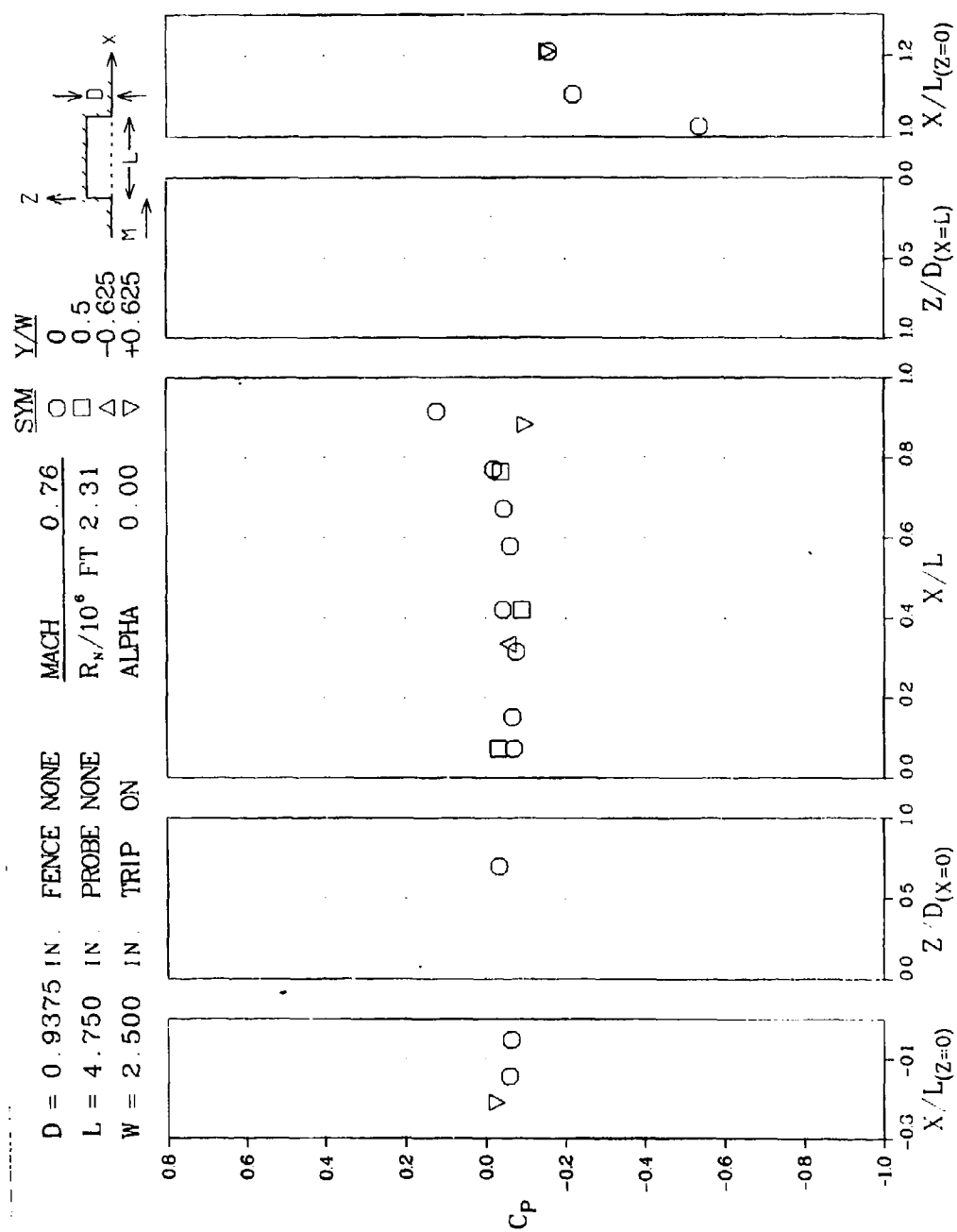


Figure 16 Pressure Coefficient Distributions for  $L/D = 5.1$  Cavity with Boundary Layer Trip,  $M_\infty = 0.76$

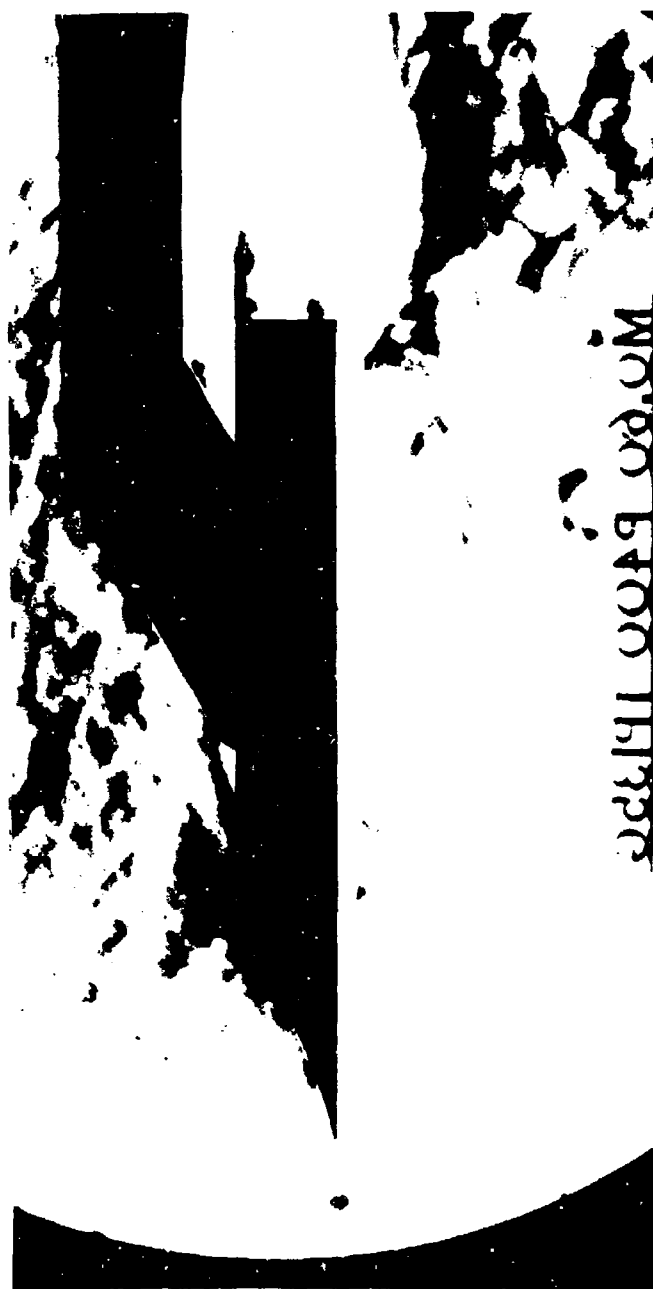


Figure 17 Schlieren Flow Photograph,  $L/D = 5.1$  Cavity with Boundary Layer Trip,  $M_{\infty} = 0.60$





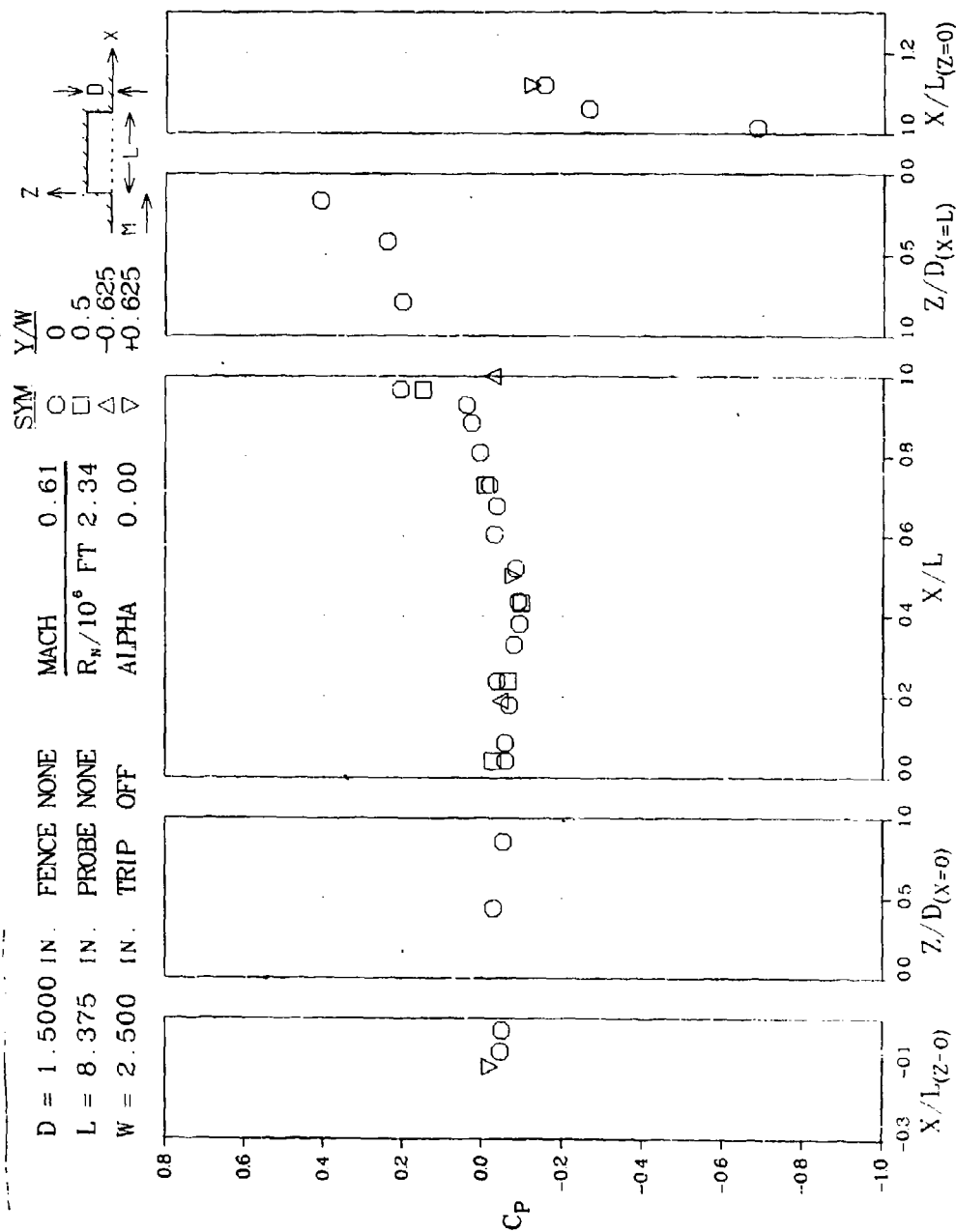


Figure 19 Pressure Coefficient Distributions for  $L/D = 5.6$  Cavity,  $M_\infty = 0.61$

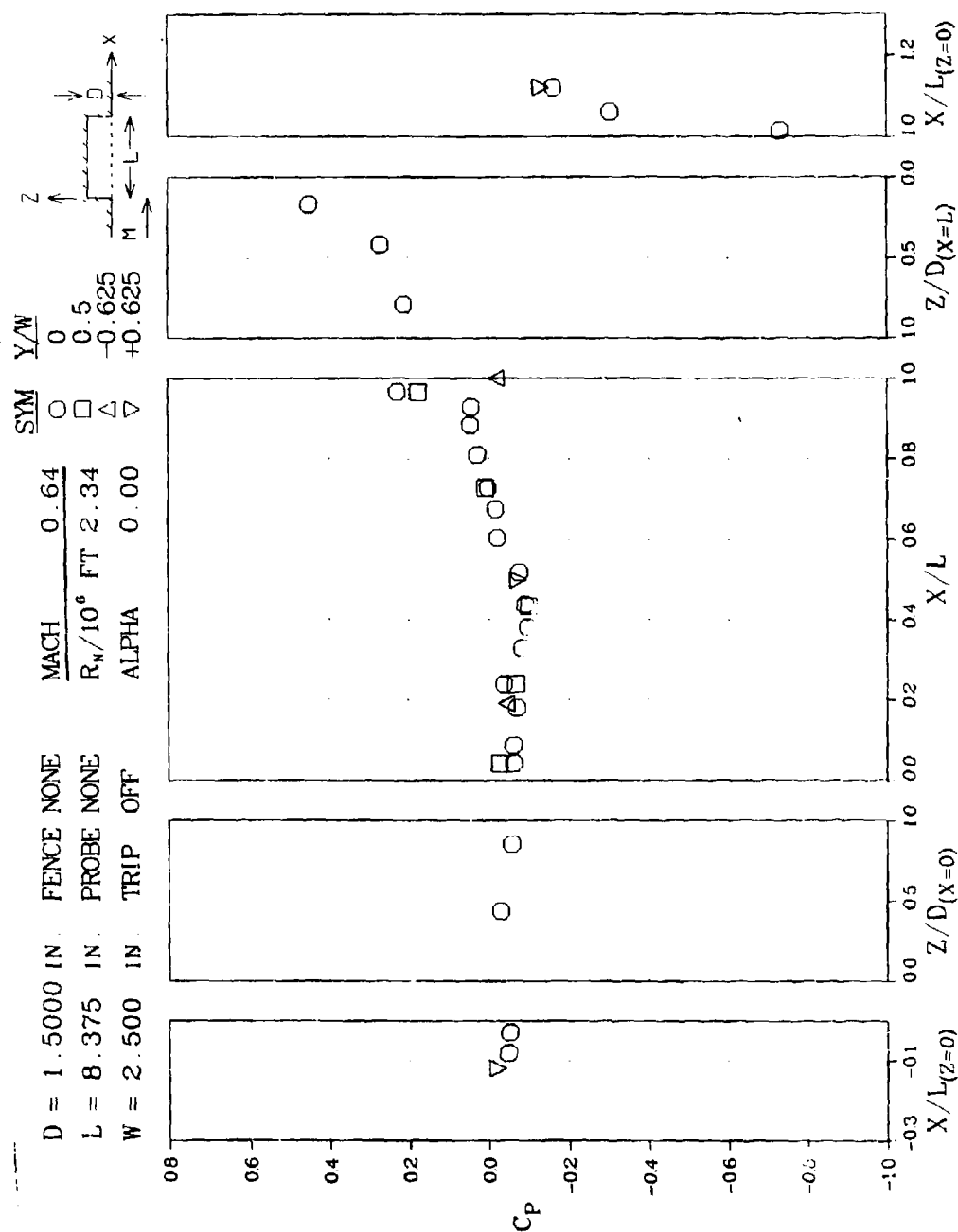


Figure 20 Pressure Coefficient Distributions for  $L/D = 5.6$  Cavity,  $M_\infty = 0.64$

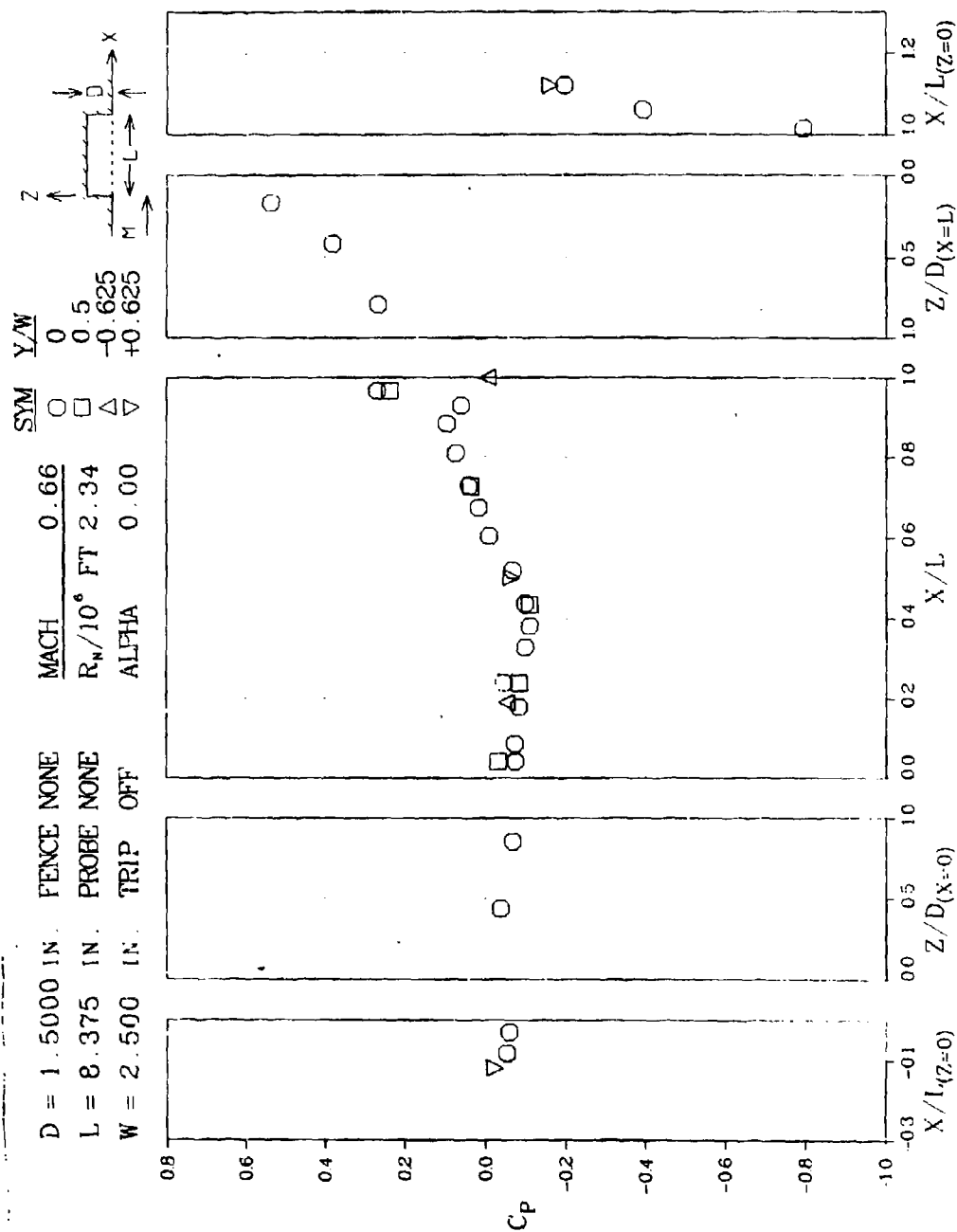


Figure 21 Pressure Coefficient Distributions for  $L/D = 5.6$  Cavity,  $M_\infty = 0.66$

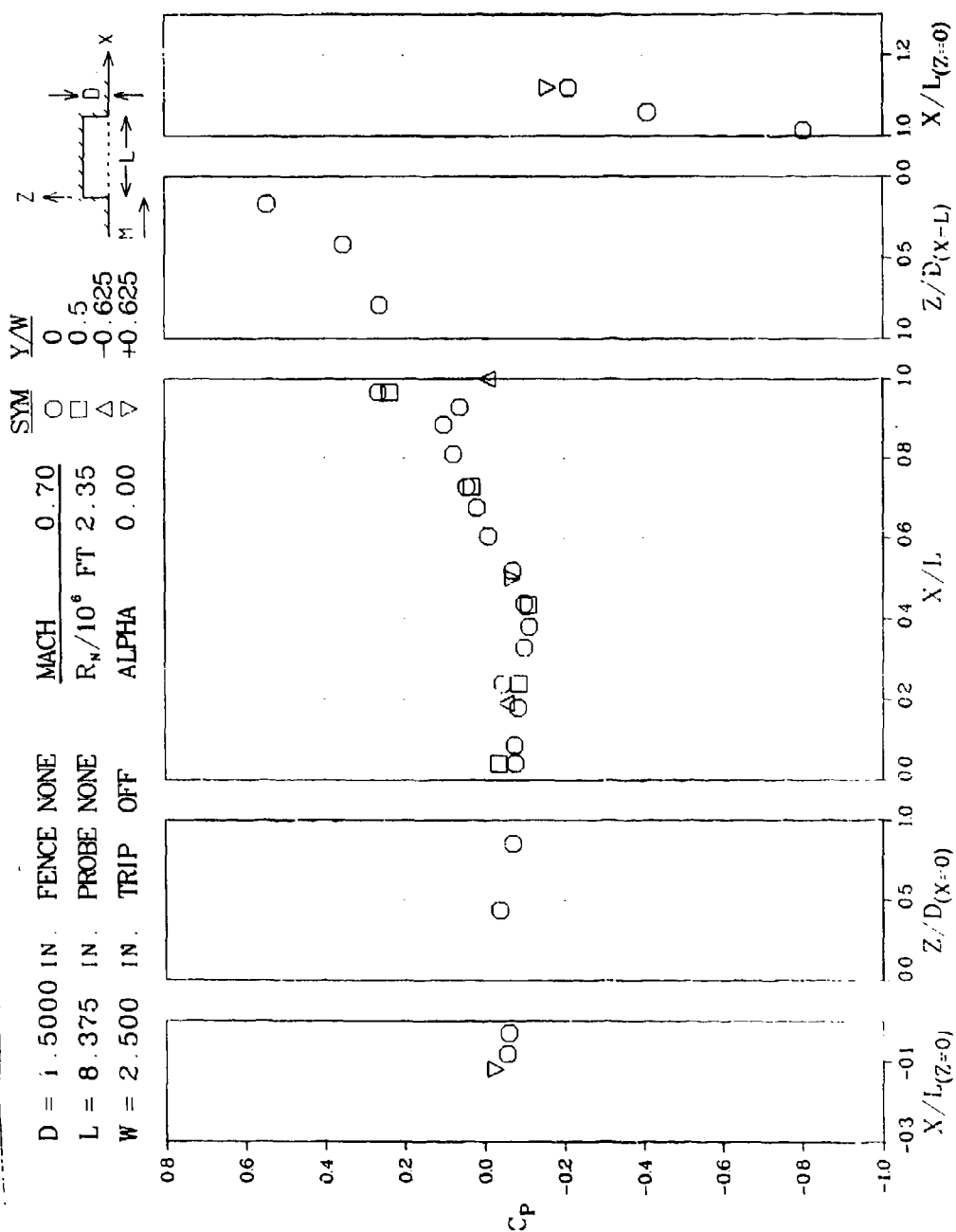


Figure 22 Pressure Coefficient Distributions for  $L/D = 5.6$  Cavity,  $M_\infty = 0.70$

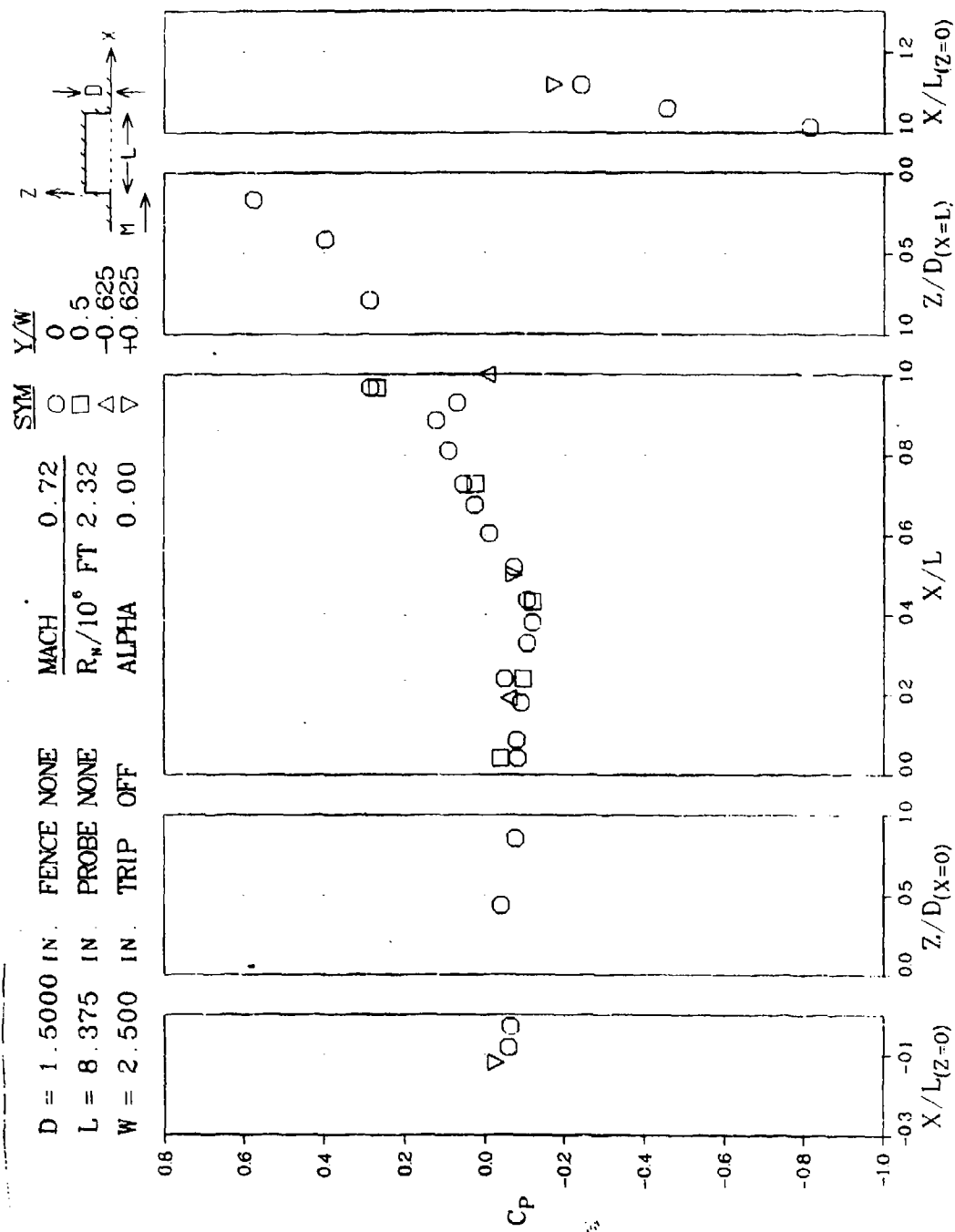


Figure 23 Pressure Coefficient Distributions for  $L/D = 5.6$  Cavity,  $M_\infty = 0.72$

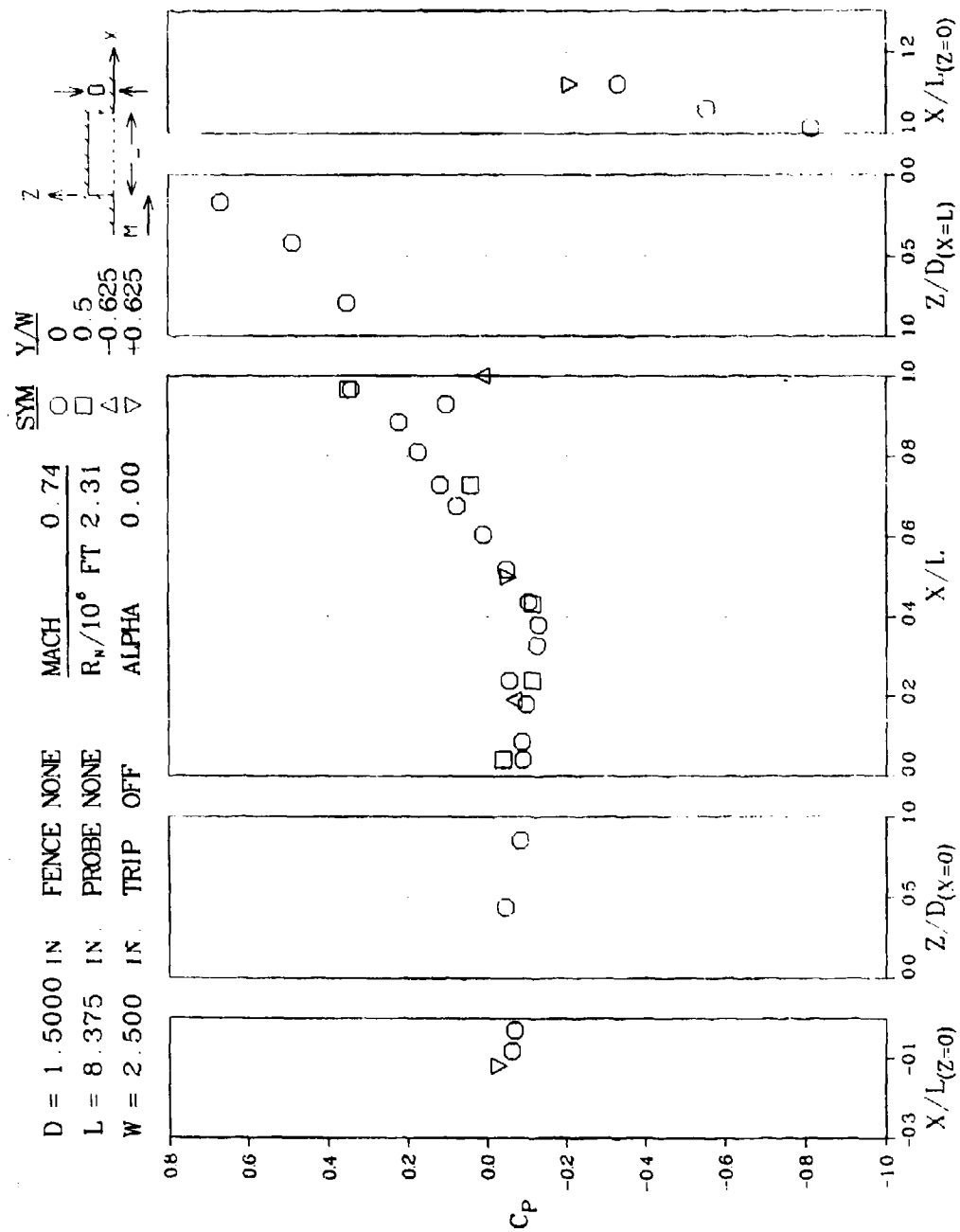


Figure 24 Pressure Coefficient Distributions for  $L/D = 5.6$  Cavity,  $M_\infty = 0.74$

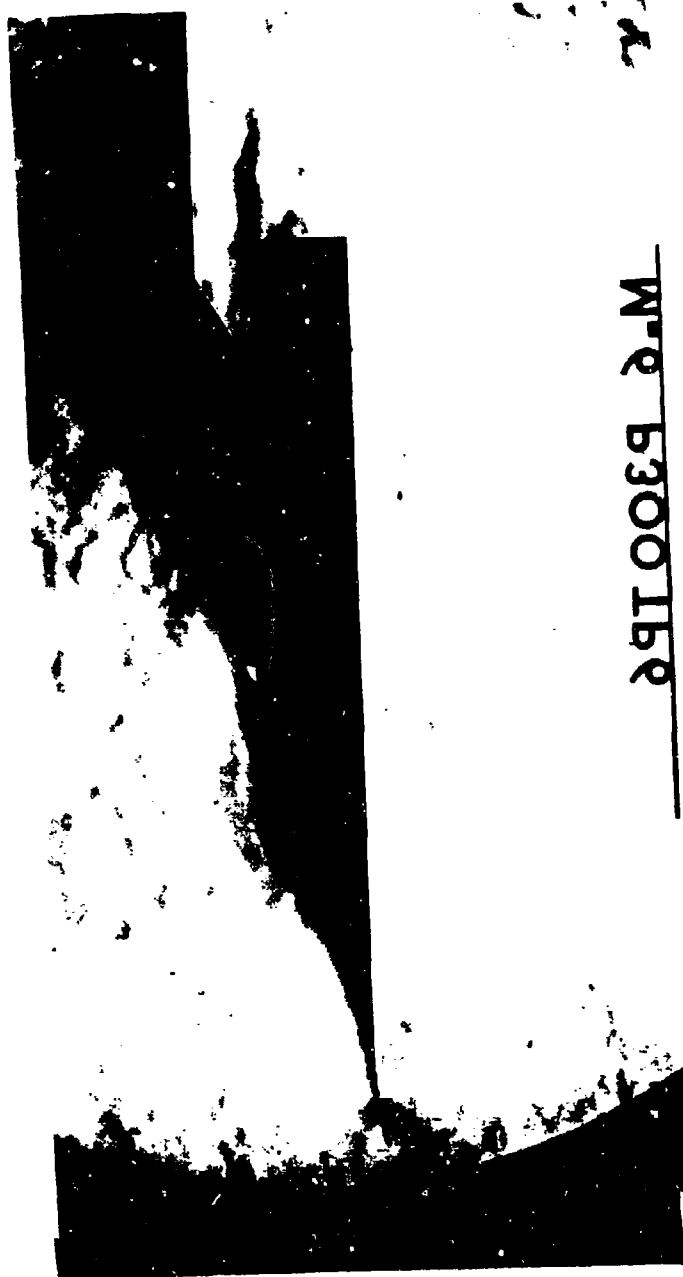


Figure 25 Schlieren Flow Photograph,  $L/D = 5.6$  Cavity,  $M_\infty = 0.60$



Fig 26 Schlieren Flow Photograph,  $L/D = 5.6$  Cavity,  $M_\infty = 0.61$



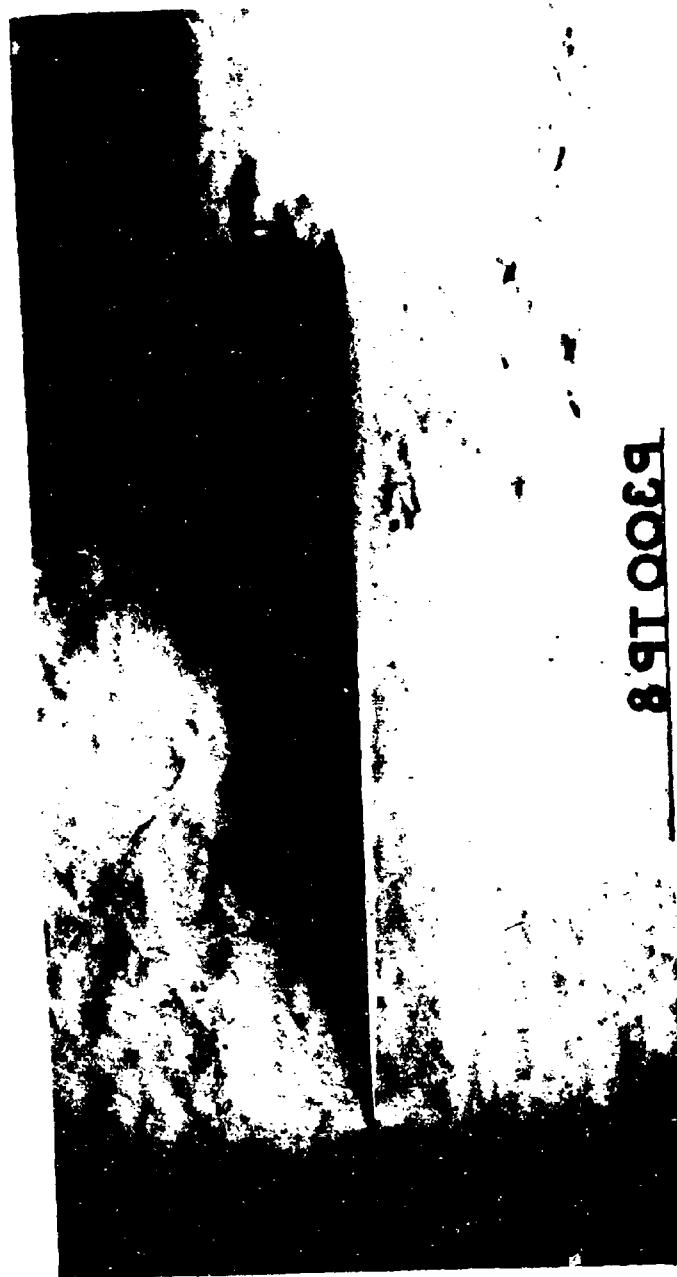


Figure 27 Schlieren Flow Photograph,  $L/D = 5.6$  Cavity,  $M_{\infty} = 0.64$

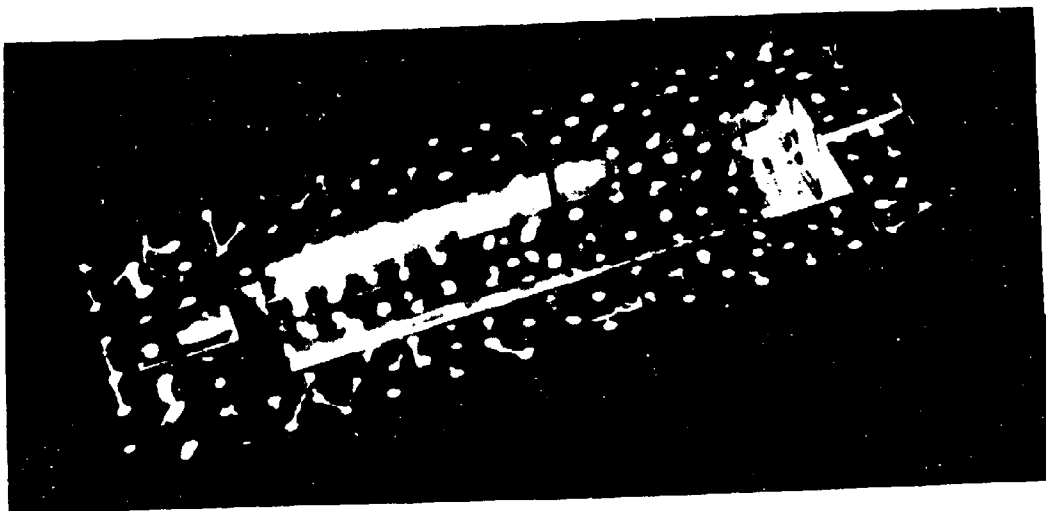


Figure 28 Oil Drop Pattern Prior to Test Run,  $L/D = 5.6$  Cavity

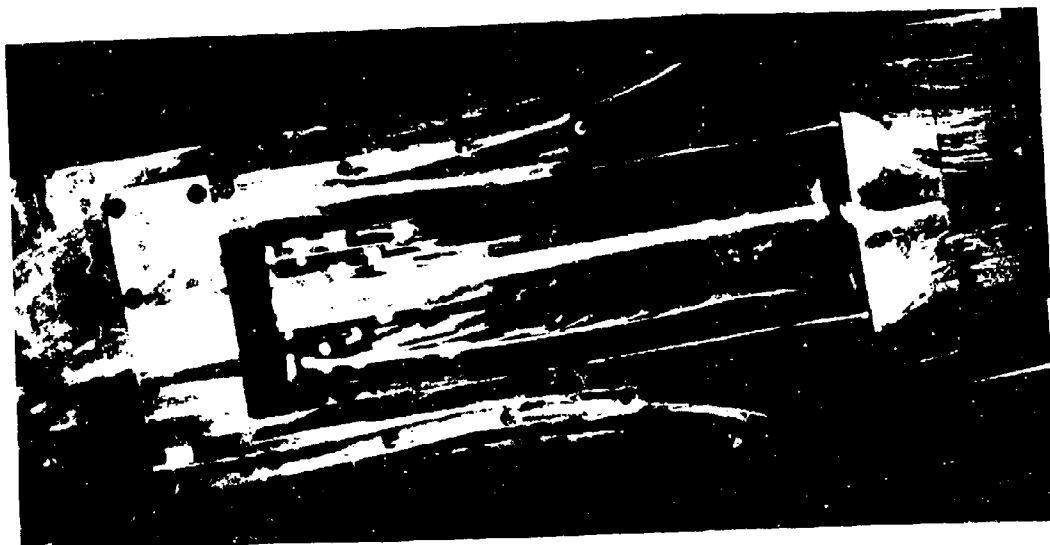


Figure 29 Oil Flow in  $L/D = 5.6$  Cavity at  $M_{\infty} = 0.75$ , Ceiling



Figure 30 Oil Flow in  $L/D = 5.6$  Cavity at  $M_\infty = 0.75$ , Port Side

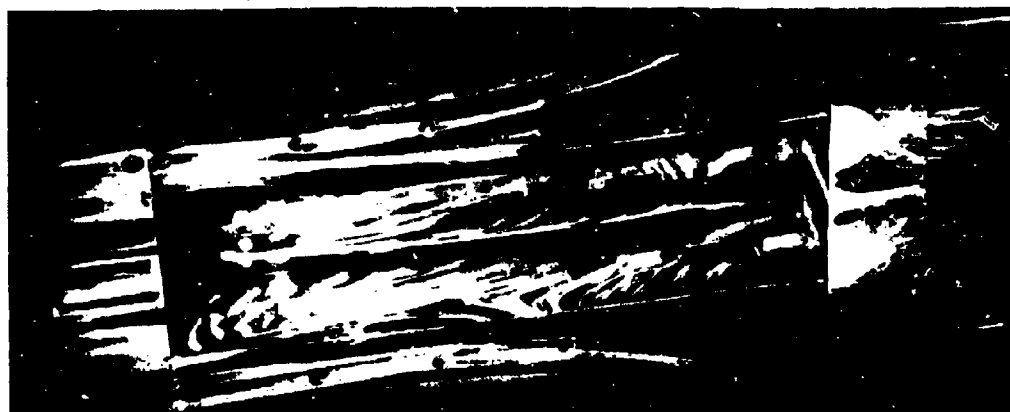
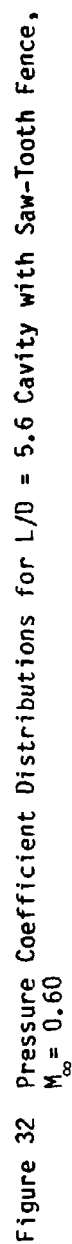
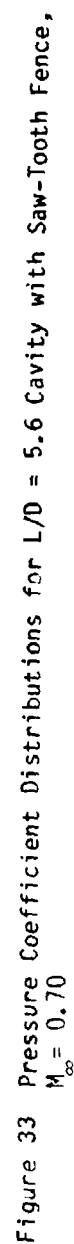


Figure 31 Oil Flow in  $L/D = 5.6$  Cavity at  $M_\infty = 0.75$ , Starboard Side





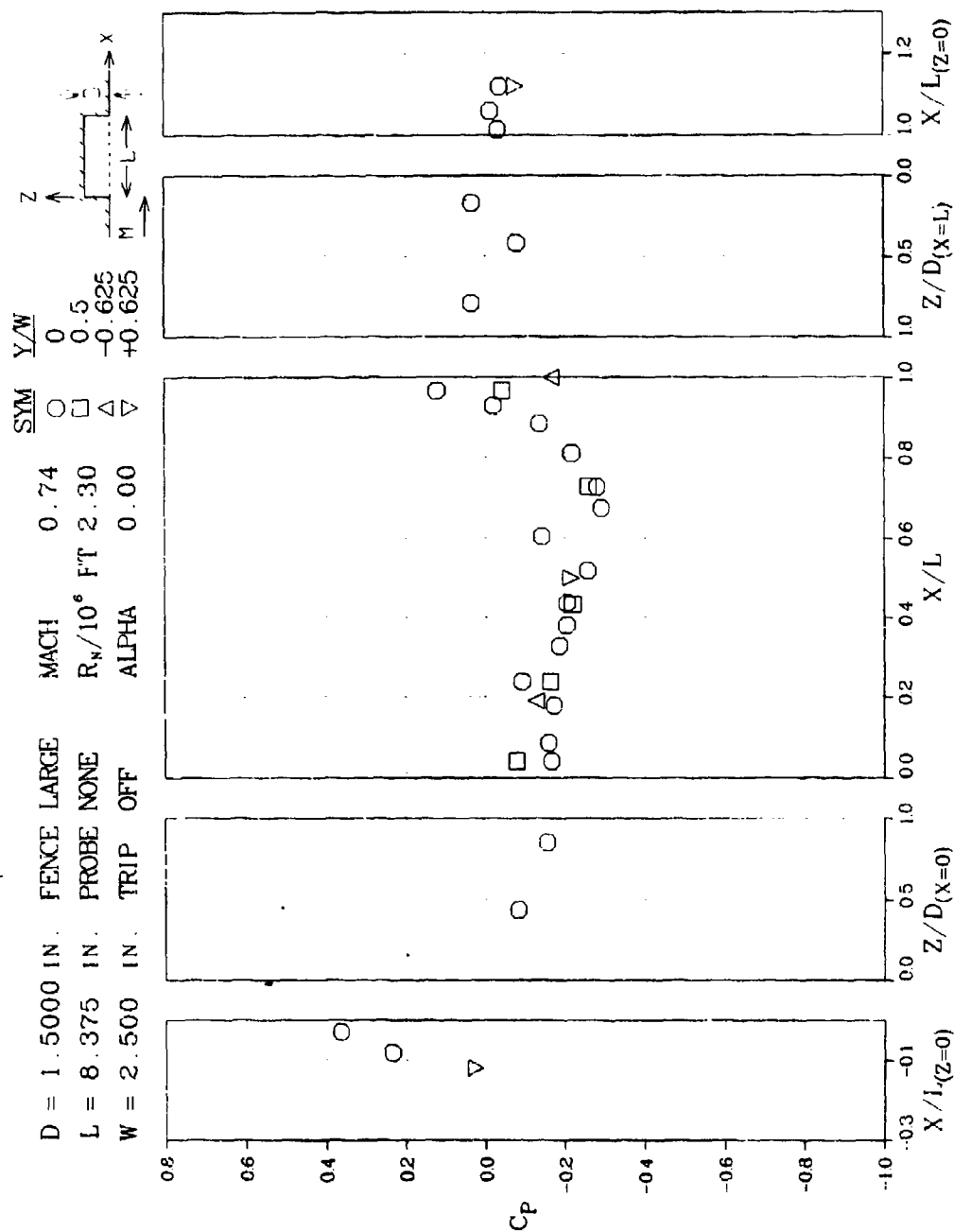


Figure 34 Pressure Coefficient Distributions for  $L/D = 5.6$  Cavity with Saw-Tooth Fence,  $M_\infty = 0.74$



Figure 35 Oil Drop Pattern Prior to Test Run,  $L/D = 5.6$  Cavity with Saw-Tooth Fence

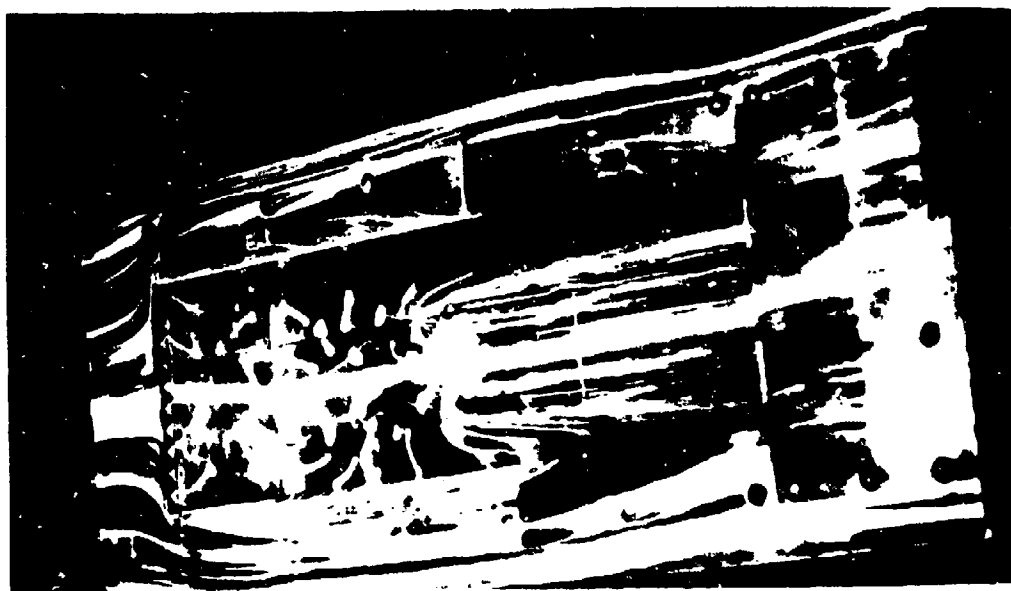


Figure 36 Oil Flow in  $L/D = 5.6$  Cavity with Saw-tooth Fence,  $M_u = 0.70$ , Ceiling

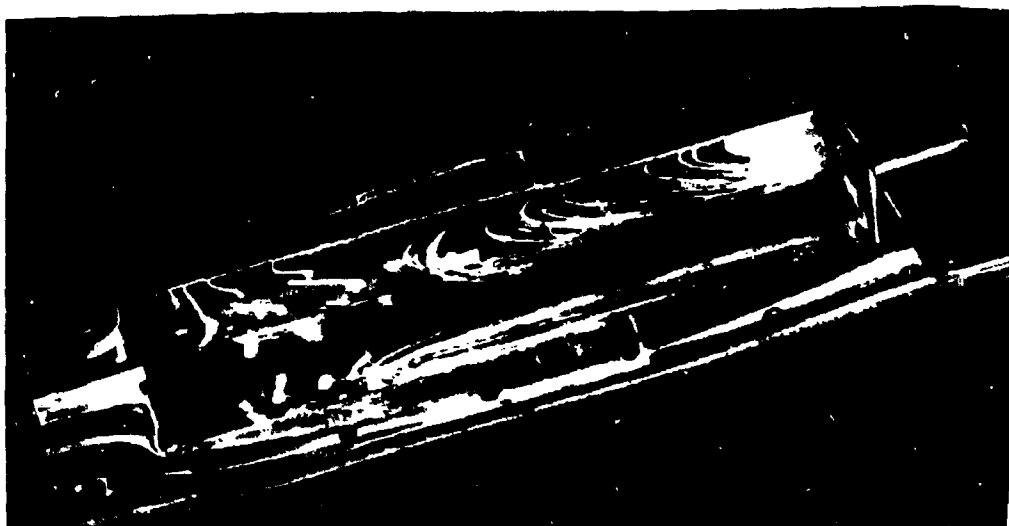


Figure 37 Oil Flow in  $L/D = 5.6$  Cavity with Saw-Tooth Fence,  $M_{\infty} = 0.70$ , Port Side

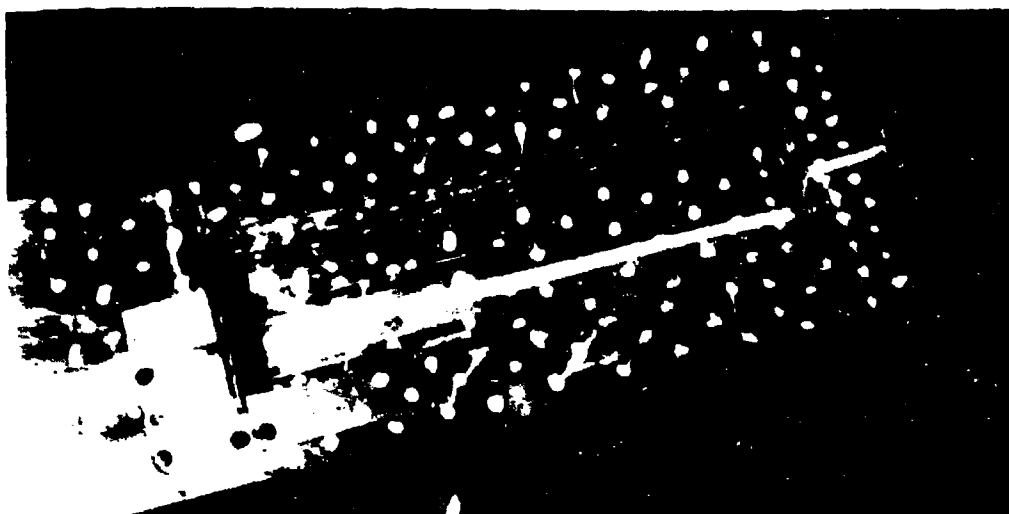


Figure 38 Oil Drop Pattern Prior to Test Run,  $L/D = 5.6$  Cavity with Perforated Fence



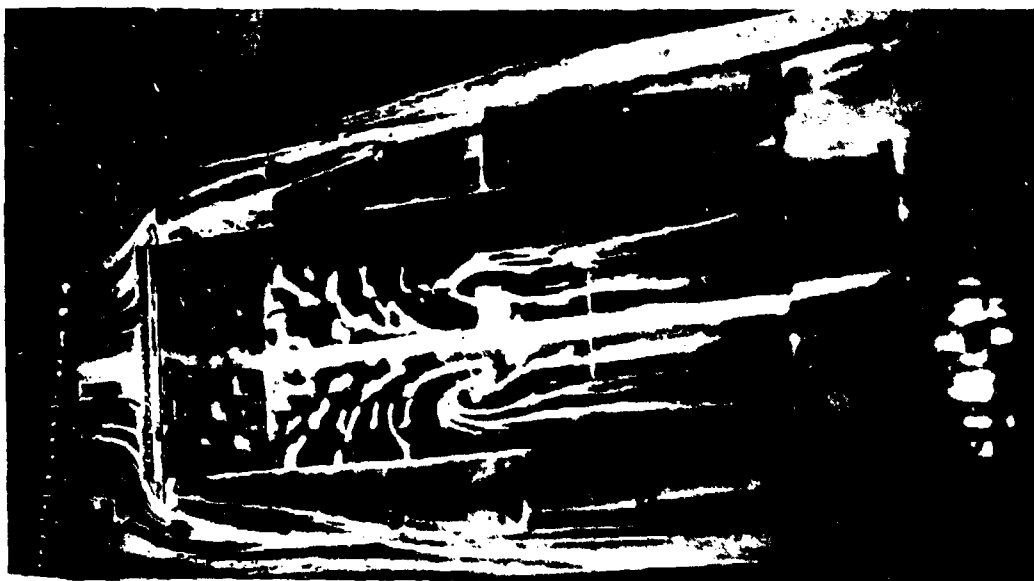


Figure 39 Oil Flow in  $L/D = 5.6$  Cavity with Perforated Fence,  $M_\infty = 0.70$ , Ceiling

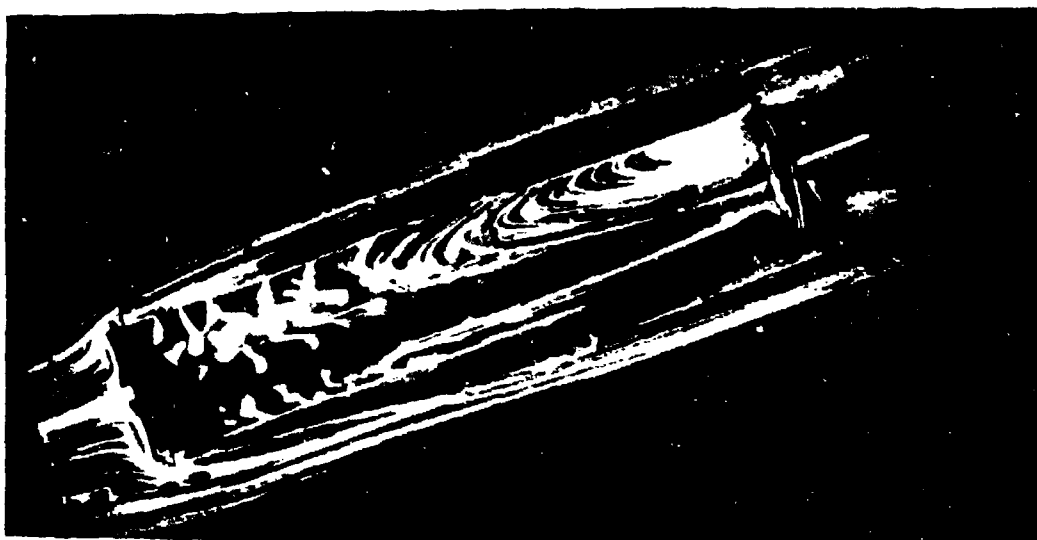


Figure 40 Oil Flow in  $L/D = 5.6$  Cavity with Perforated Fence,  $M_\infty = 0.70$ , Port Side

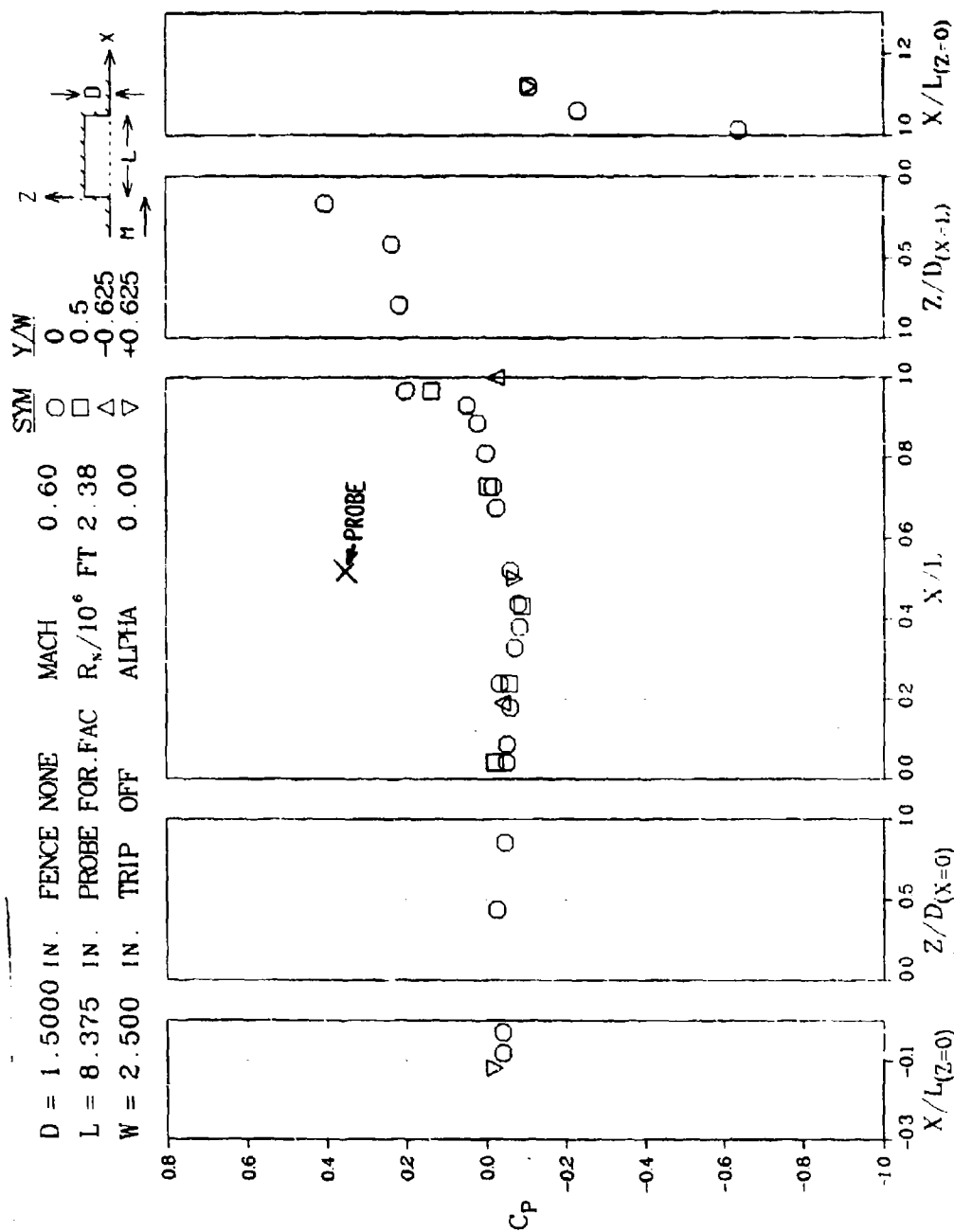
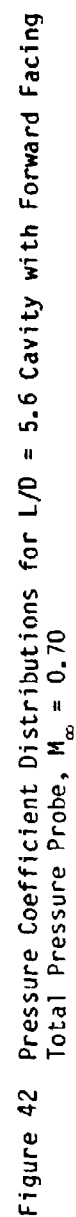
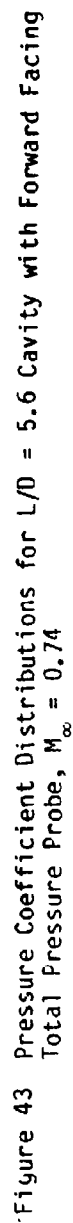


Figure 41 Pressure Coefficient Distributions for  $L/D = 5.6$  Cavity with Forward Facing Total Pressure Probe,  $M_\infty = 0.60$





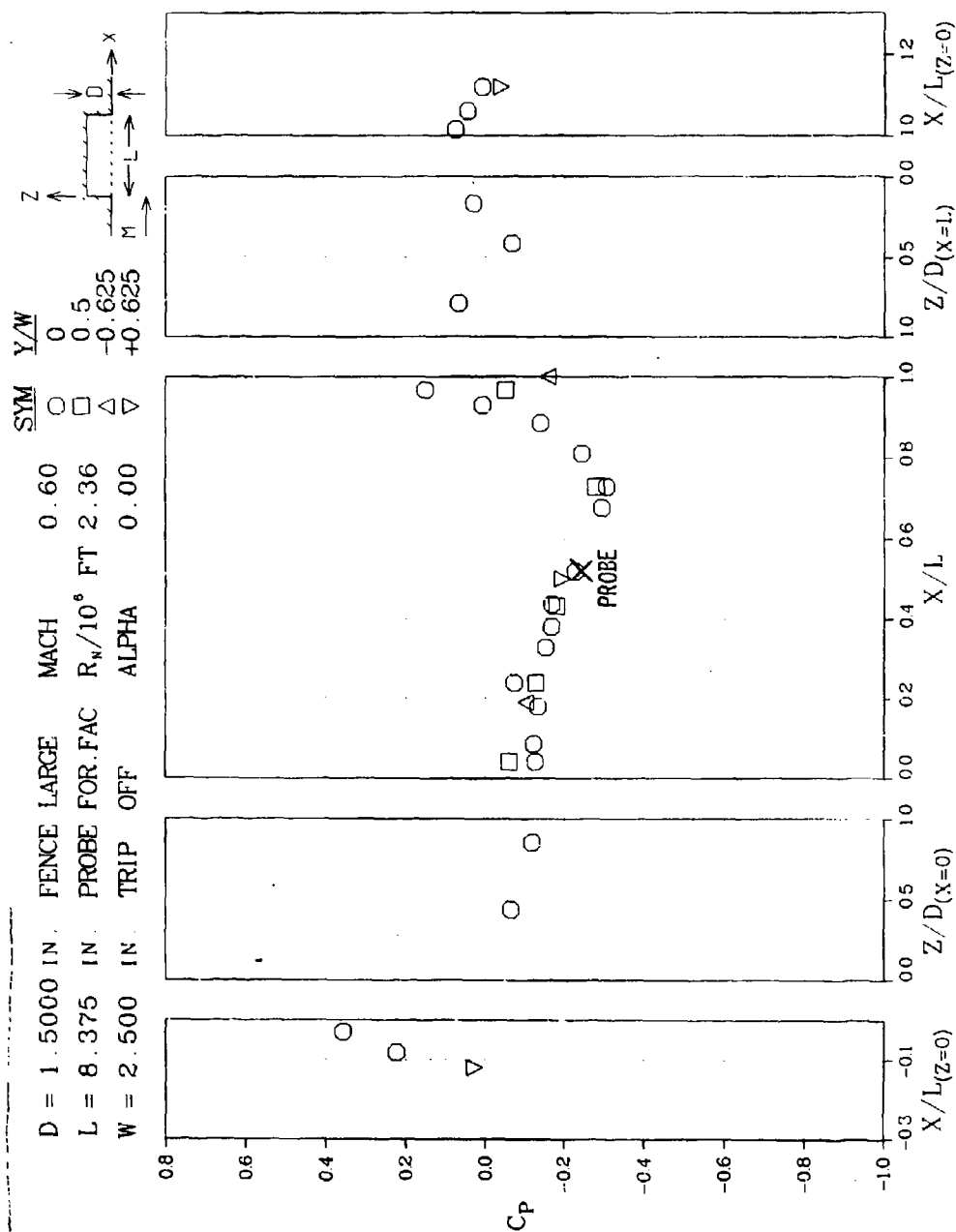


Figure 44 Pressure Coefficient Distributions for  $L/D = 5.6$  Cavity with Saw-Tooth Fence and Forward-Facing Total Pressure Probe,  $M_\infty = 0.60$

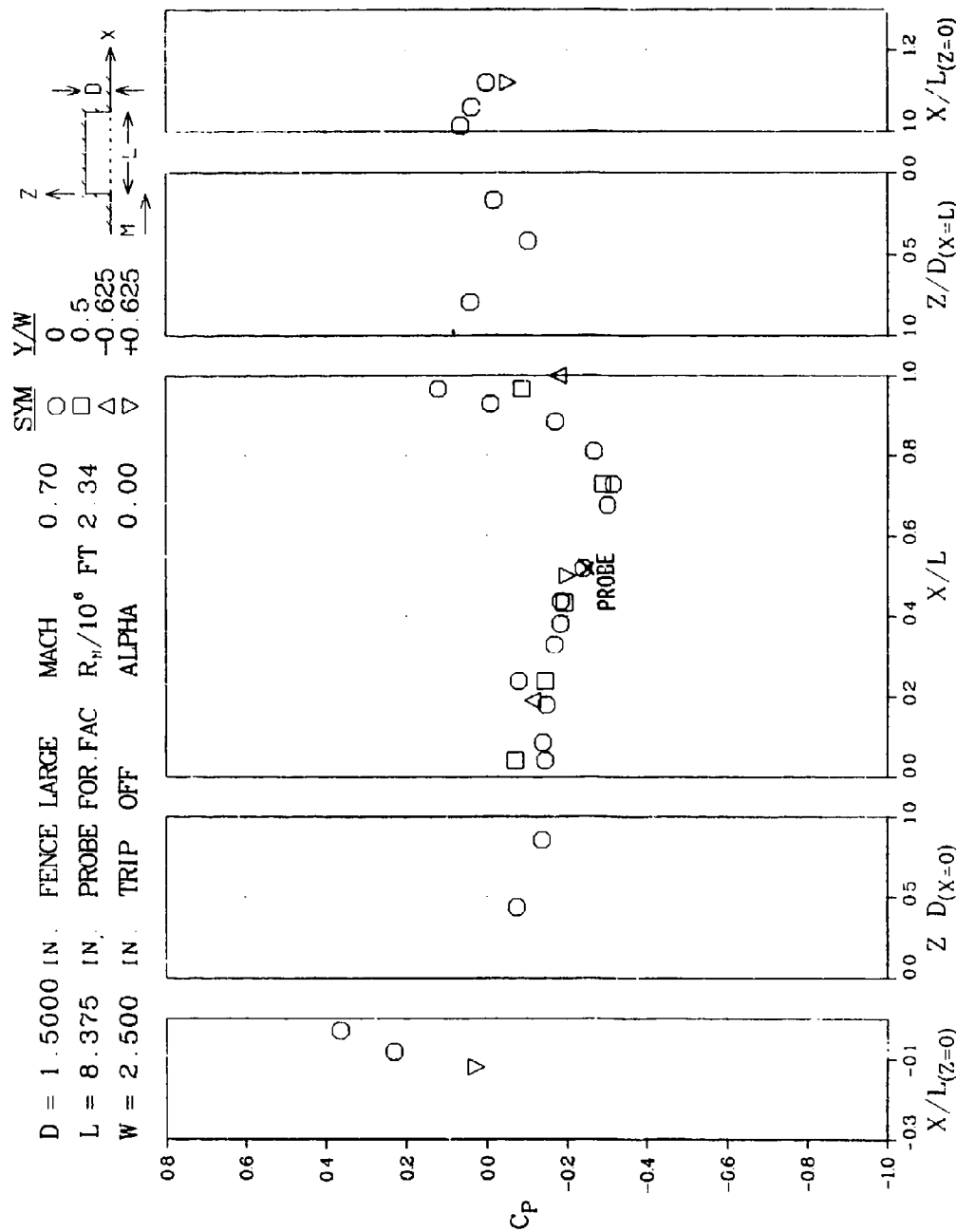


Figure 45 Pressure Coefficient Distributions for  $L/D = 5.6$  Cavity with Saw-Tooth Fence and Forward-Facing Total Pressure Probe,  $M_\infty = 0.70$

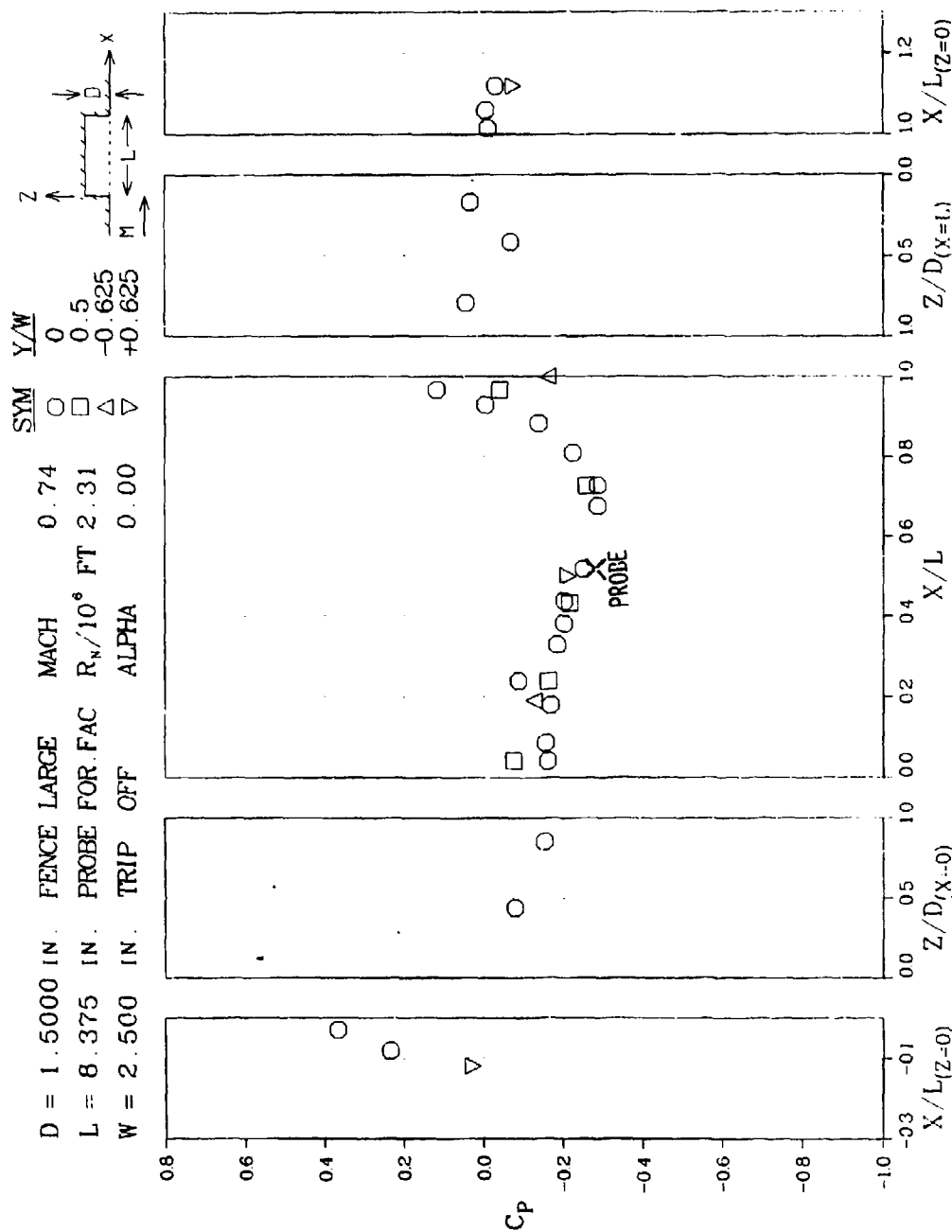


Figure 46 Pressure Coefficient Distributions for  $L/D = 5.6$  Cavity with Saw-Tooth Fence and Forward-Facing Total Pressure Probe,  $M_\infty = 0.74$





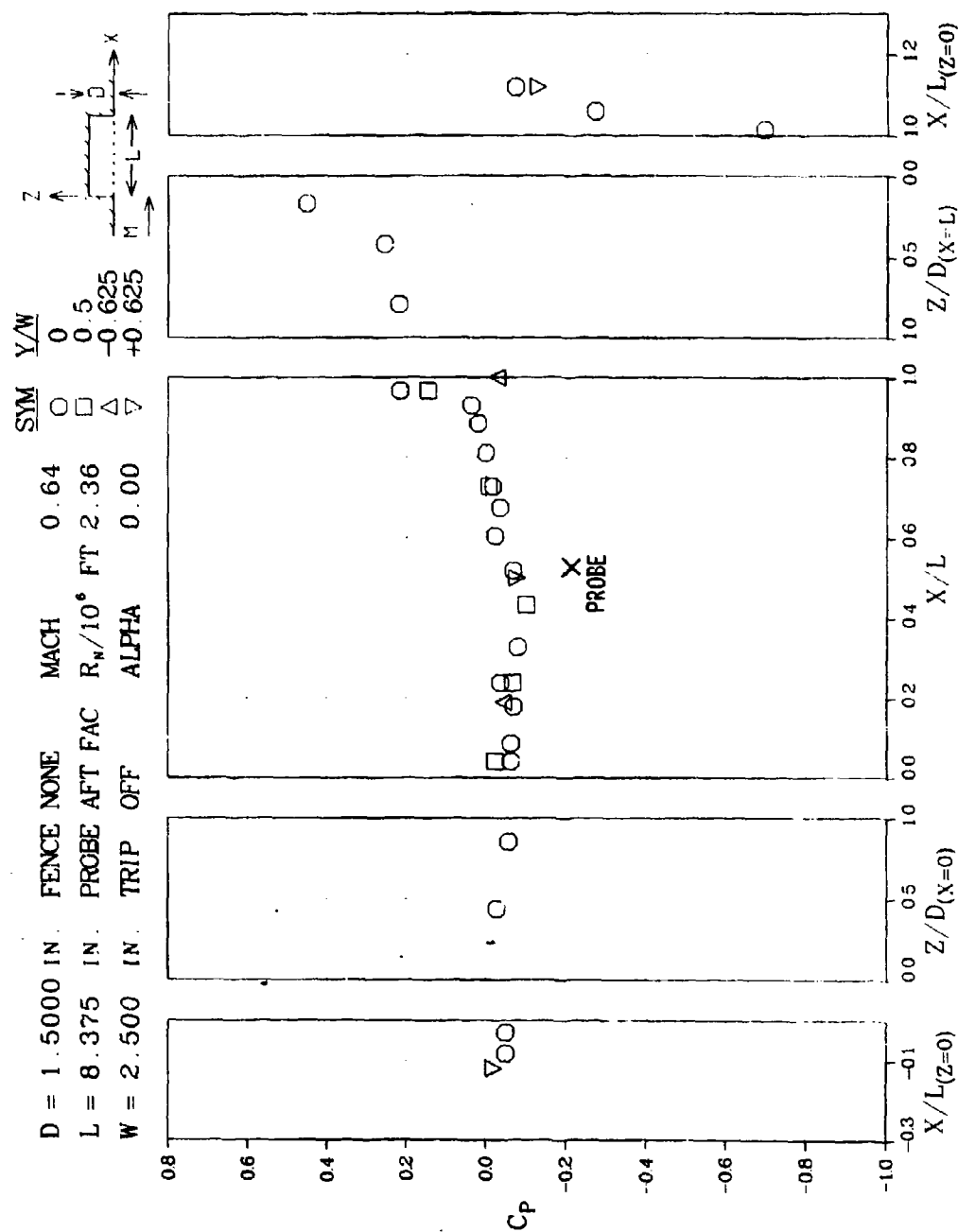


Figure 48 Pressure Coefficient Distributions for  $L/D = 5.6$  Cavity with Aft-Facing Total Pressure Probe,  $M_\infty = 0.64$

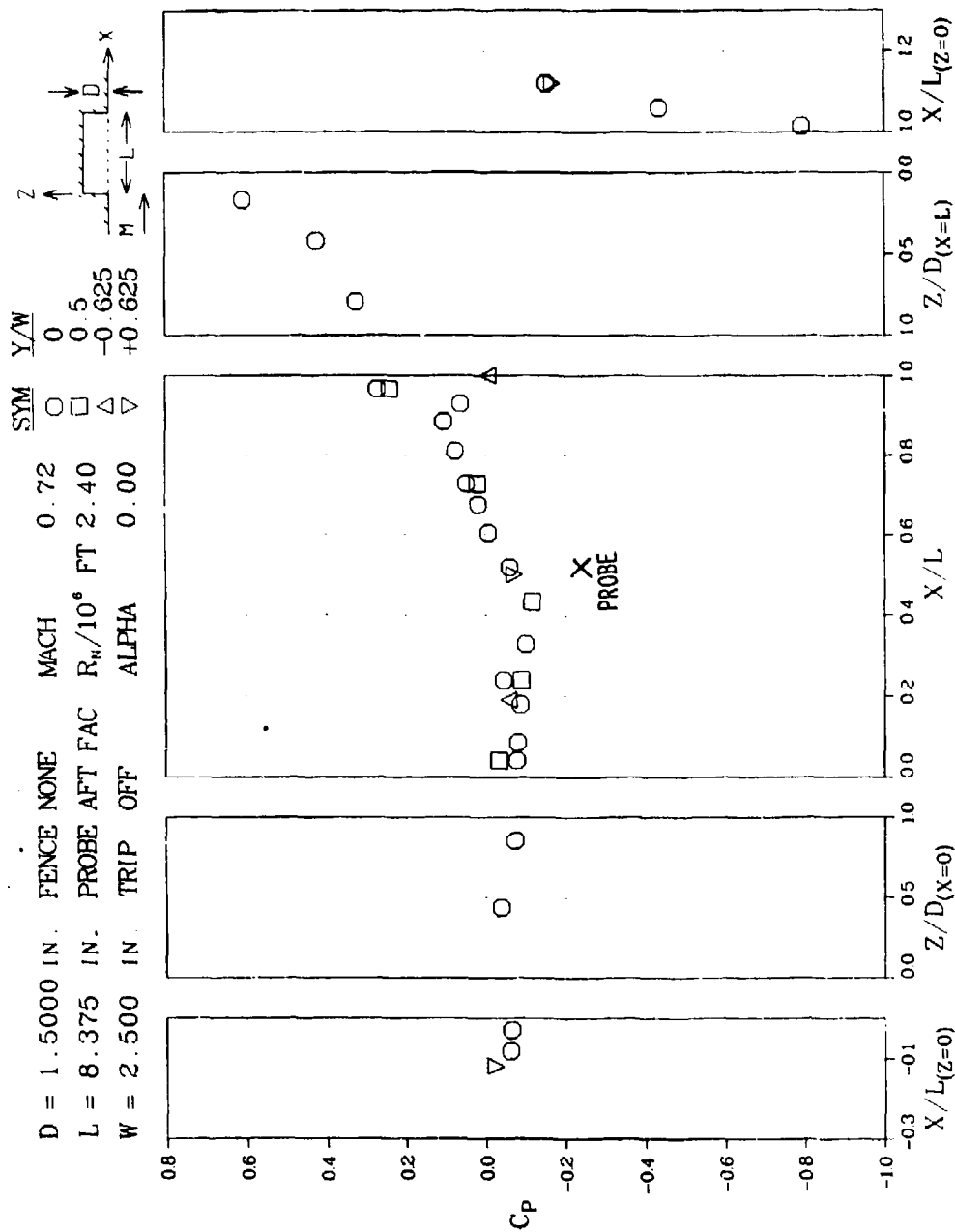
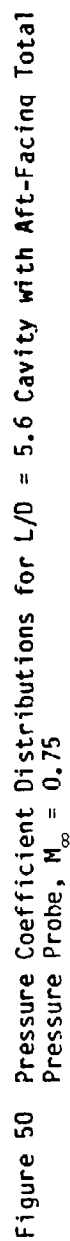


Figure 49 Pressure Coefficient Distributions for  $L/D = 5.6$  Cavity with Aft-Facing Total Pressure Probe,  $M_\infty = 0.72$



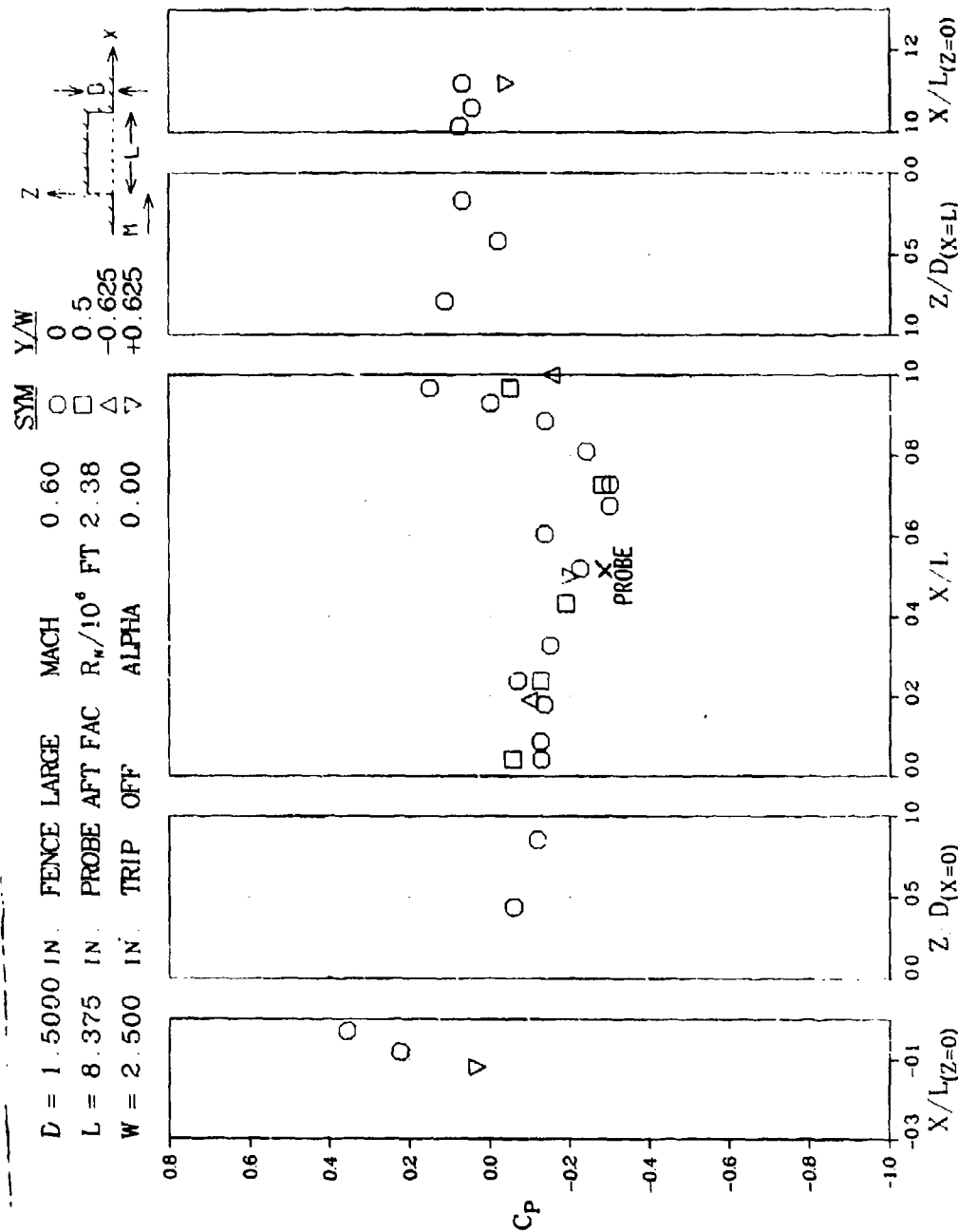
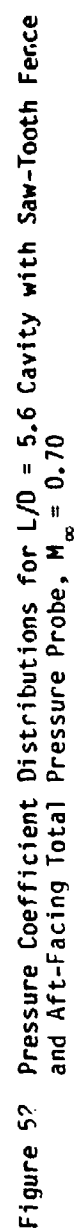


Figure 51 Pressure Coefficient Distributions for  $L/D = 5.6$  Cavity with Saw-Tooth Fence and Aft-Facing Total Pressure Probe,  $M_\infty = 0.60$



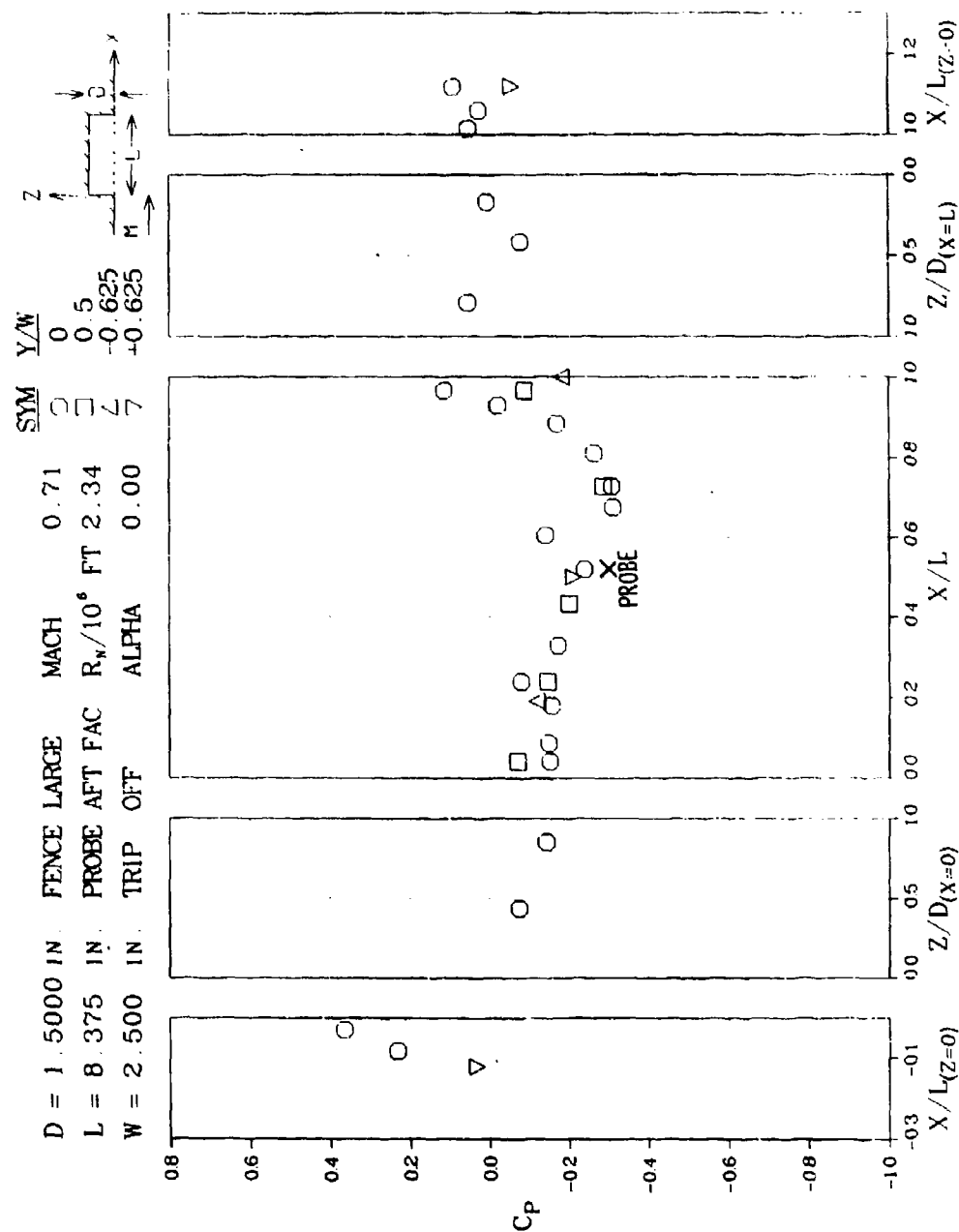


Figure 53 Pressure Coefficient Distributions for  $L/D = 5.6$  Cavity with Saw-Tooth Fence and Aft-Facing Total Pressure Probe,  $M_\infty = 0.71$



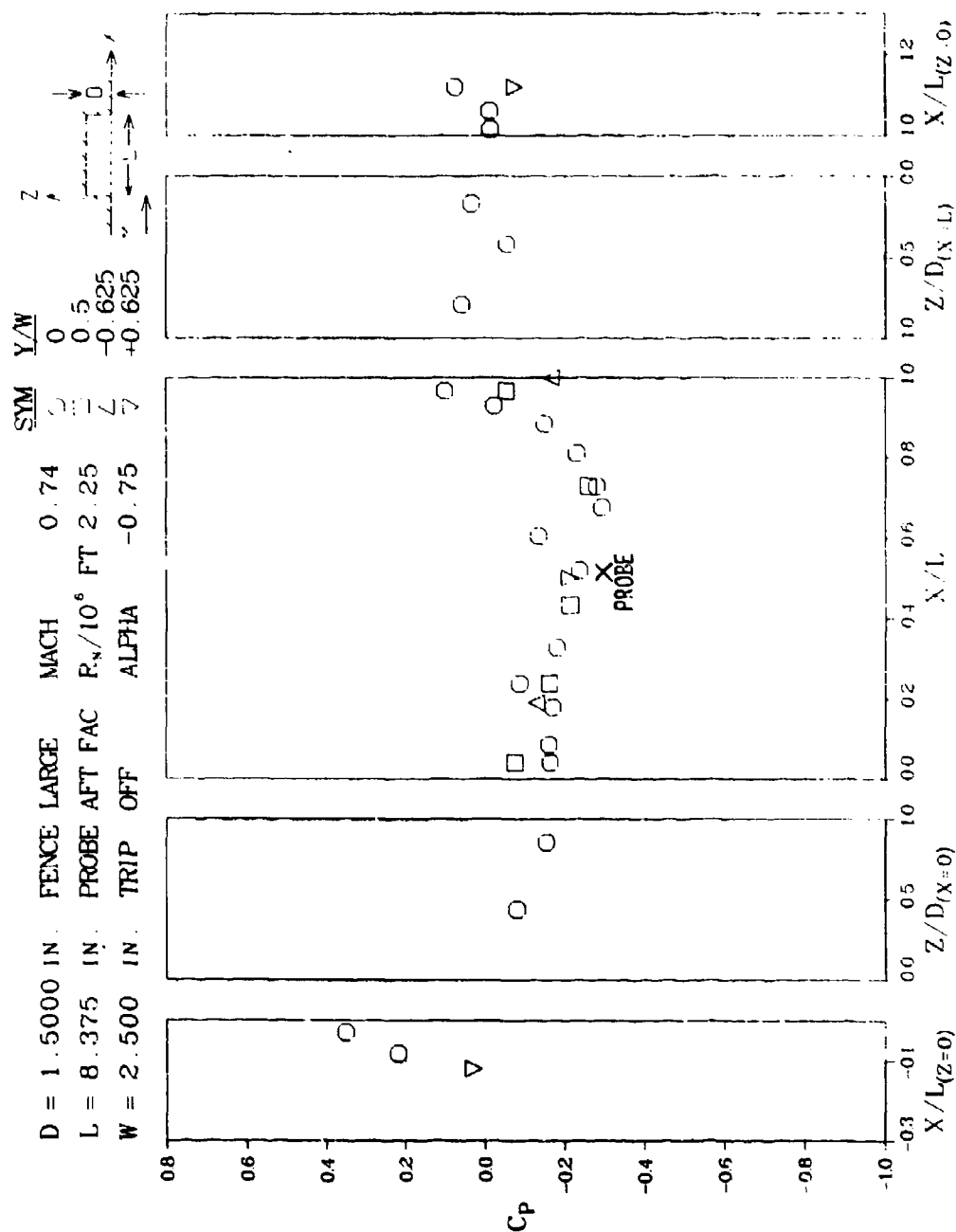


Figure 55 Pressure Coefficient Distributions for  $L/D = 5.6$  Cavity with Saw-Tooth Fence and Aft-Facing Total Pressure Probe,  $M_\infty = 0.74$ , Model Pitched Nose Down  $3/4^\circ$



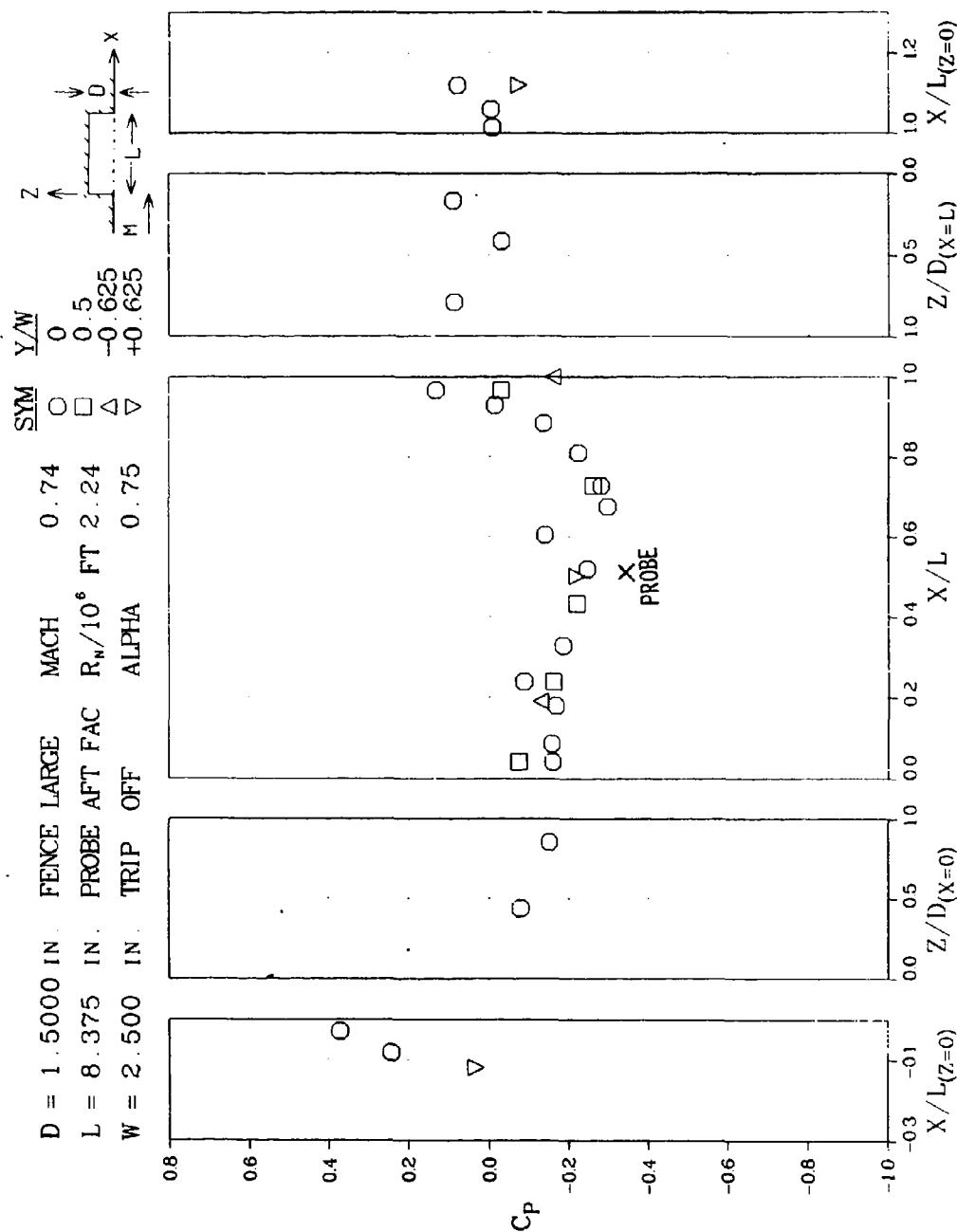


Figure 56 Pressure Coefficient Distributions for  $L/D = 5.6$  Cavity with Saw-Tooth Fence and Aft-Facing Total Pressure Probe,  $M_\infty = 0.74$ , Model Pitched Nose Up  $3/4^\circ$

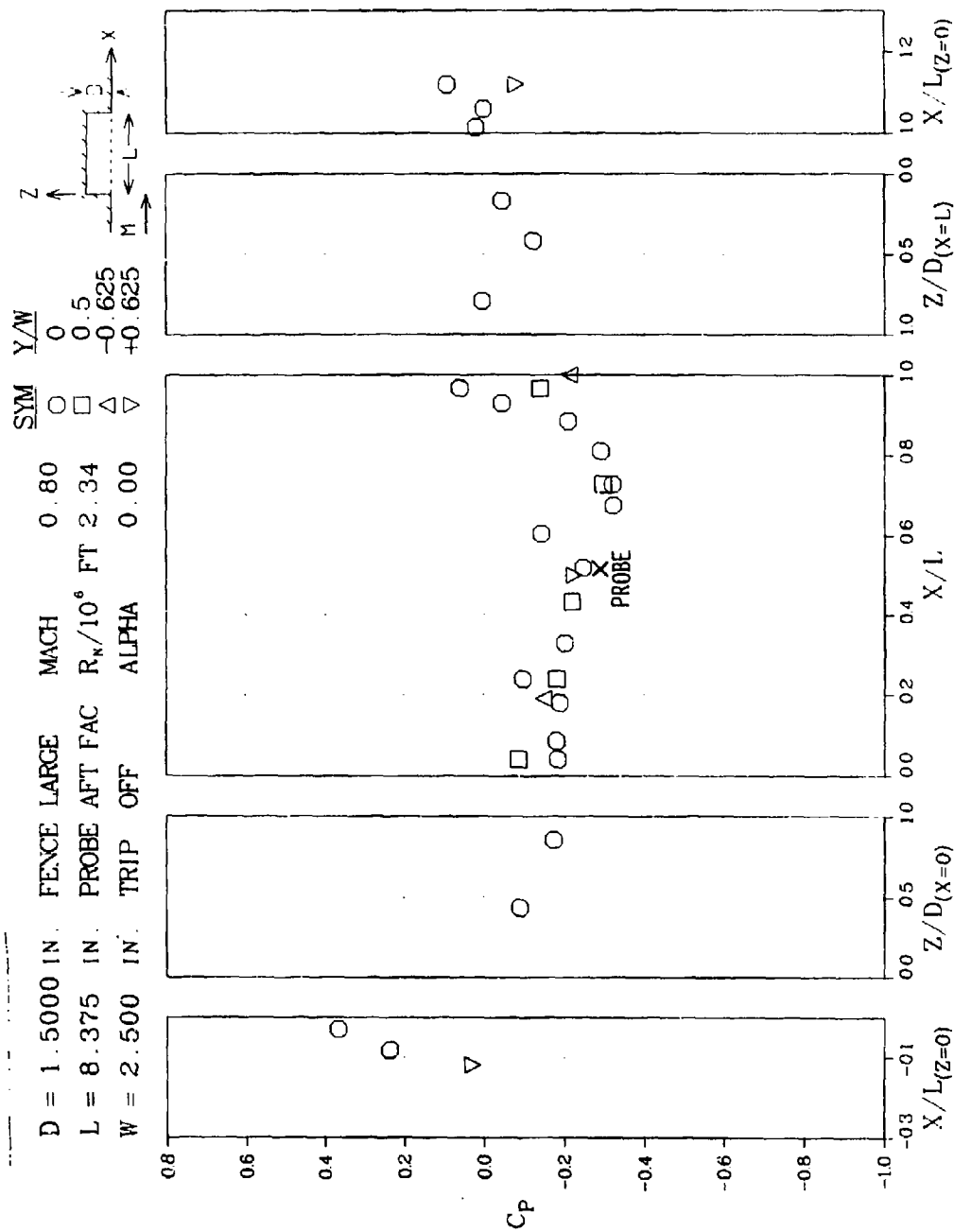


Figure 57 Pressure Coefficient Distributions for  $L/D = 5.6$  Cavity with Saw-Tooth Fence and Aft-Facing Total Pressure Probe,  $M_\infty = 0.80$



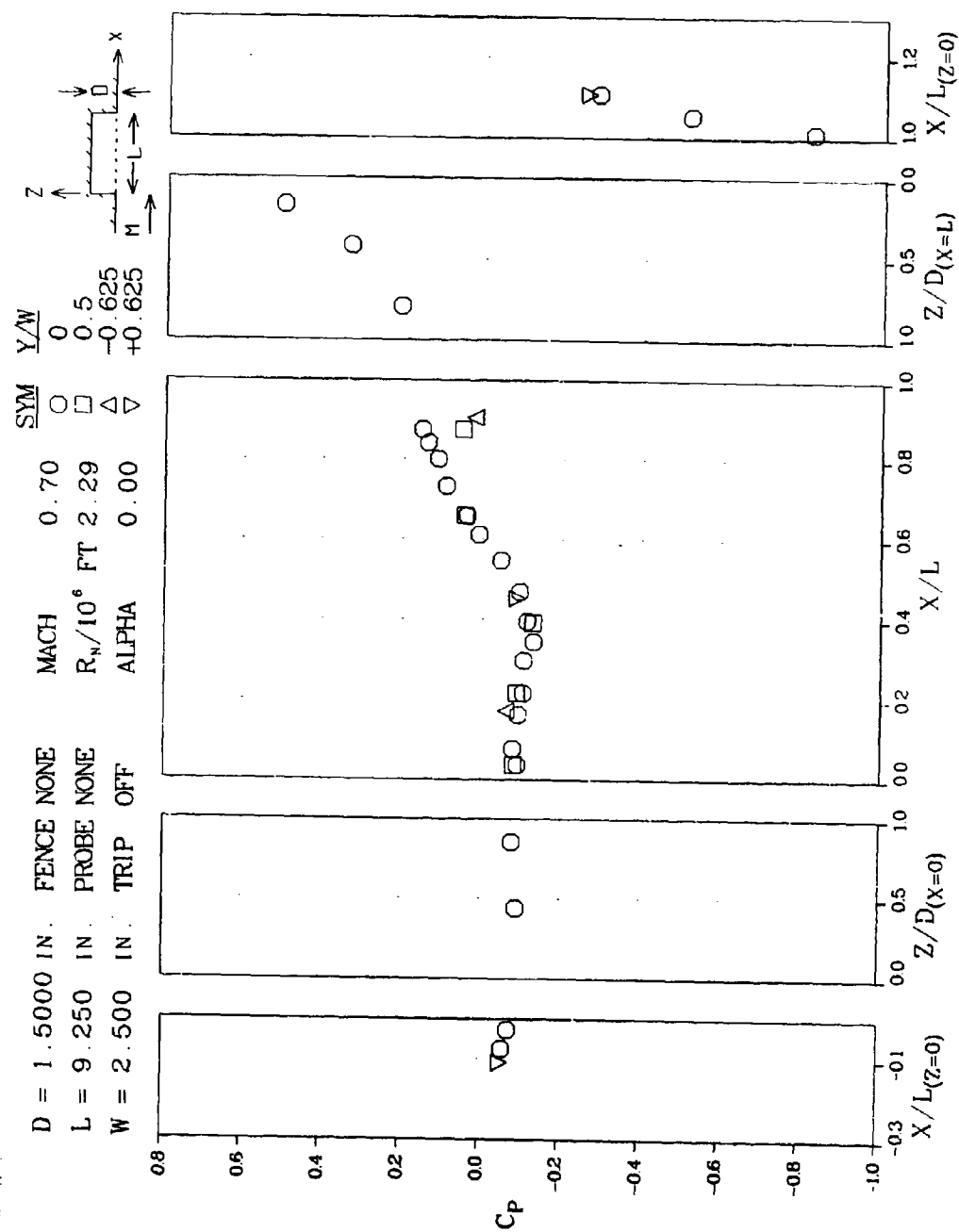
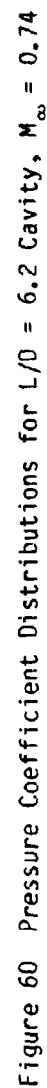


Figure 59 Pressure Coefficient Distributions for  $L/D = 6.2$  Cavity,  $M_\infty = 0.70$



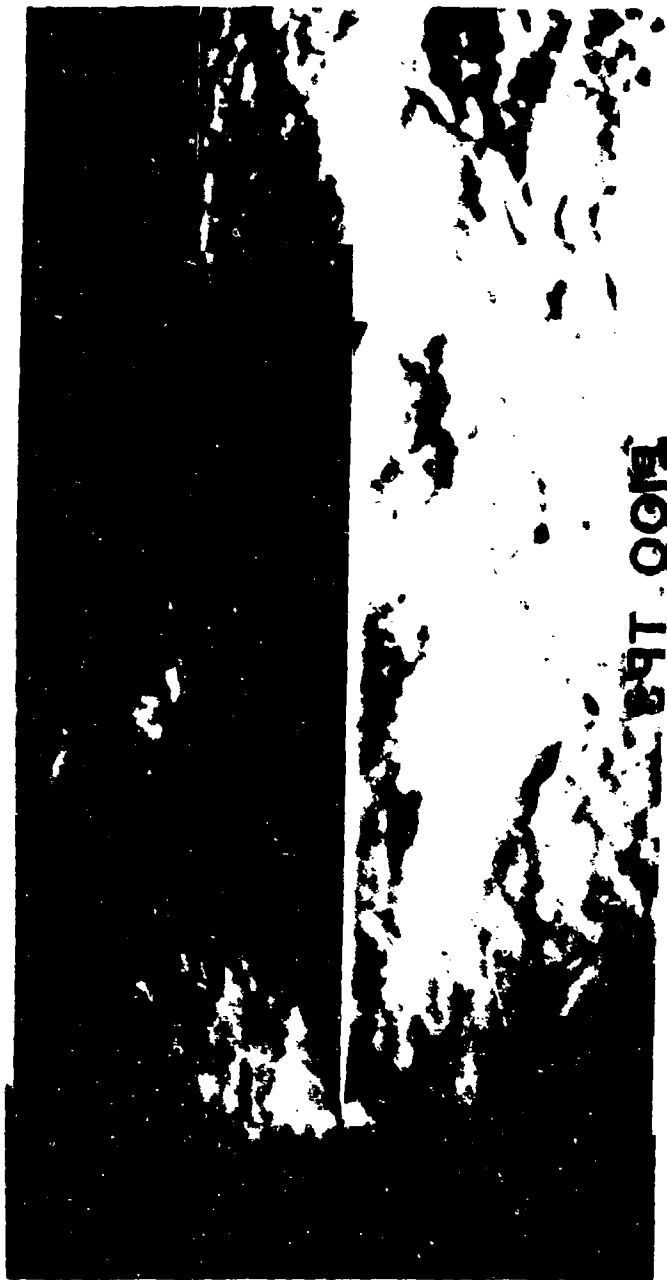


Figure 61 Schlieren Flow Photograph,  $L/D = 6.2$  Cavity,  $M_\infty = 0.70$



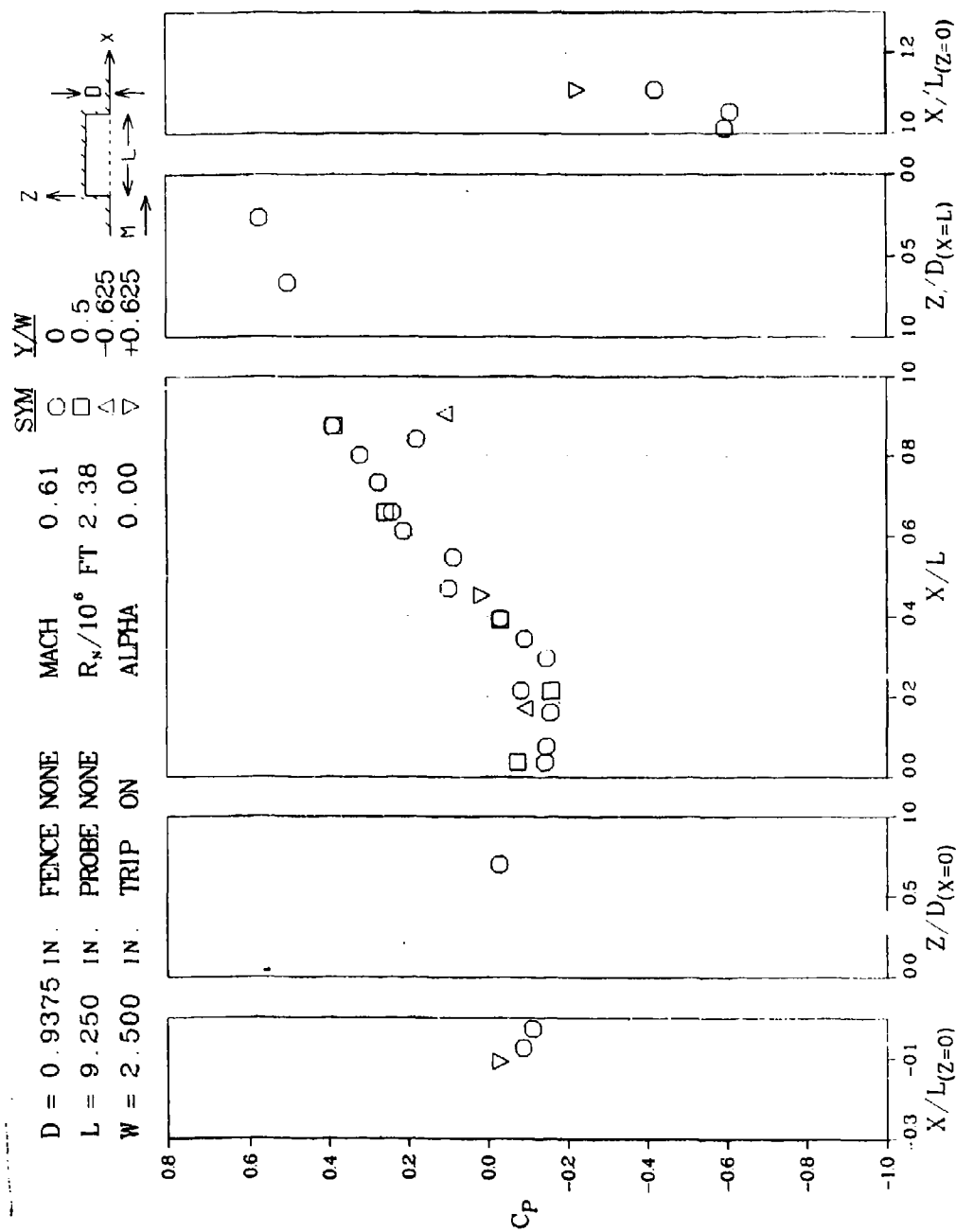


Figure 63 Pressure Coefficient Distributions for  $L/D = 9.9$  Cavity with Boundary Layer Trip,  $M_\infty = 0.61$



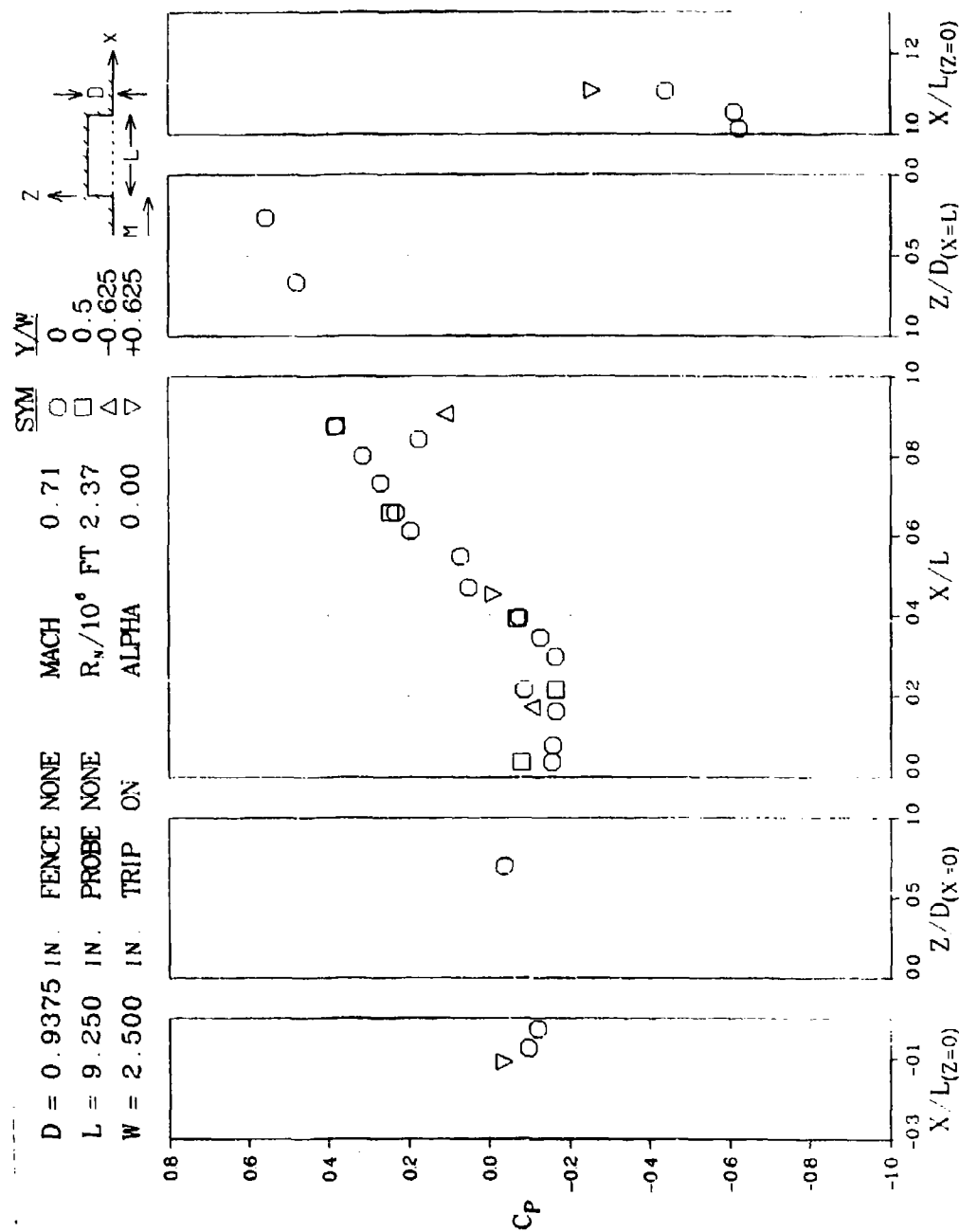


Figure 64 Pressure Coefficient Distributions for  $L/D = 9.9$  Cavity with Boundary Layer Trip,  $M_\infty = 0.71$

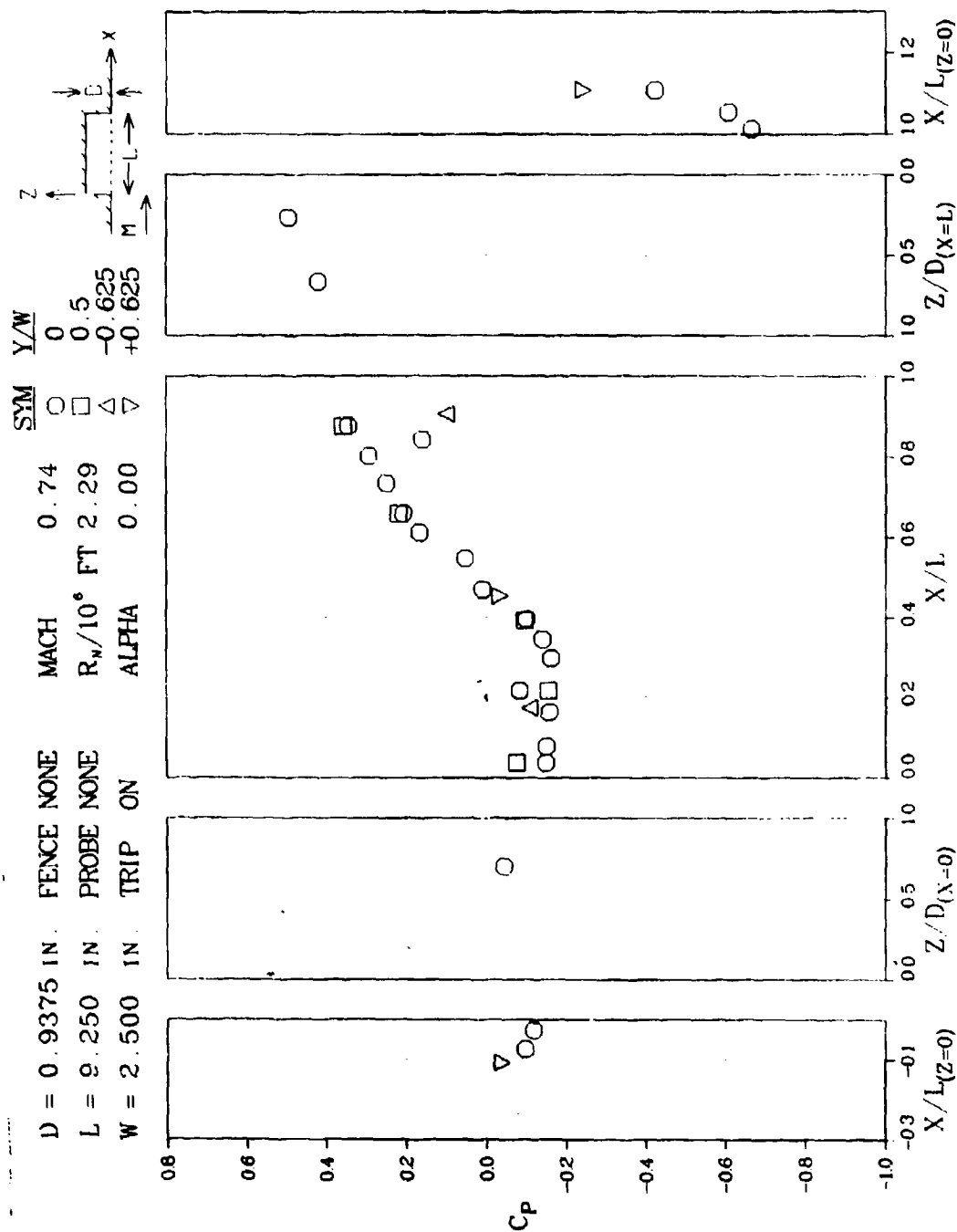


Figure 65 Pressure Coefficient Distributions for  $L/D = 9.9$  Cavity with Boundary Layer Trip,  $M_\infty = 0.74$

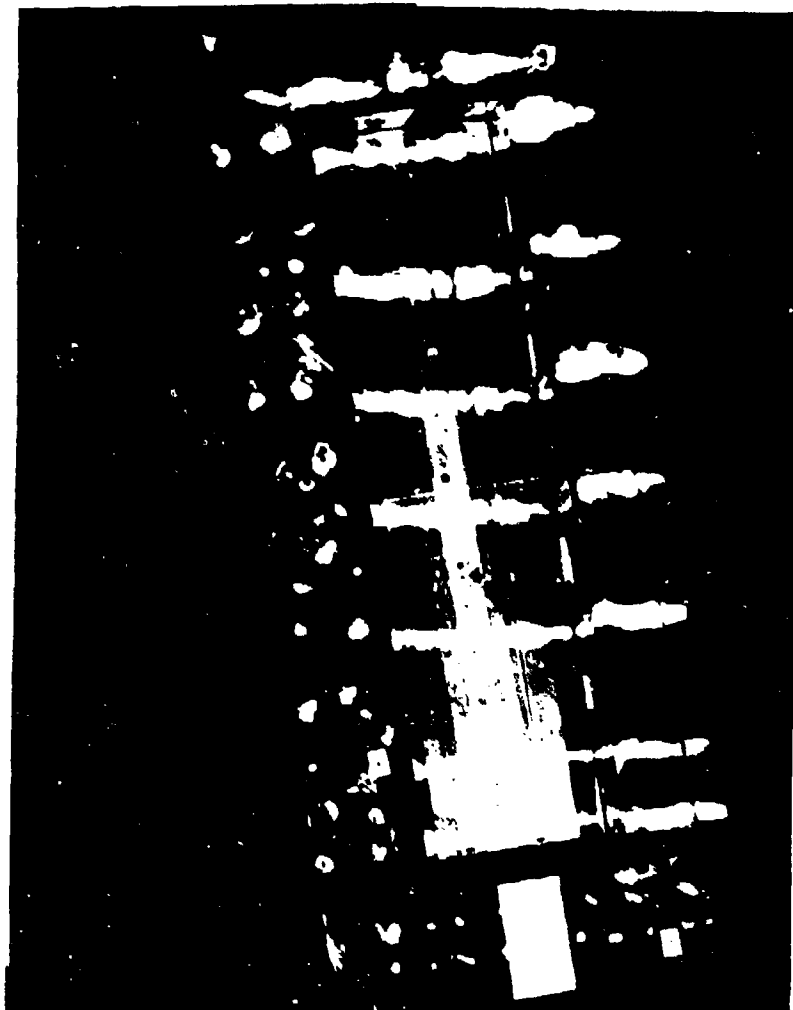


Figure 66 Oil Pattern Prior to Test Run,  $L/D = 9.9$  Cavity



Figure 67 Oil Flow in  $L/D = 9.9$  Cavity at  $M_\infty = 0.70$ , Ceiling

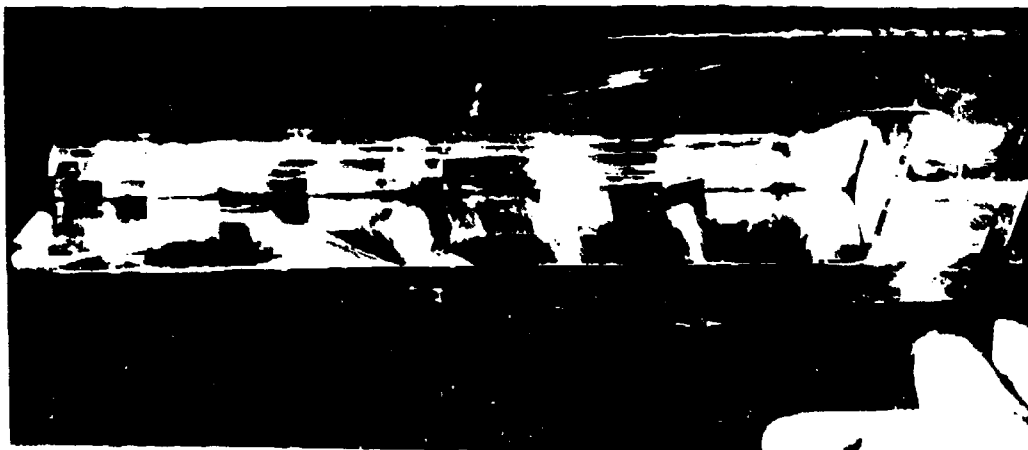
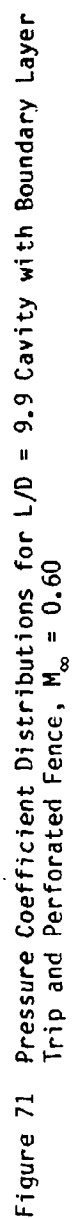


Figure 68 Oil Flow in  $L/D = 9.9$  Cavity at  $M_\infty = 0.70$ , Starboard Side



Figure 69 Schlieren Flow Photograph,  $L/D = 9.9$  Cavity,  $M_\infty = 0.61$









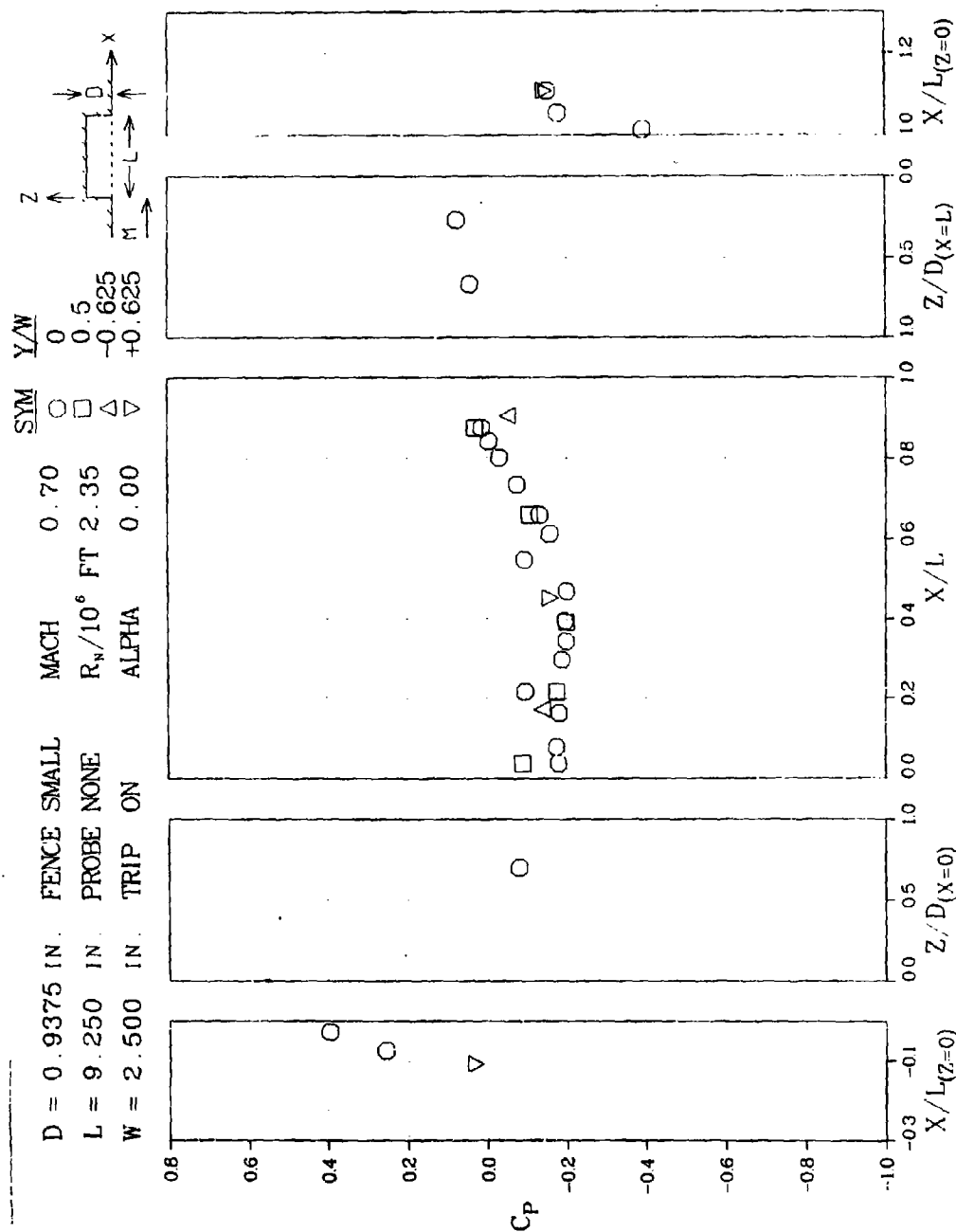


Figure 73 Pressure Coefficient Distributions for  $L/D = 9.9$  Cavity with Boundary Layer Trip and Perforated Fence,  $M_\infty = 0.70$



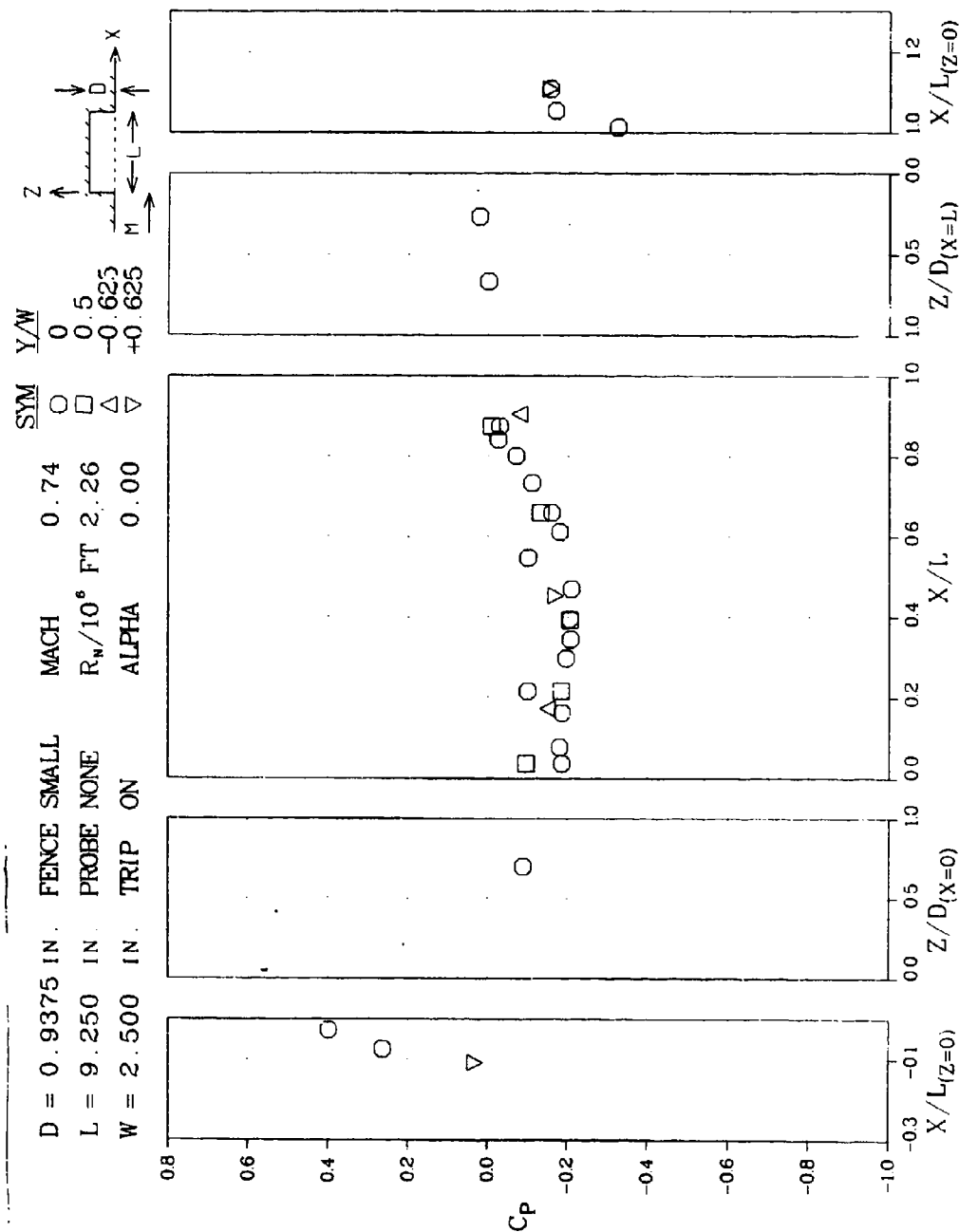


Figure 75 Pressure Coefficient Distributions for  $L/D = 9.9$  Cavity with Boundary Layer Trip and Perforated Fence,  $M_\infty = 0.74$

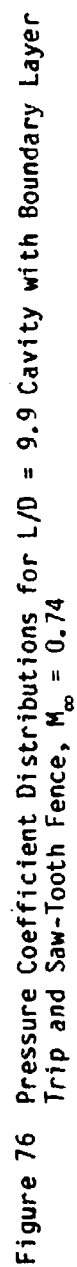




Figure 77 Schlieren Flow Photograph,  $L/D = 9.9$  Cavity with Boundary Layer Trip and Perforated Fence,  $M_\infty = 0.70$



Figure 78 Schlieren Flow Photograph,  $L/D = 9.9$  Cavity with Boundary Layer Trip and Saw-Tooth Fence,  $M_\infty = 0.70$



Figure 79 Oil Drop Pattern Prior to Test Run,  $L/D = 9.9$  Cavity with Boundary Layer Trip and Perforated Fence

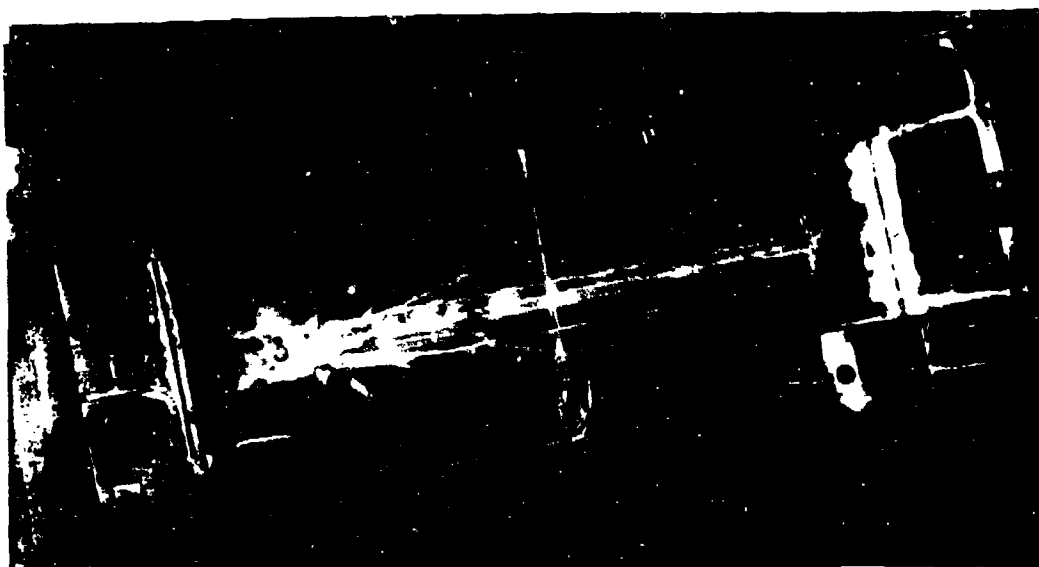


Figure 80 Oil Flow in  $L/D = 9.9$  Cavity with Boundary Layer Trip and Perforated Fence,  $M_\infty = 0.70$ , Ceiling View 1



Figure 81 Oil Flow in  $L/D = 9.9$  Cavity with Boundary Layer Trip and Perforated Fence,  $M_\infty = 0.70$ , Ceiling View 2



Figure 82 Oil Flow in  $L/D = 9.9$  Cavity with Boundary Layer Trip and Perforated Fence,  $M_\infty = 0.70$ , Starboard Side





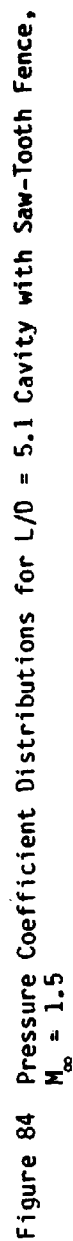
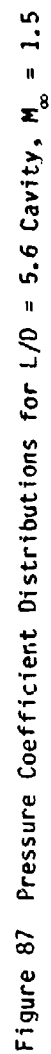




Figure 85 Schlieren Flow Photograph,  $L/D = 5.1$  Cavity,  $M_{\infty} = 1.5$



Figure 86 Schlieren Flow Photograph,  $L/D = 5.1$  Cavity, Saw-Tooth Fence,  $M_{\infty} = 1.5$



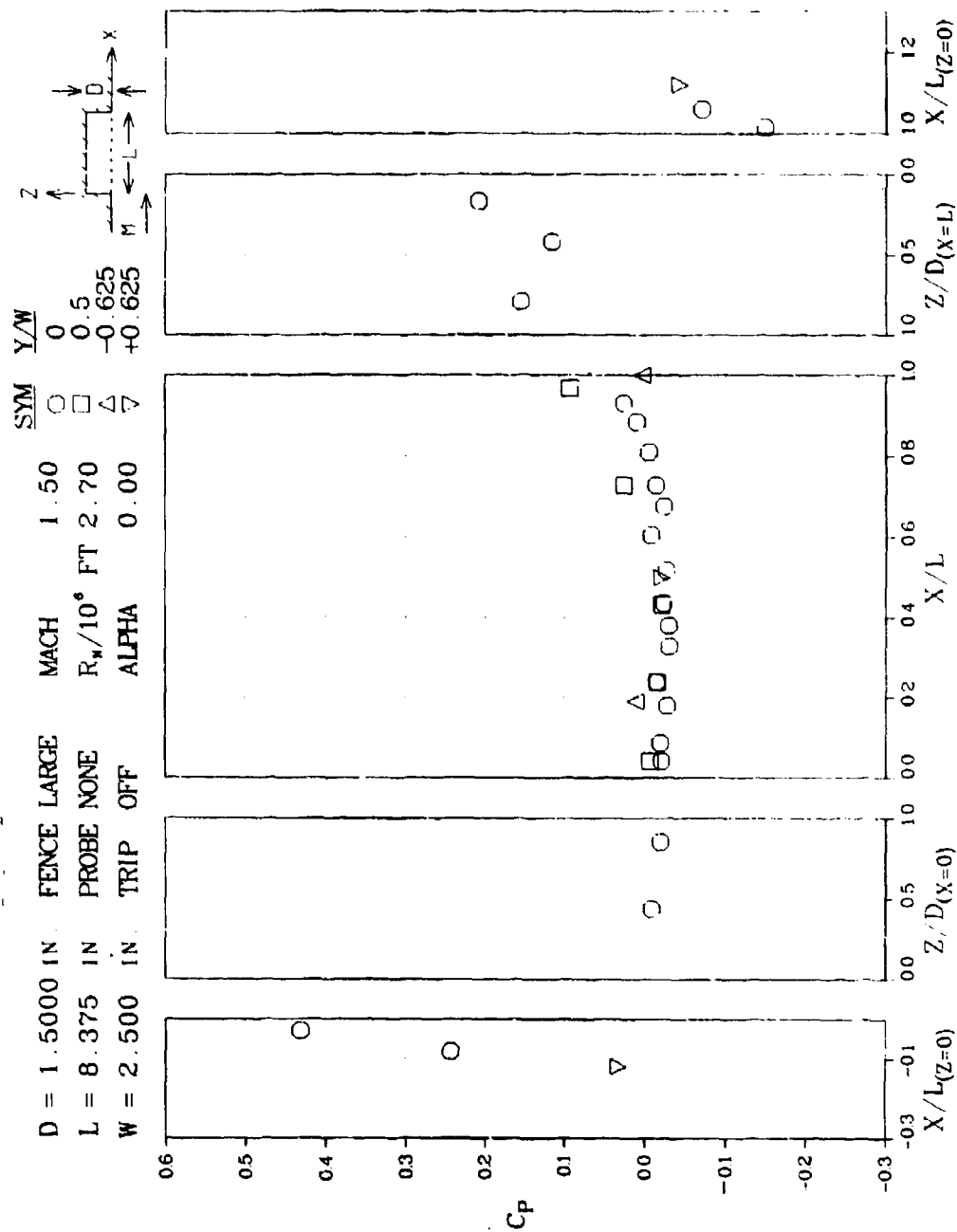


Figure 88 Pressure Coefficient Distributions for  $L/D = 5.6$  Cavity with Saw-Tooth Fence,  $M_\infty = 1.5$

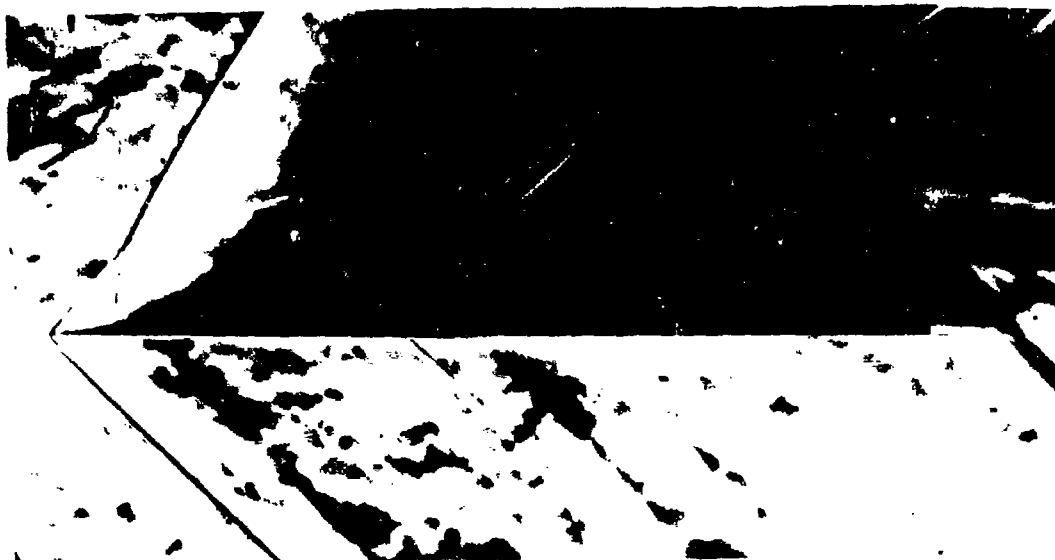


Figure 89 Schlieren Flow Photograph,  $L/D = 5.6$  Cavity,  $M_\infty = 1.5$



Figure 90 Schlieren Flow Photograph,  $L/D = 5.6$  Cavity, Saw-Tooth Fence,  $M_\infty = 1.5$

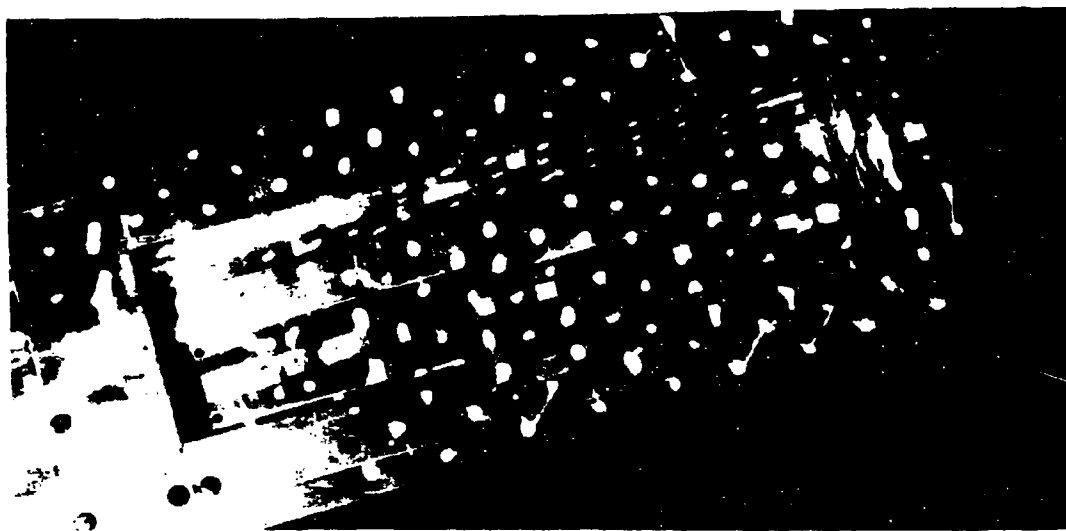


Figure 91 Oil Drop Pattern Prior to Test Run,  $L/D = 5.6$  Cavity



Figure 92 Oil Flow in  $L/D = 5.6$  Cavity at  $M_\infty = 1.5$ , Forward Portion

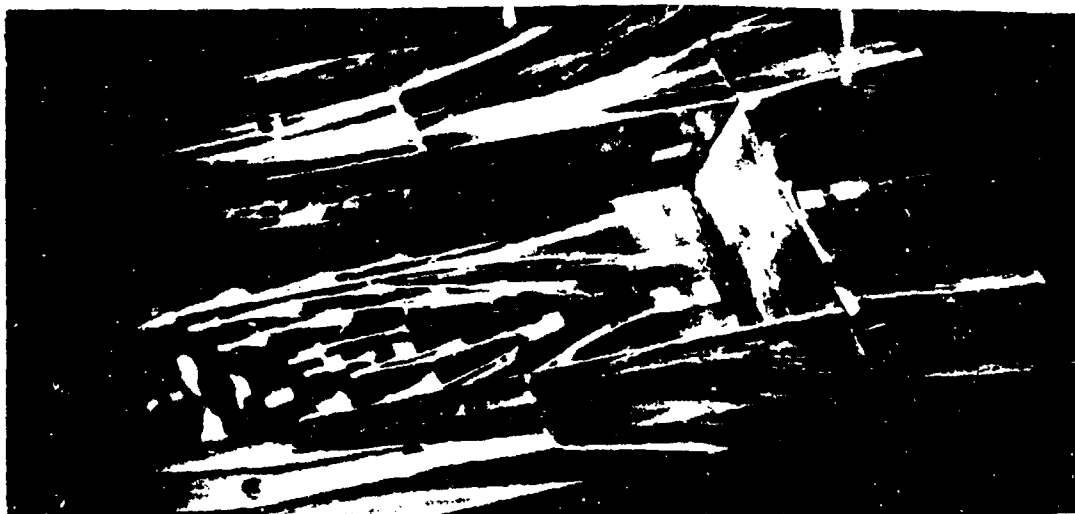


Figure 93 Oil Flow in  $L/D = 5.6$  Cavity at  $M_{\infty} = 1.5$ , Aft Portion

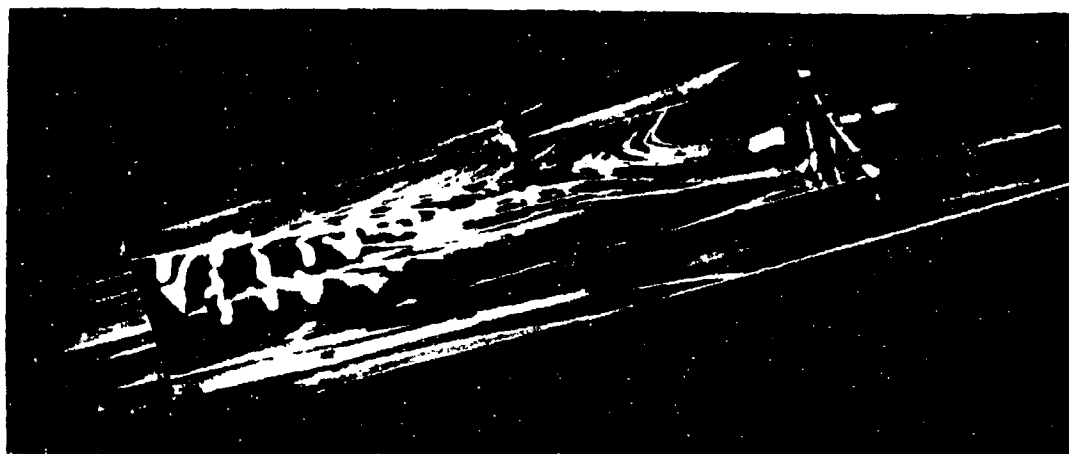


Figure 94 Oil Flow in  $L/D = 5.6$  Cavity at  $M_{\infty} = 1.5$ , Port Side

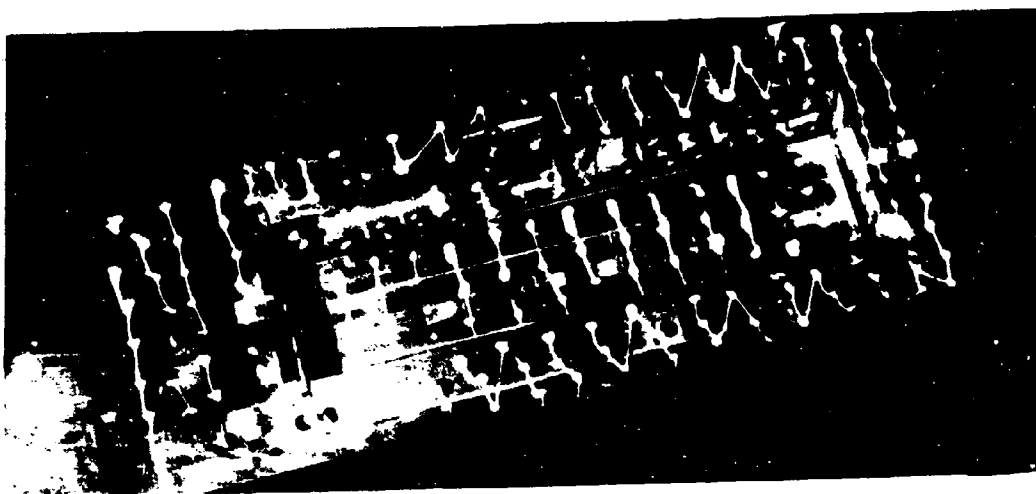


Figure 95 Oil Drop Pattern Prior to Test Run,  $L/D = 5.6$  Cavity with Perforated Fence



Figure 96 Oil Flow in  $L/D = 5.6$  Cavity, Perforated Fence Attached,  $M_\infty = 1.5$ , Ceiling



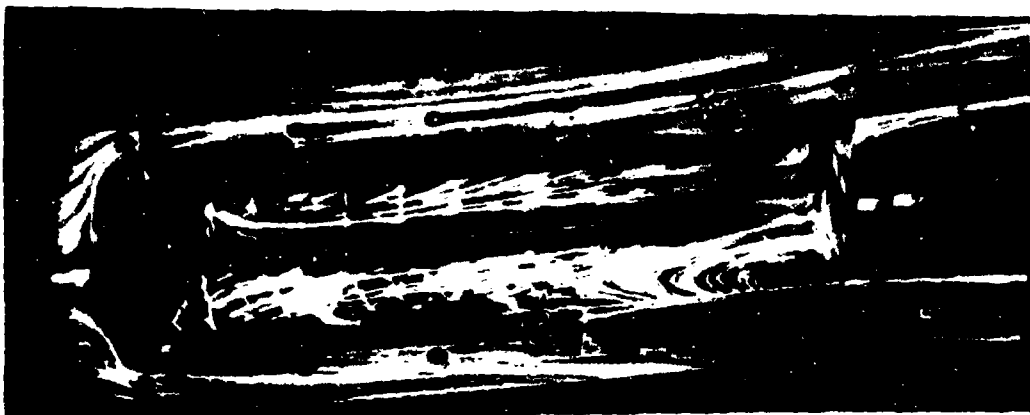


Figure 97 Oil Flow in  $L/D = 5.6$  Cavity, Perforated Fence Attached,  
 $M_{\infty} = 1.5$ , Starboard Side



Figure 98 Oil Flow in  $L/D = 5.6$  Cavity, Perforated Fence Attached,  
 $M_{\infty} = 1.5$ , Port Side

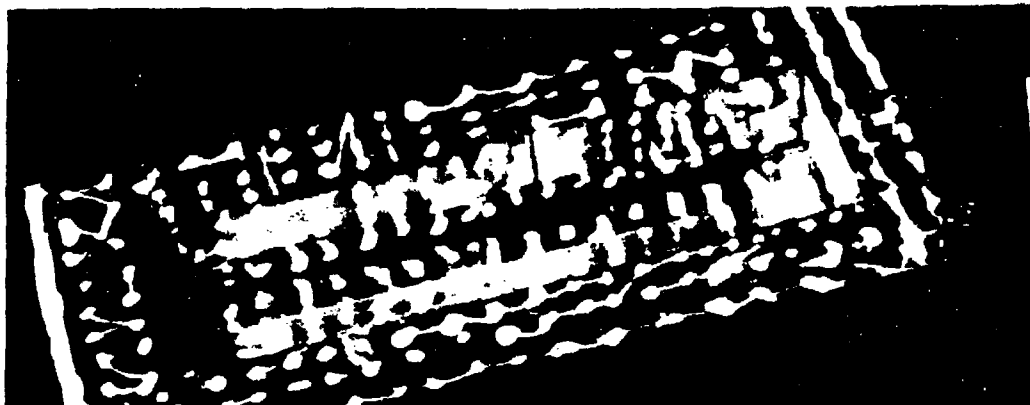


Figure 99 Oil Pattern Prior to Test Run;  $L/D = 5.6$  Cavity with Saw-Tooth Fence



Figure 100 Oil Flow in  $L/D = 5.6$  Cavity, Saw-Tooth Fence Attached,  
 $M_{\infty} = 1.5$ , Ceiling



Figure 101 Oil Flow in  $L/D = 5.6$  Cavity, Saw-Tooth Fence Attached,  
 $M_{\infty} = 1.5$ , Port Side



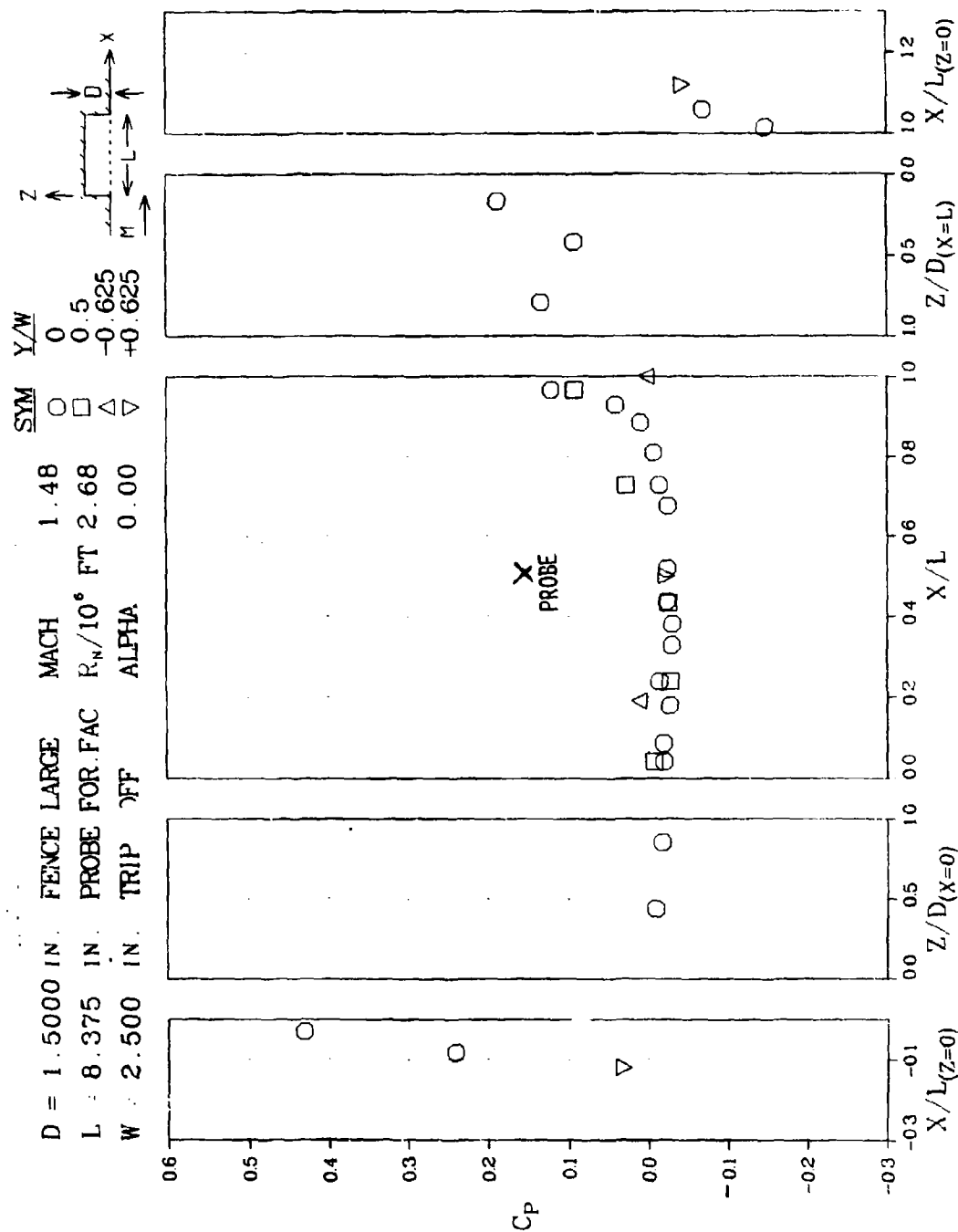


Figure 103 Pressure Coefficient Distributions for  $L/D = 5.6$  Cavity with Saw-Tooth Fence and Forward Facing Total Pressure Probe,  $M_\infty = 1.5$



Figure 104 Schlieren Flow Photograph,  $L/D = 5.6$  Cavity, Forward-Facing Total Pressure Probe,  $M_\infty = 1.5$



Figure 105 Schlieren Flow Photograph,  $L/D = 5.6$  Cavity, Saw-Tooth Fence and Forward-Facing Total Pressure Probe,  $M_\infty = 1.5$

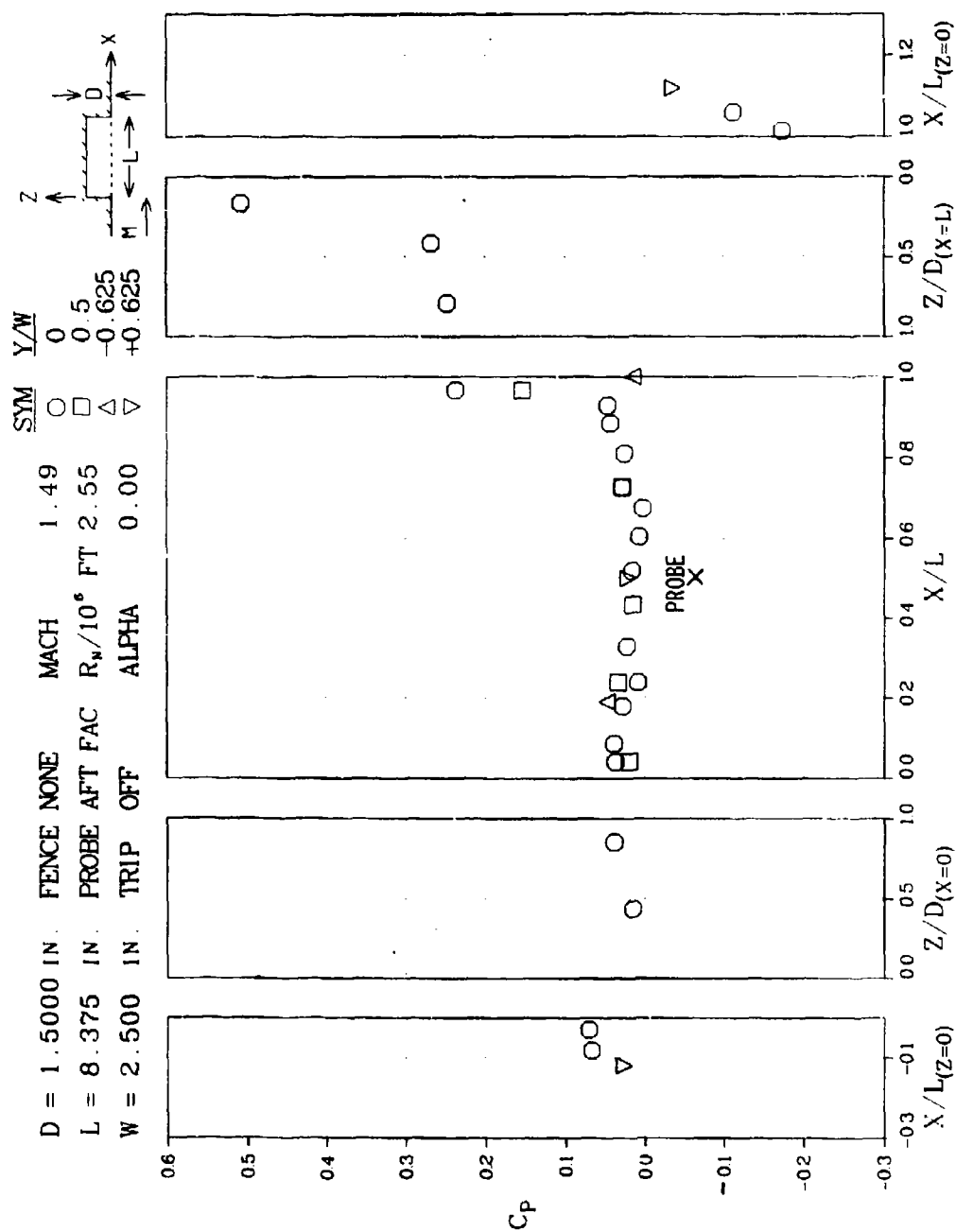


Figure 106 Pressure Coefficient Distributions for  $L/D = 5.6$  Cavity with Aft-Facing Total Pressure Probe,  $M_\infty = 1.5$ , Run 1

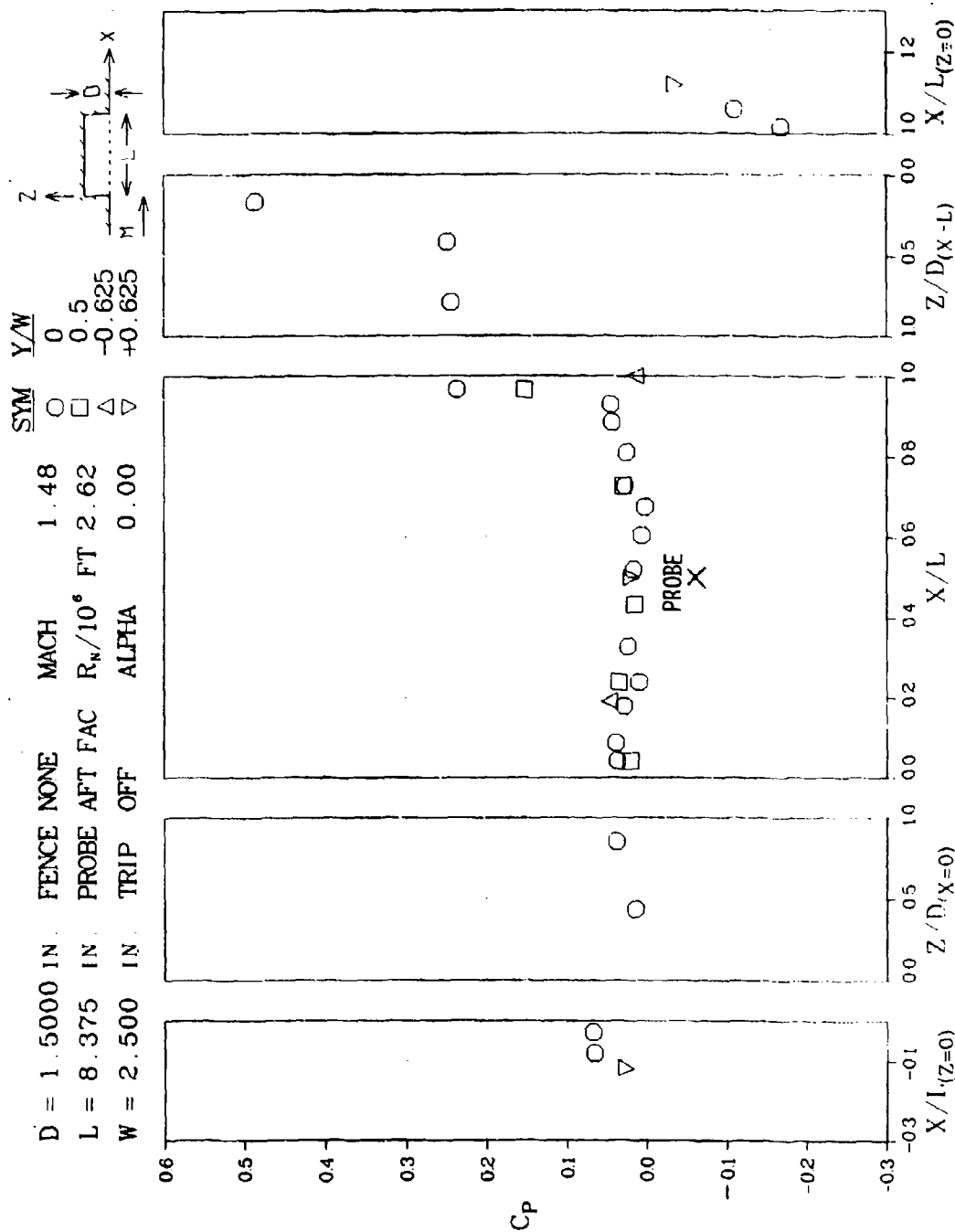


Figure 107 Pressure Coefficient Distributions for  $L/D = 5.6$  Cavity with Aft-Facing Total Pressure Probe,  $M_\infty = 1.5$ , Run 2

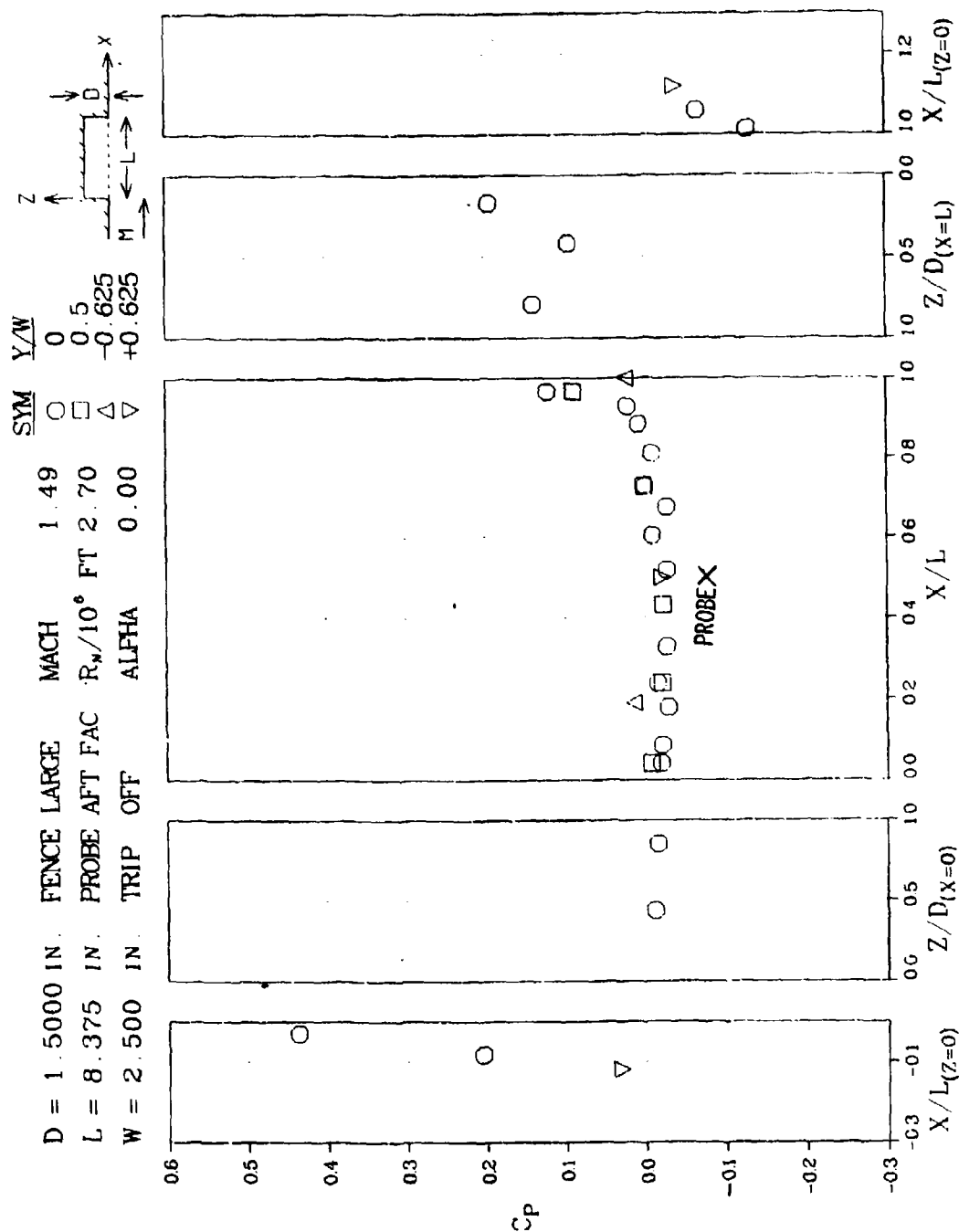


Figure 108 Pressure Coefficient Distributions for  $L/D = 5.6$  Cavity with Saw-Tooth Fence and Aft-Facing Total Pressure Probe,  $M_\infty = 1.5$





Figure 109 Schlieren Flow Photograph,  $L/D = 5.6$  Cavity with Saw-Tooth Fence and Aft-Facing Total Pressure Probe,  $M_\infty = 1.5$

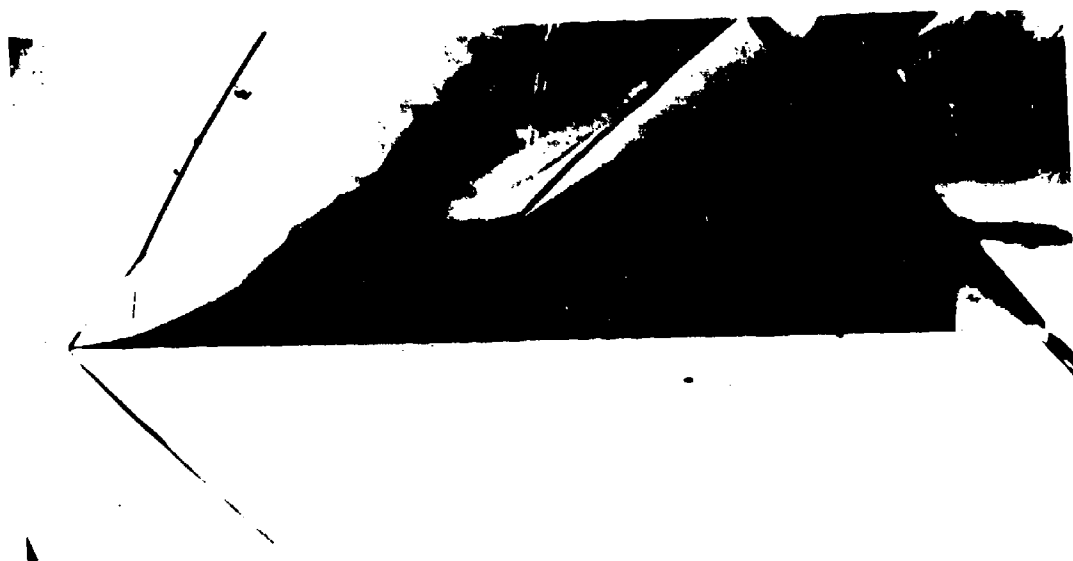


Figure 110 Schlieren Flow Photograph,  $L/D = 5.6$  Cavity with Aft-Facing Total Pressure Probe,  $M_\infty = 1.5$







Figure 113 Schlieren Flow Photograph,  $L/D = 6.2$  Cavity,  $M_{\infty} = 1.5$



Figure 114 Schlieren Flow Photograph,  $L/D = 6.2$  Cavity with Saw-Tooth Fence,  $M_{\infty} = 1.5$



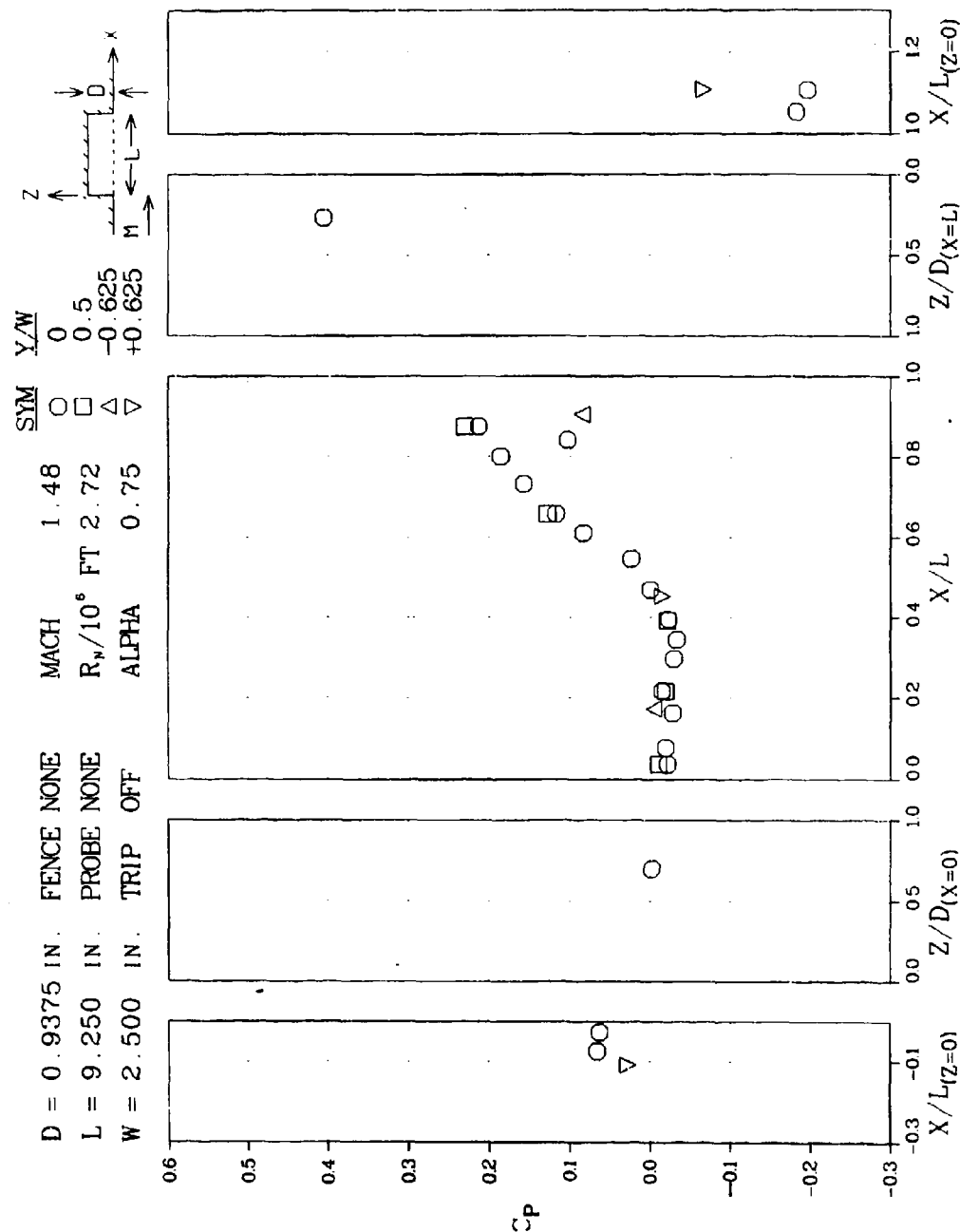
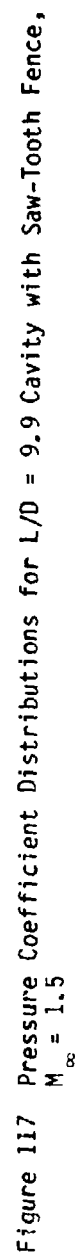


Figure 116 Pressure Coefficient Distributions for  $L/D = 9.9$  Cavity, Model Pitched Nose  
Up  $3/4^\circ$ ,  $M_\infty = 1.5$



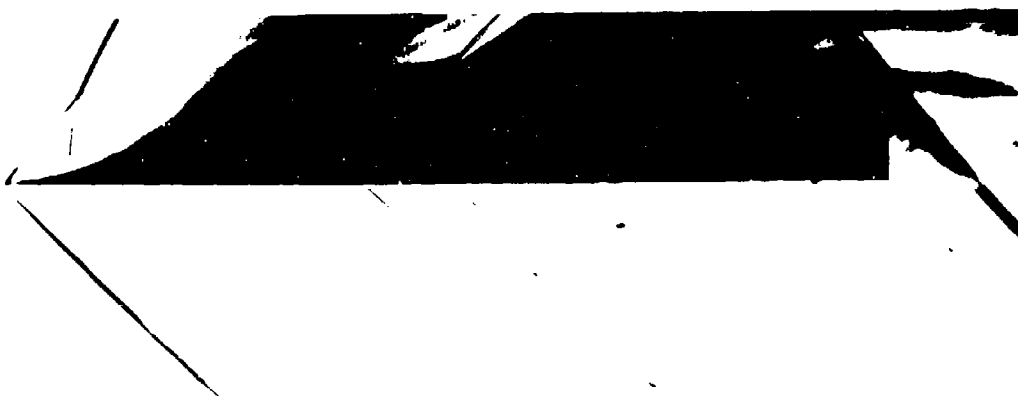


Figure 118 Schlieren Flow Photograph,  $L/D = 9.9$  Cavity,  $M_{\infty} = 1.5$



Figure 119 Schlieren Flow Photograph,  $L/D = 9.9$  Cavity, Model Pitched Nose  
Up  $3/4^{\circ}$   $M_{\infty} = 1.5$



Figure 120 Schlieren Flow Photograph,  $L/D = 9.9$  Cavity with Saw-Tooth Fence,  
 $M_{\infty} = 1.5$



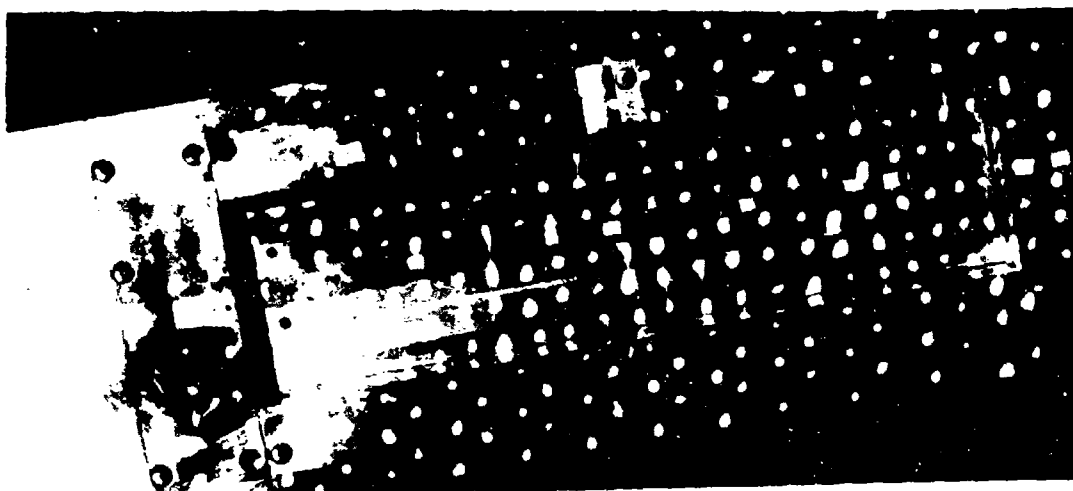


Figure 121 Oil Drop Pattern Prior to Test Run,  $L/D = 9.9$  Cavity

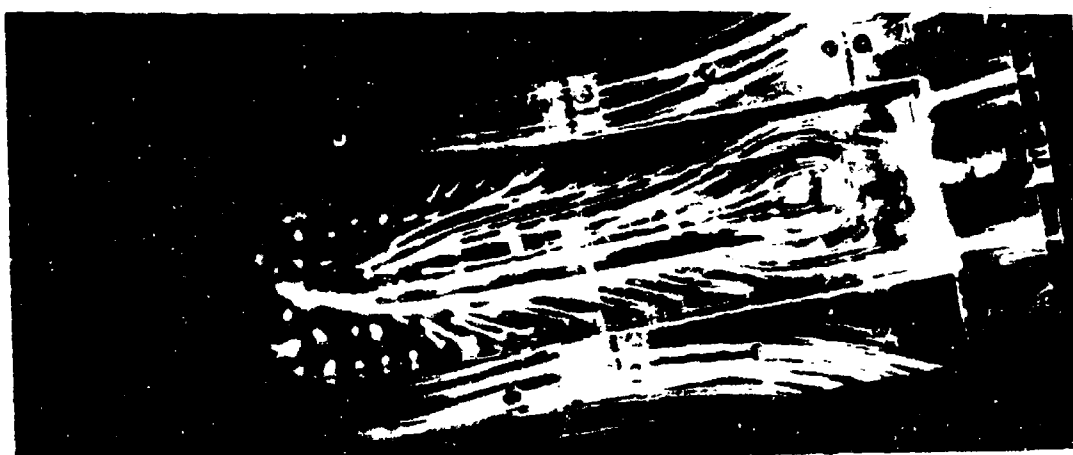


Figure 122 Oil Flow in  $L/D = 9.9$  Cavity,  $M_\infty = 1.5$ , Ceiling

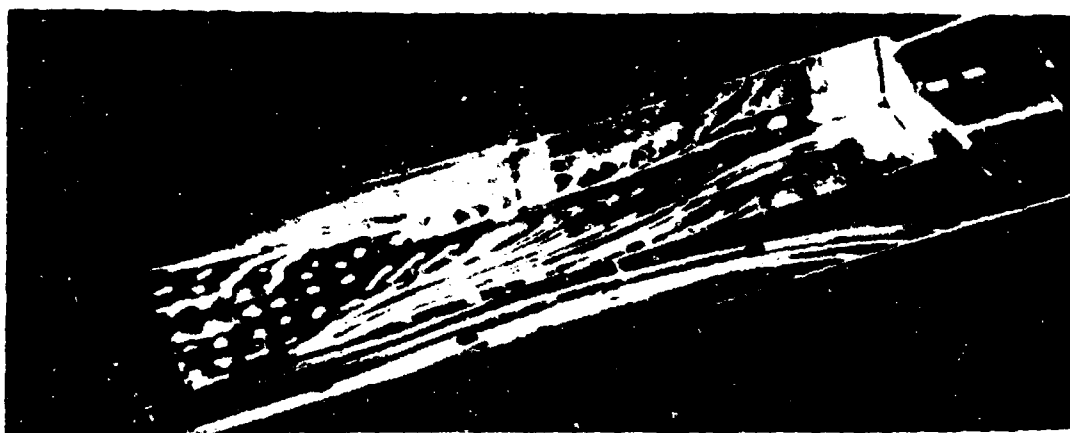


Figure 123 Oil Flow in  $L/D = 9.9$  Cavity,  $M_{\infty} = 1.5$ , Port Side



Figure 124 Oil Flow in  $L/D = 9.9$  Cavity,  $M_{\infty} = 1.5$ , Starboard Side

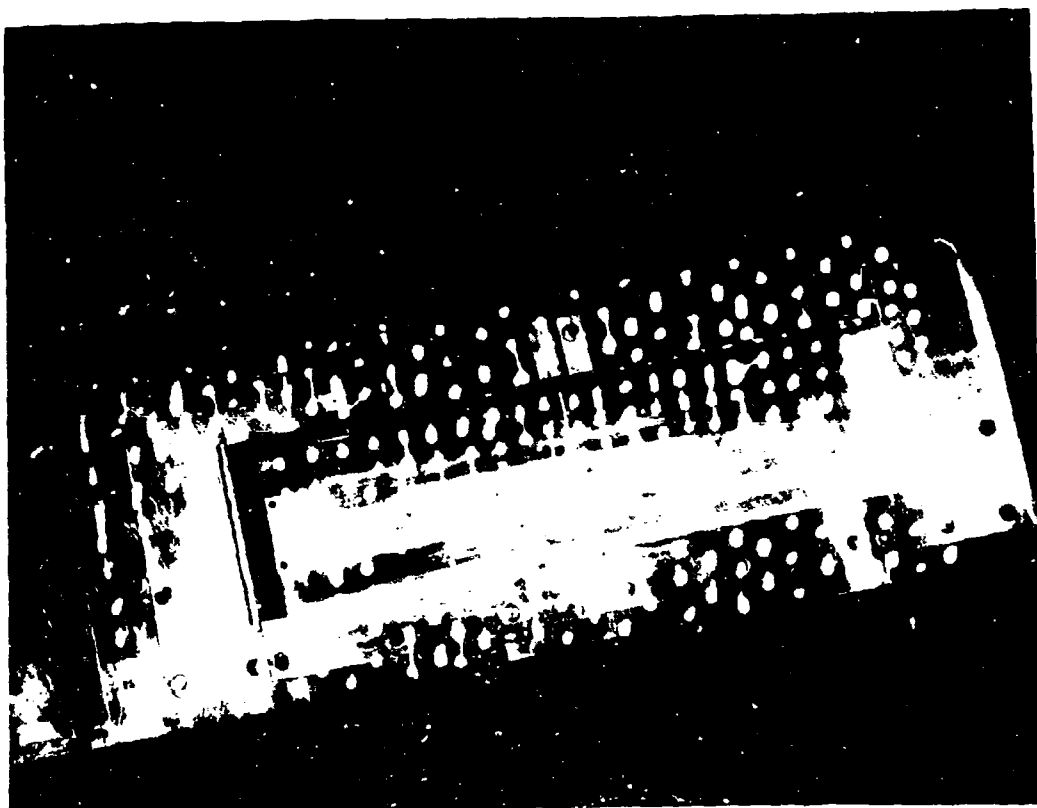


Figure 125 Oil Drop Pattern Prior to Test Run,  $L/D = 9.9$  Cavity, Perforated Fence Attached

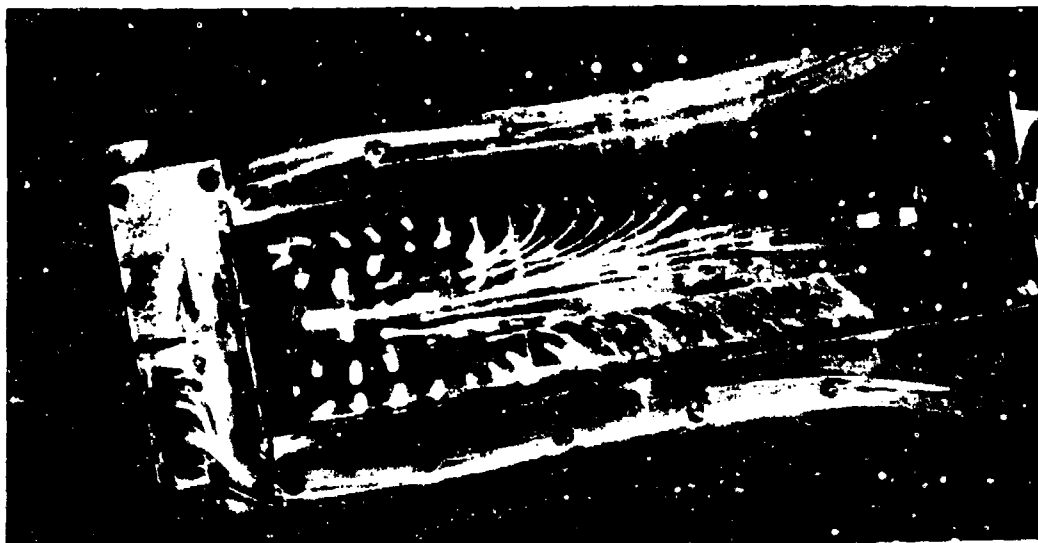


Figure 126 Oil Flow in  $L/D = 9.9$  Cavity, Perforated Fence Attached,  
 $M_{\infty} = 1.5$ , Ceiling

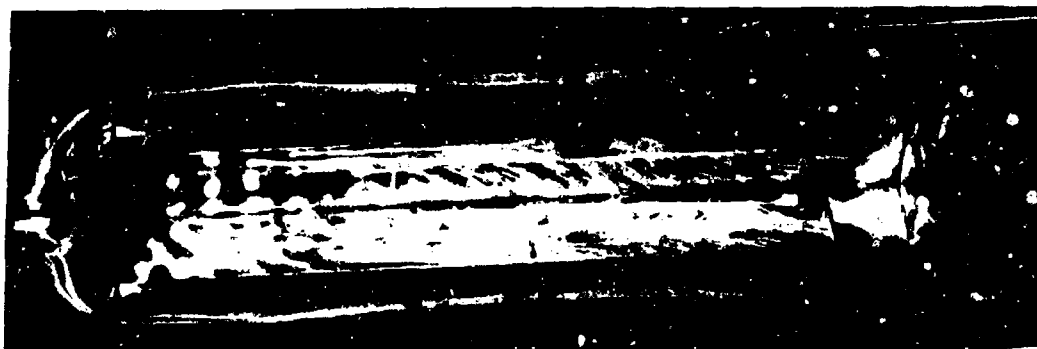


Figure 127 Oil Flow in  $L/D = 9.9$  Cavity, Perforated Fence Attached,  
 $M_{\infty} = 1.5$ , Starboard Side

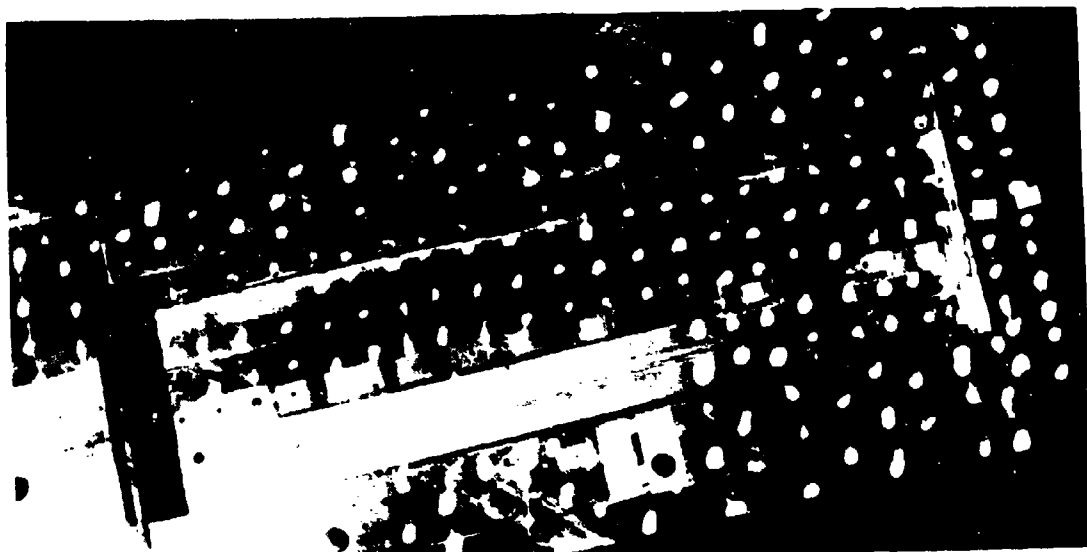


Figure 128 Oil Drop Pattern Prior to Test Run,  $L/D = 8.9$  Cavity, Perforated Fence Attached

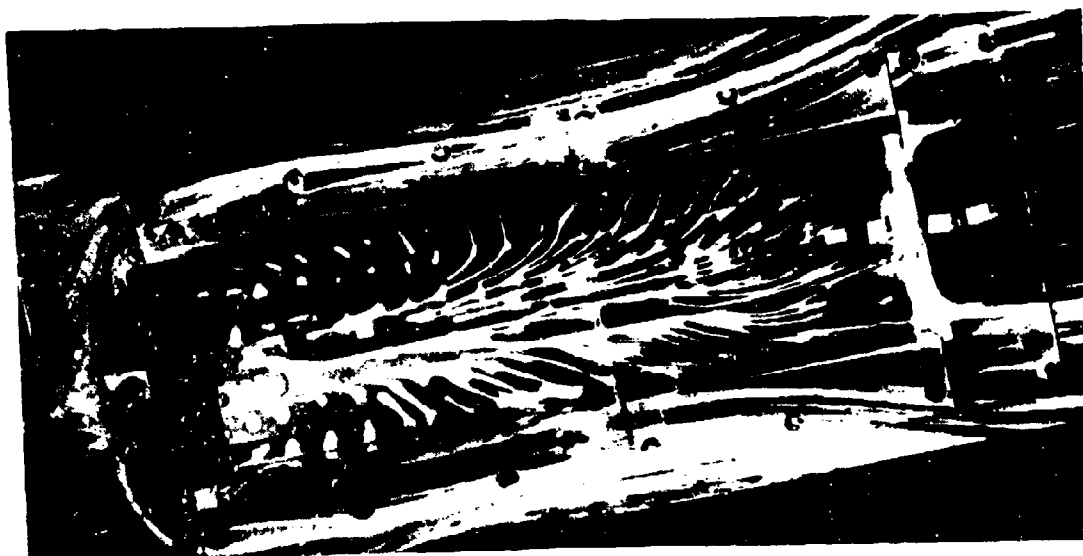


Figure 129 Oil Flow in  $L/D = 8.9$  Cavity, Perforated Fence Attached,  $M_\infty = 1.5$ , Ceiling



Figure 130 Oil Flow in  $L/D = 8.9$  Cavity, Perforated Fence Attached,  
 $M_{\infty} = 1.5$ , Starboard Side

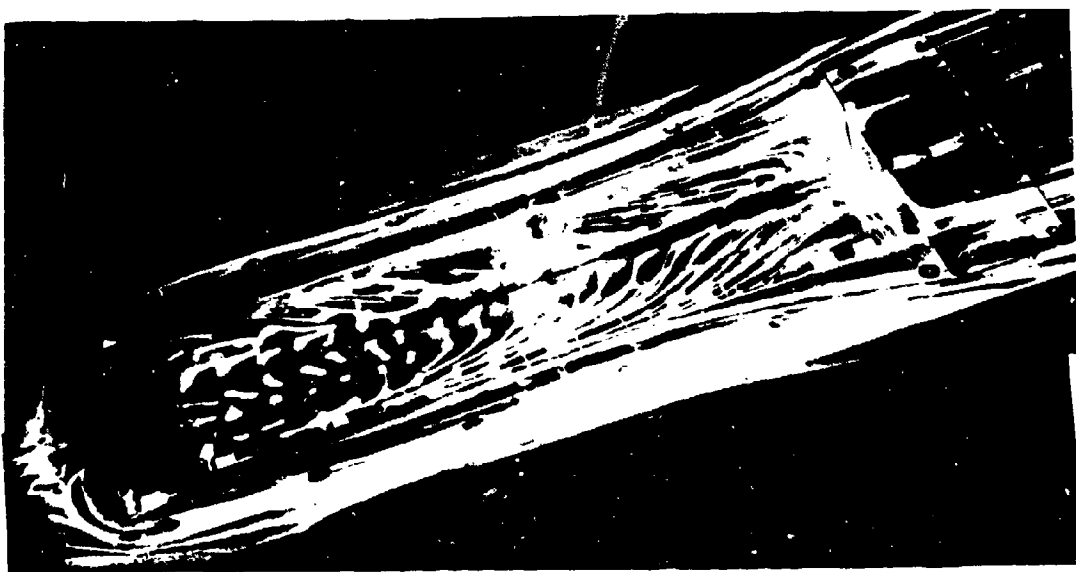


Figure 131 Oil Flow in  $L/D = 8.9$  Cavity, Perforated Fence Attached,  
 $M_{\infty} = 1.5$ , Port Side

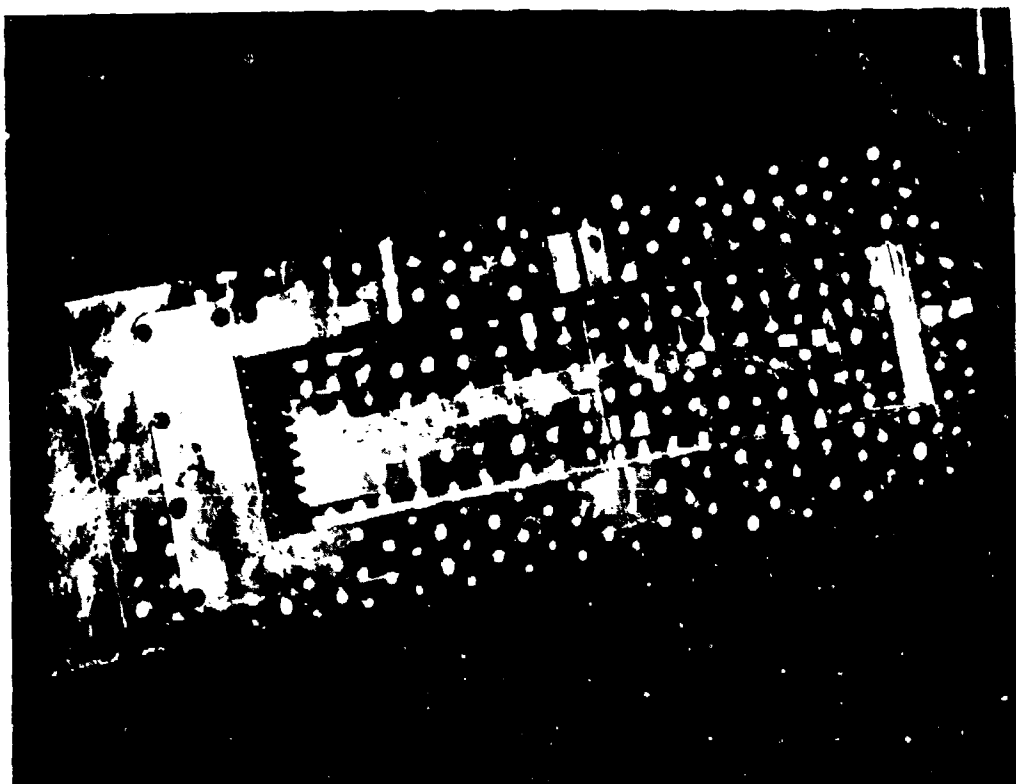


Figure 132 Oil Drop Pattern Prior to Test Run,  $L/D = 9.0$  Cavity,  
Saw-Tooth Fence Attached.



Figure 133 Oil Flow in  $L/D = 9.9$  Cavity, Saw-Tooth Fence Attached,  
 $M_{\infty} = 1.5$ , Ceiling



Figure 134 Oil Flow in  $L/D = 9.9$  Cavity, Saw-Tooth Fence Attached,  
 $M_{\infty} = 1.5$ , Port Side



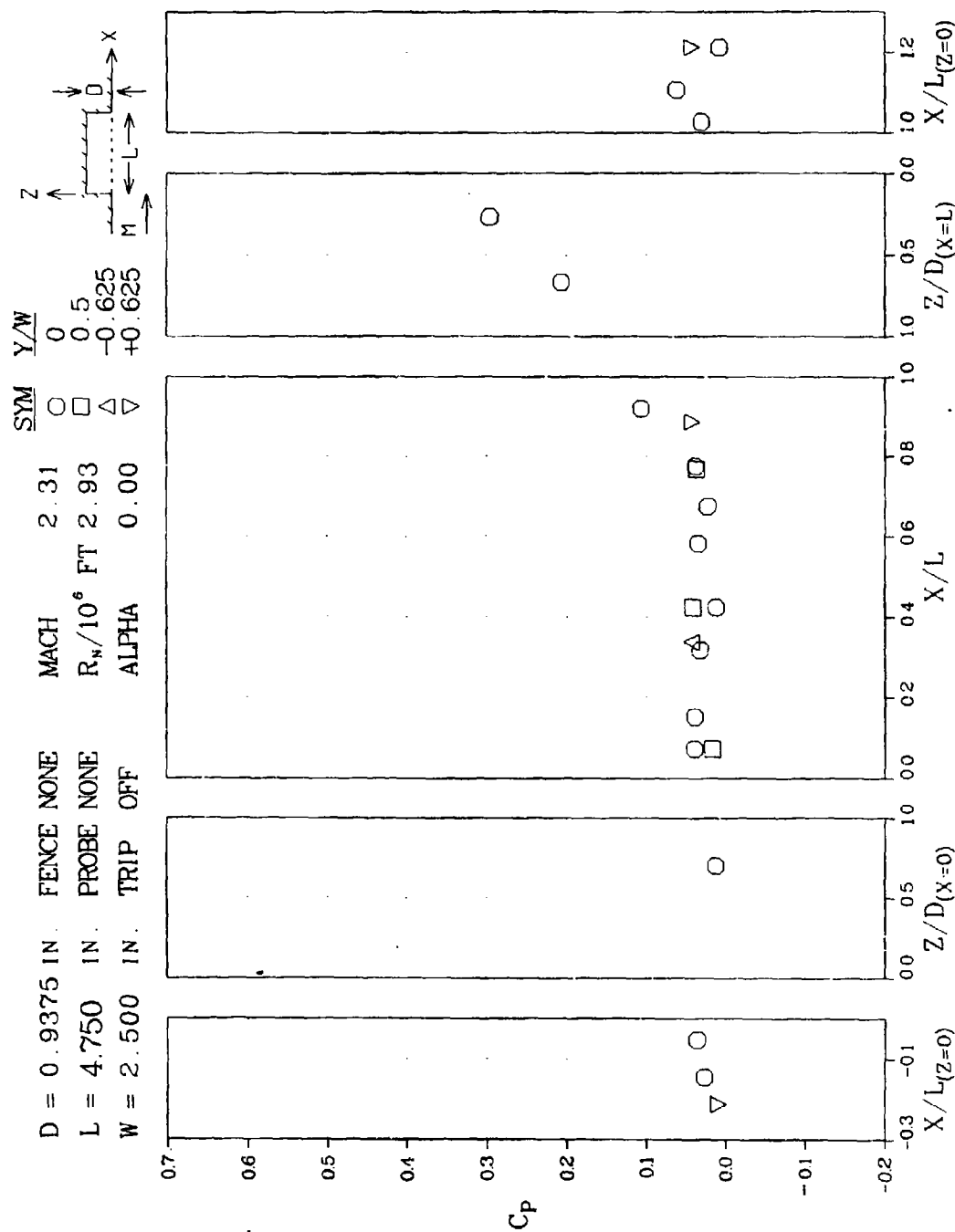


Figure 135 Pressure Coefficient Distributions for  $L/D = 5.1$  Cavity,  $M_\infty = 2.3$ ,  
 $Re/10^6 = 2.9$

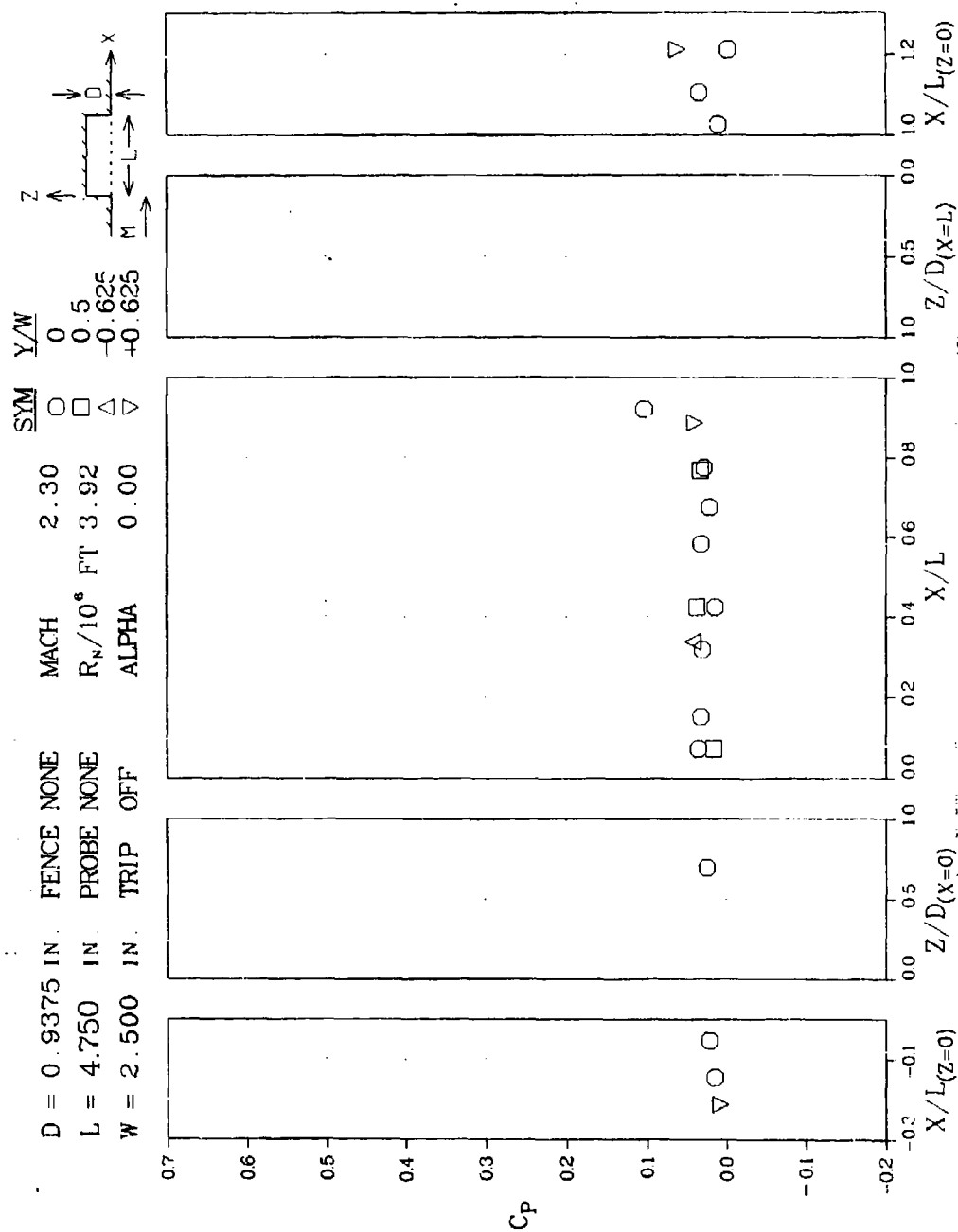


Figure 136 Pressure Coefficient Distributions for  $L/D = 5.1$  Cavity,  $M_\infty = 2.3$ ,  $Re/10^6 = 3.9$

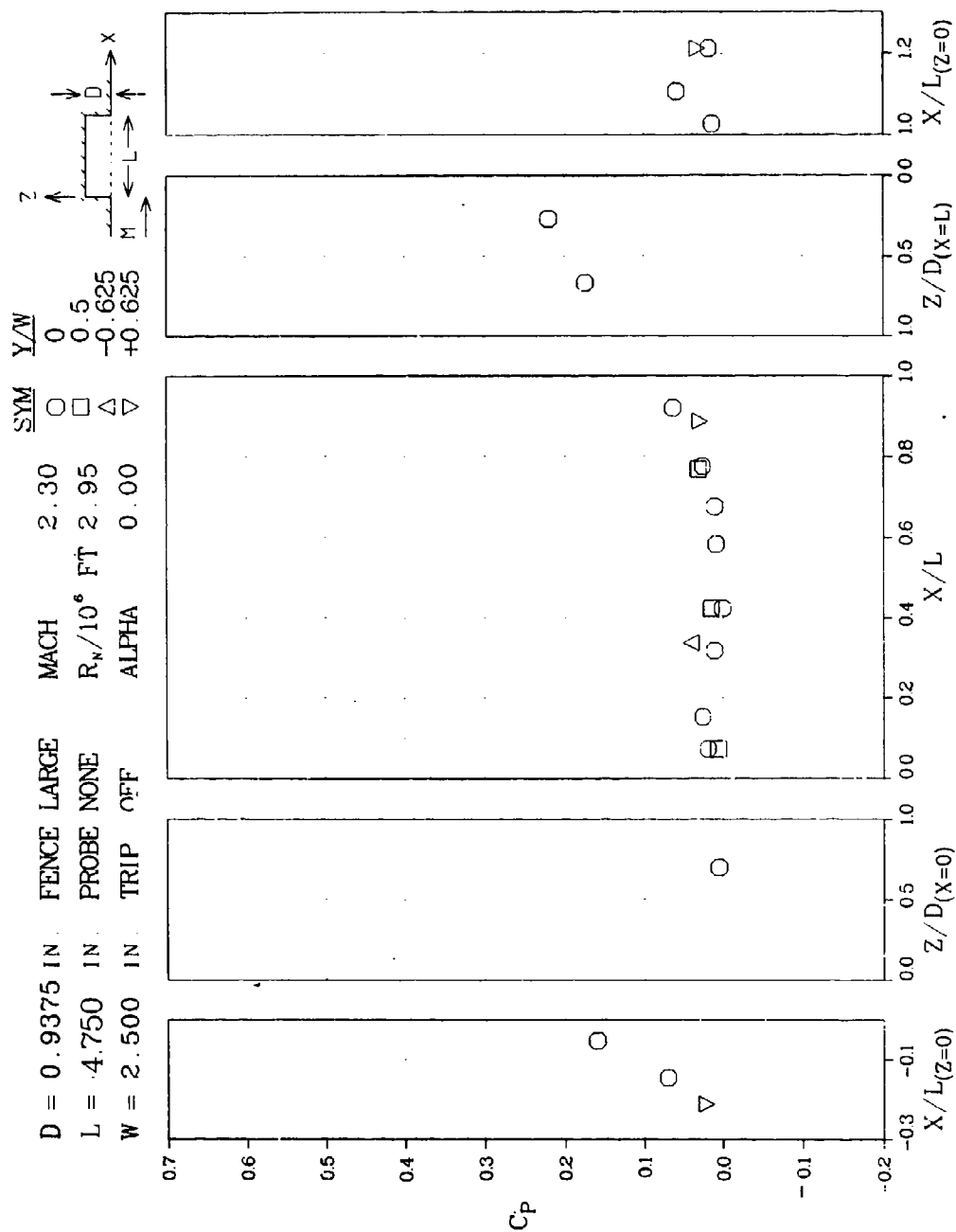
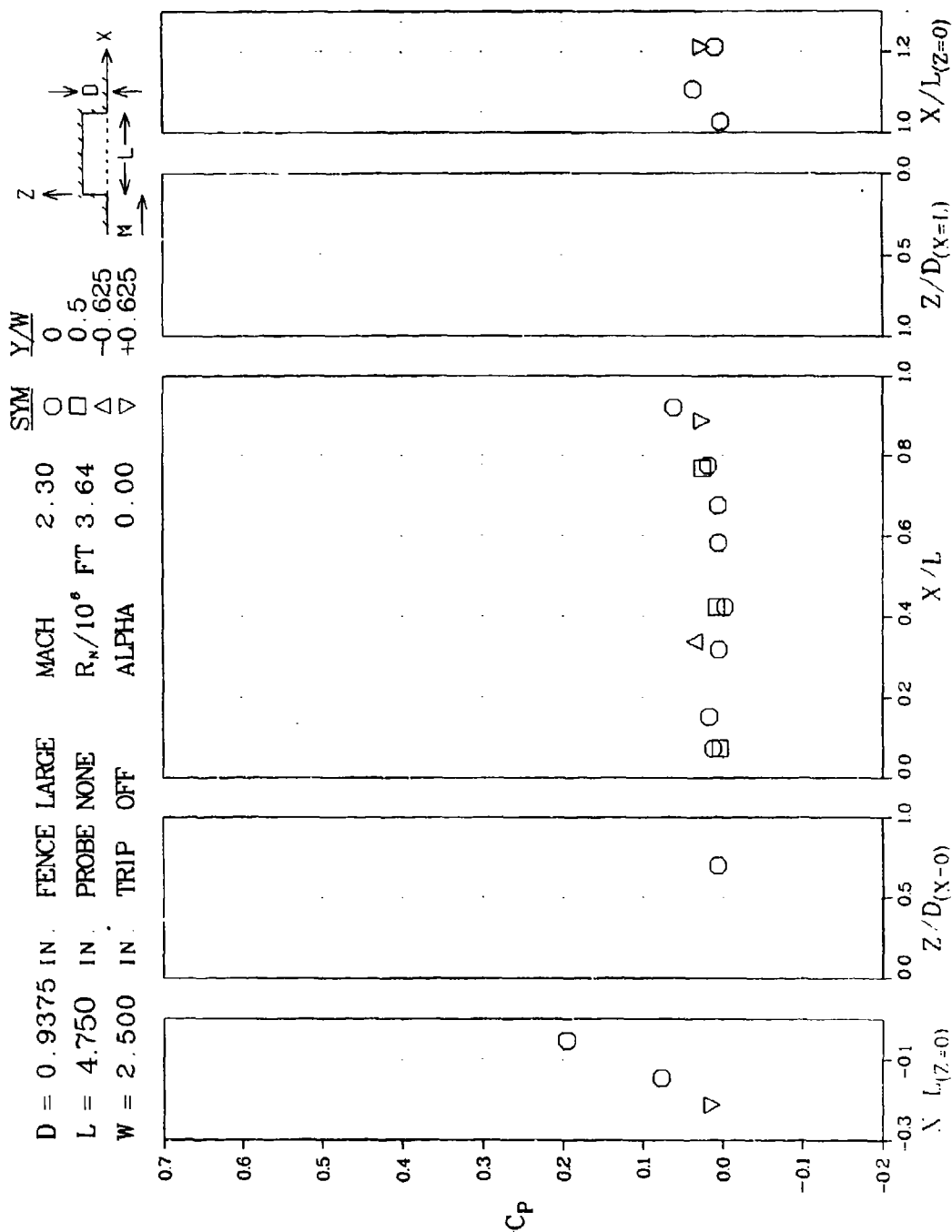


Figure 137 Pressure Coefficient Distributions for  $L/D = 5.1$  Cavity with Saw-Tooth Fence,  
 $M_\infty = 2.3$ ,  $Re/10^6 = 3.0$



1331-001P

Figure 138 Pressure Coefficient Distributions for  $L/D = 5.1$  Cavity with Saw-Tooth Fence,  $M_\infty = 2.3$ ,  $Re/10^6 = 3.6$



Figure 139 Schlieren Flow Photograph,  $L/D = 5.1$  Cavity,  $M_\infty = 2.3$ ,  
 $Re/10^6 = 2.9$



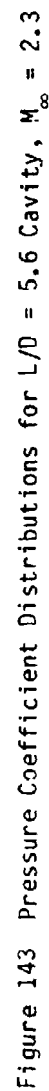
Figure 140 Schlieren Flow Photograph,  $L/D = 5.1$  Cavity,  $M_\infty = 2.3$ ,  
 $Re/10^6 = 3.9$

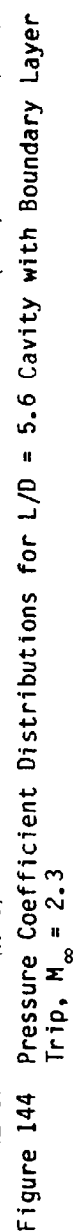


Figure 141 Schlieren Flow Photograph,  $L/D = 5.1$  Cavity with Saw-Tooth Fence,  
 $M_{\infty} = 2.3$ ,  $Re/10^6 = 3.0$

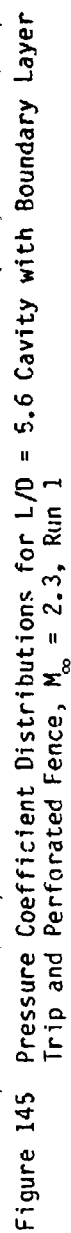


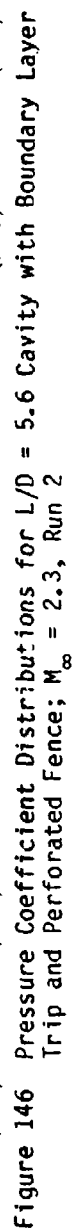
Figure 142 Schlieren Flow Photograph,  $L/D = 5.1$  Cavity with Saw-Tooth Fence,  
 $M_{\infty} = 2.3$ ,  $Re/10^6 = 3.6$













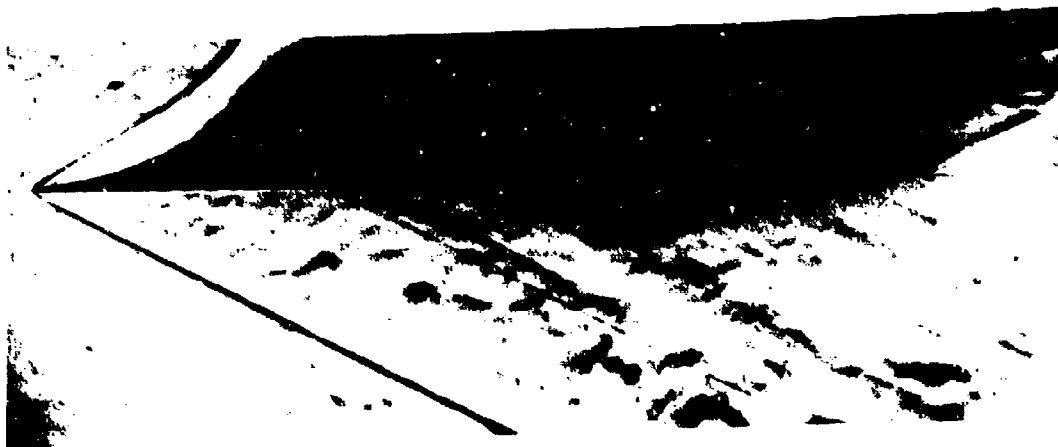


Figure 148 Schlieren Flow Photograph,  $L/D = 5.6$  Cavity,  $M_{\infty} = 2.3$



Figure 149 Schlieren Flow Photograph,  $L/D = 5.6$  Cavity with Boundary Layer Trip,  $M_{\infty} = 2.3$



Figure 150 Schlieren Flow Photograph,  $L/D = 5.6$  Cavity with Boundary Layer Trip and Perforated Fence,  $M_\infty = 2.3$ , Run 1



Figure 151 Schlieren Flow Photograph,  $L/D = 5.6$  Cavity with Boundary Layer Trip and Perforated Fence,  $M_\infty = 2.3$ , Run 2

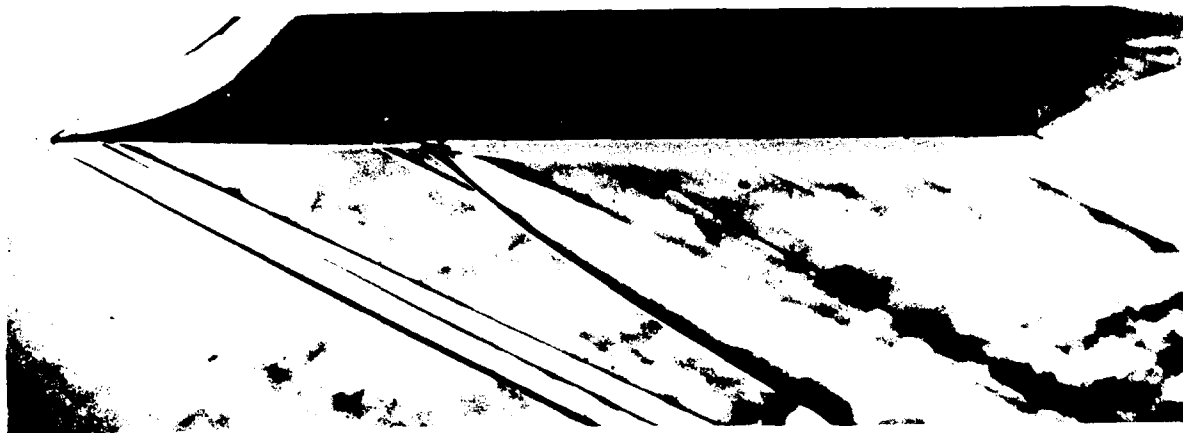


Figure 152 Schlieren Flow Photograph,  $L/D = 5.6$  Cavity with Boundary Layer Trip and Saw Tooth Fence,  $M_\infty = 2.3$

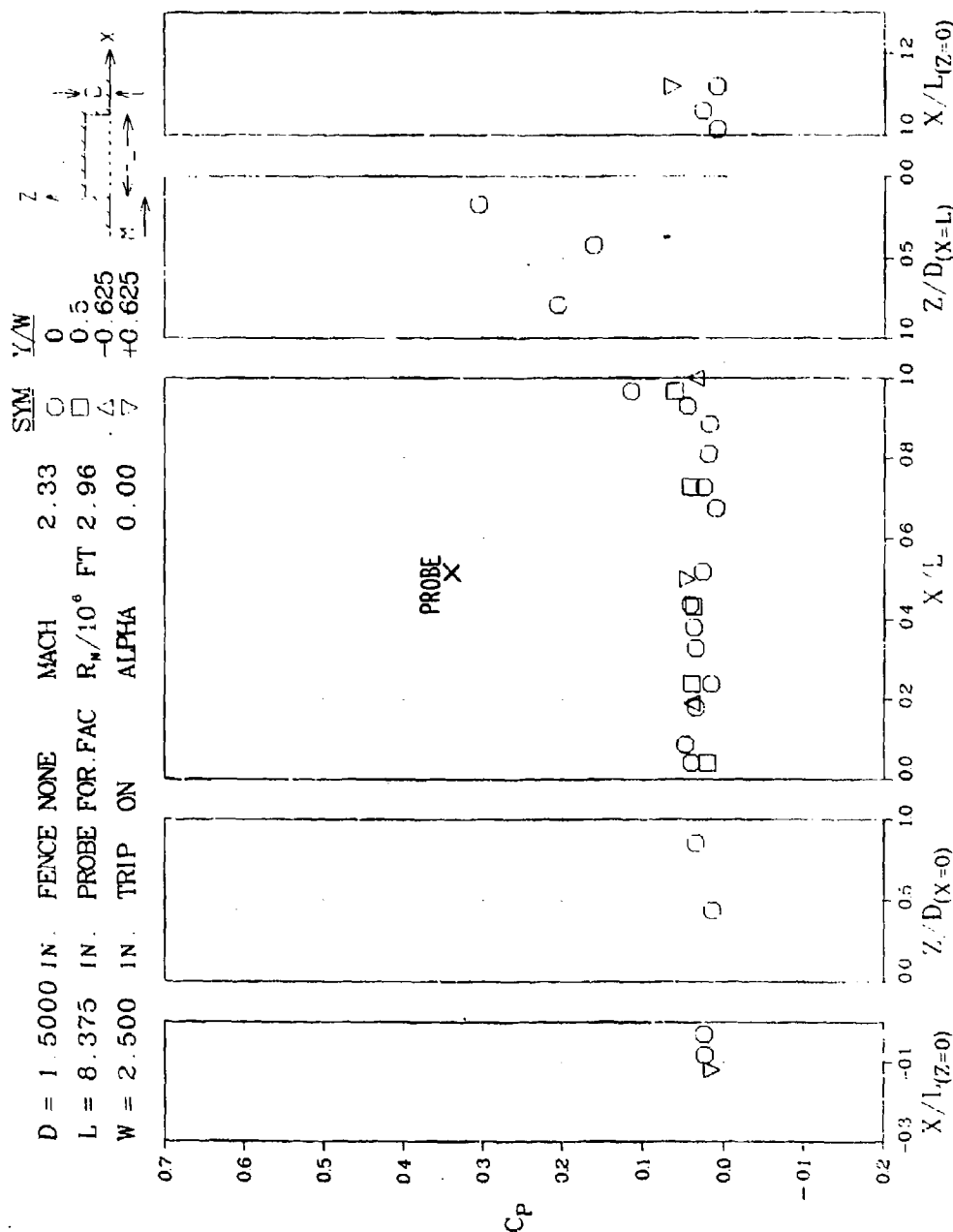


Figure 153 Pressure Coefficient Distributions for  $L/D = 5.6$  Cavity with Boundary Layer Trip and Forward Facing Probe,  $M_\infty = 2.3$

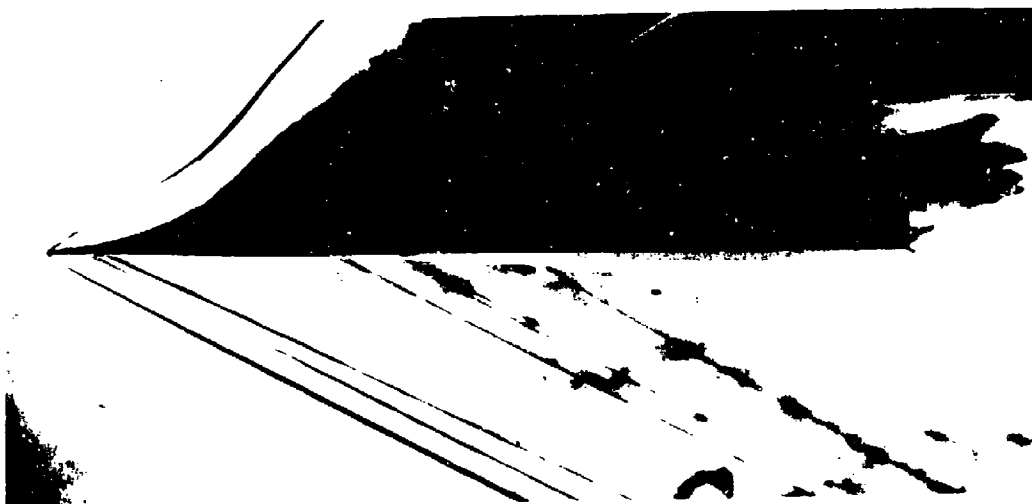


Figure 154 Schlieren Flow Photograph,  $L/D = 5.6$  Cavity with Boundary Layer Trip and Forward Facing Probe,  $M_\infty = 2.3$





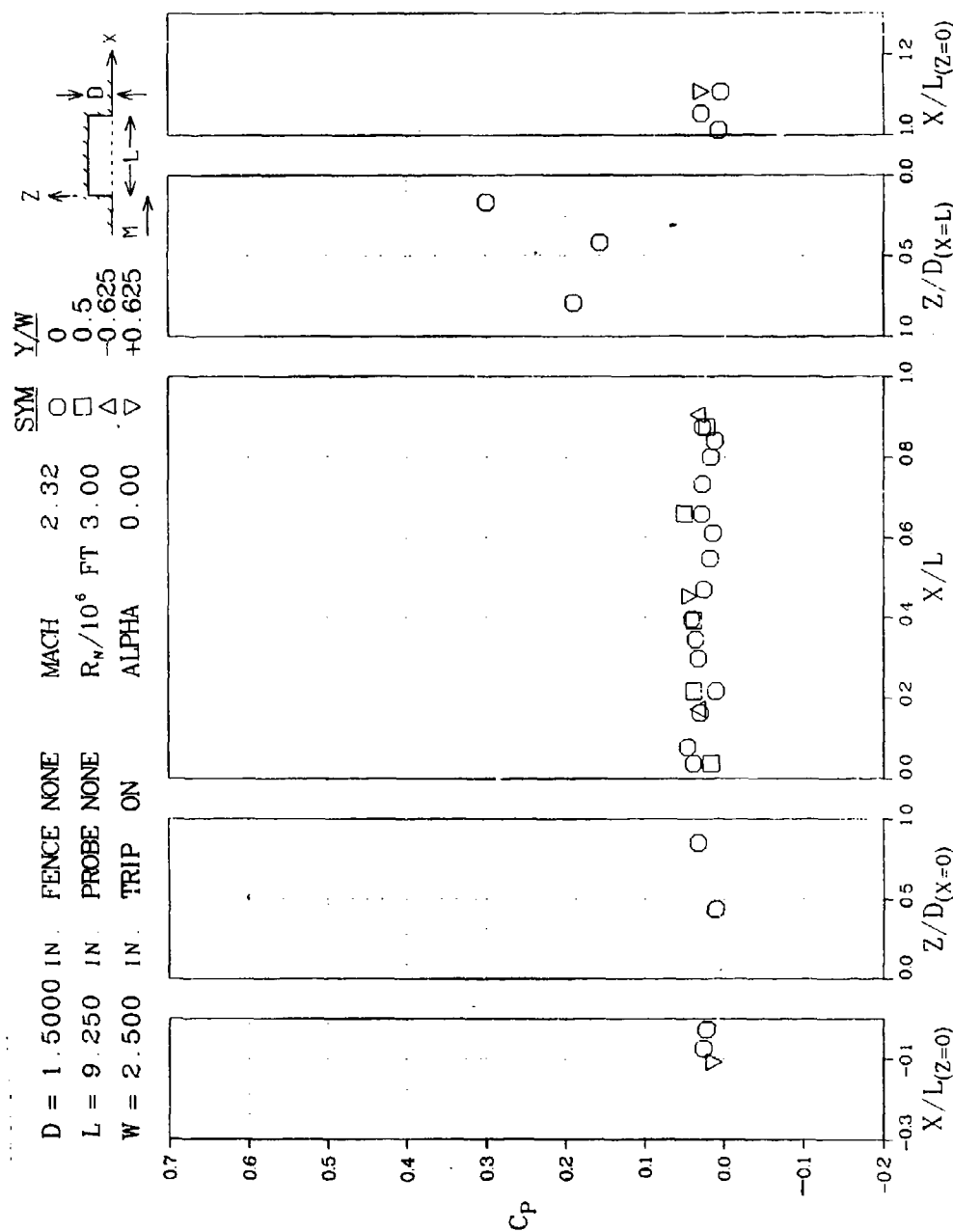


Figure 156 Pressure Coefficient Distributions for  $L/D = 6.2$  Cavity with Boundary Layer Trip,  $M_\infty = 2.3$

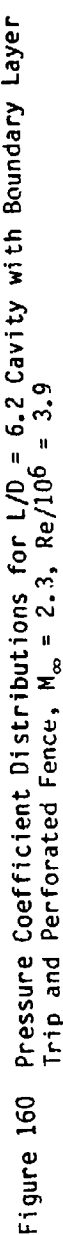


Figure 157 Schlieren Flow Photograph,  $L/D = 6.2$  Cavity,  $M_\infty = 2.3$



Figure 158 Schlieren Flow Photograph,  $L/D = 6.2$  Cavity with Boundary Layer Trip,  $M_\infty = 2.3$





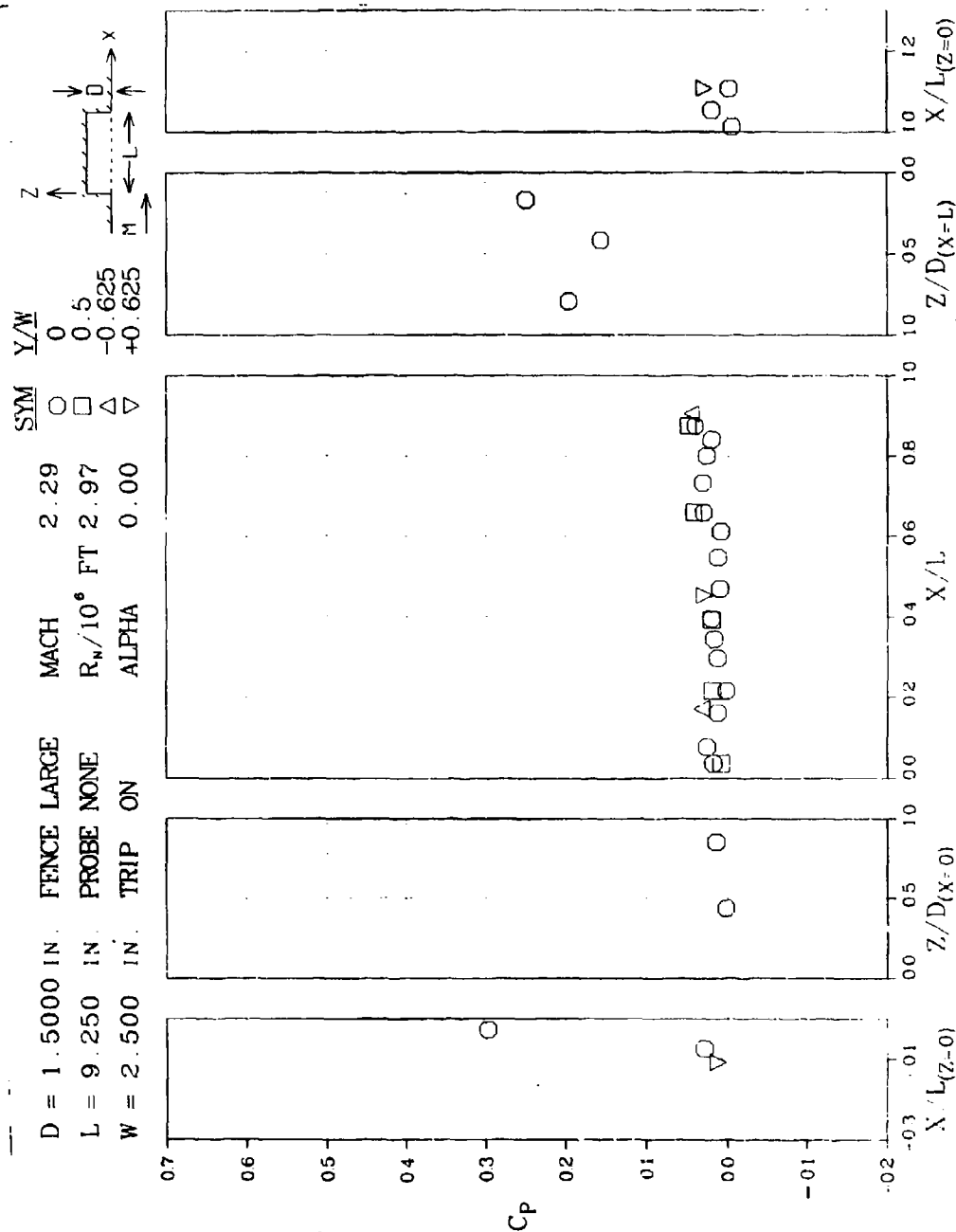


Figure 161 Pressure Coefficient Distributions for  $L/D = 6.2$  Cavity with Boundary Layer Trip and Saw-Tooth Fence,  $M_\infty = 2.3$

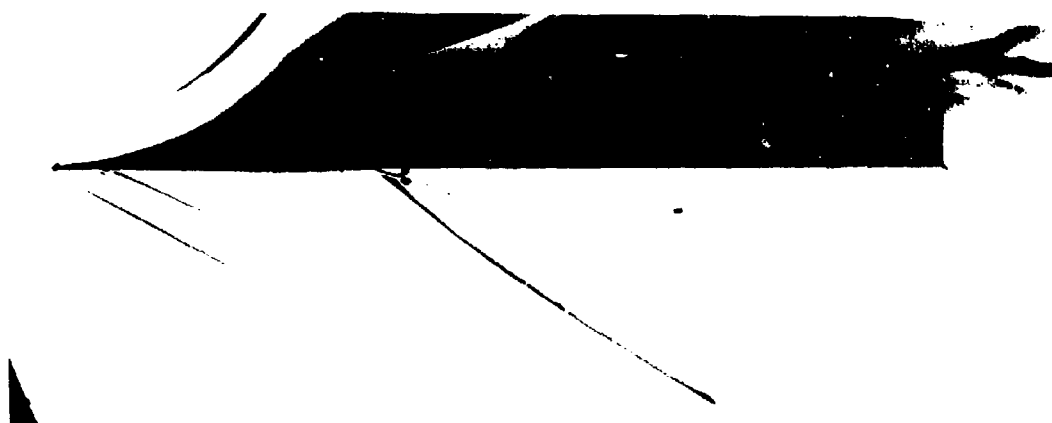


Figure 162 Schlieren Flow Photograph,  $L/D = 6.2$  Cavity with Boundary Layer Trip and Perforated Fence,  $M_\infty = 2.3$ ,  $Re/10^6 = 2.9$



Figure 163 Schlieren Flow Photograph,  $L/D = 6.2$  Cavity with Boundary Layer Trip and Perforated Fence,  $M_\infty = 2.3$ ,  $Re/10^6 = 3.9$

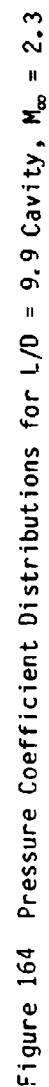








Figure 166 Schlieren Flow Photograph,  $L/D = 9.9$  Cavity,  $M_{\infty} = 2.3$



Figure 167 Schlieren Flow Photograph,  $L/D = 9.9$  Cavity with Boundary Layer Trip,  $M_{\infty} = 2.3$

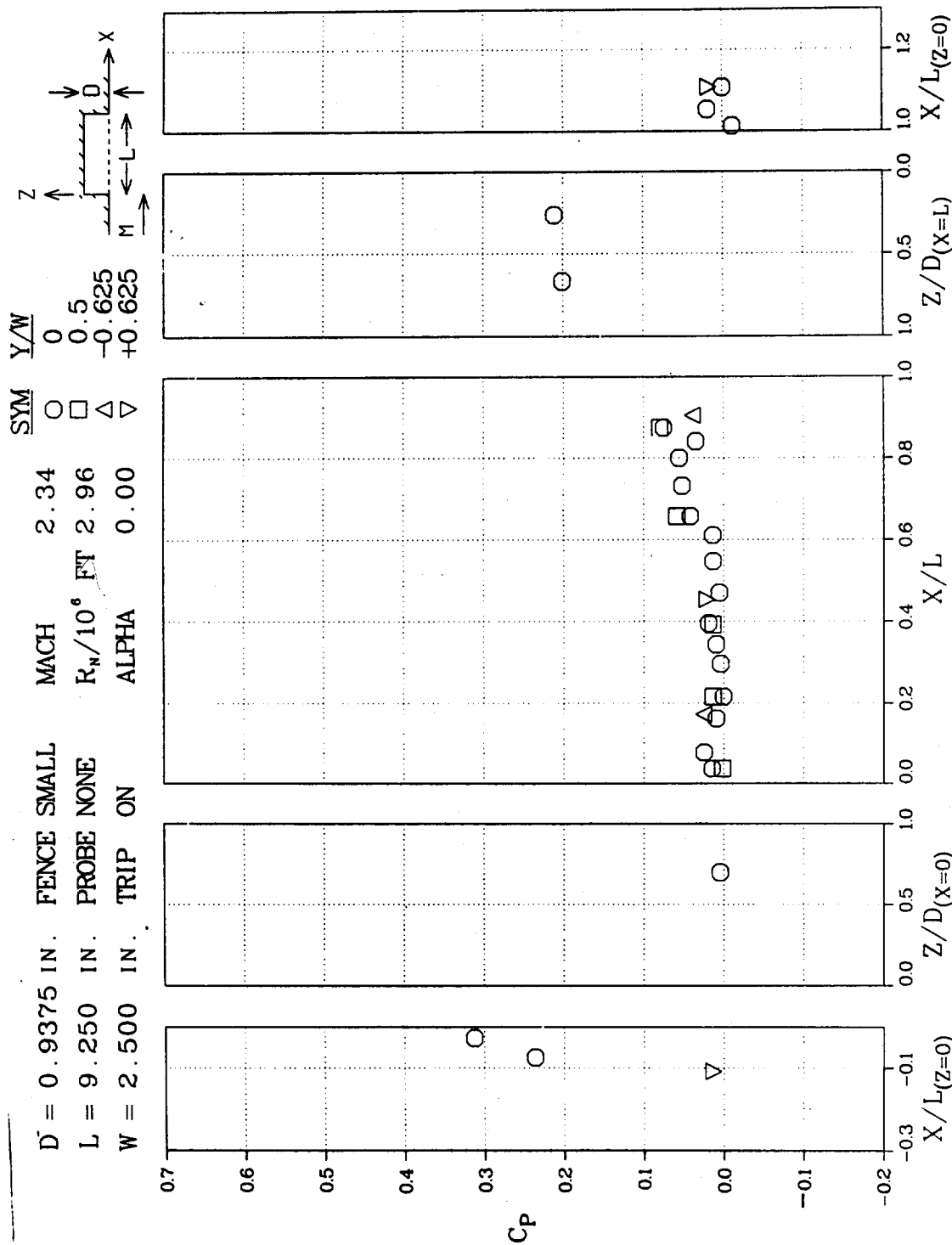


Figure 168 Pressure Coefficient Distributions for  $L/D = 9.9$  Cavity with Boundary Layer Trip and Perforated Fence,  $M_\infty = 2.3$

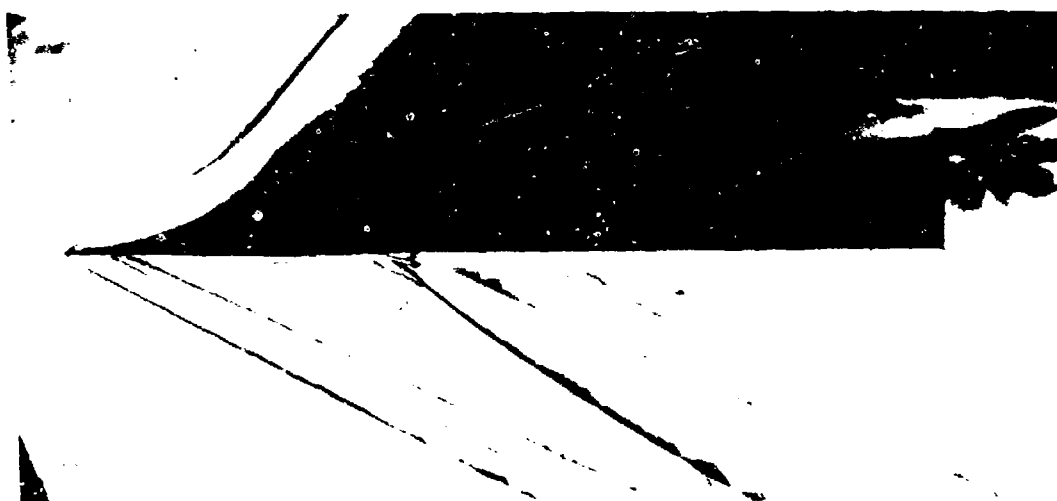


Figure 169 Schlieren Flow Photograph,  $L/D = 9.9$  Cavity with  
Boundary Layer Trip and Perforated Fence,  $M_{\infty} = 2.3$

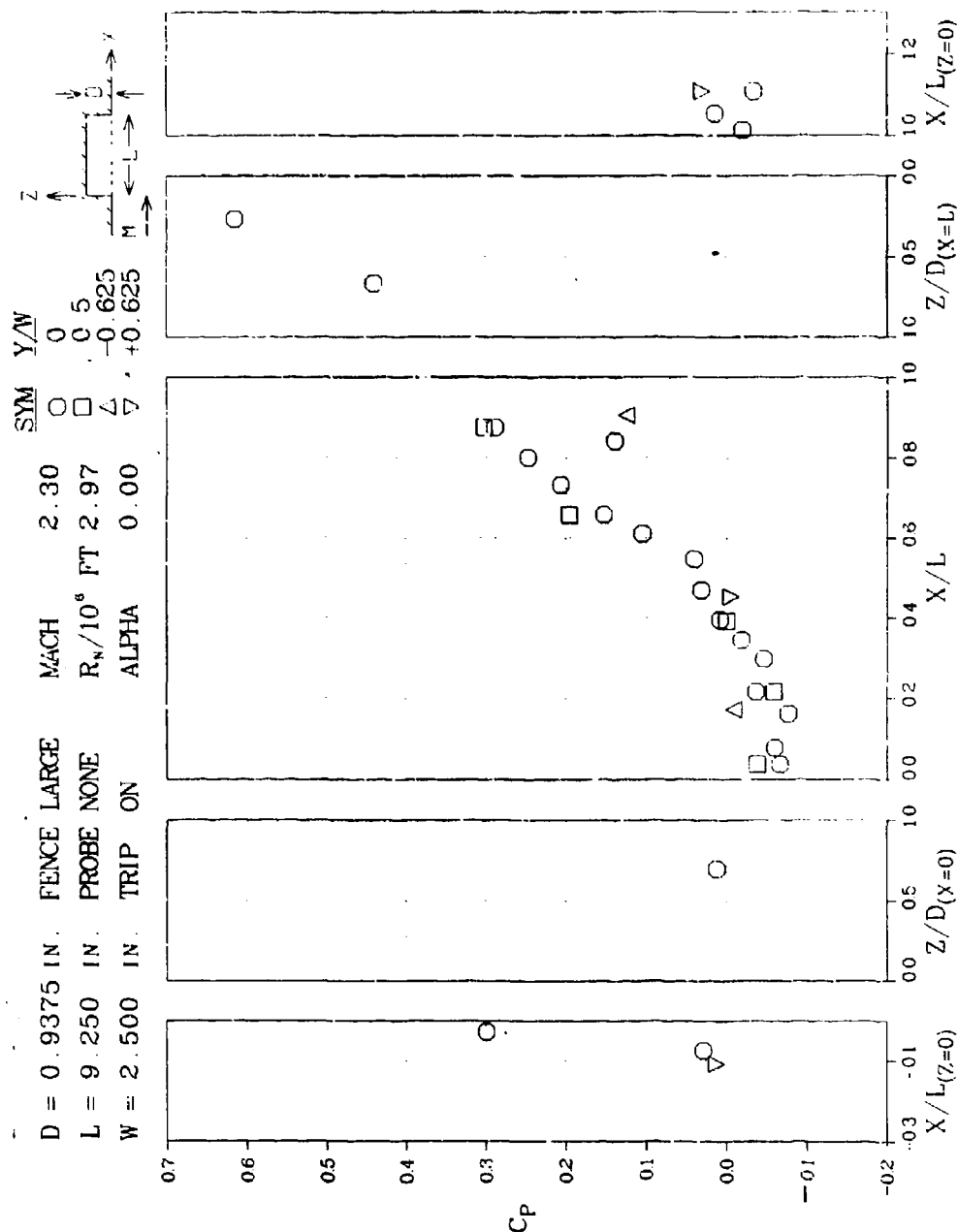


Figure 170 Pressure Coefficient Distributions for  $L/D = 9.9$  Cavity with Boundary Layer Trip and Saw-Tooth Fence,  $M_\infty = 2.3$ , Run 1

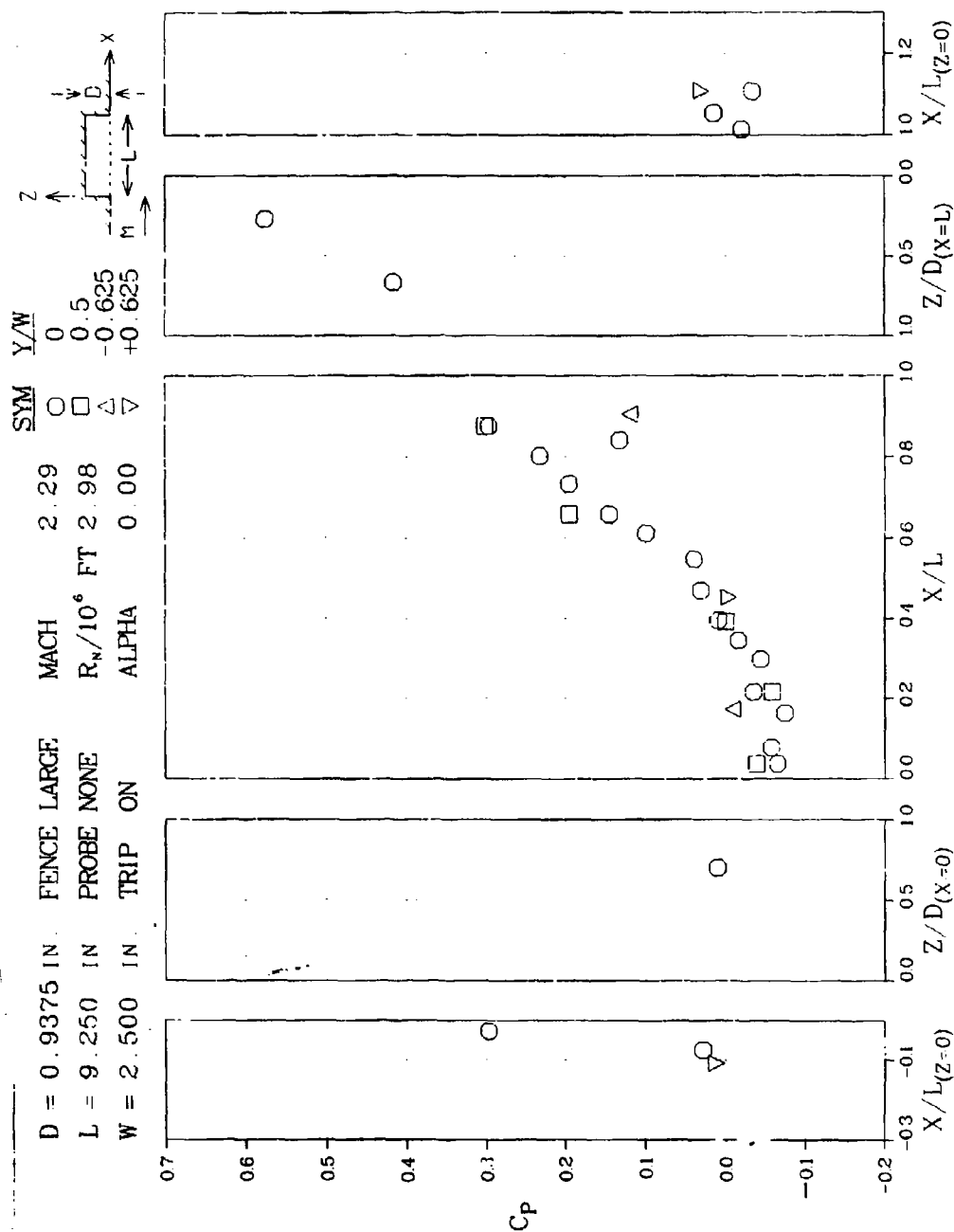


Figure 171 Pressure Coefficient Distributions for  $L/D = 9.9$  Cavity with Boundary Layer Trip and Saw-Tooth Fence,  $M_\infty = 2.3$ , Run 2

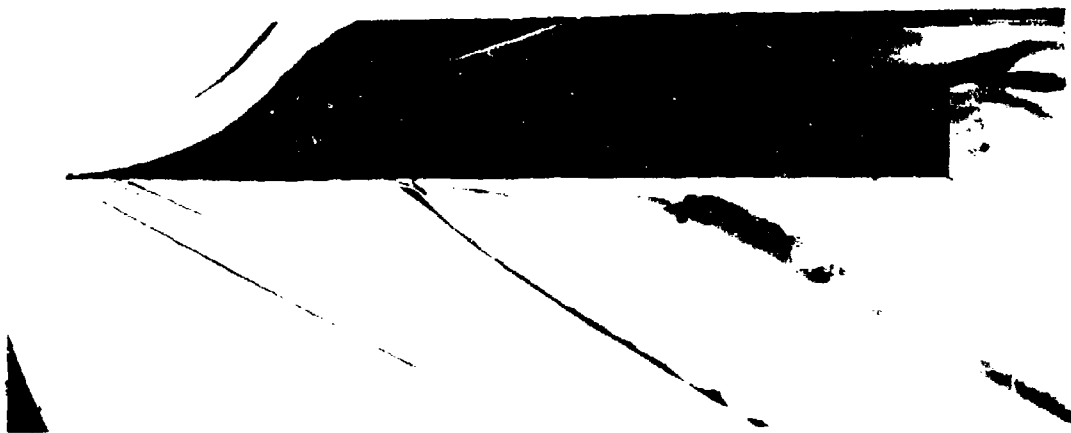


Figure 172 Schlieren Flow Photograph,  $L/D = 9.9$  Cavity with Boundary Layer Trip and Saw-Tooth Fence,  $M_\infty = 2.3$ , Time T1

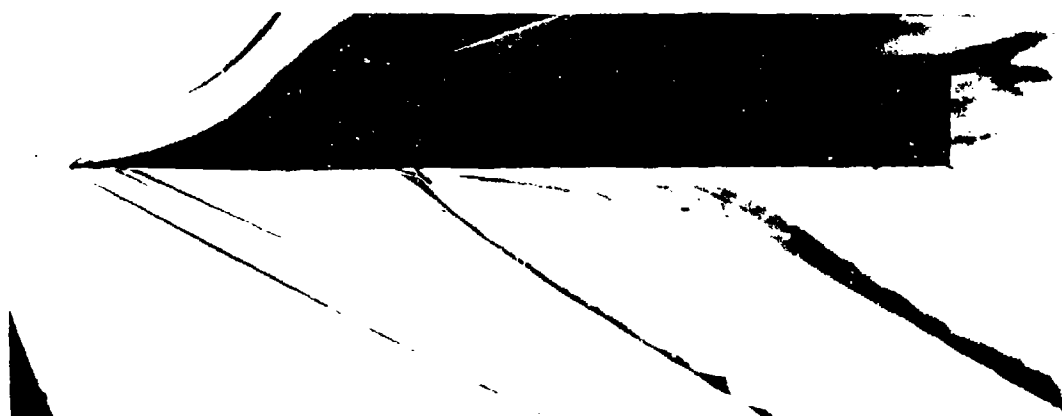


Figure 173 Schlieren Flow Photograph,  $L/D = 9.9$  Cavity with Boundary Layer Trip and Saw-Tooth Fence,  $M_\infty = 2.3$ , Time T2



Figure 174 Schlieren Flow Photograph,  $L/D = 9.9$  Cavity with Boundary Layer Trip and Saw-Tooth Fence,  $M_\infty = 2.3$ , Time T3

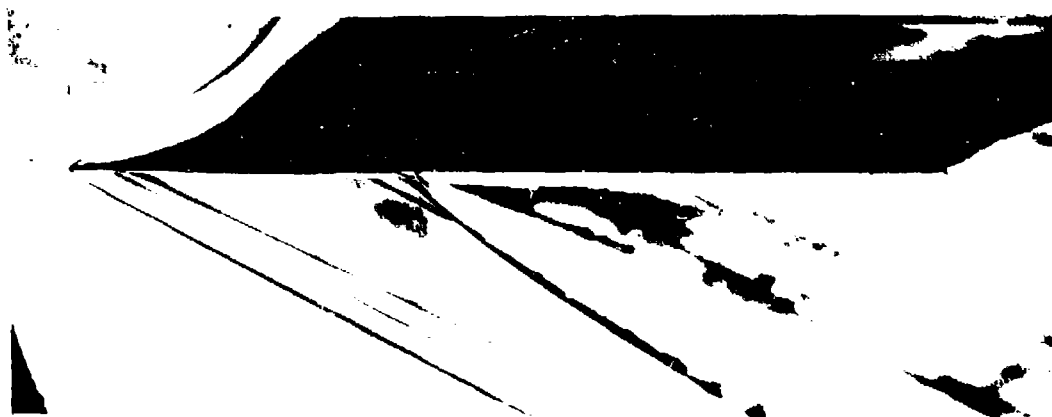


Figure 175 Schlieren Flow Photograph,  $L/D = 9.9$  Cavity with Boundary Layer Trip and Saw-Tooth Fence,  $M_\infty = 2.3$ , Time T4

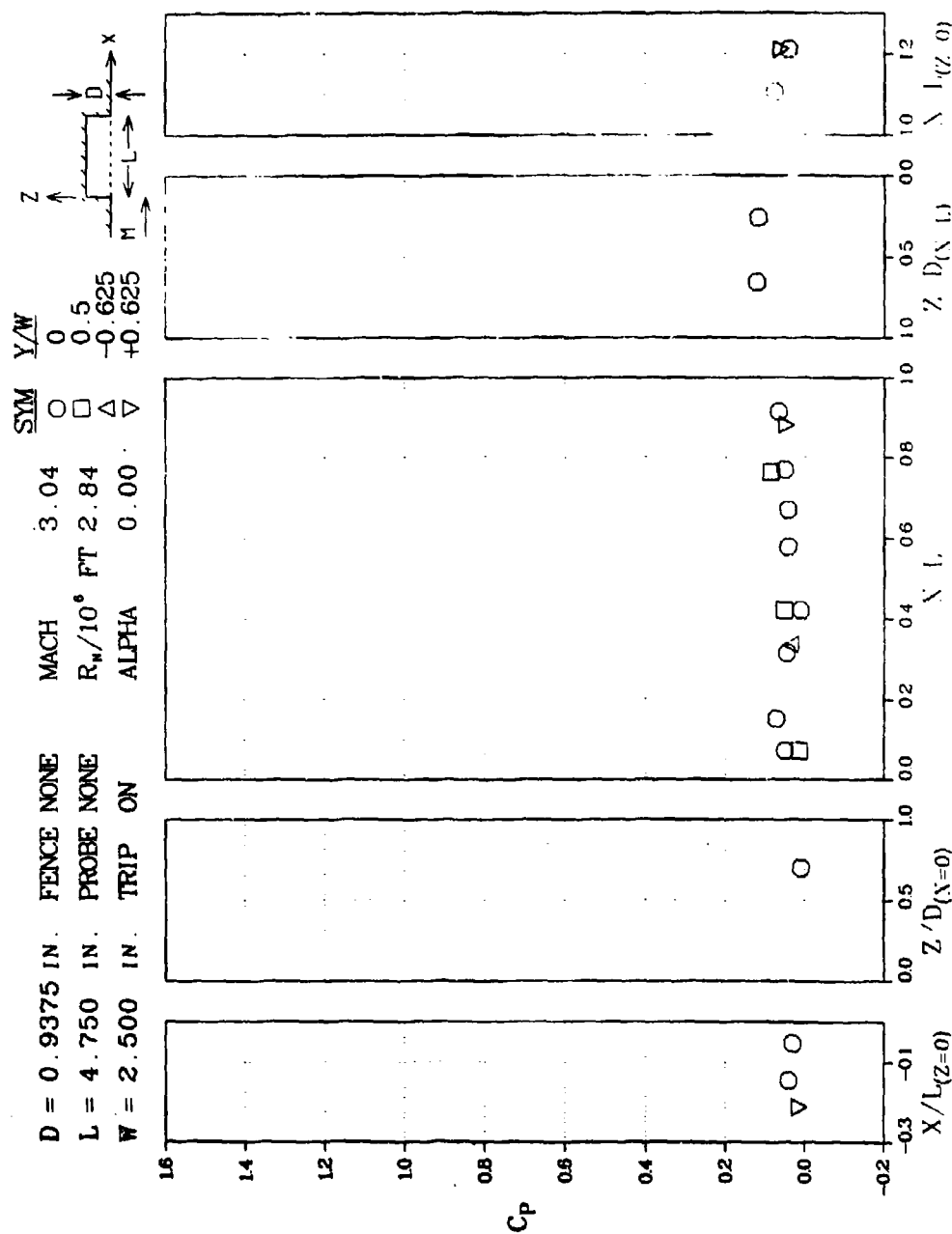


Figure 176 Pressure Coefficient Distributions for  $L/D = 5.1$  Cavity with Boundary Layer Trip,  $M_\infty = 3.0$ , Run 1









Figure 179 Oil Flow on Ceiling of  $L/D = 5.1$  Cavity,  $M_\infty = 3.0$



Figure 180 Oil Flow on Port Side of  $L/D = 5.1$  Cavity,  $M_\infty = 3.0$

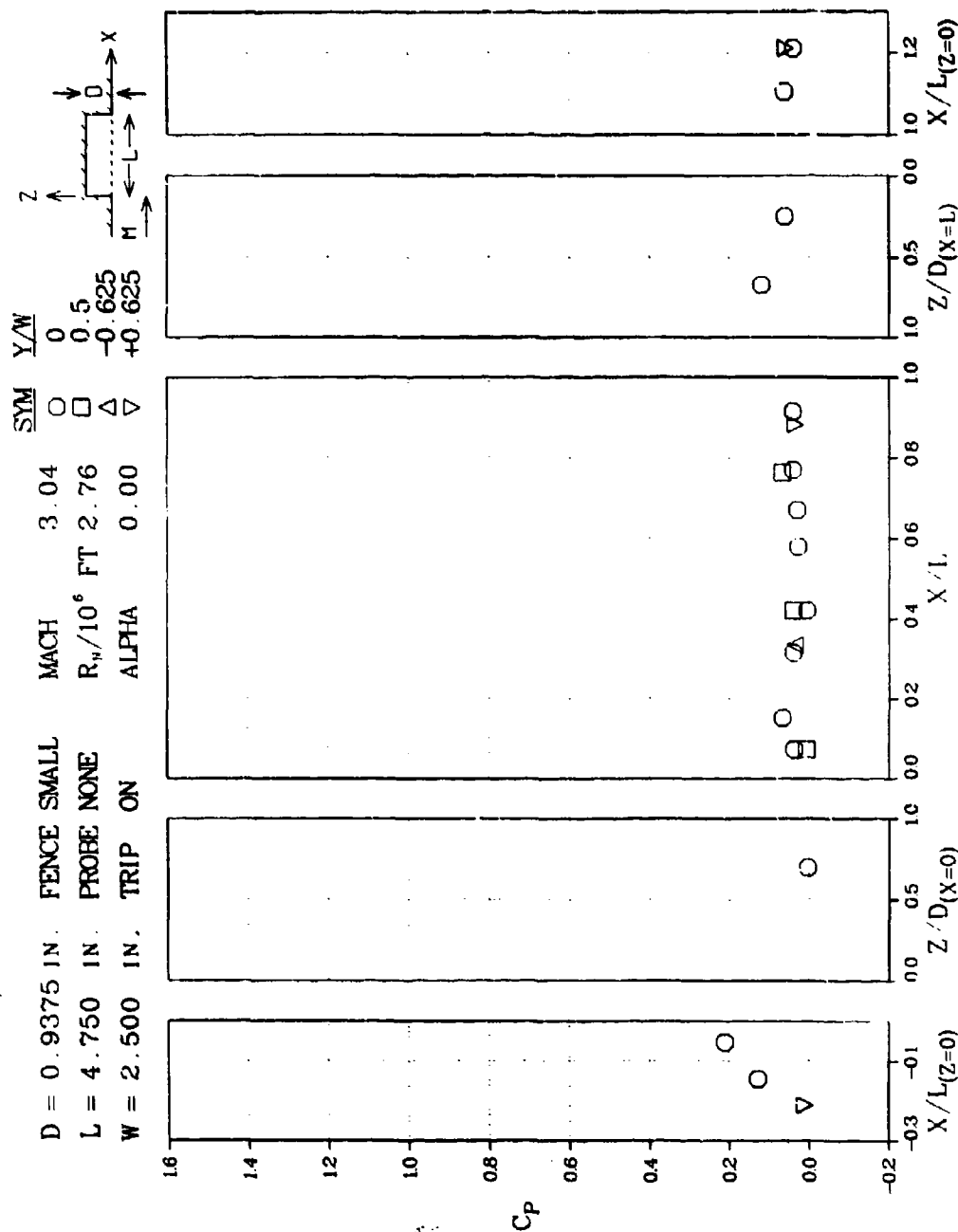
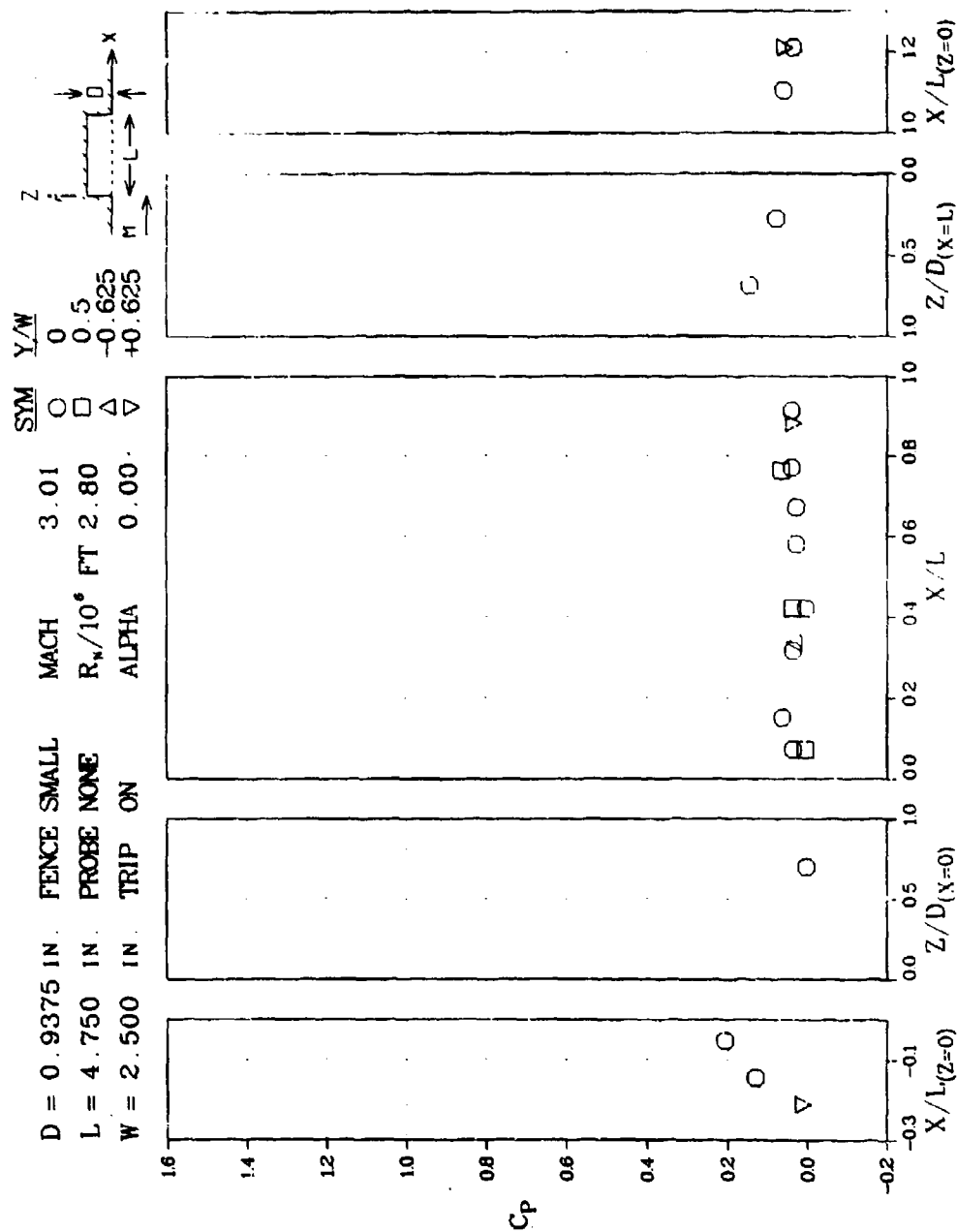


Figure 181 Pressure Coefficient Distributions for  $L/D = 5.1$  Cavity with Boundary Layer Trip and Perforated Fence,  $M_\infty = 3.0$ , Run 1



1331-006P

Figure 182 Pressure Coefficient Distributions for  $L/D = 5.1$  Cavity with Boundary Layer Trip and Perforated Fence,  $M_\infty = 3.0$ , Run 2

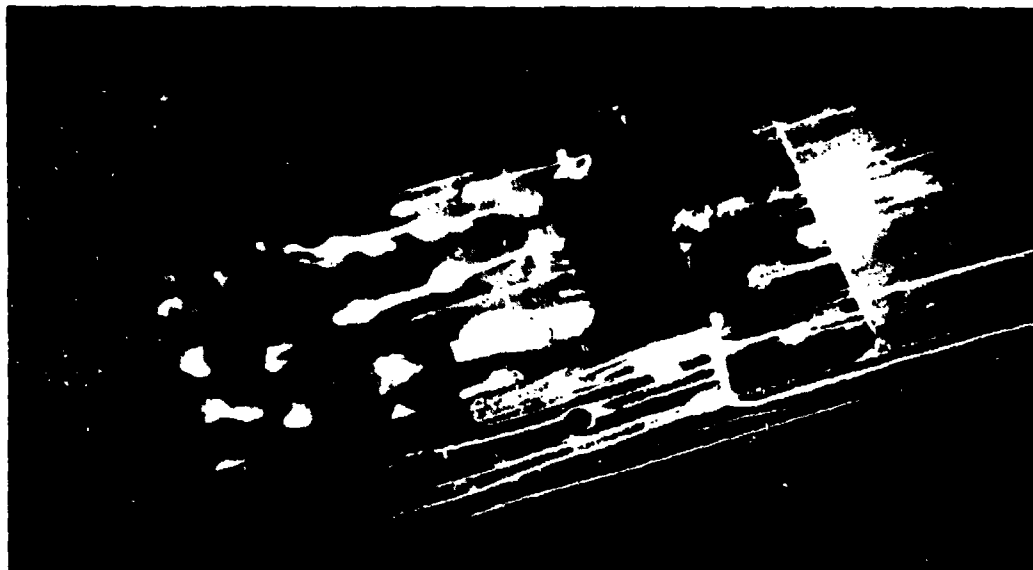
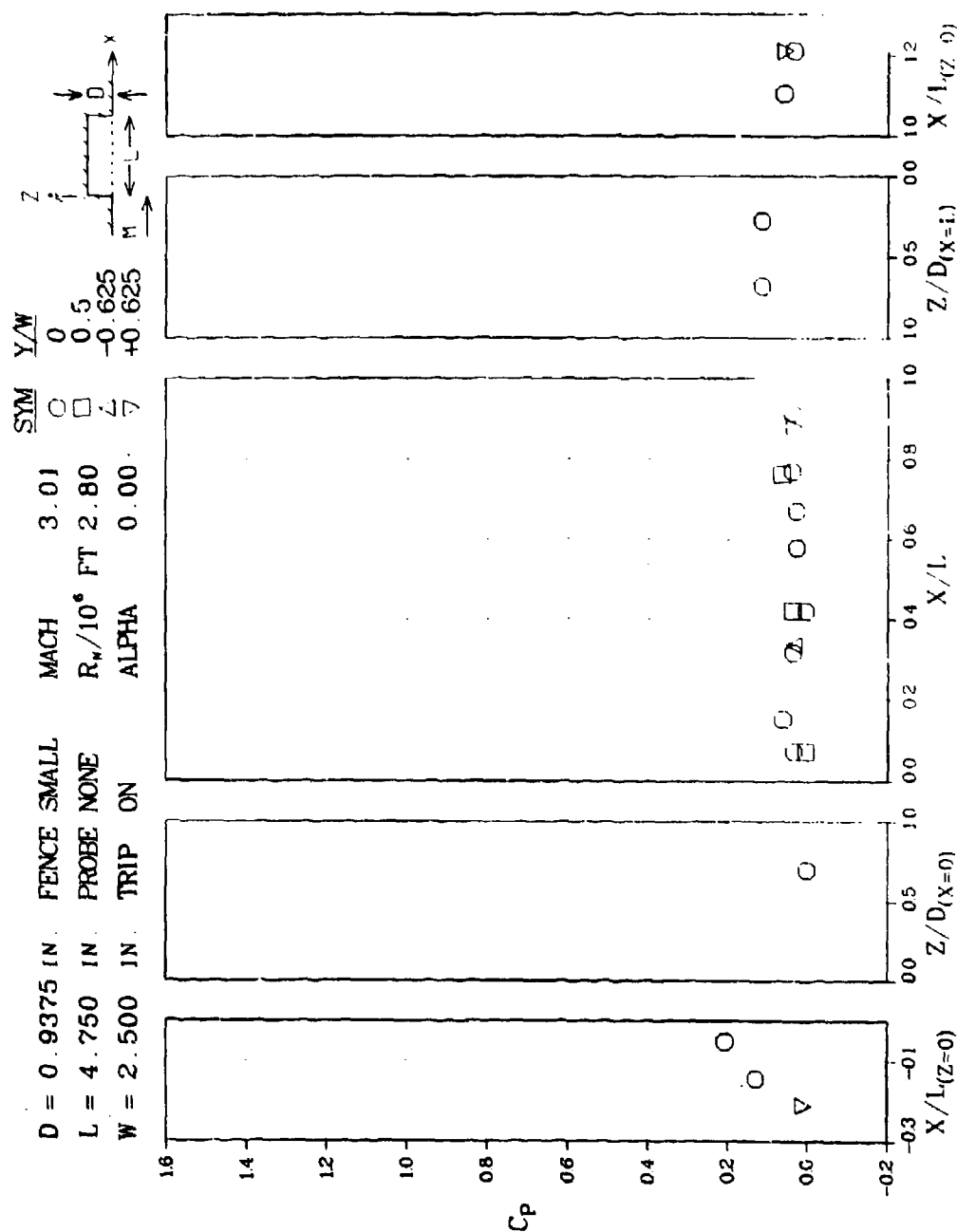


Figure 183 Oil Flow on Ceiling and Port Side of  $L/D = 5.1$  Cavity, Perforated Fence Attached,  $M_\infty = 3.0$ , Photograph 1



Figure 184 Oil Flow on Ceiling and Port Side of  $L/D = 5.1$  Cavity, Perforated Fence Attached,  $M_\infty = 3.0$ , Photograph 2



1331-007P

Figure 185 Pressure Coefficient Distributions for  $L/D = 5.1$  Cavity with Boundary Layer Trip and Saw Tooth Fence,  $M_\infty = 3.0$ .



Figure 186 Schlieren Flow Photograph,  $L/D = 5.1$  Cavity with Boundary Layer Trip,  $M_\infty = 3.0$



Figure 187 Schlieren Flow Photograph,  $L/D = 5.1$  Cavity with Boundary Layer Trip and Perforated Fence,  $M_\infty = 3.0$



Figure 188 Schlieren Flow Photograph,  $L/D = 5.1$  Cavity with Boundary Layer Trip and Saw-Tooth Fence,  $M_\infty = 3.0$







Trip, M = 3.0, Run 2



Figure 191 Oil Flow on Ceiling and Port Side of  $L/D = 5.6$  Cavity,  $M_\infty = 3.0$

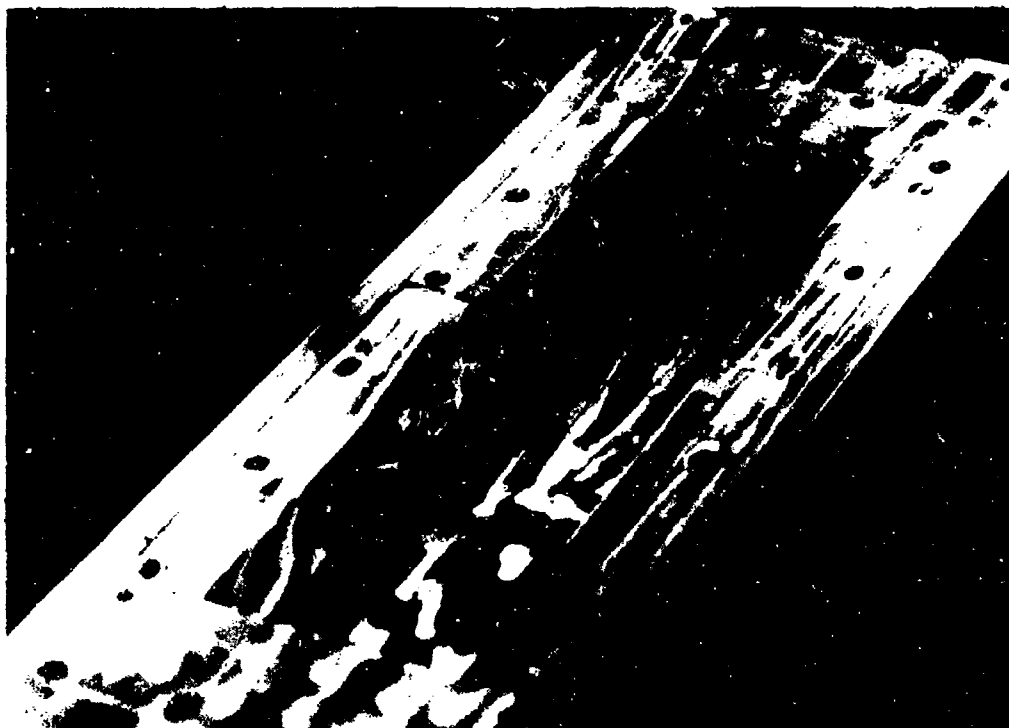


Figure 192 Oil Flow on Ceiling, Port Side and Aft Bulkhead of  $L/D = 5.6$  Cavity,  $M_\infty = 3.0$



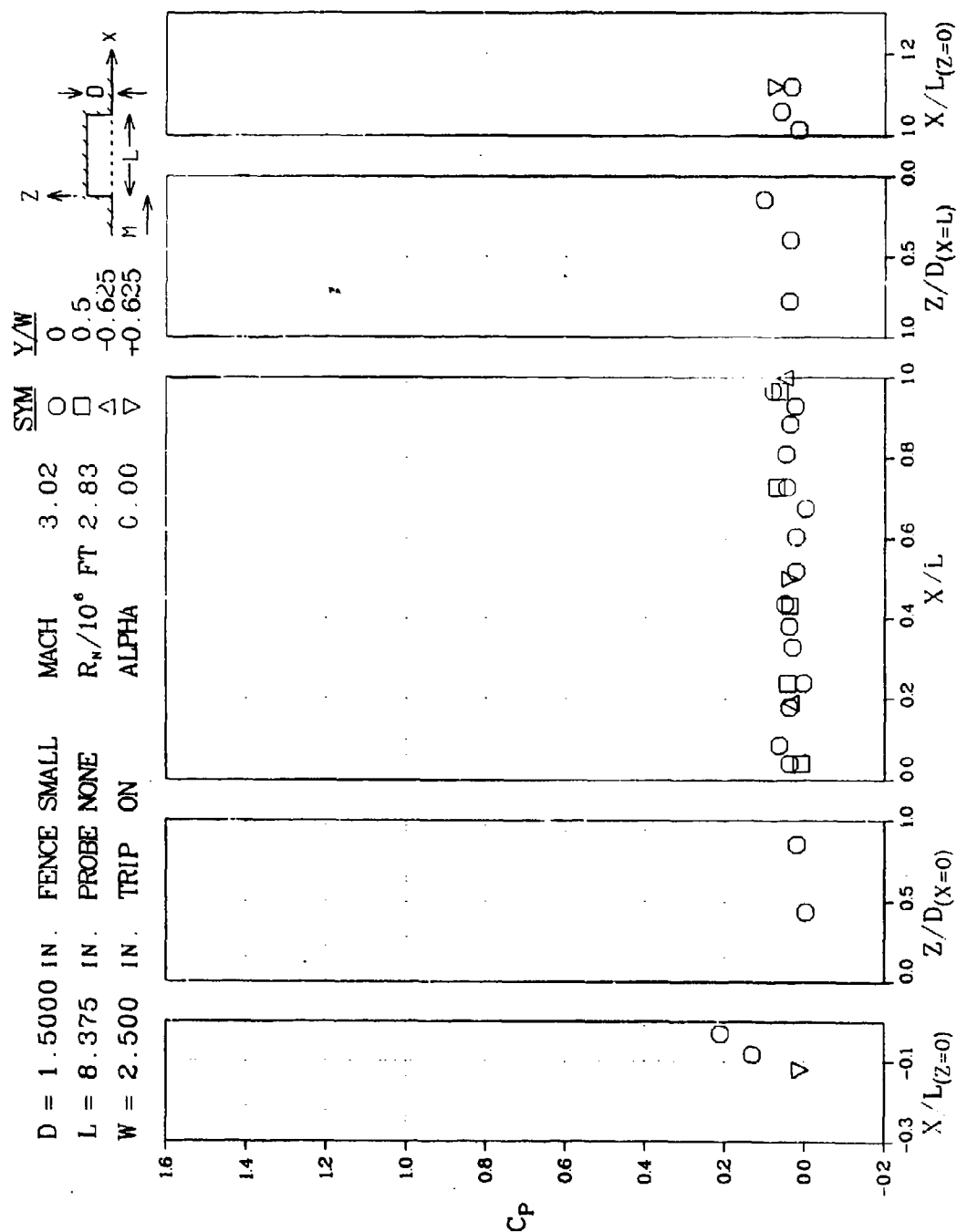


Figure 194 Pressure Coefficient Distributions for  $L/D = 5.6$  Cavity with Boundary Layer Trip and Perforated Fence,  $M_\infty = 3.0$ , Run 2



Figure 195 Schlieren Flow Photograph,  $L/D = 5.6$  Cavity with Boundary Layer Trip,  $M_\infty = 3.0$

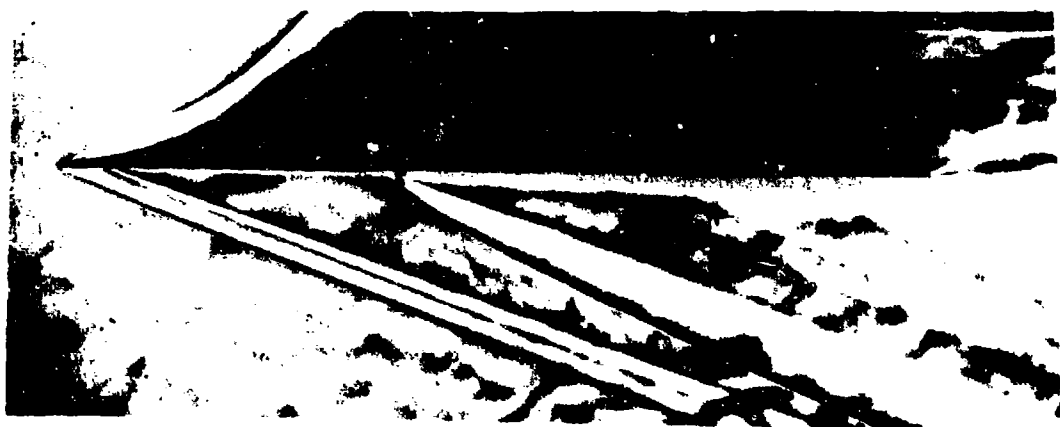


Figure 196 Schlieren Flow Photograph,  $L/D = 5.6$  Cavity with Boundary Layer Trip and Perforated Fence,  $M_\infty = 3.0$





Figure 198 Schlieren Flow Photograph,  $L/D = 5.6$  Cavity with Boundary Layer Trip and Saw-Tooth Fence,  $M_\infty = 3.0$





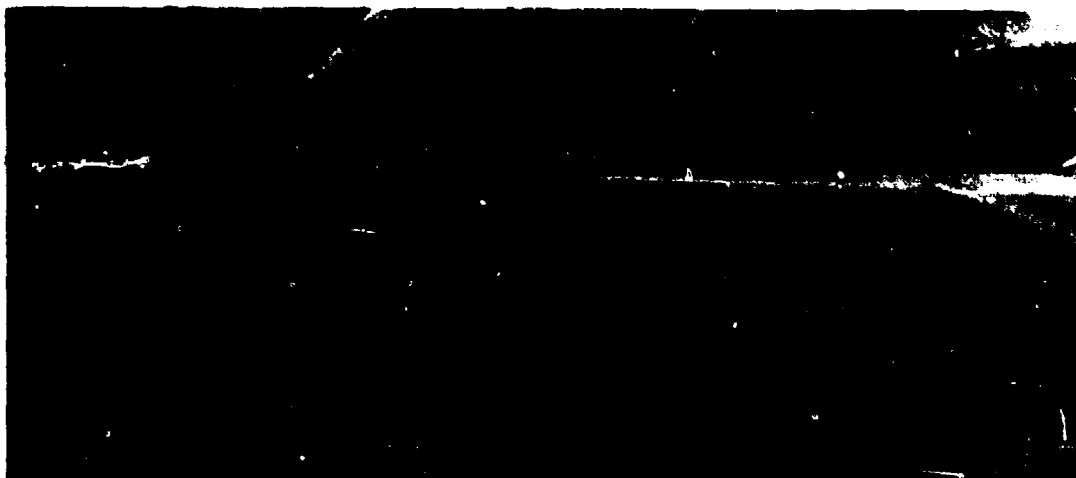
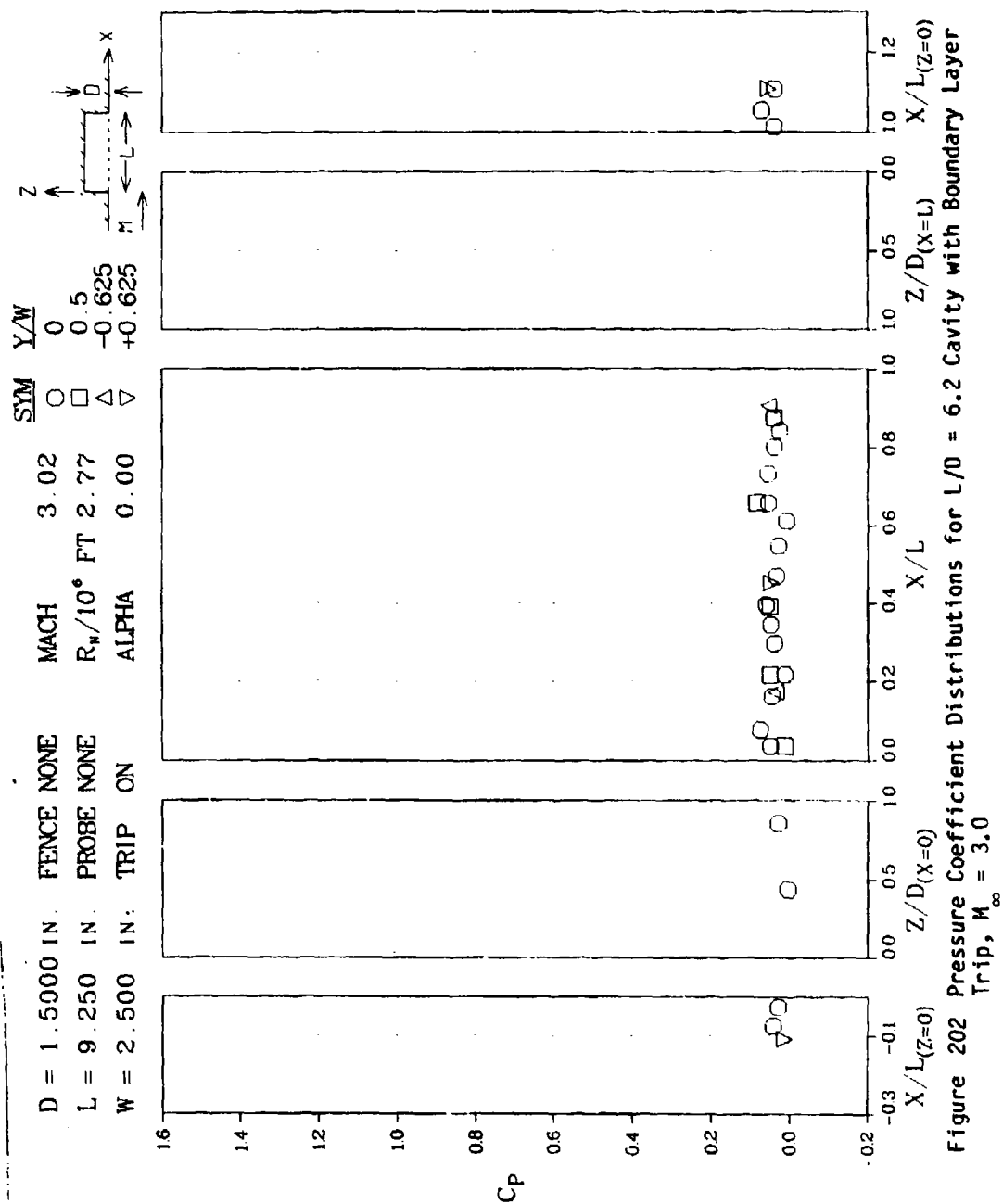


Figure 200 Schlieren Flow Photograph,  $L/D = 5.6$  Cavity with Boundary Layer Trip and Forward Facing Probe,  $M_\infty = 3.0$



Figure 201 Schlieren Flow Photograph,  $L/D = 5.6$  Cavity with Boundary Layer Trip and Forward Facing Probe, Model Pitched 5 Degrees Nose Up



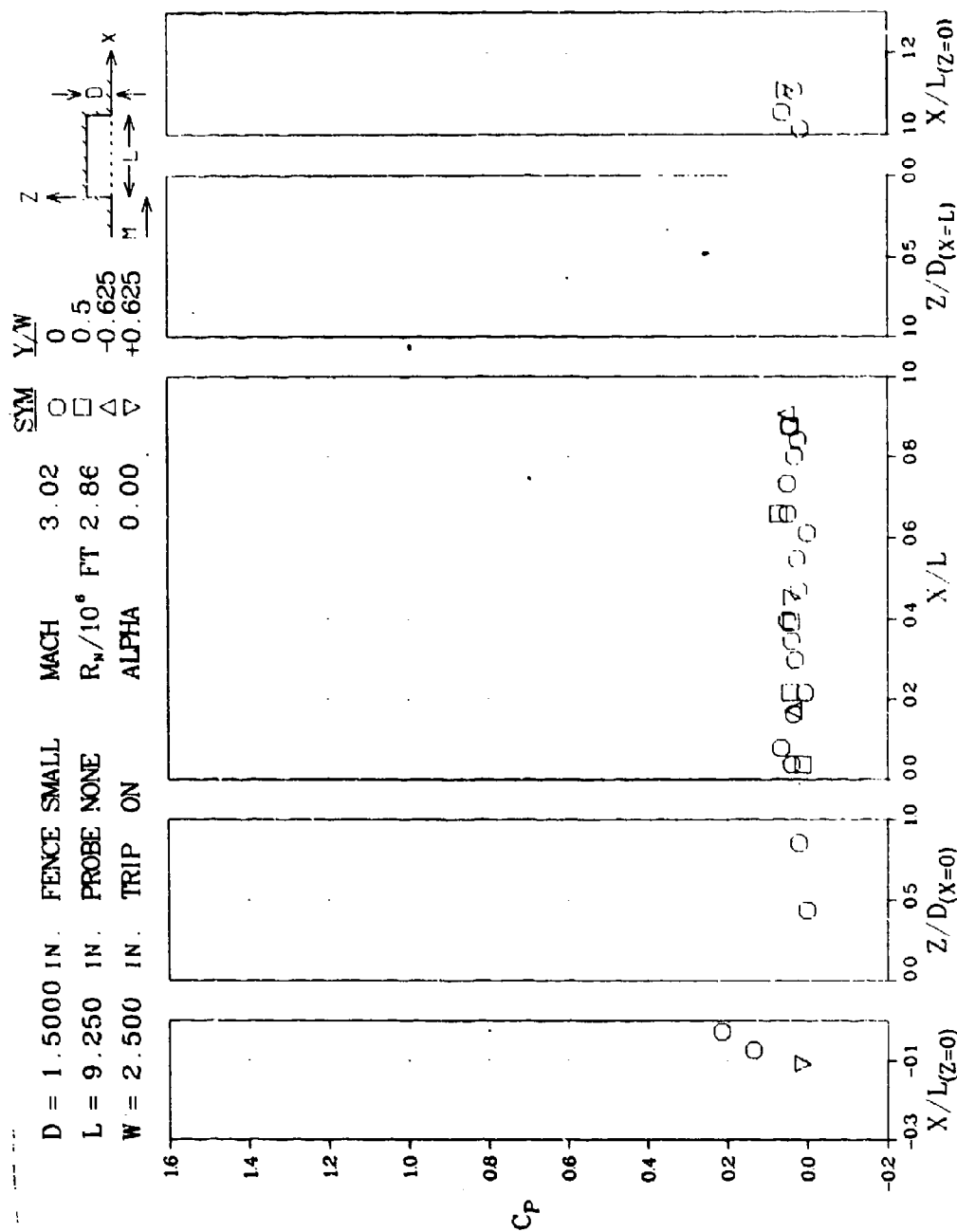


Figure 203 Pressure Coefficient Distributions for  $L/D = 6.2$  Cavity with Boundary Layer Trip and Perforated Fence,  $M_\infty = 3.0$ , Run 1

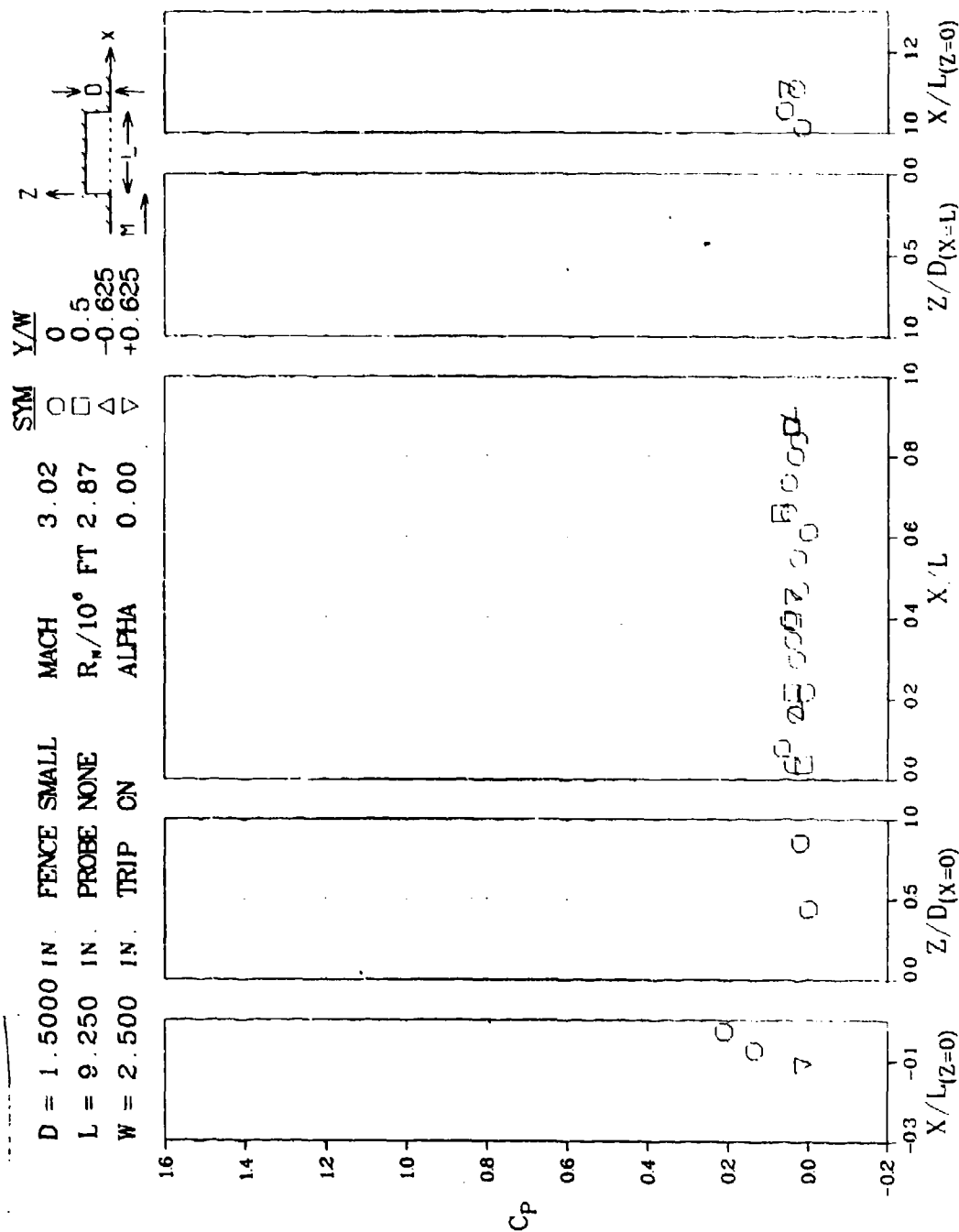


Figure 204 Pressure Coefficient Distributions for  $L/D = 6.2$  Cavity with Boundary Layer Trip and Perforated Fence,  $M_\infty = 3.0$ , Run 2

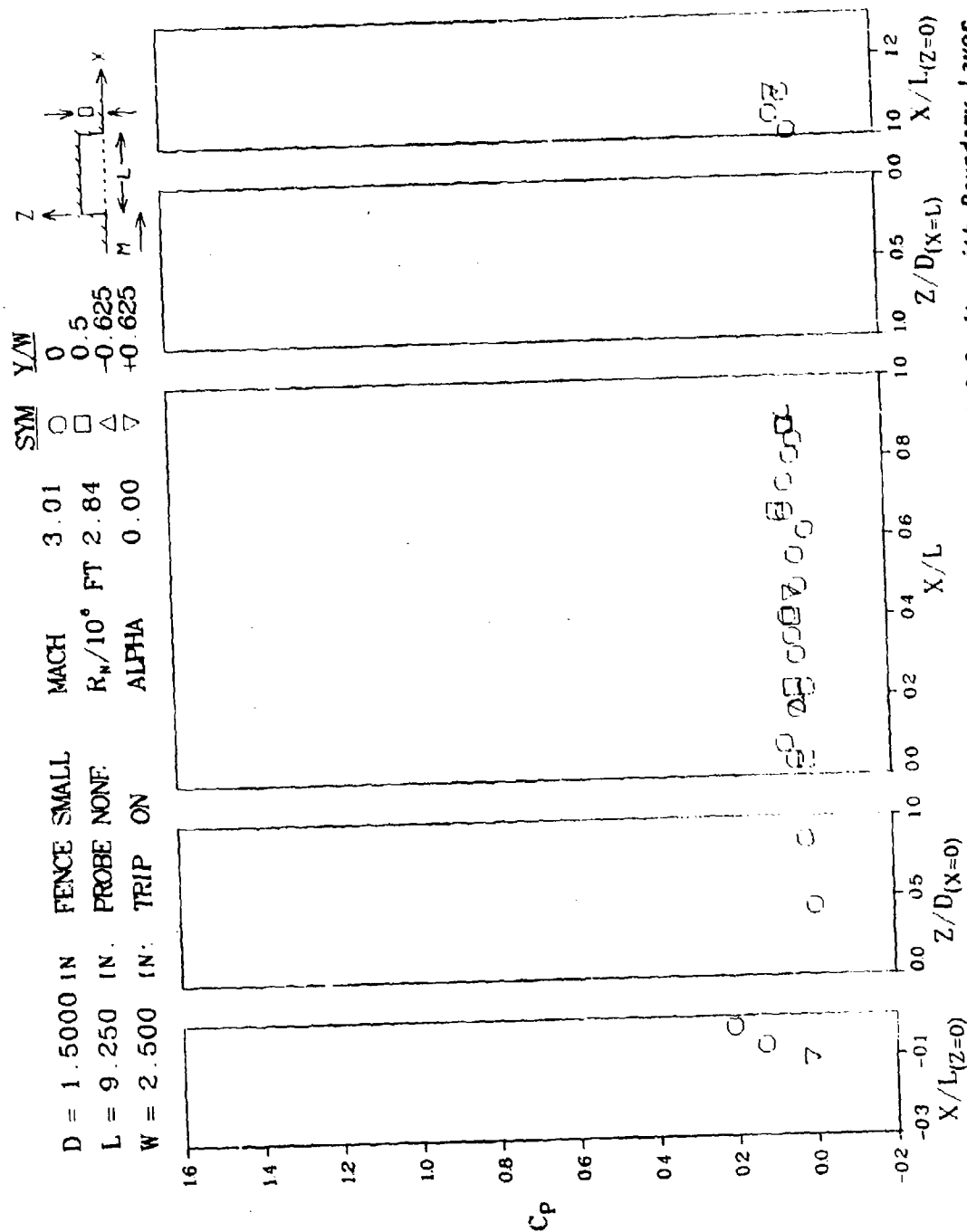


Figure 205 Pressure Coefficient Distributions for  $L/D = 6.2$  Cavity with Boundary Layer  
 Trip and Perforated Fence,  $M_\infty = 3.0$ , Run 3

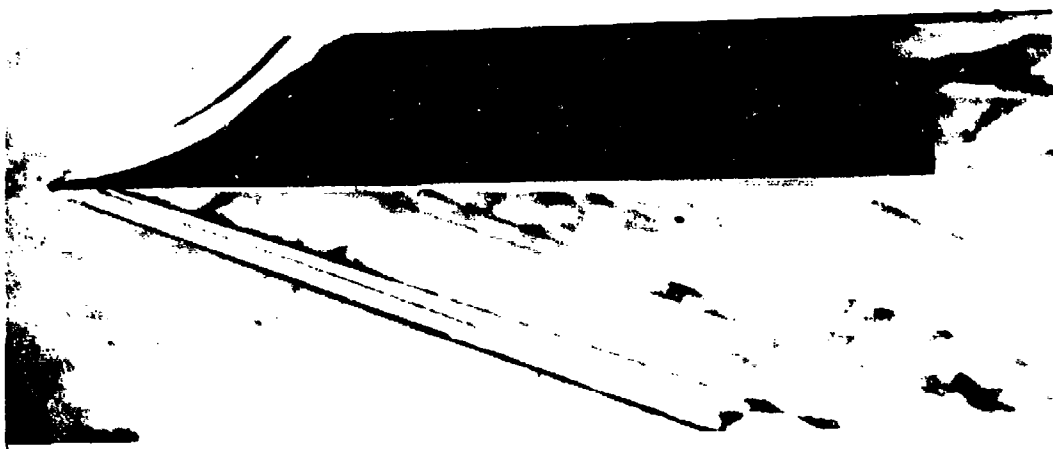


Figure 206 Schlieren Flow Photograph,  $L/D = 6.2$  Cavity with Boundary Layer Trip,  $M_\infty = 3.0$

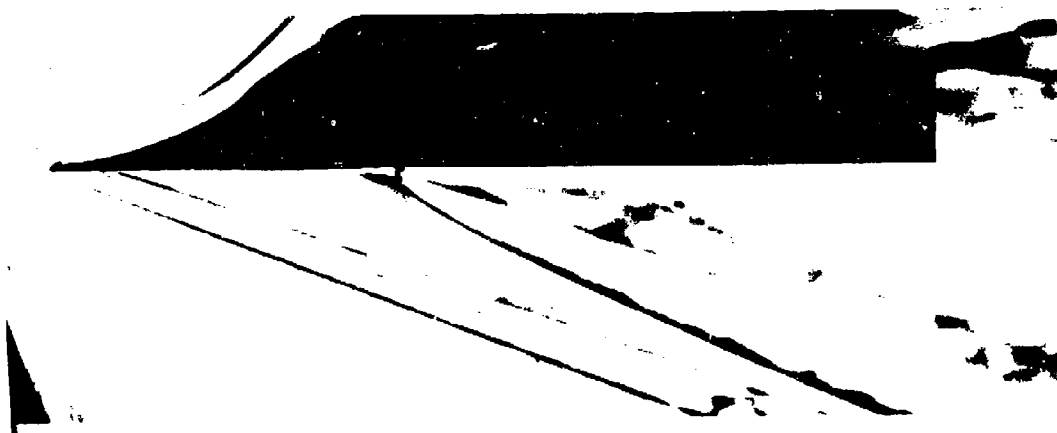
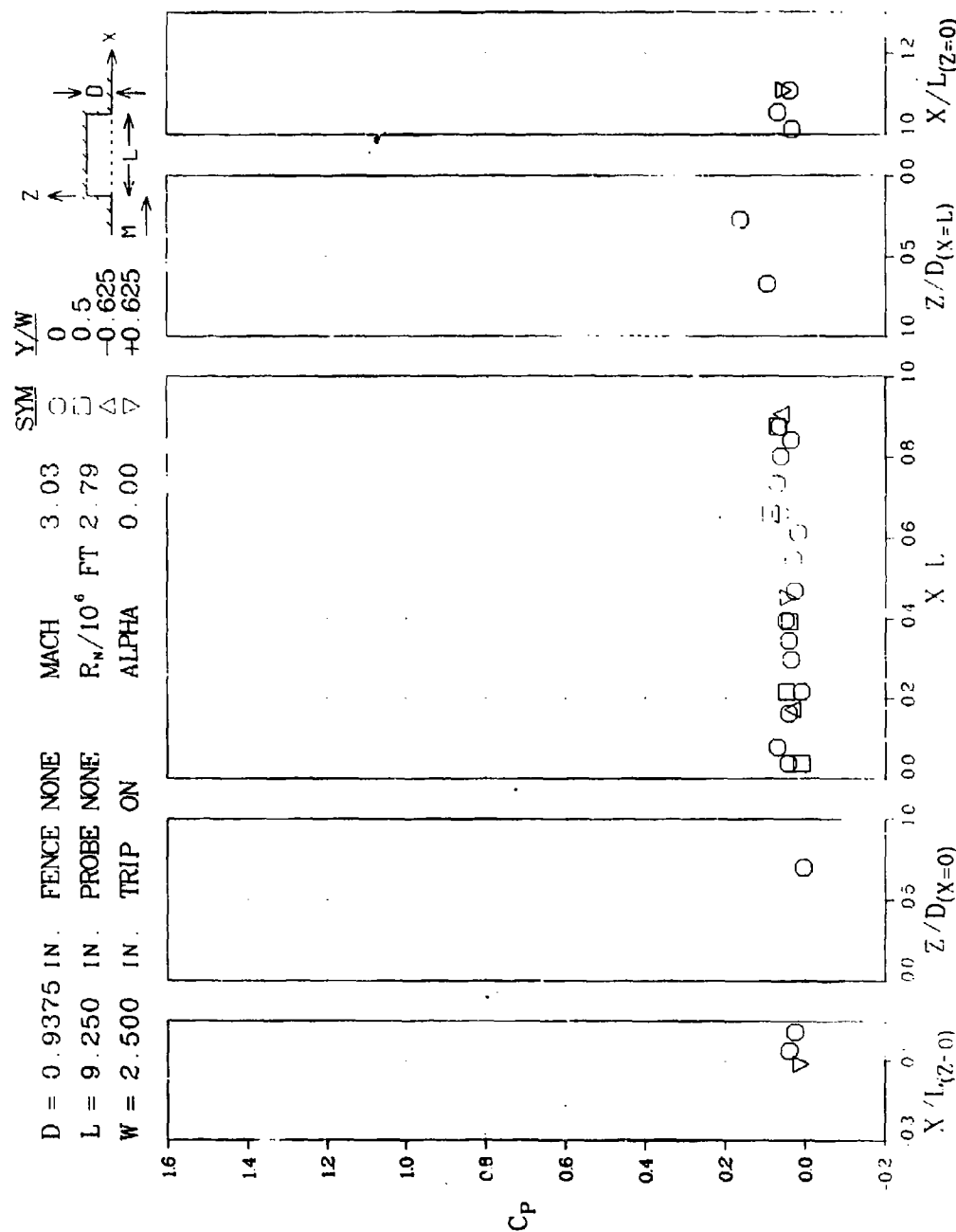


Figure 207 Schlieren Flow Photograph,  $L/D = 6.2$  Cavity with Boundary Layer Trip and Perforated Fence,  $M_\infty = 3.0$



1331-014P

Figure 208 Pressure Coefficient Distributions for  $L/D = 9.9$  Cavity with Boundary Layer Trip,  $M_\infty = 3.0$ , Run 1





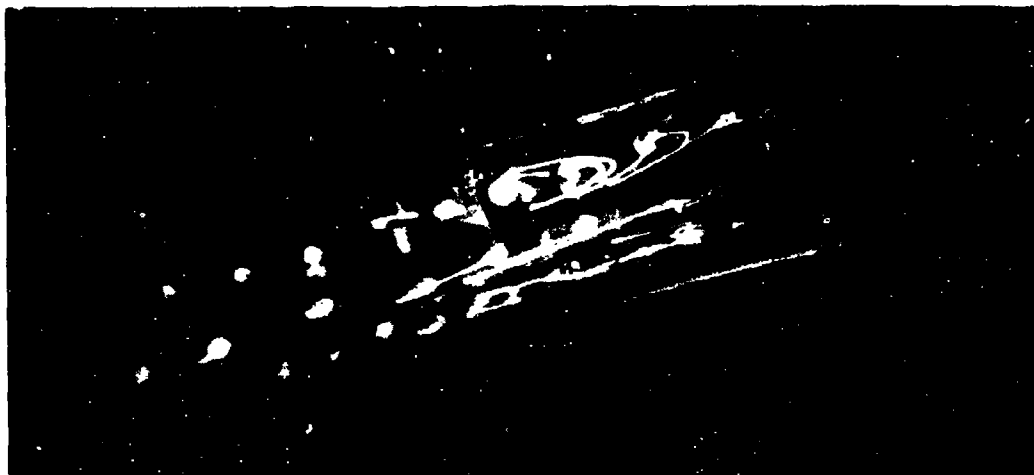


Figure 210 Oil Flow on Ceiling and Port side of  $L/D = 9.9$  Cavity,  $M_{\infty} = 3.0$



Figure 211 Oil Flow on Ceiling and Starboard Side of  $L/D = 9.9$  Cavity,  
 $M_{\infty} = 3.0$

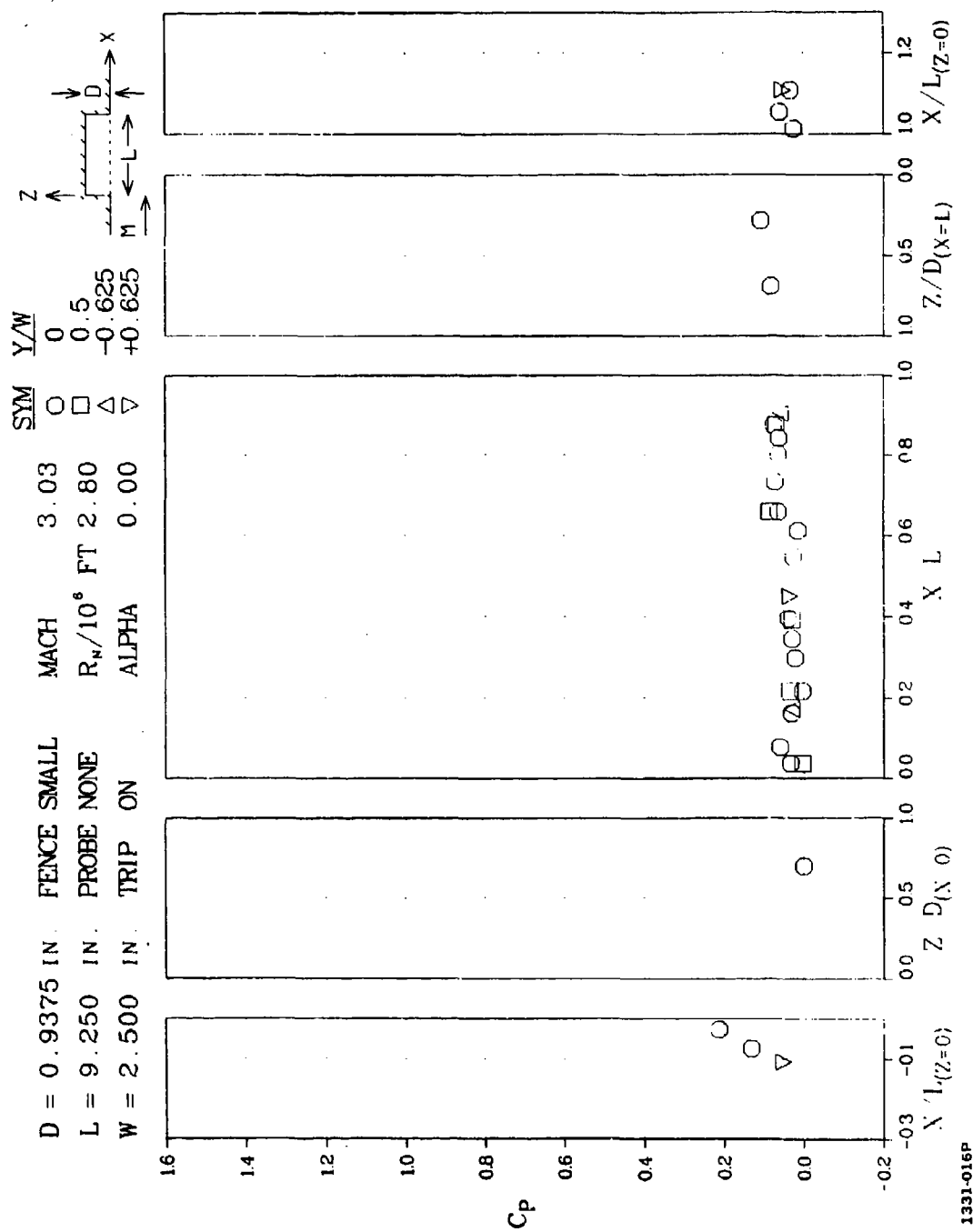


Figure 212 Pressure Coefficient Distributions for  $L/D = 9.9$  Cavity with Boundary Layer Trip and Perforated Fence,  $M_\infty = 3.0$ , Run 1

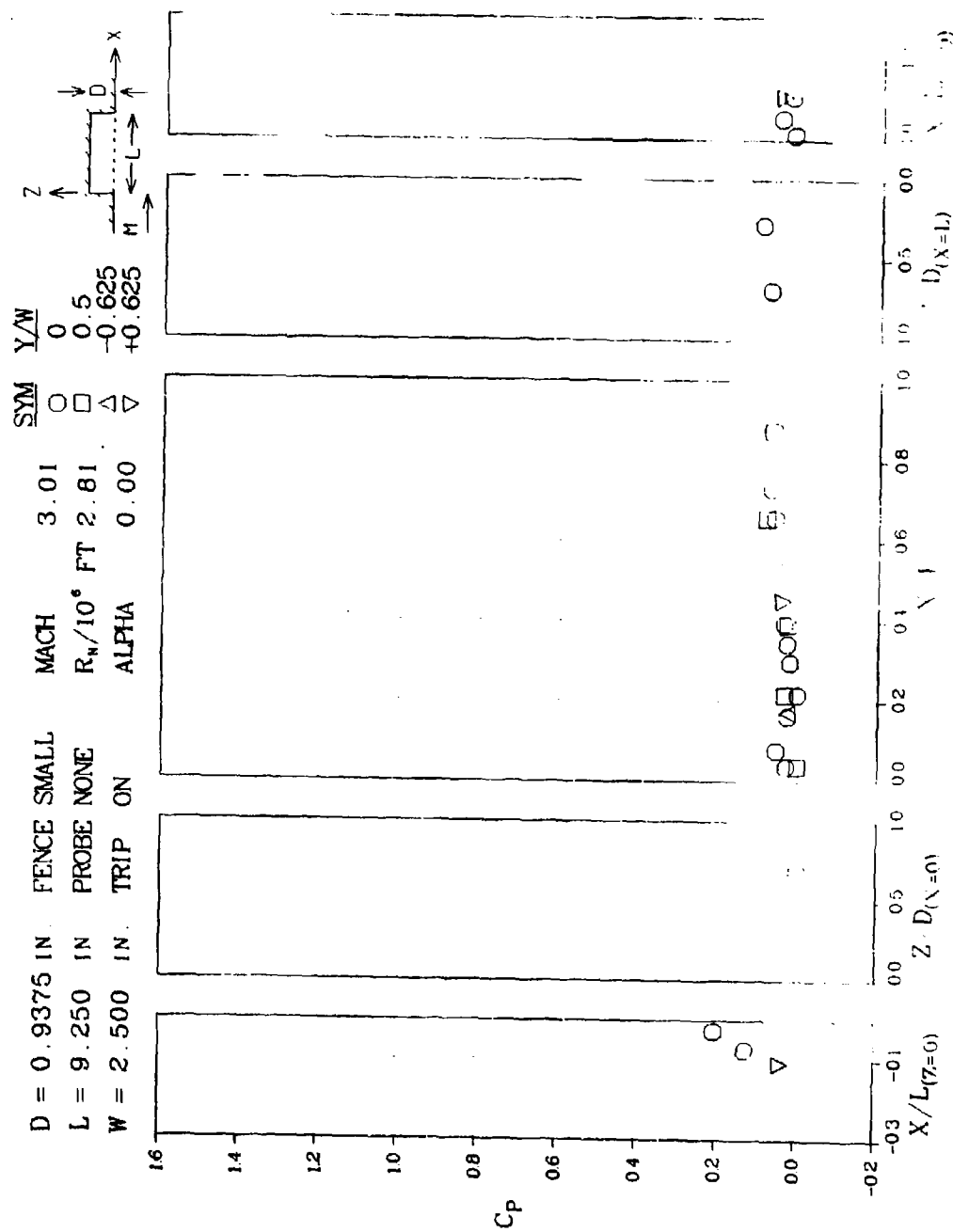


Figure 213 Pressure Coefficient Distributions for  $L/D = 9.9$  Cavity with Boundary Layer Trip and Perforated Fence,  $M_\infty = 3.0$ , Run 2



Figure 214 Schlieren Flow Photograph,  $L/D = 9.9$  Cavity with Boundary Layer Trip,  $M_\infty = 3.0$

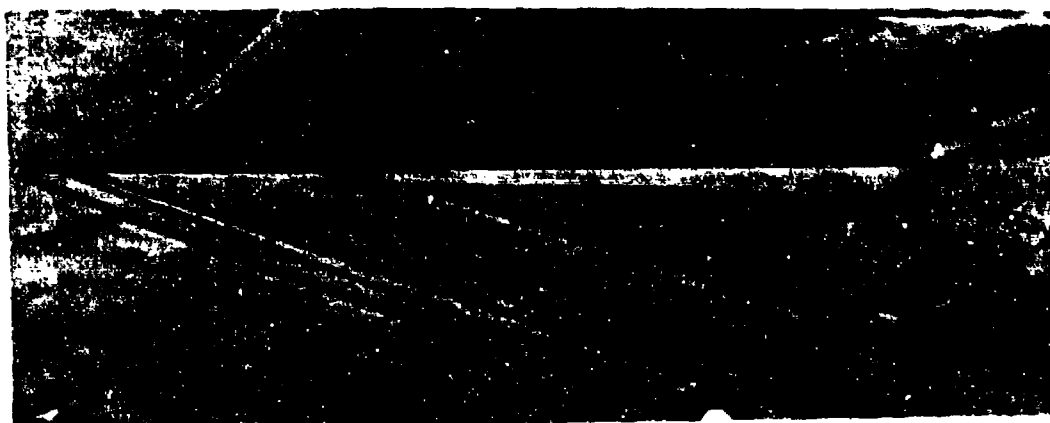


Figure 215 Schlieren Flow Photograph,  $L/D = 9.9$  Cavity with Boundary Layer Trip and Perforated Fence,  $M_\infty = 3.0$

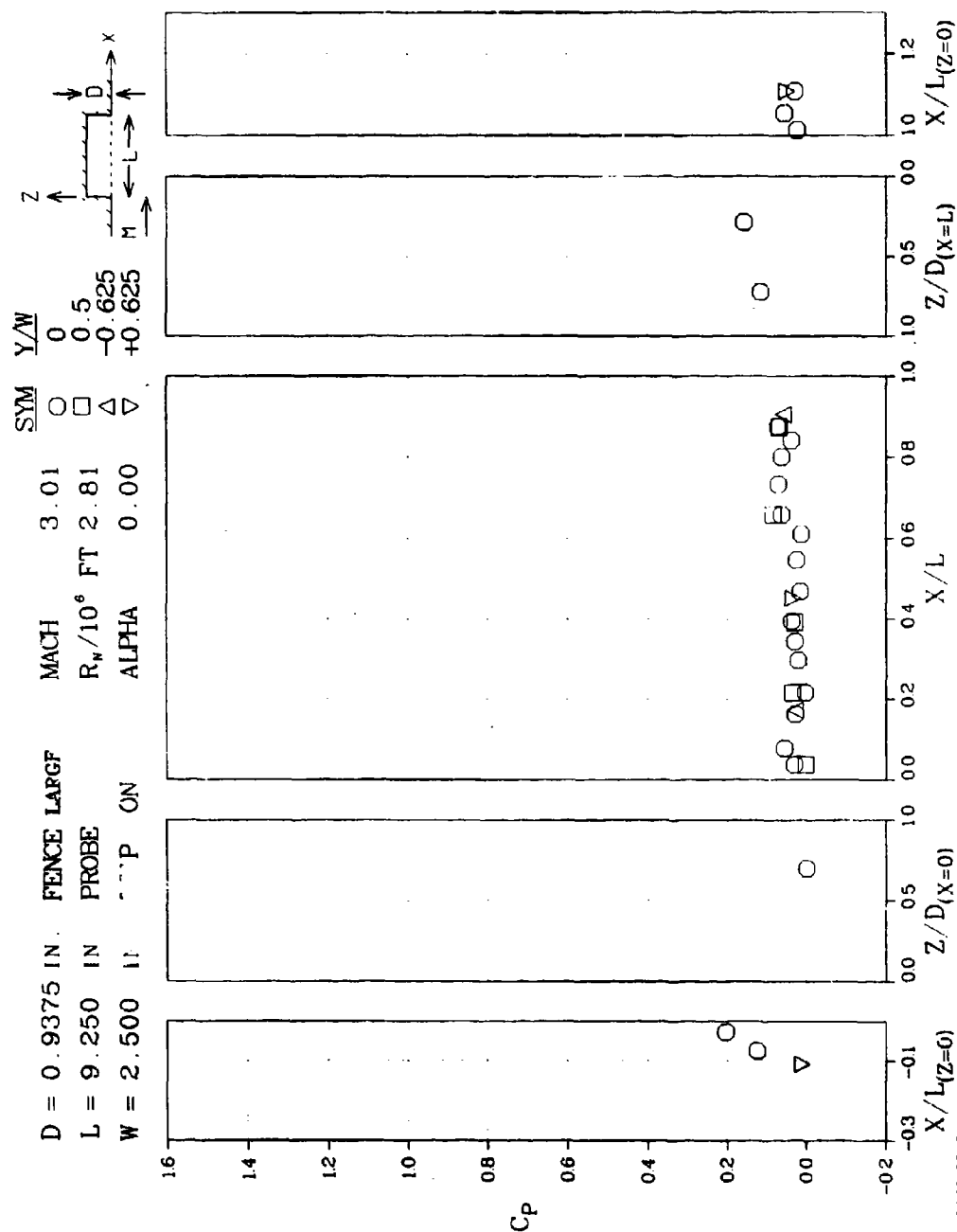


Figure 216 Pressure Coefficient Distributions for  $L/D = 9.9$  Cavity with Boundary Layer Trip and Saw Tooth Fence,  $M_\infty = 3.0$



Figure 217 Schlieren Flow Photograph,  $L/D = 0.9$  cavity with boundary layer  
Trip and Saw-Tooth fence,  $M = 3.0$

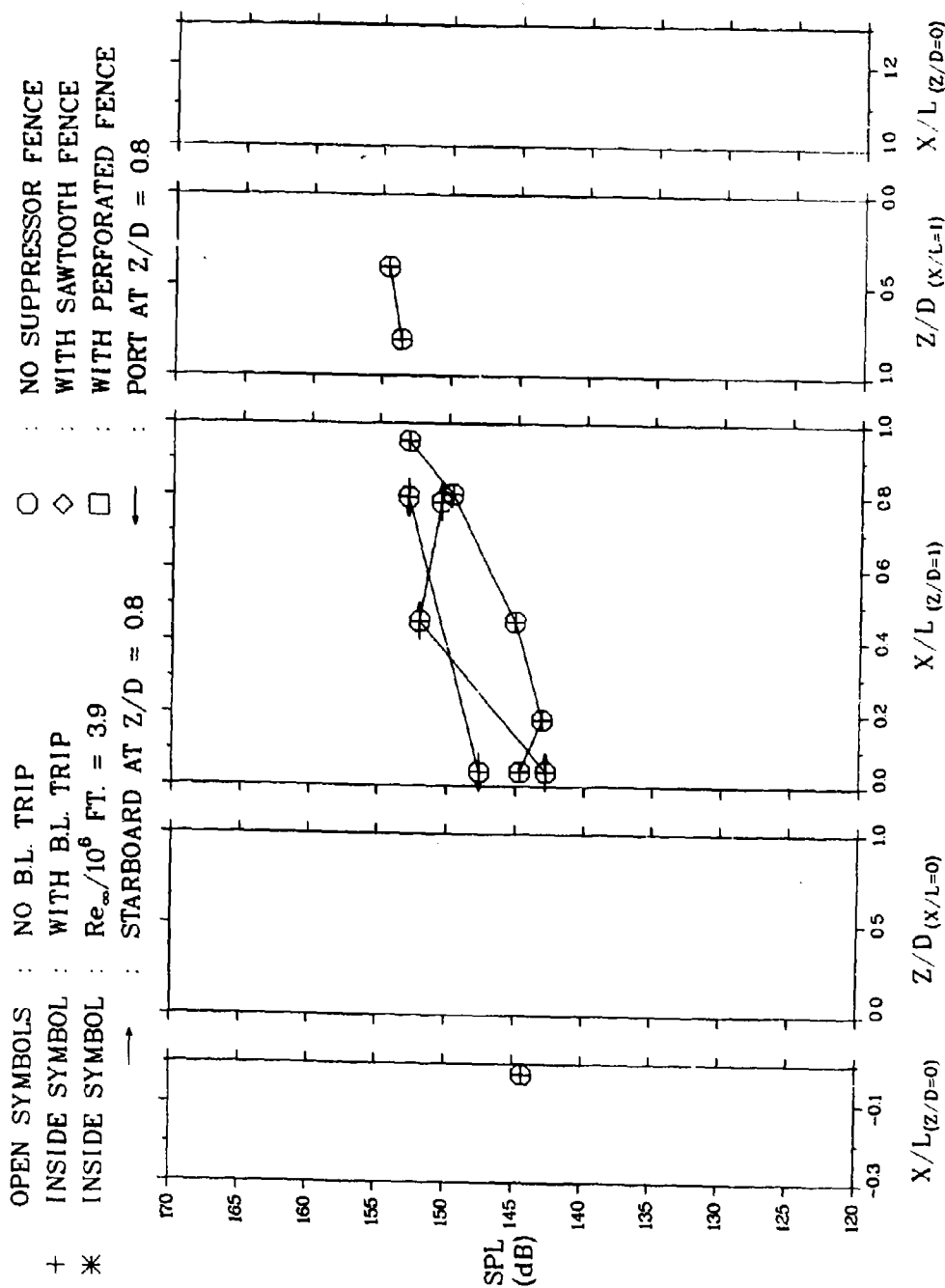


Figure 218 Acoustic Pressure Distributions in  $L/D = 5.1$  Cavity at  $M_{\infty} = 0.6$



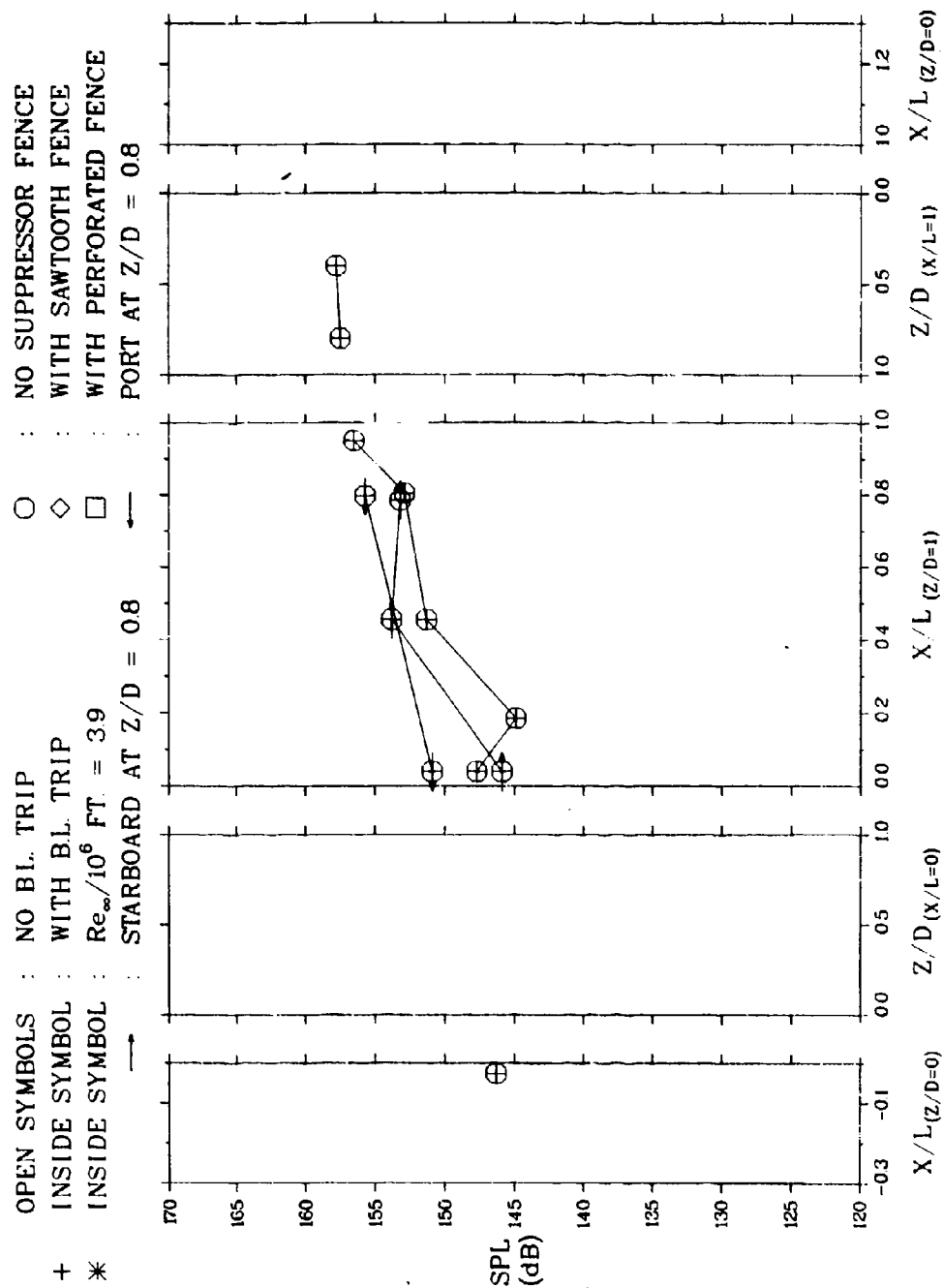


Figure 219 Acoustic Pressure Distributions in  $L/D = 5.1$  Cavity at  $M_{\infty} = 0.71$

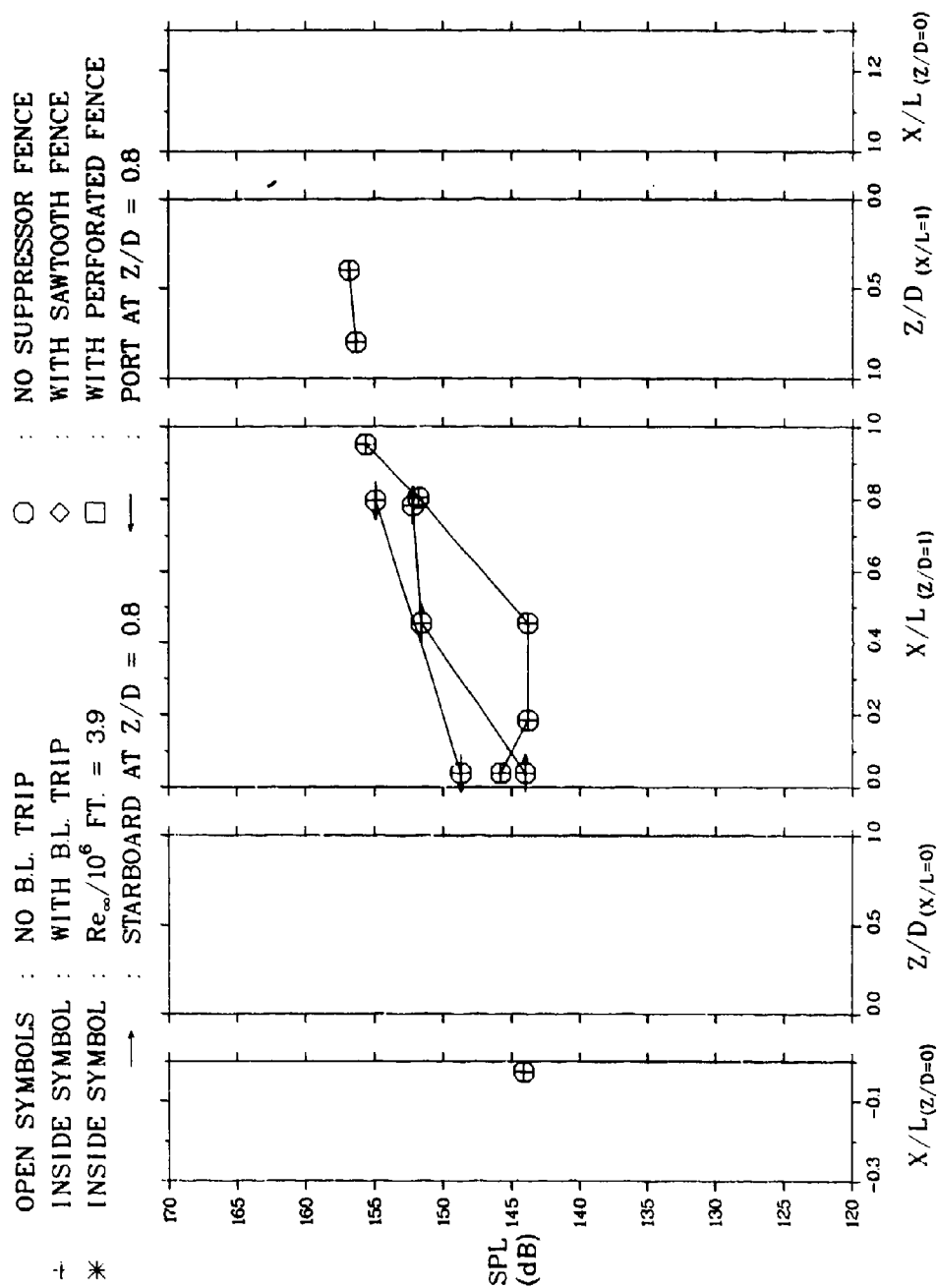


Figure 220 Acoustic Pressure Distributions in  $L/D = 5.1$  Cavity at  $M_{\infty} = 0.76$

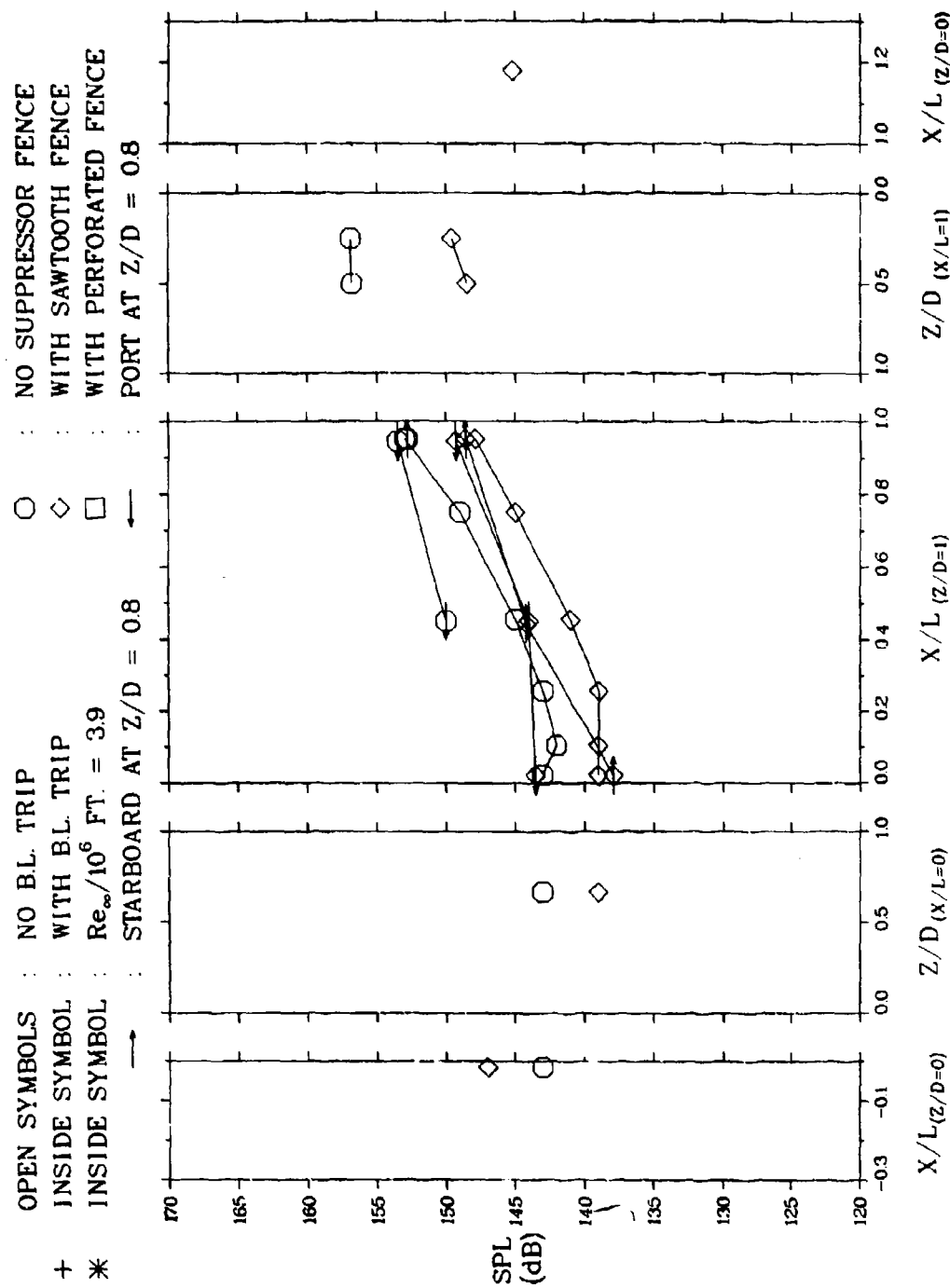


Figure 221 Acoustic Pressure Distributions in  $L/D = 5.6$  Cavity at  $M_{\infty} = 0.60$

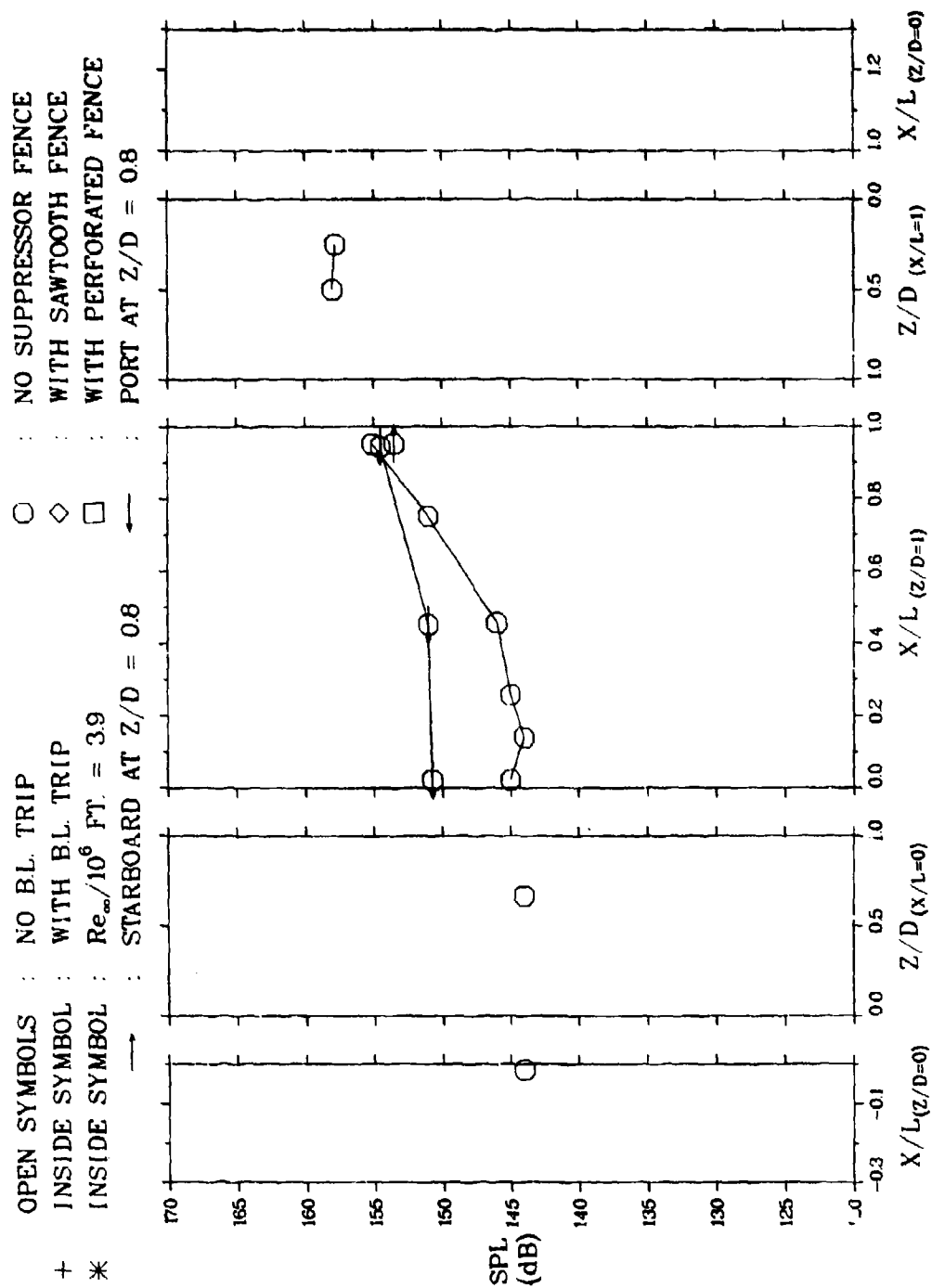


Figure 222 Acoustic Pressure Distributions in  $L/D = 5.6$  Cavity at  $M_{\infty} = 0.64$

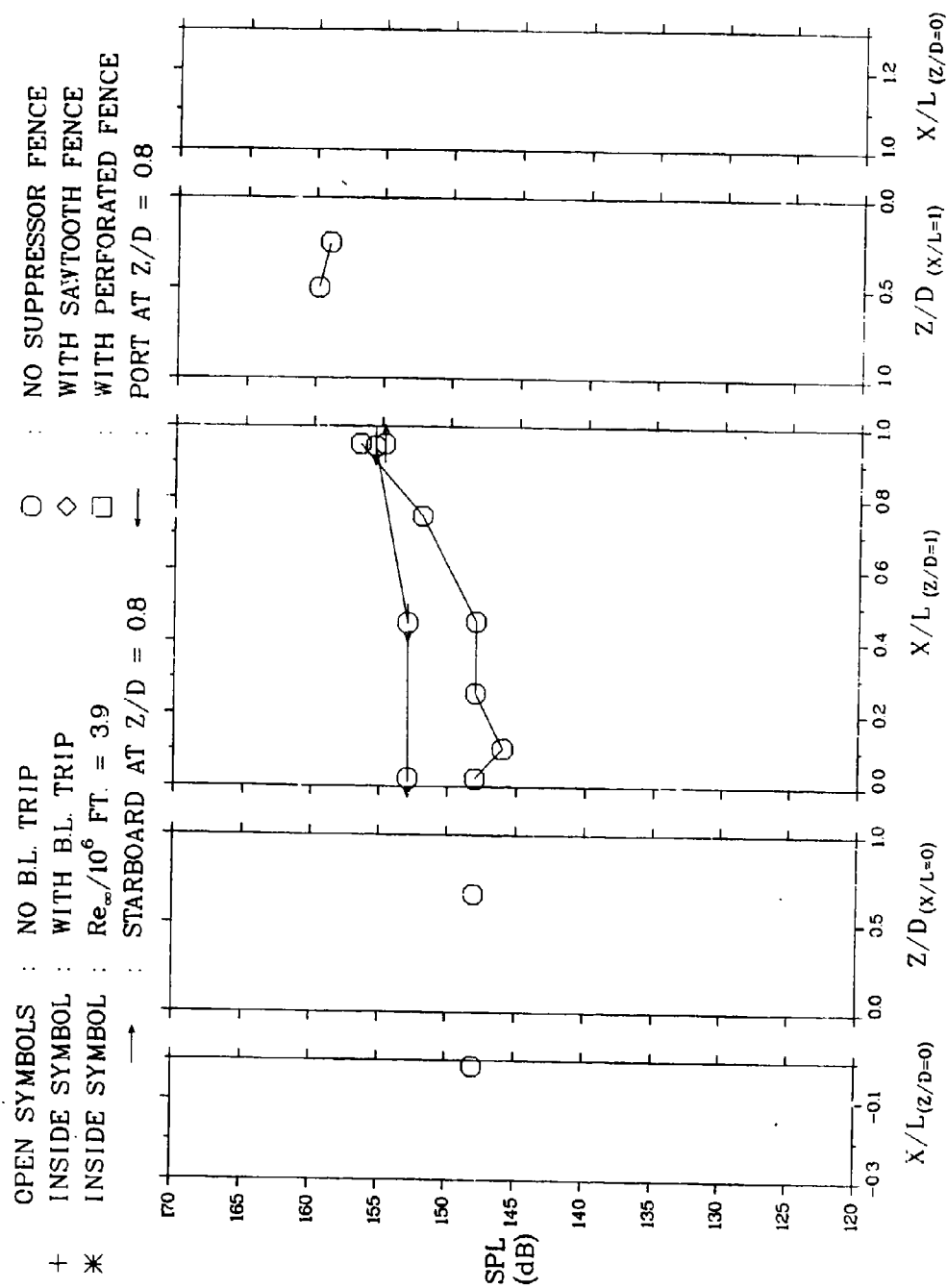


Figure 223 Acoustic Pressure Distributions in  $L/D = 5.6$  Cavity at  $M_{\infty} = 0.66$

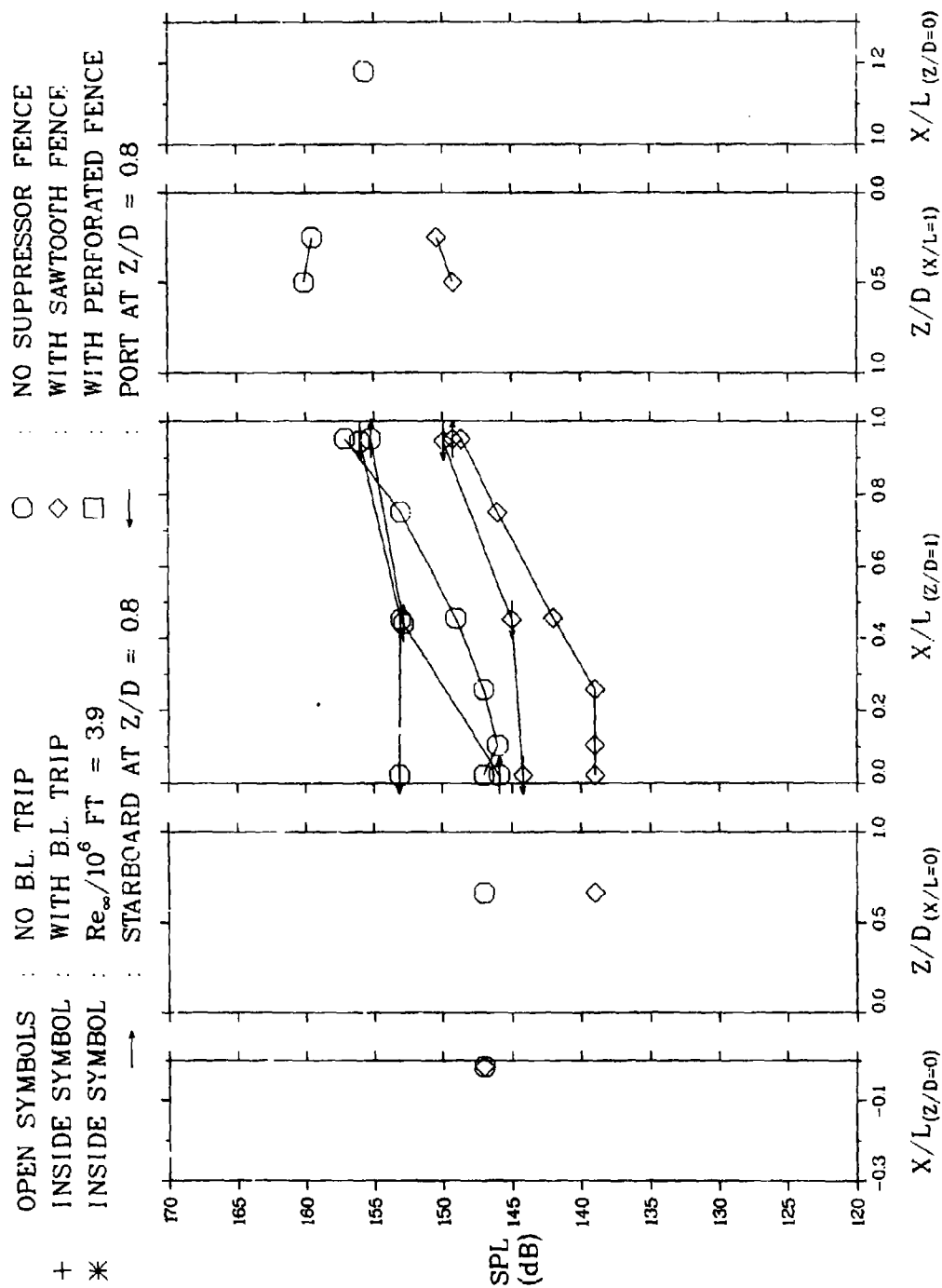


Figure 224 Acoustic Pressure Distributions in  $L/D = 5.6$  Cavity at  $M_{\infty} = 0.70$

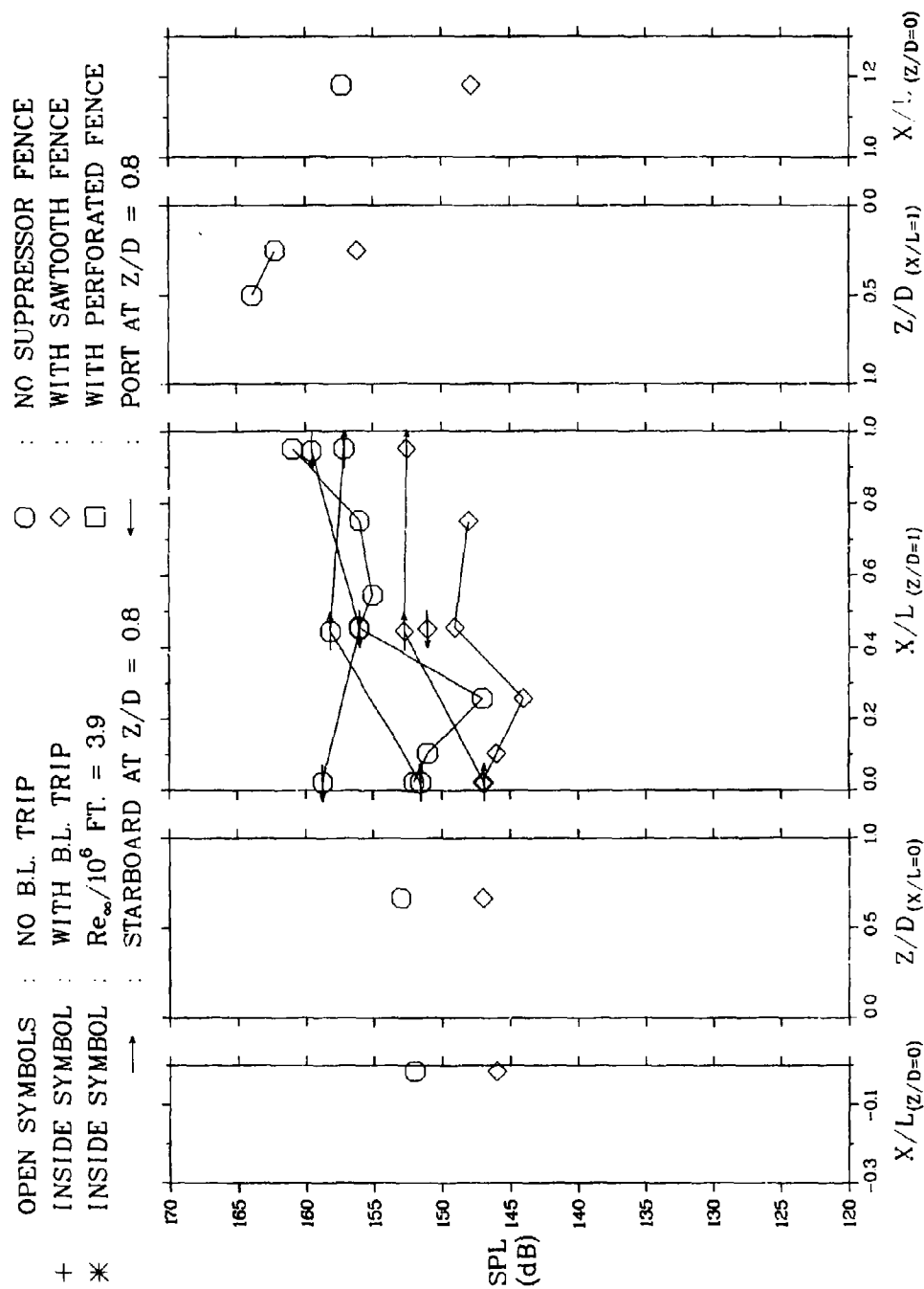


Figure 225 Acoustic Pressure Distributions in  $L/D = 5.6$  Cavity at  $M_{\infty} = 0.74$

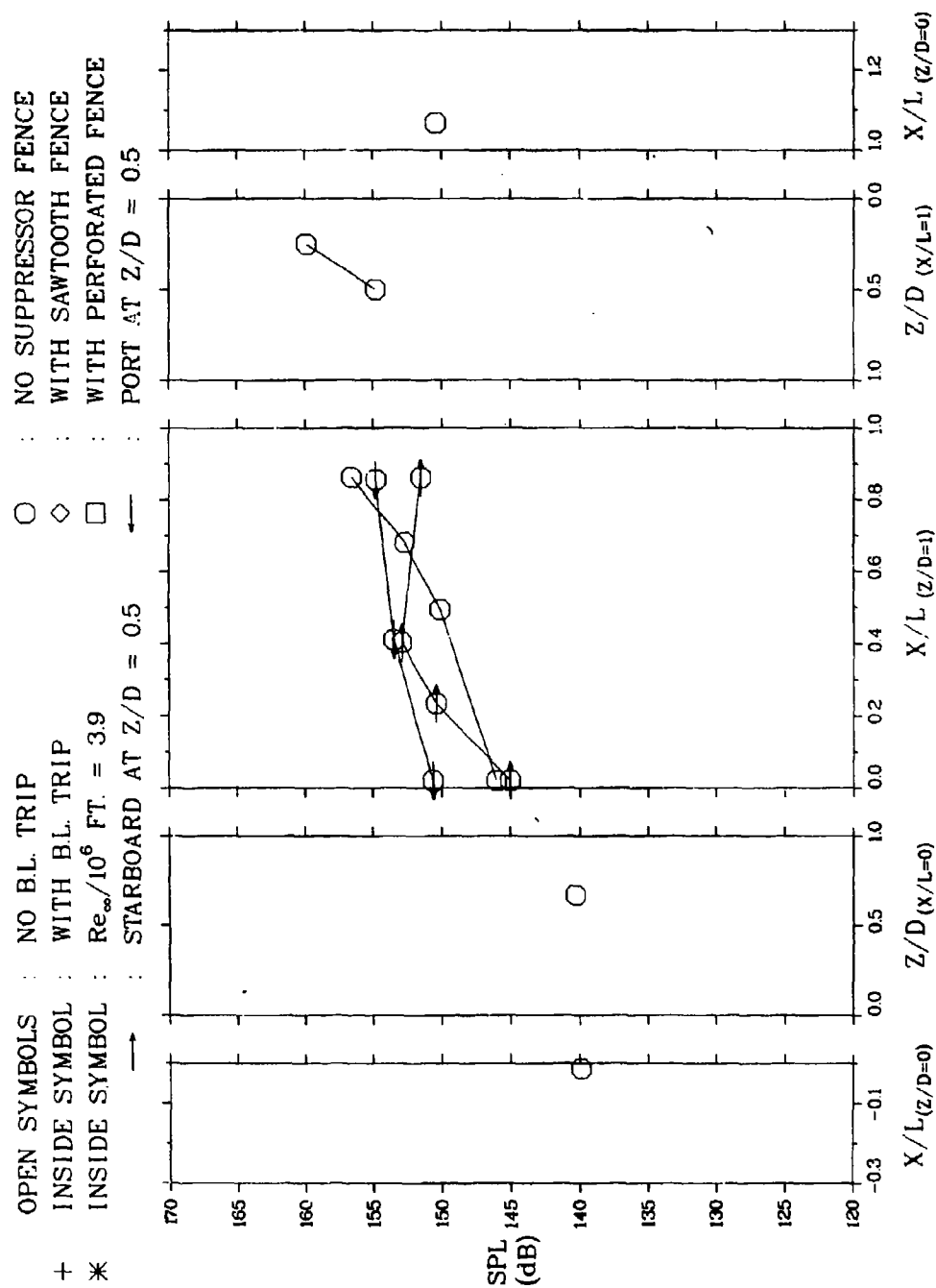
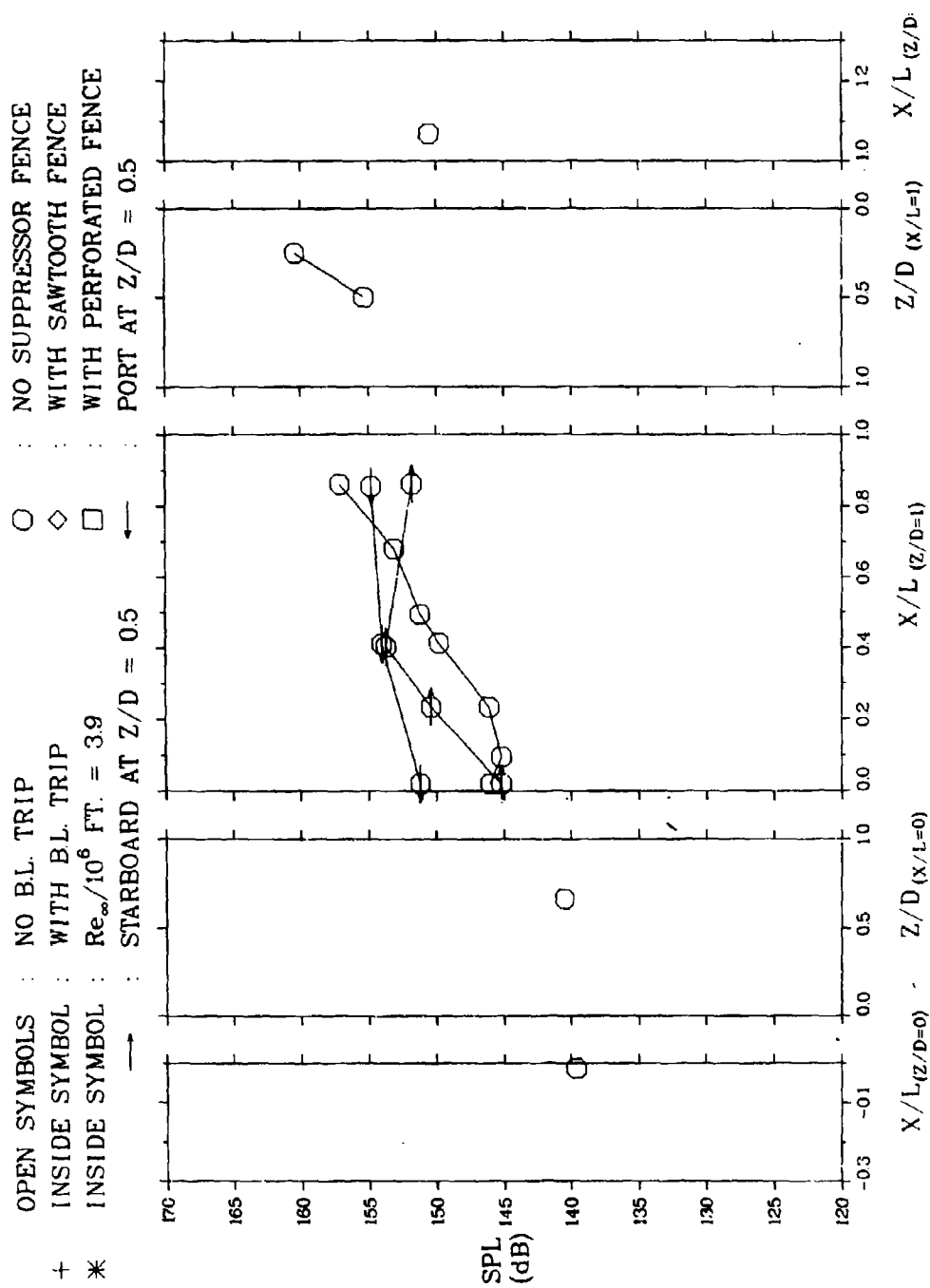


Figure 226 Acoustic Pressure Distributions in  $L/D = 6.2$  Cavity at  $M_{\infty} = 0.60$



Figure 227 Acoustic Pressure Distributions in  $L/D = 6.2$  Cavity at  $M_\infty = 0.70$

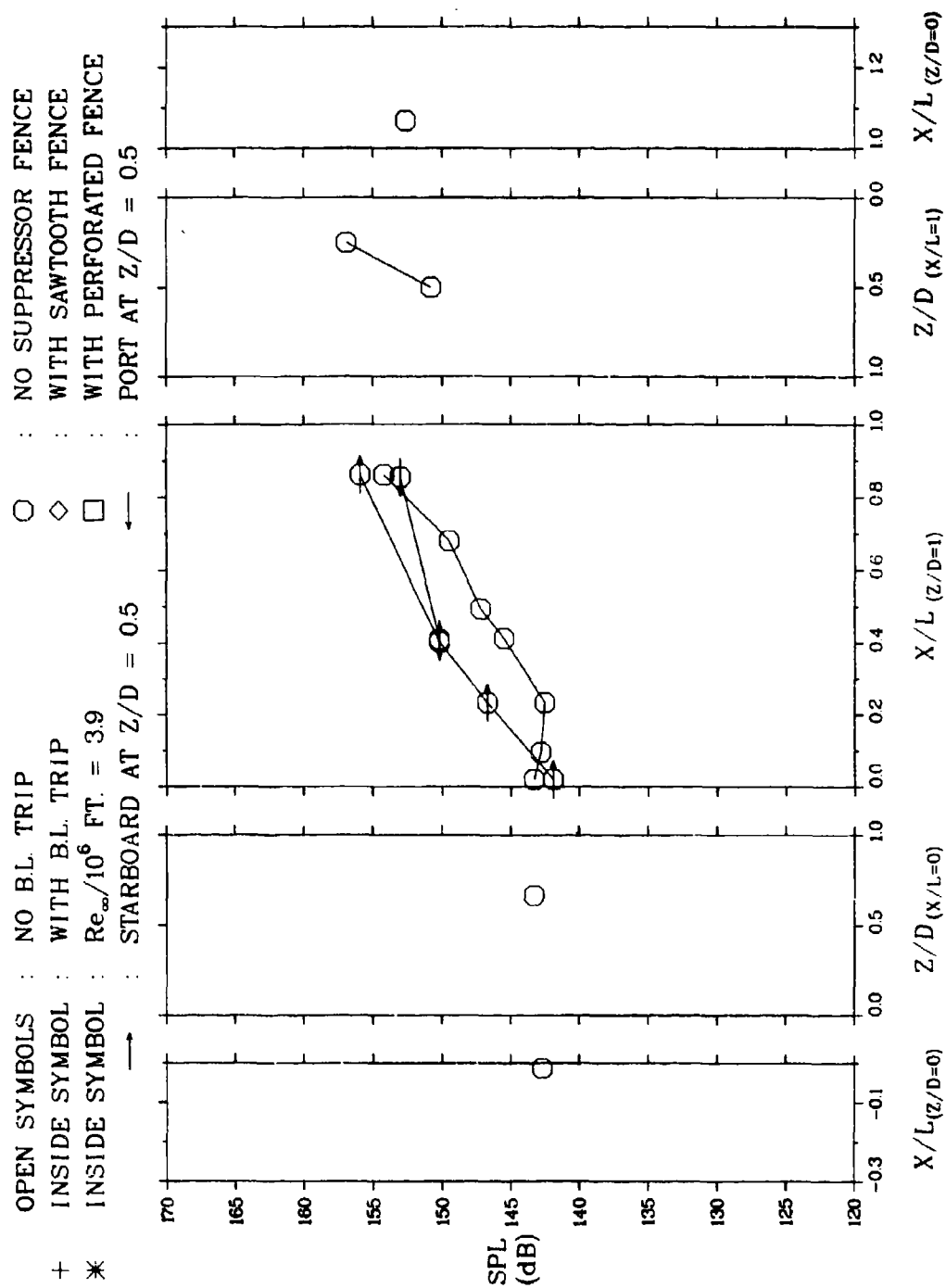


Figure 228 Acoustic Pressure Distributions in  $L/D = 6.2$  Cavity at  $M_{\infty} = 0.74$

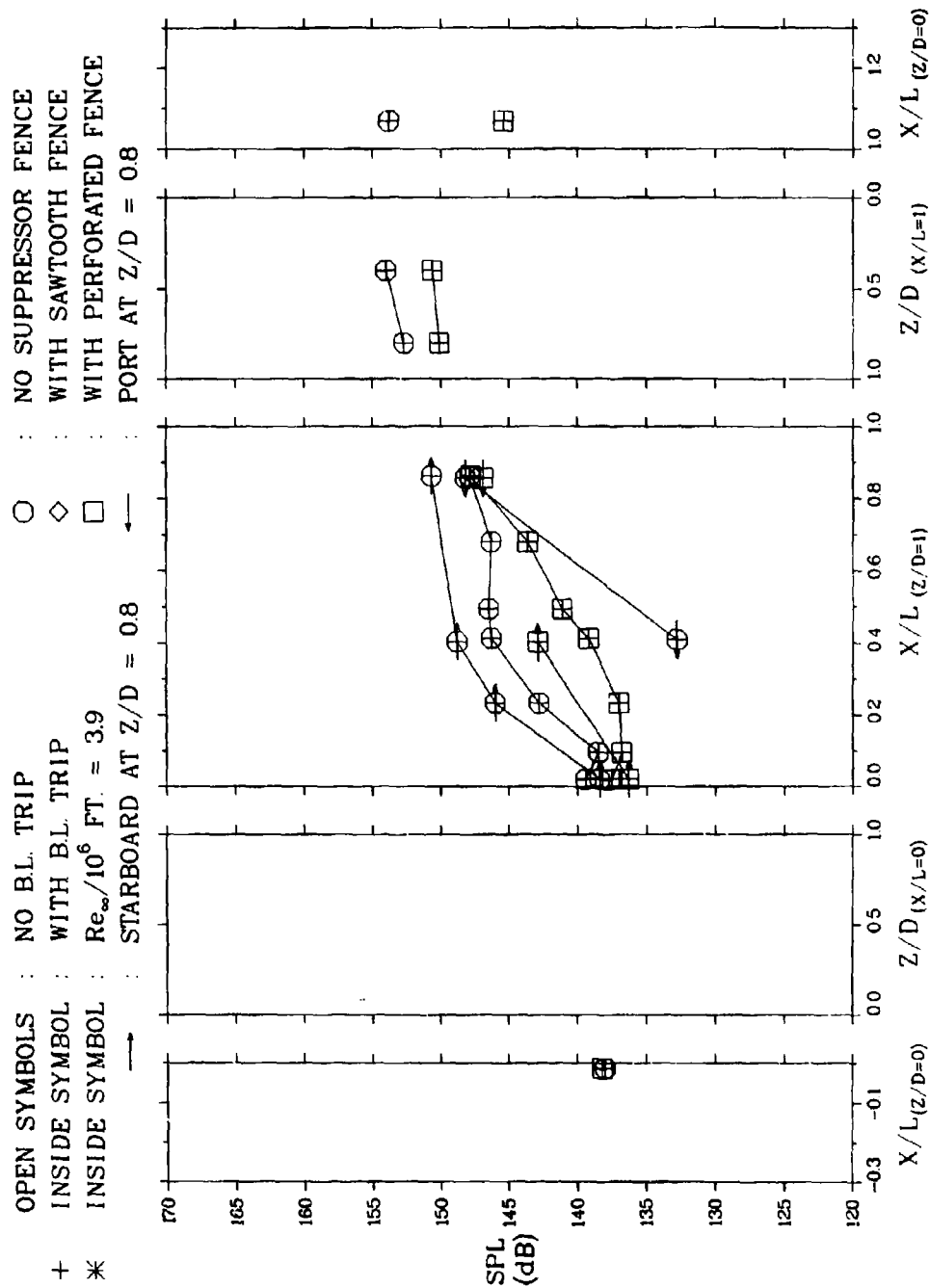


Figure 229 Acoustic Pressure Distributions in  $L/D = 9.9$  Cavity at  $M_{\infty} = 0.60$

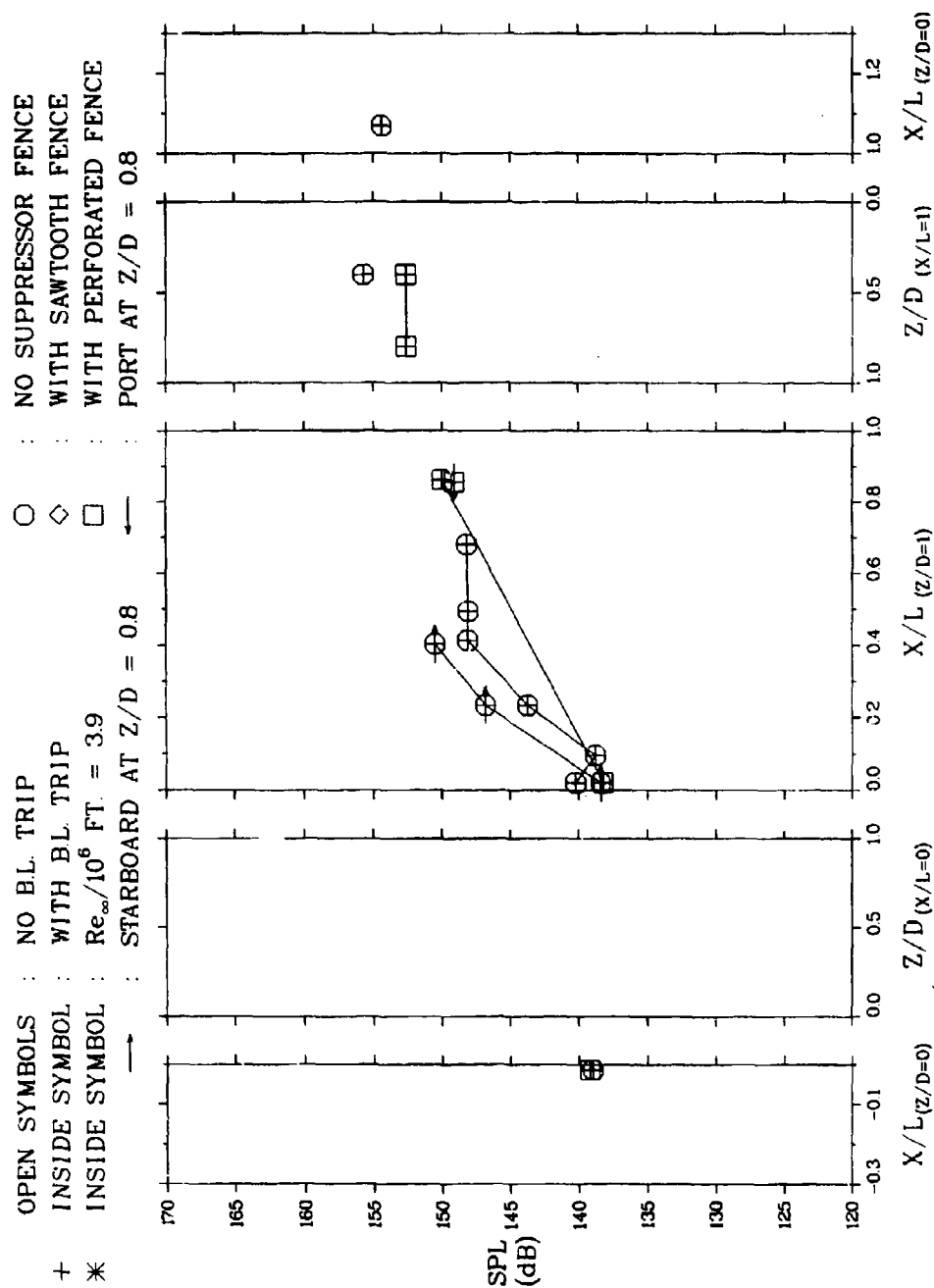
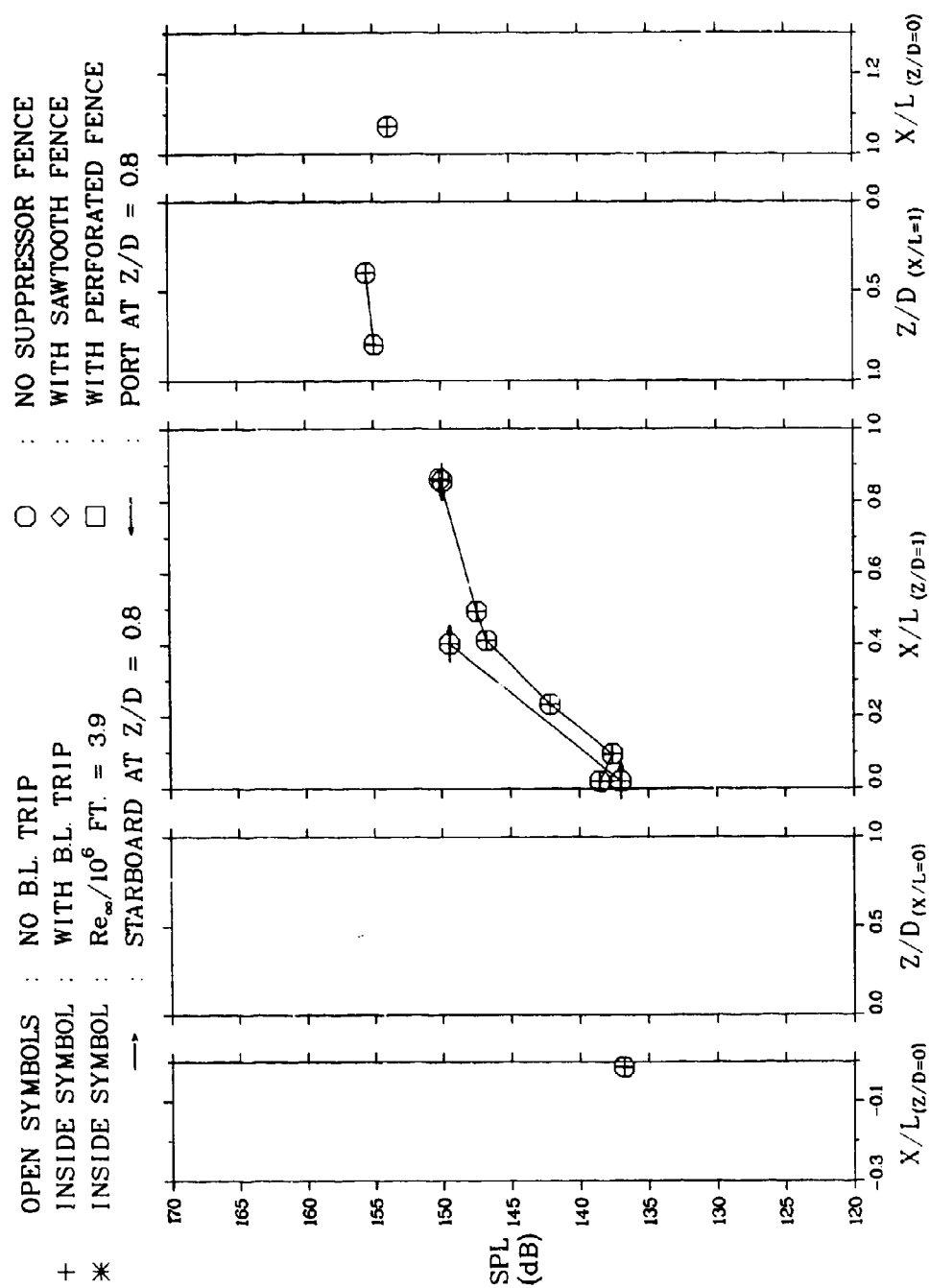


Figure 230 Acoustic Pressure Distributions in  $L/D = 9.9$  Cavity at  $M_{\infty} = 0.70$



**Figure 231** Acoustic Pressure Distributions in  $L/D = 9.9$  Cavity at  $M_\infty = 0.74$

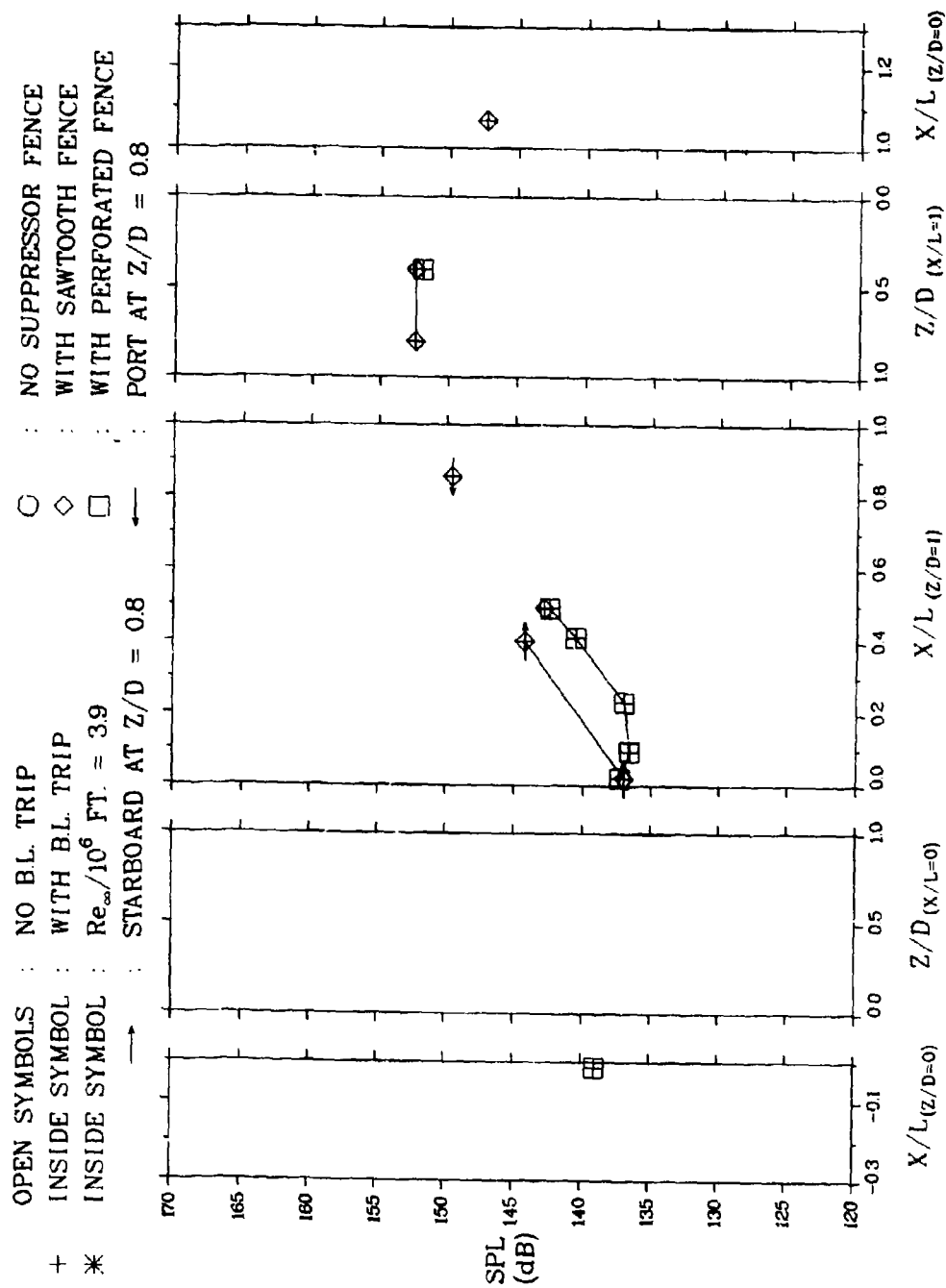


Figure 232 Acoustic Pressure Distributions in  $L/D = 9.9$  Cavity at  $M_{\infty} = 0.75$

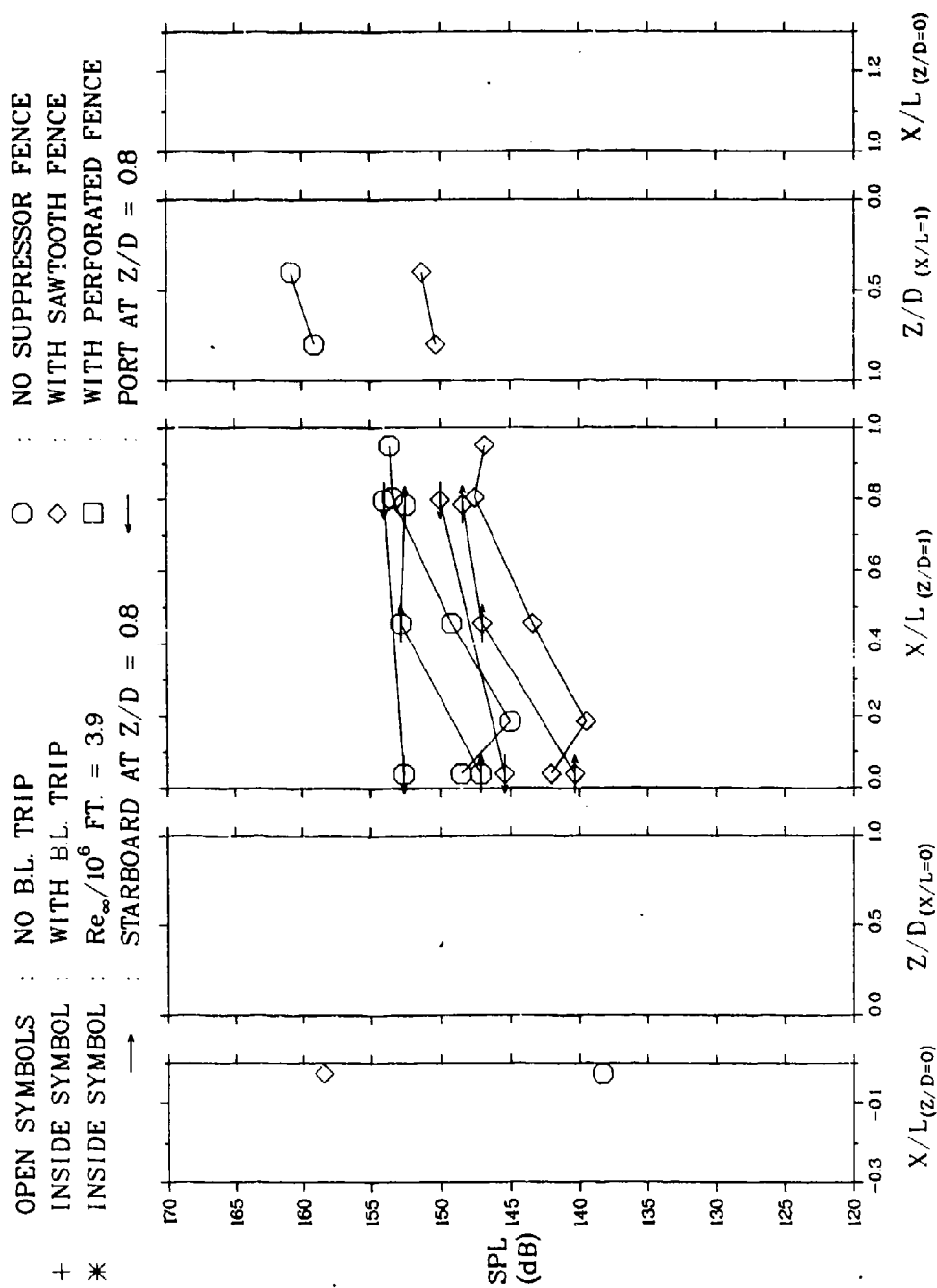


Figure 233 Acoustic Pressure Distributions at  $M_{\infty} = 1.5$  in  $L/D = 5.1$  Cavity

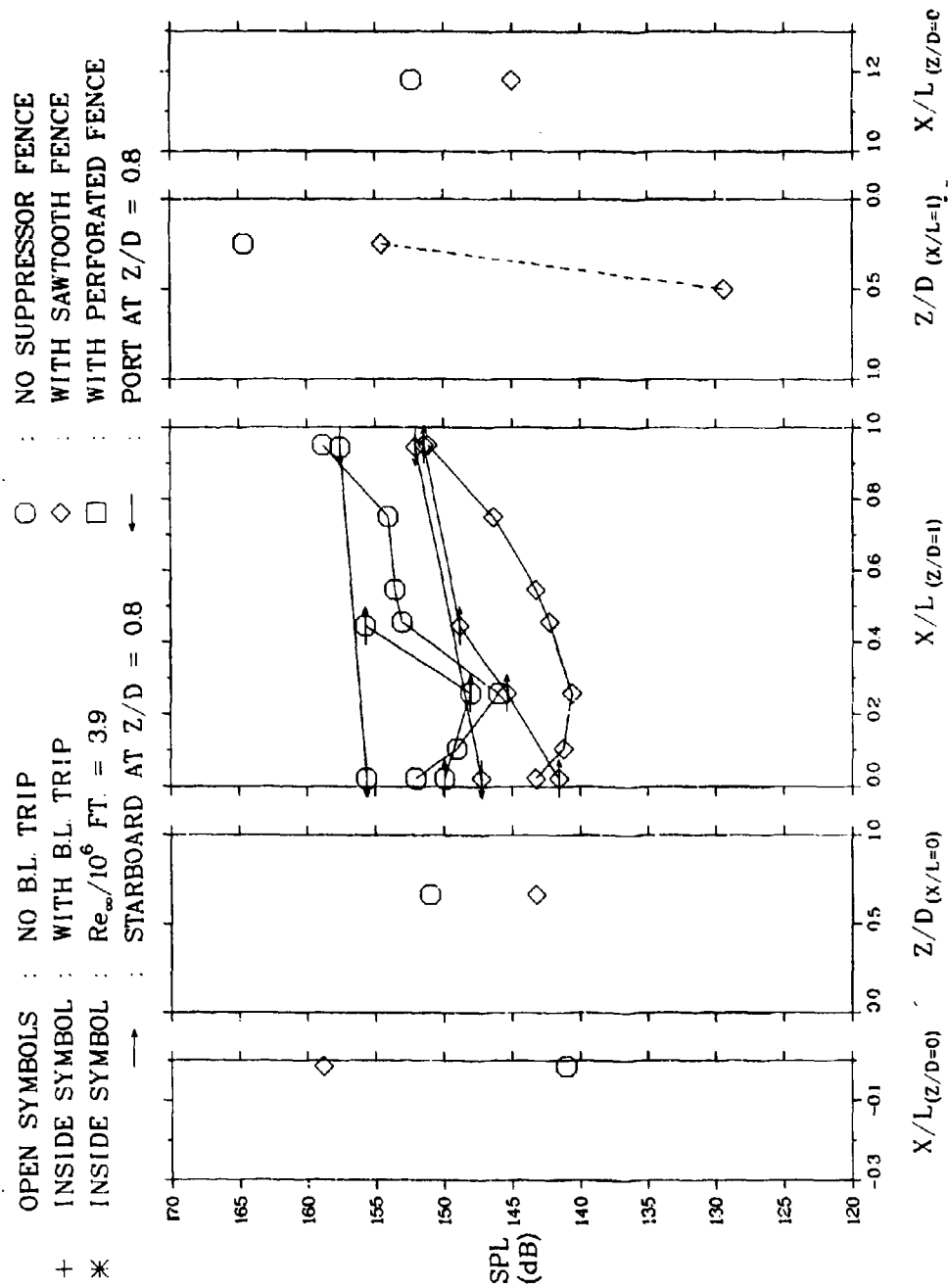


Figure 234 Acoustic Pressure Distributions at  $M_{\infty} = 1.5$  in  $L/D = 5.6$  Cavity



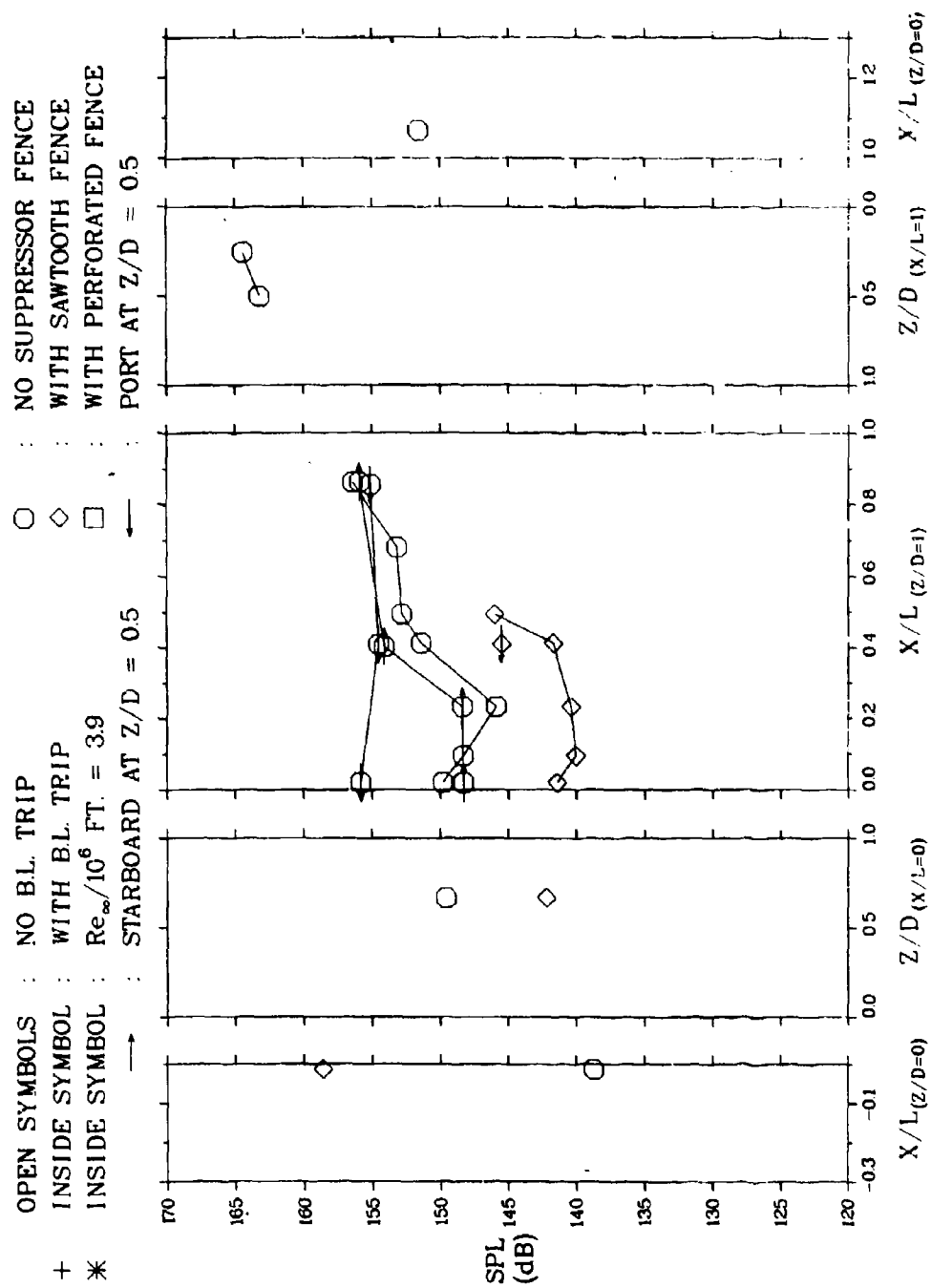


Figure 235 Acoustic Pressure Distributions at  $M_{\infty} = 1.5$  in  $L/D = 6.2$  Cavity

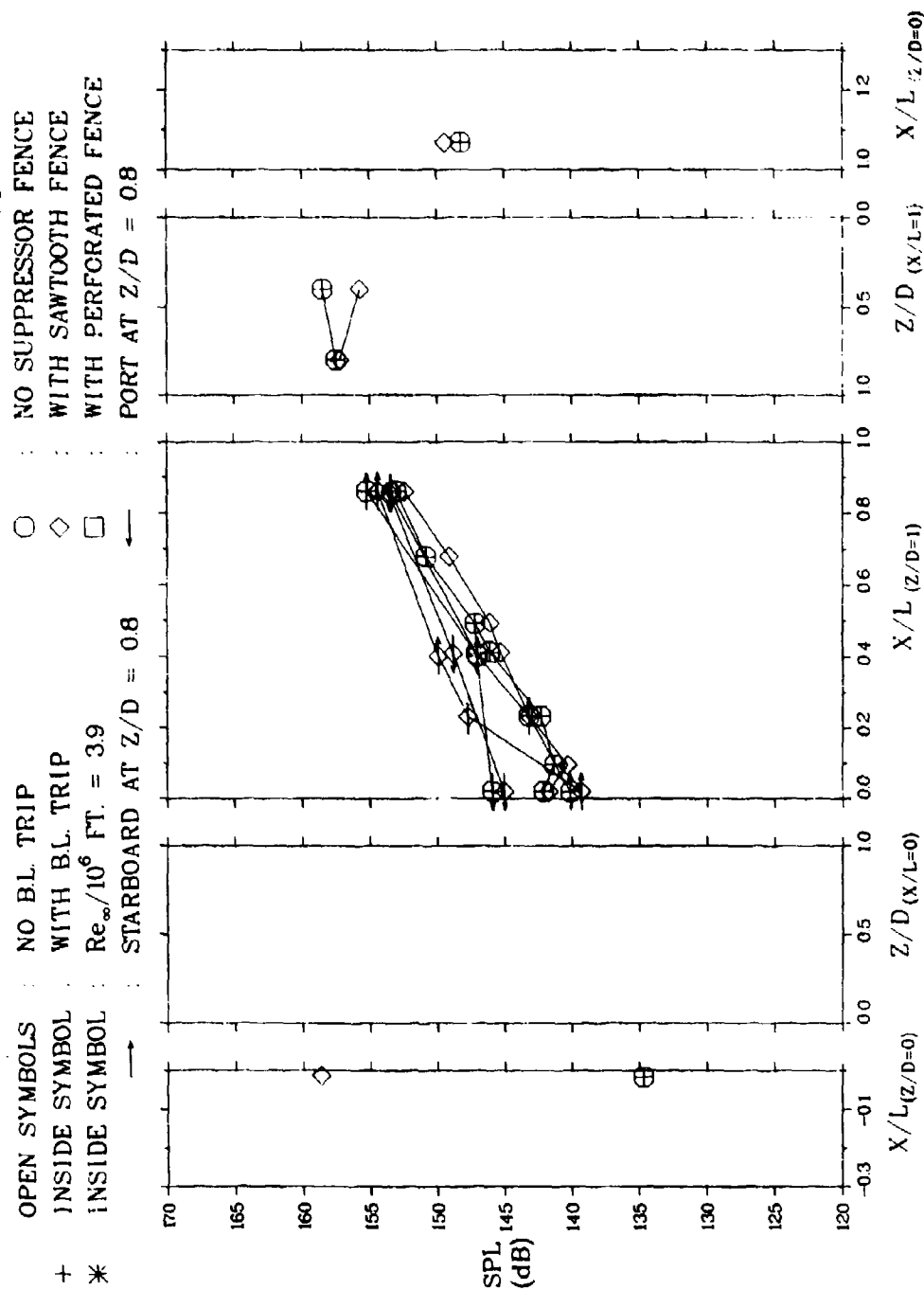


Figure 236 Acoustic Pressure Distributions at  $M_{\infty} = 1.5$  in  $L/D = 9.9$  Cavity

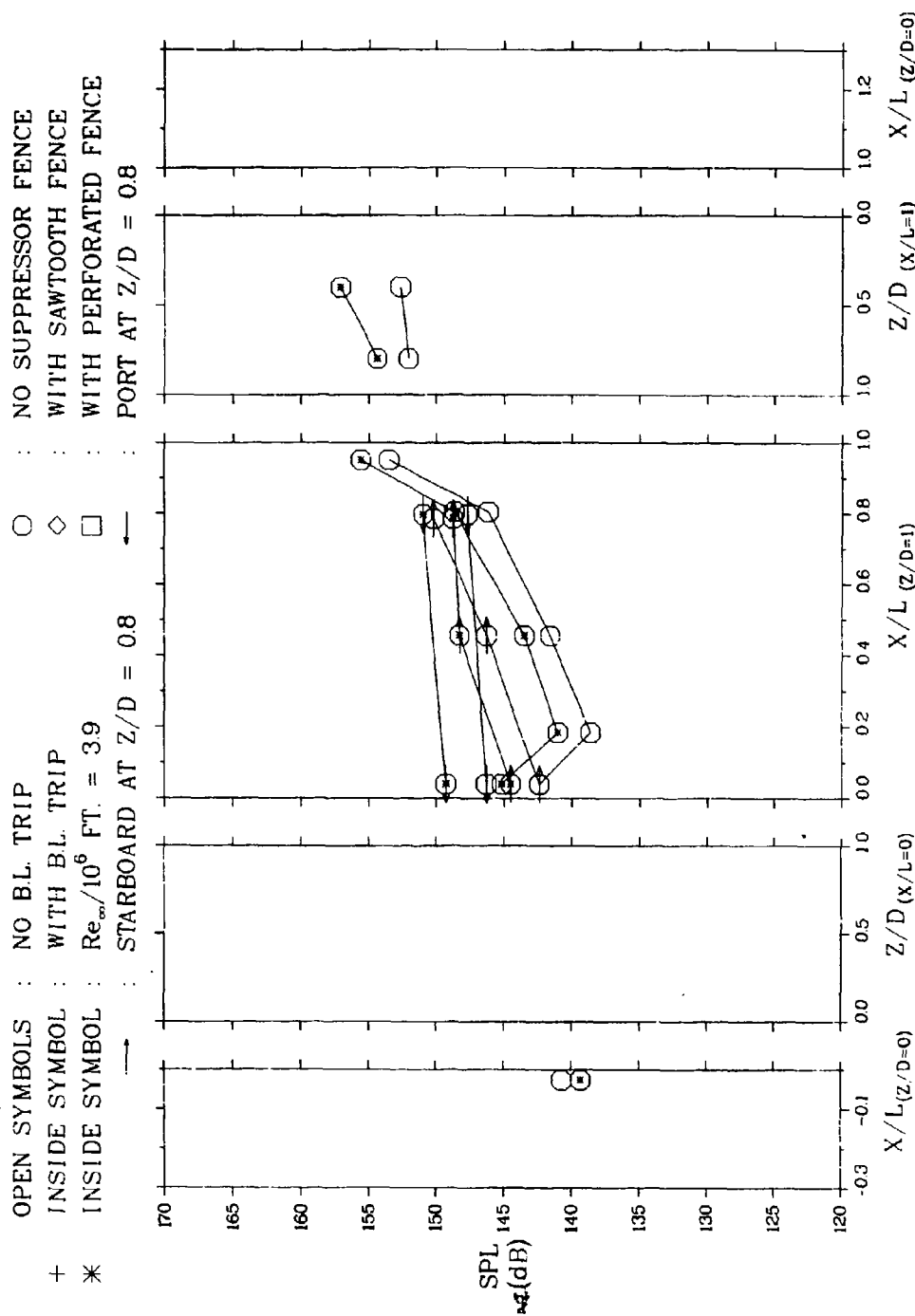


Figure 237 Acoustic Pressure Distributions at  $M_{\infty} = 2.3$  in  $L/D = 5.1$  Cavity,  
 Two Re Numbers, Without Suppressors

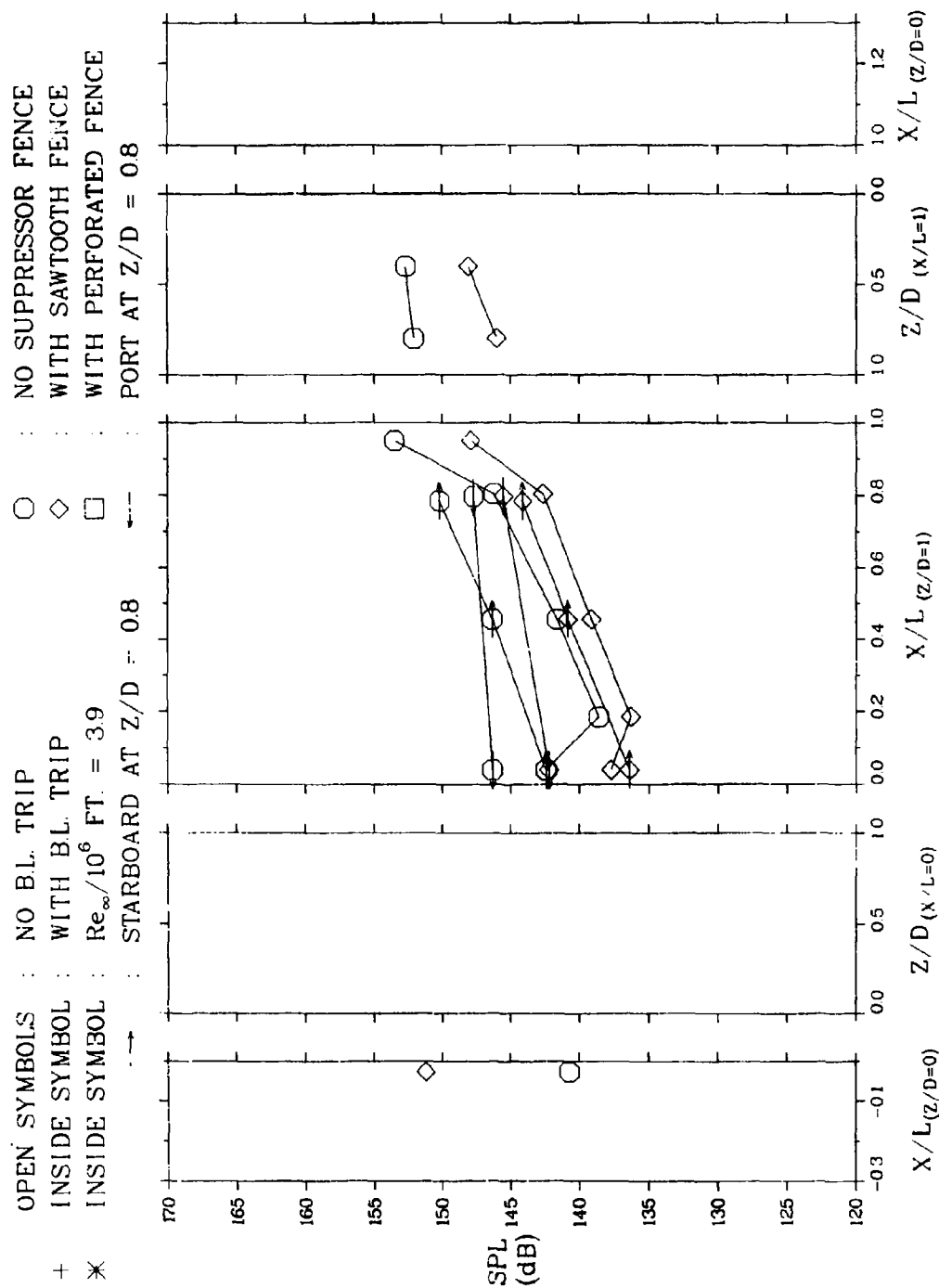


Figure 238 Acoustic Pressure Distributions at  $M_{\infty} = 2.3$  in  $L/D = 5.1$  Cavity  
 With and Without Saw-Tooth Fence

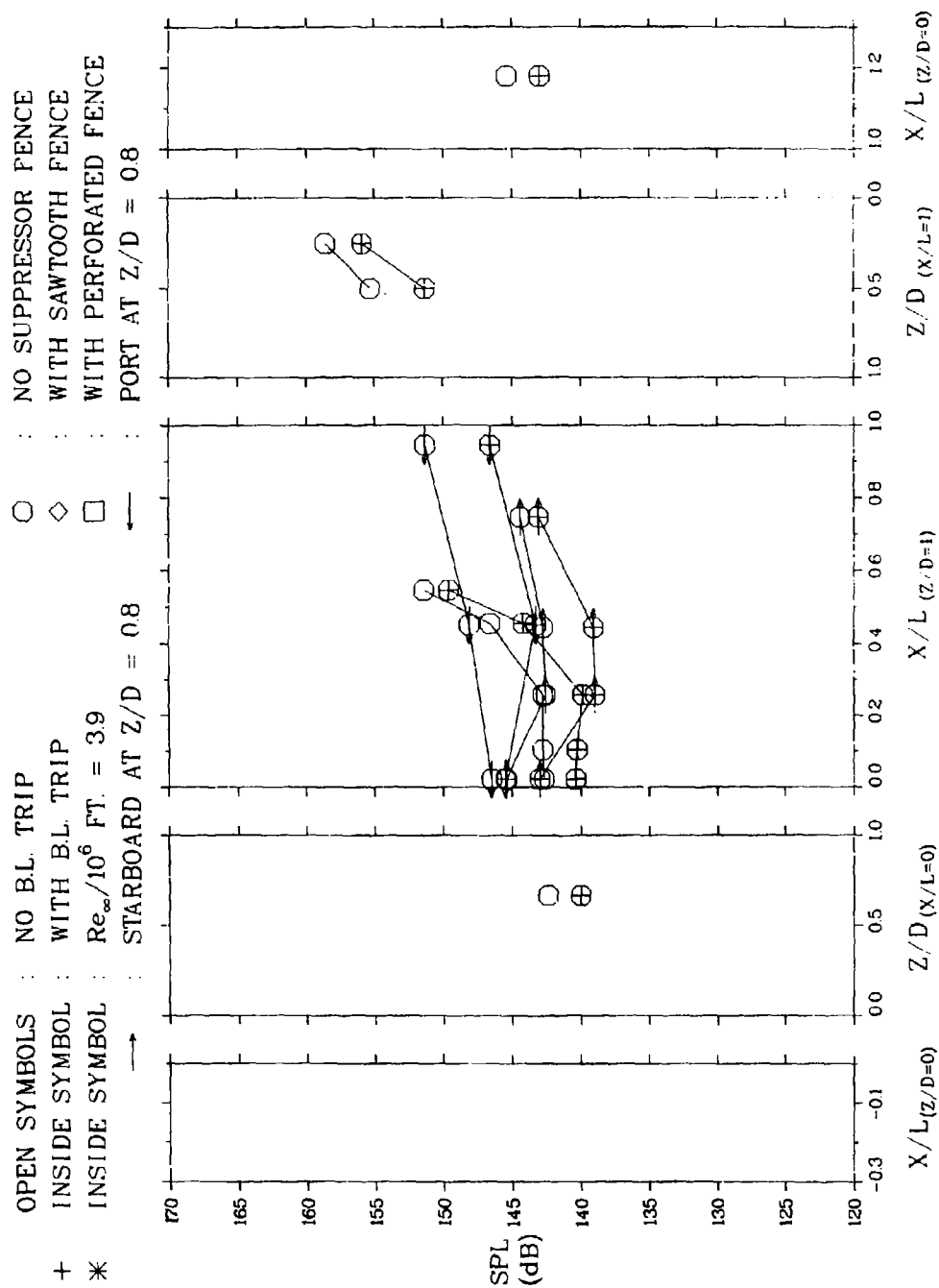


Figure 239 Acoustic Pressure Distributions at  $M_{\infty} = 2.3$  in  $L/D = 5.6$  Cavity With and Without B.L. Trip, Without Suppressors

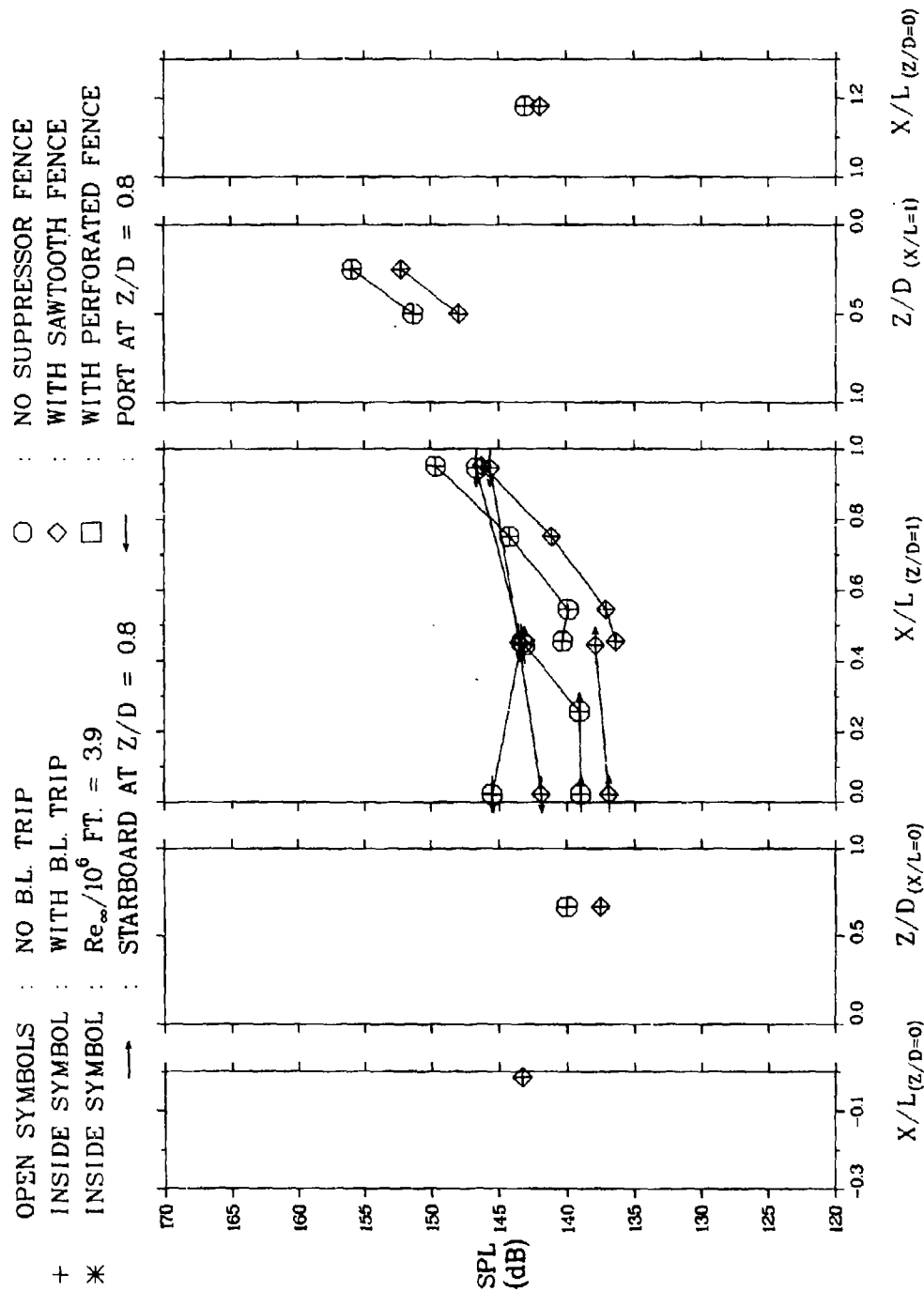


Figure 240 Acoustic Pressure Distributions at  $M_{\infty} = 2.3$  in  $L/D = 5.6$  Cavity With B.L. Trip, With and Without Saw-Tooth Suppressor

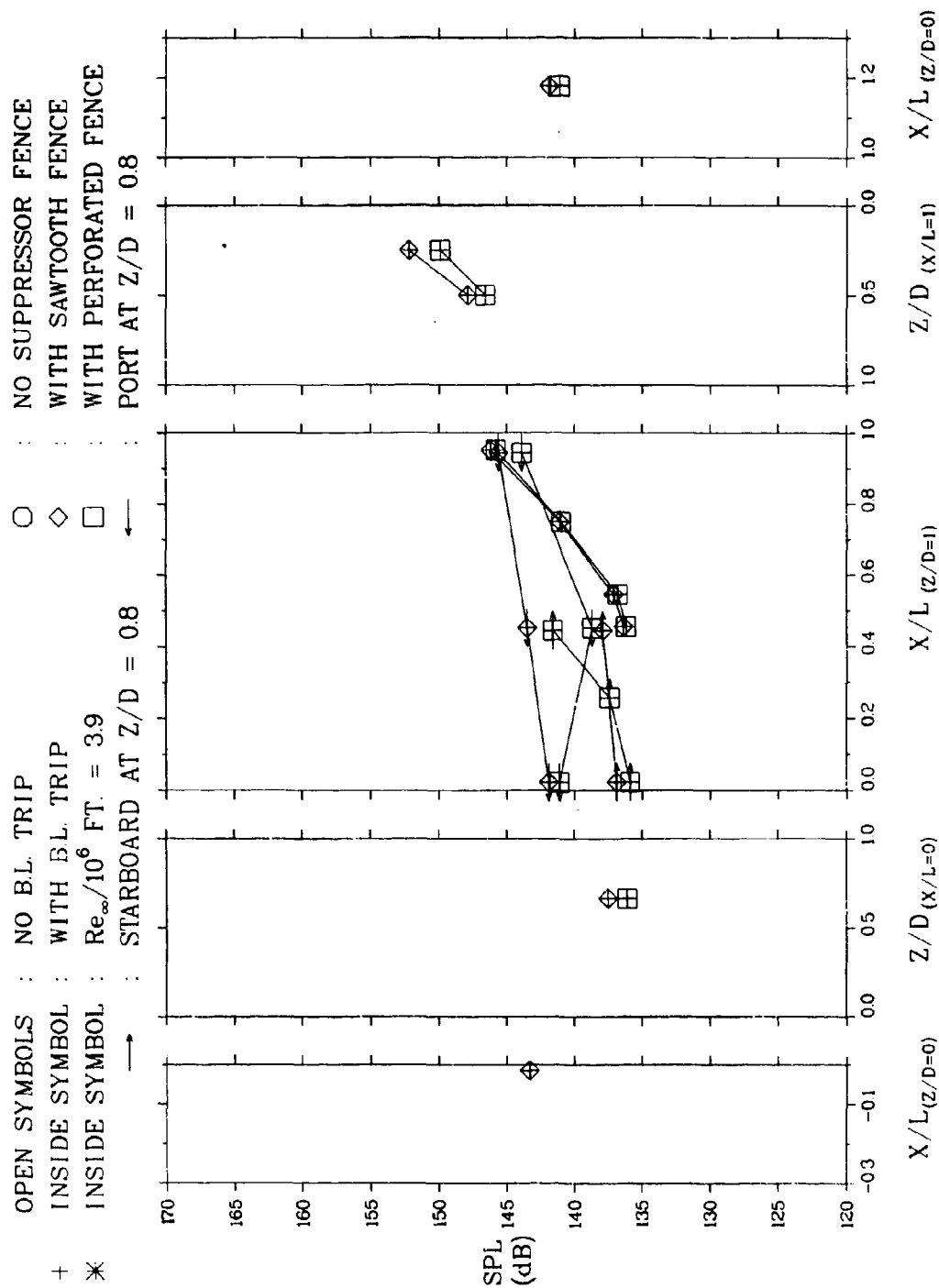


Figure 241 Acoustic Pressure Distributions at  $M_{\infty} = 2.3$  in  $L/D = 5.6$  Cavity  
 With B.L. Trip, Both Suppressor Types

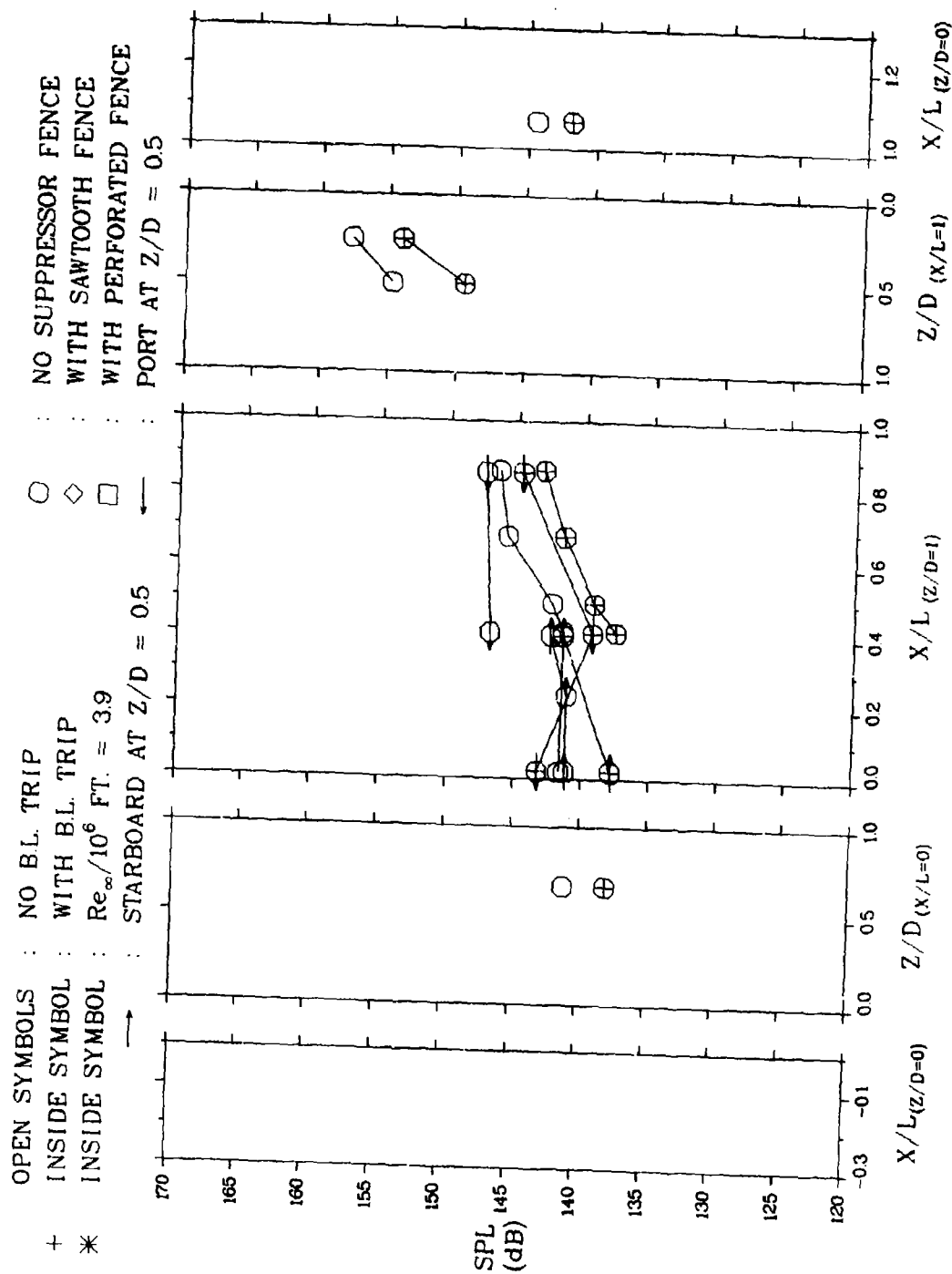


Figure 242 Acoustic Pressure Distributions at  $M_{\infty} = 2.3$  in  $L/D = 6.2$  Cavity  
 With and Without B.L. Trip, Without Suppressors



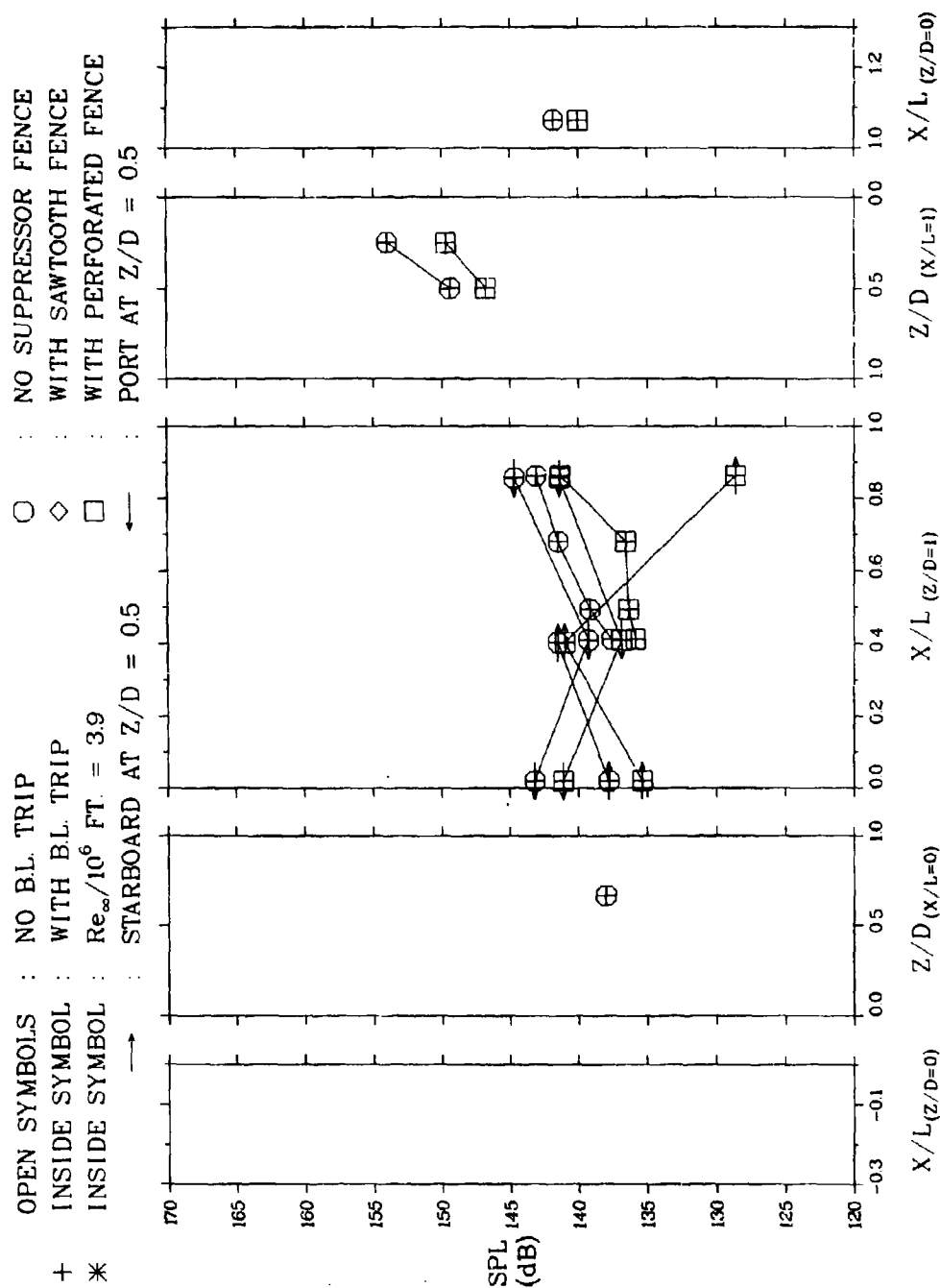


Figure 243 Acoustic Pressure Distributions at  $M_{\infty} = 2.3$  in  $L/D = 6.2$  Cavity With B.L. Trip, With and Without Perforated Suppressor

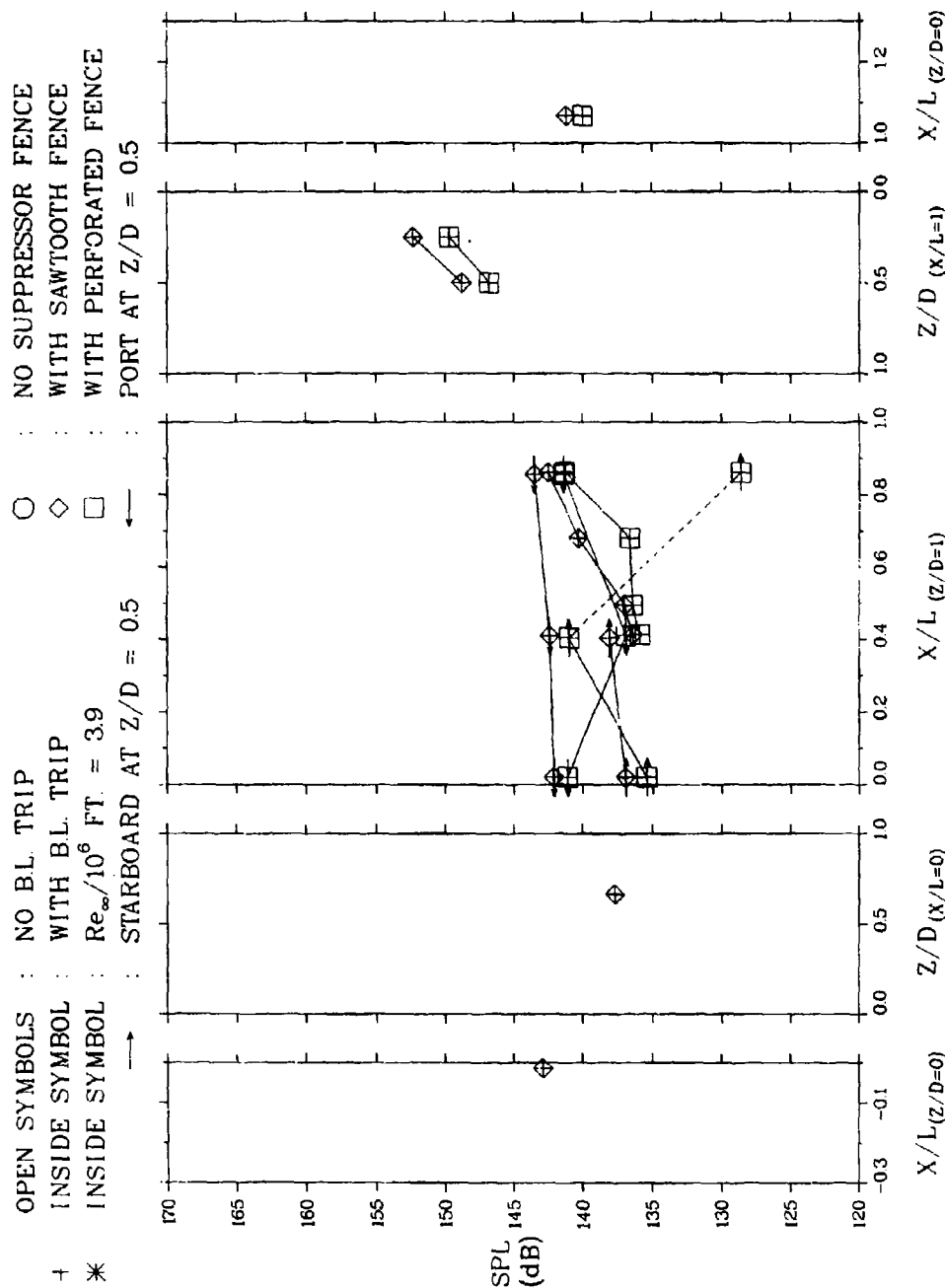


Figure 244 Acoustic Pressure Distributions at  $M_{\infty} = 2.3$  in  $L/D = 6.2$  Cavity With B.L. Trip, Both Suppressor Types

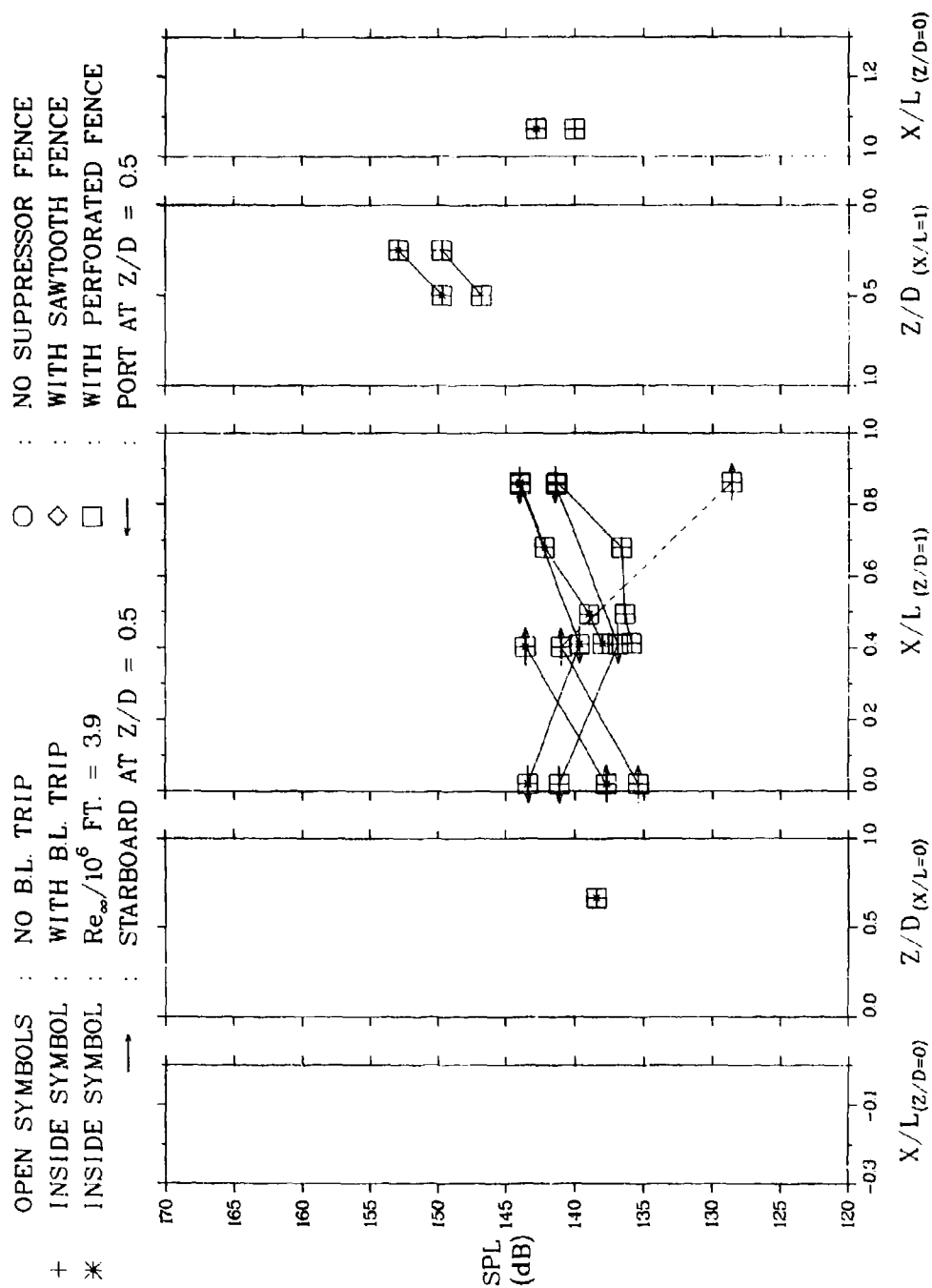


Figure 245 Acoustic Pressure Distributions at  $M_{\infty} = 2.3$  in  $L/D = 6.2$  Cavity  
 With B.L. Trip, Perforated Suppressor at Two Re

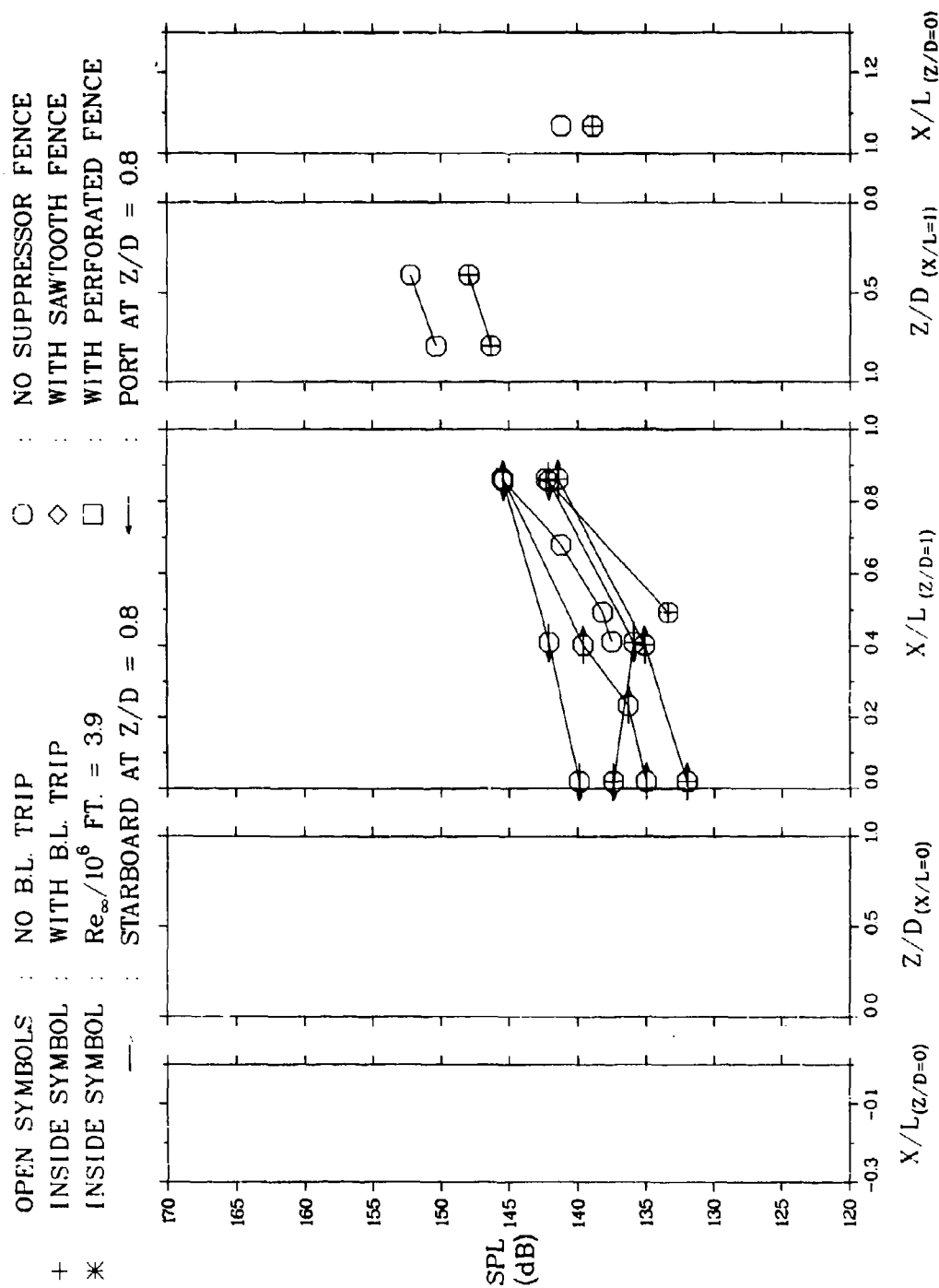


Figure 246 Acoustic Pressure Distributions at  $M_{\infty} = 2.3$  in  $L/D = 9.9$  Cavity  
 With and Without B.L. Trip, Without Suppressors

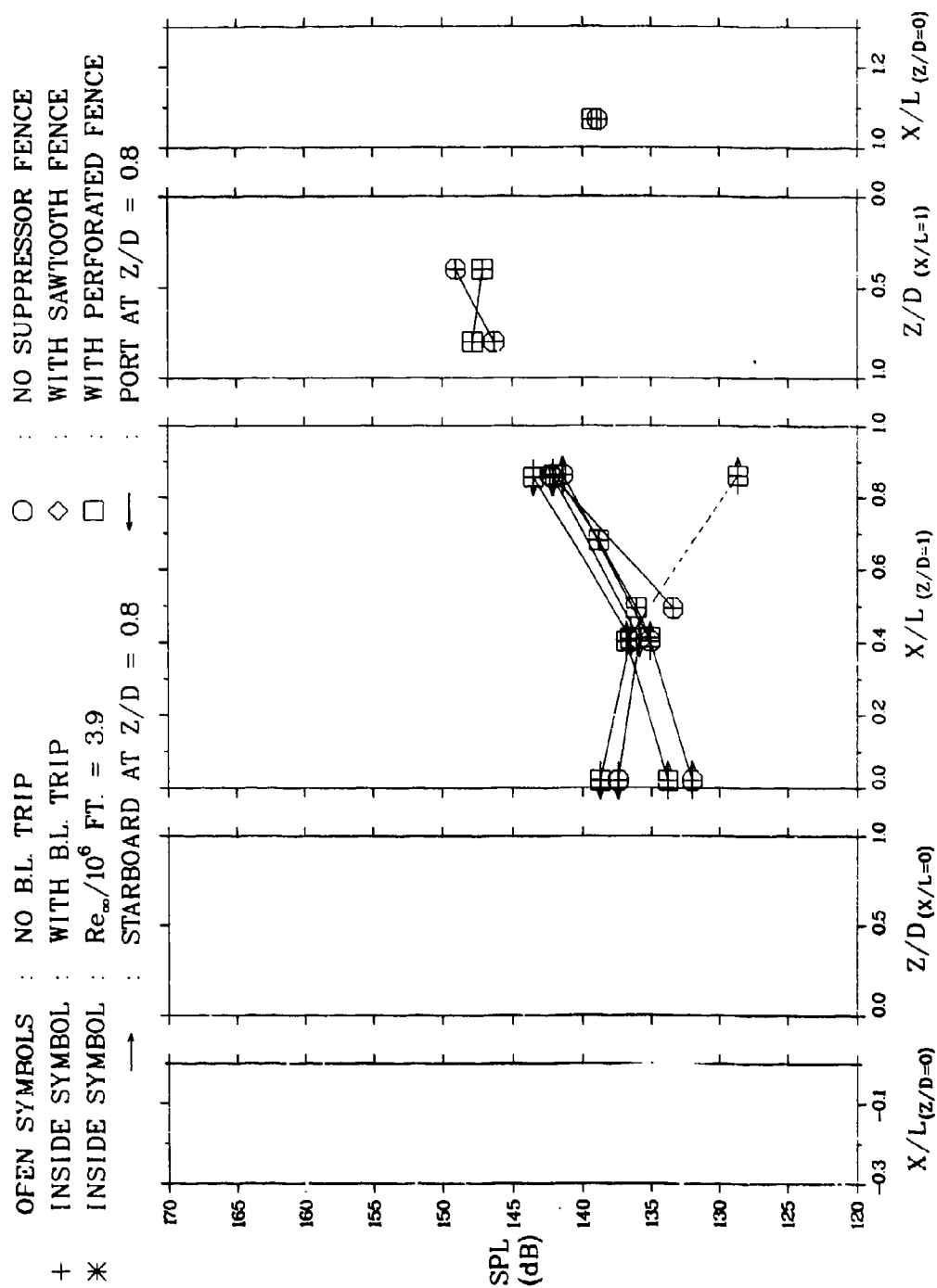


Figure 247 Acoustic Pressure Distributions at  $M_{\infty} = 2.3$  in  $L/D = 9.9$  Cavity  
 With B.L. Trip, With and Without Perforated Suppressor

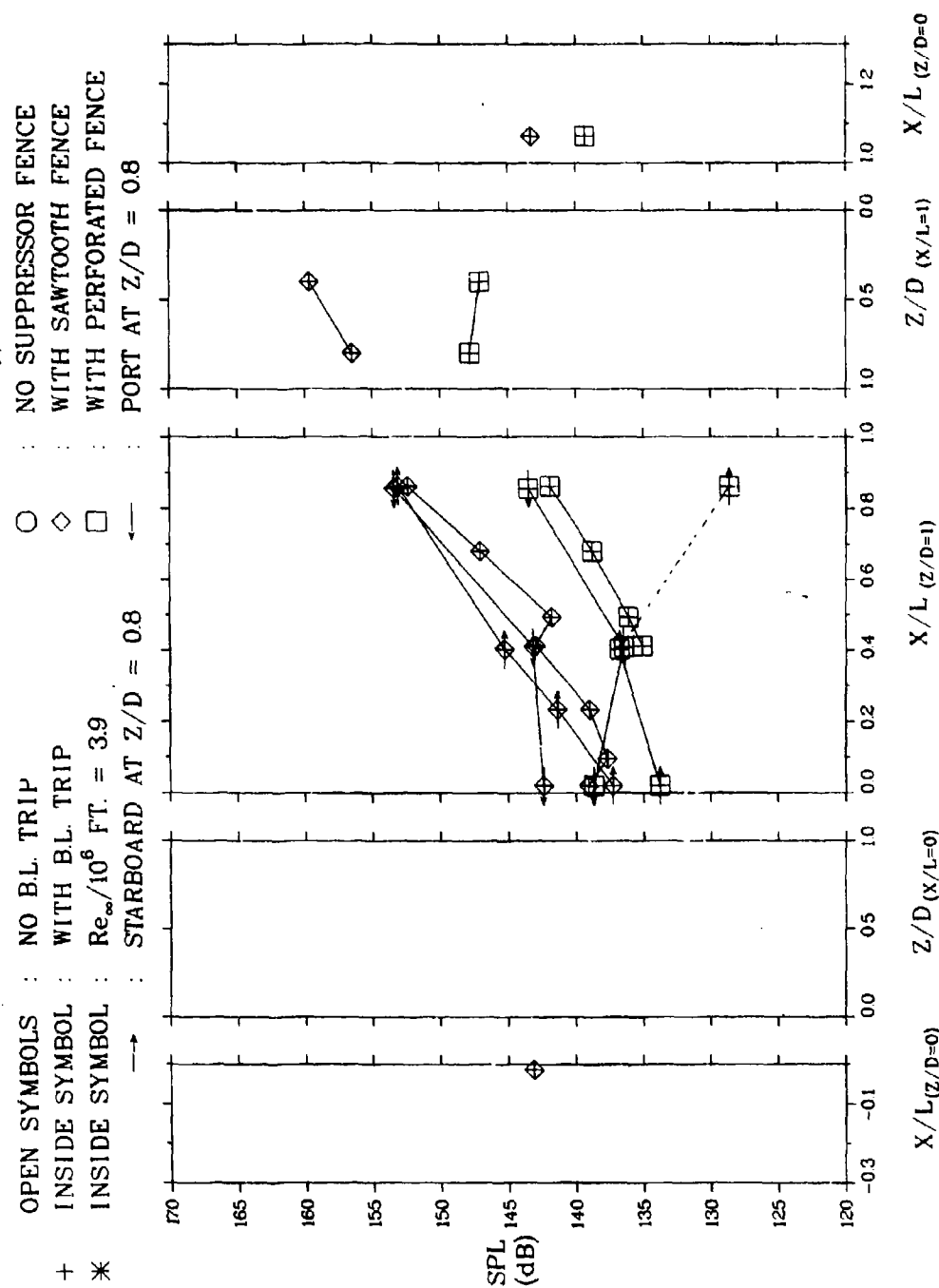


Figure 248 Acoustic Pressure Distributions at  $M_{\infty} = 2.3$  in  $L/D = 9.9$  Cavity  
 With B.L. Trip, Both Suppressor Types

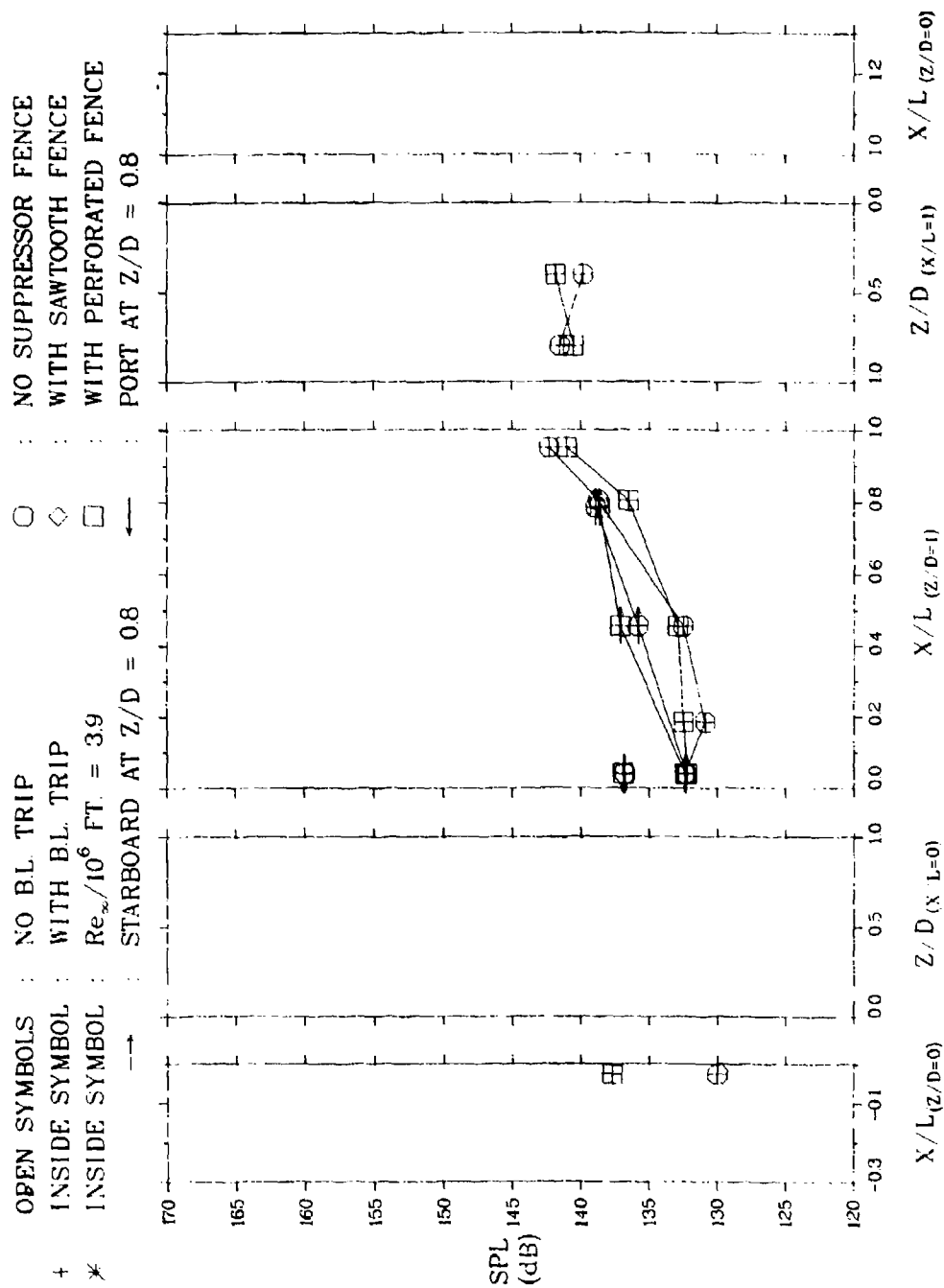


Figure 249 Acoustic Pressure Distributions at  $M_{\infty} = 3.0$  in  $L/D = 5.1$  Cavity

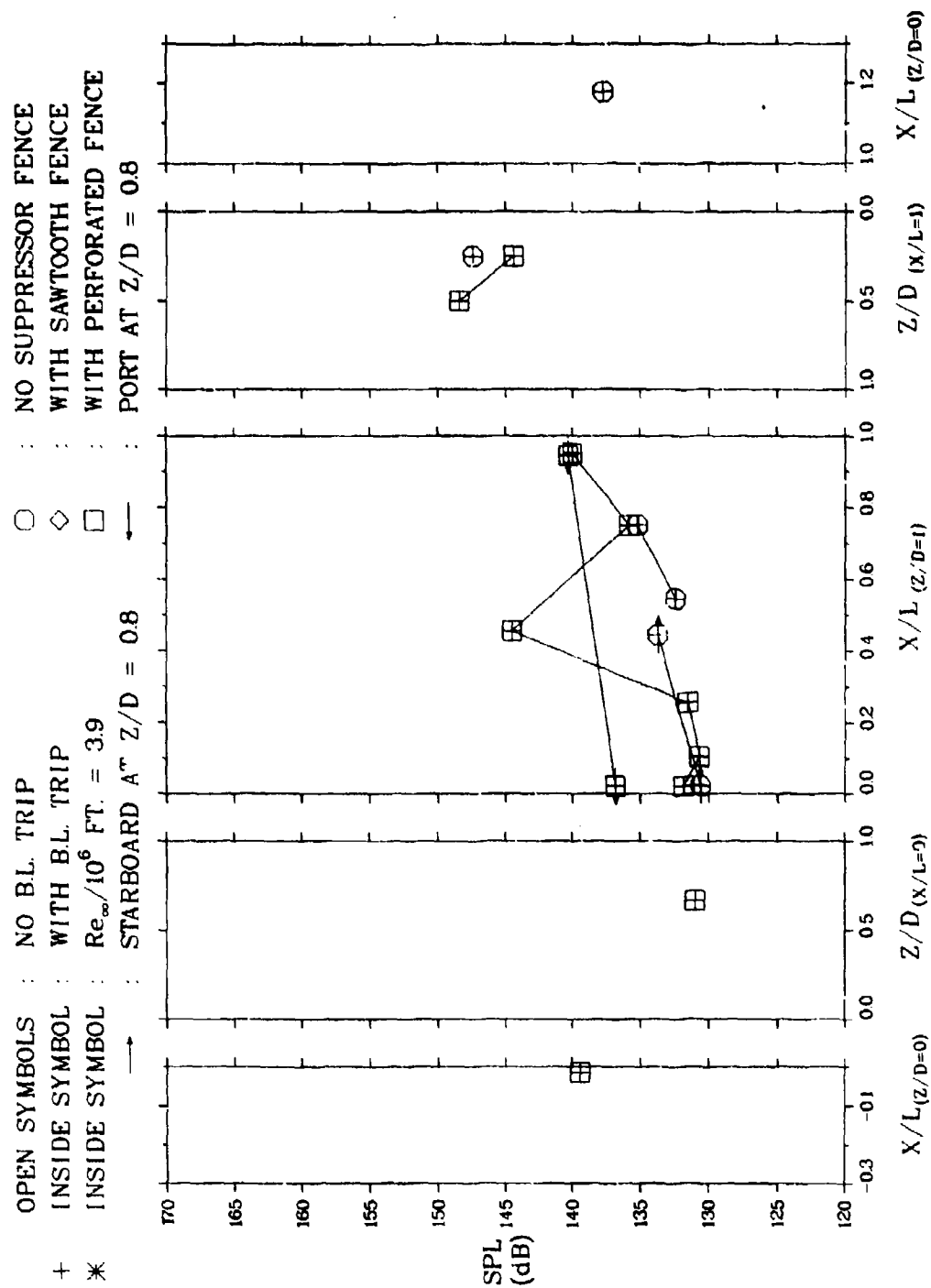


Figure 250 Acoustic Pressure Distributions at  $M_{\infty} = 3.0$  in  $L/D = 5.6$  Cavity



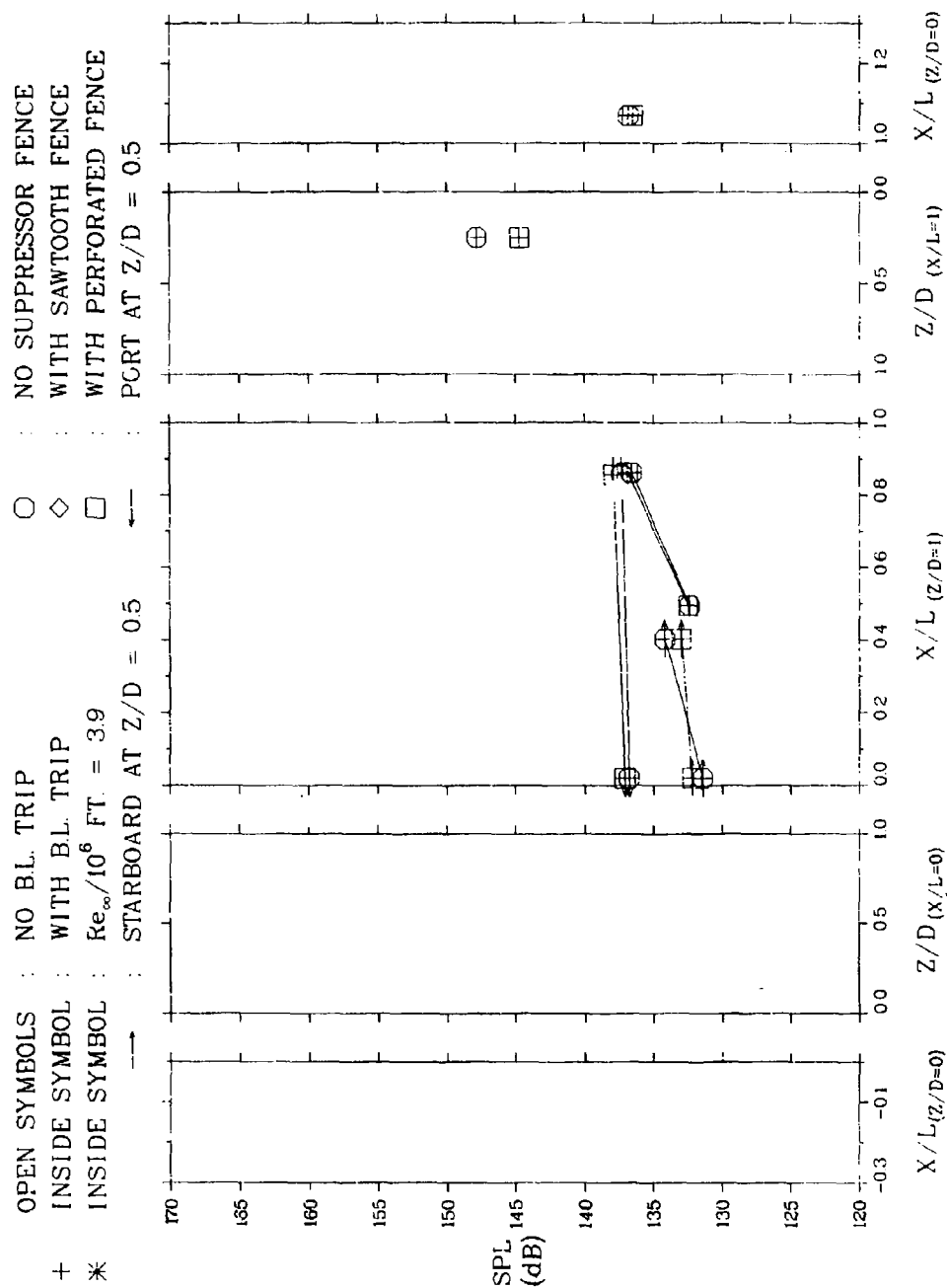


Figure 251 Acoustic Pressure Distributions at  $M_{\infty} = 3.0$  in  $L/D = 6.2$  Cavity

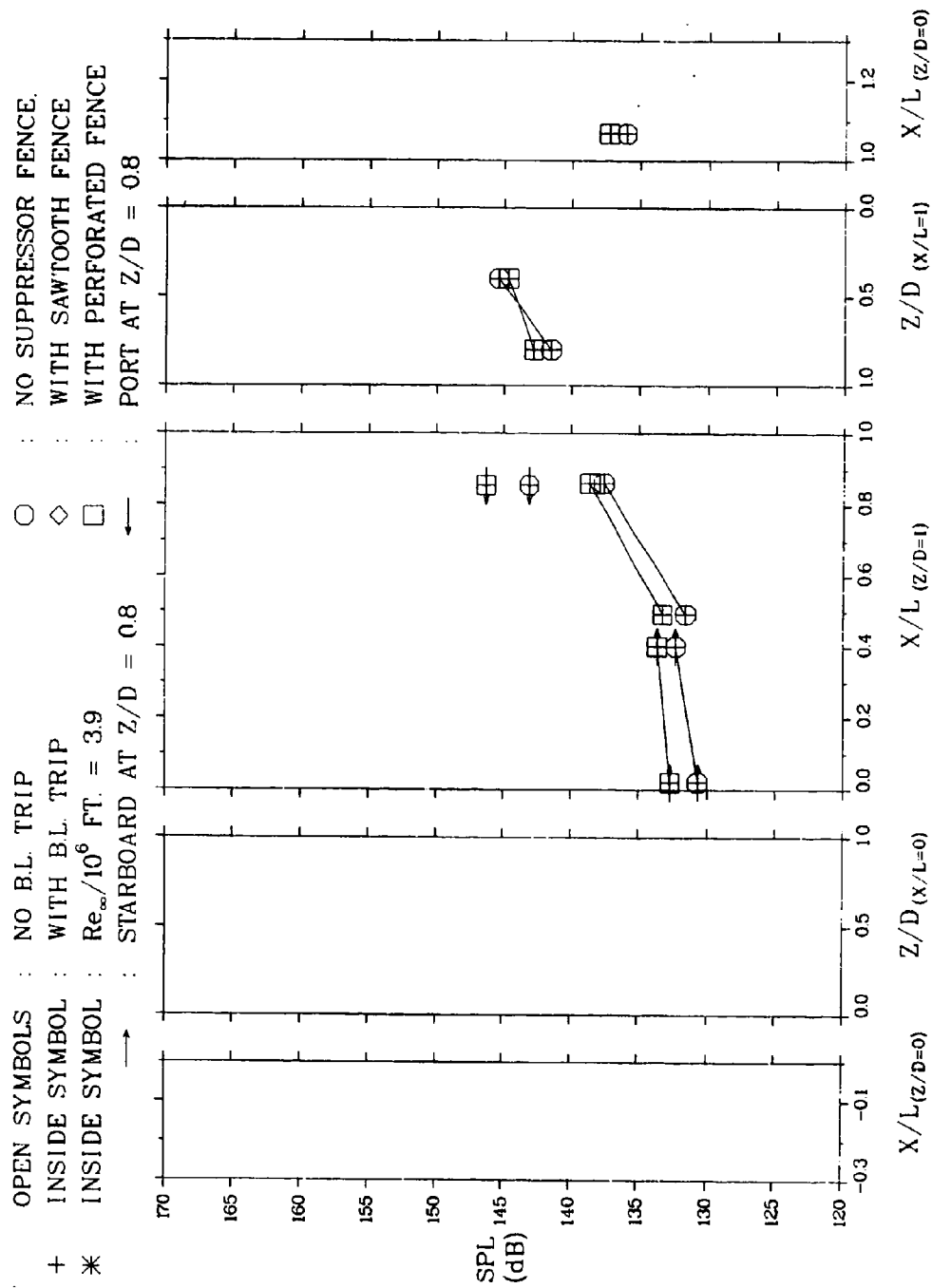
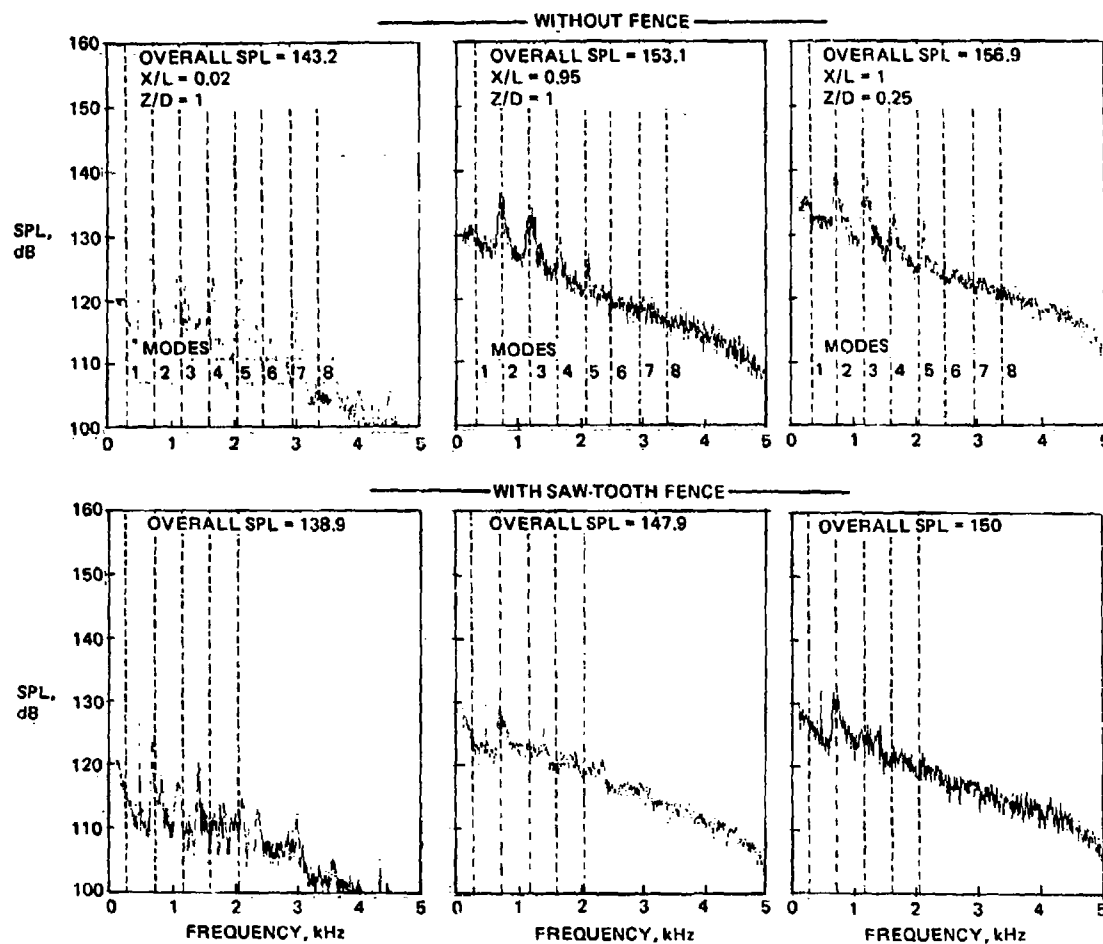
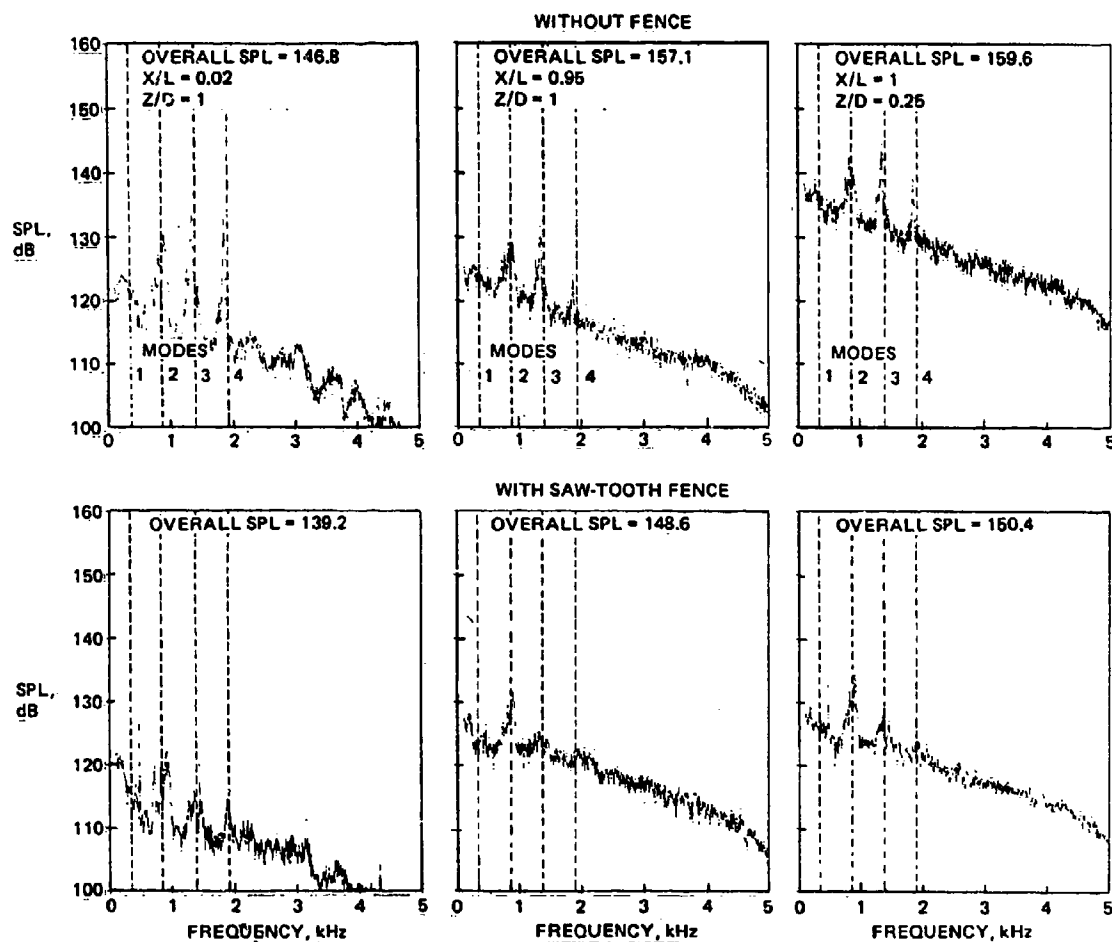


Figure 252 Acoustic Pressure Distributions at  $M_{\infty} = 3.0$  in  $L/D = 9.9$  Cavity



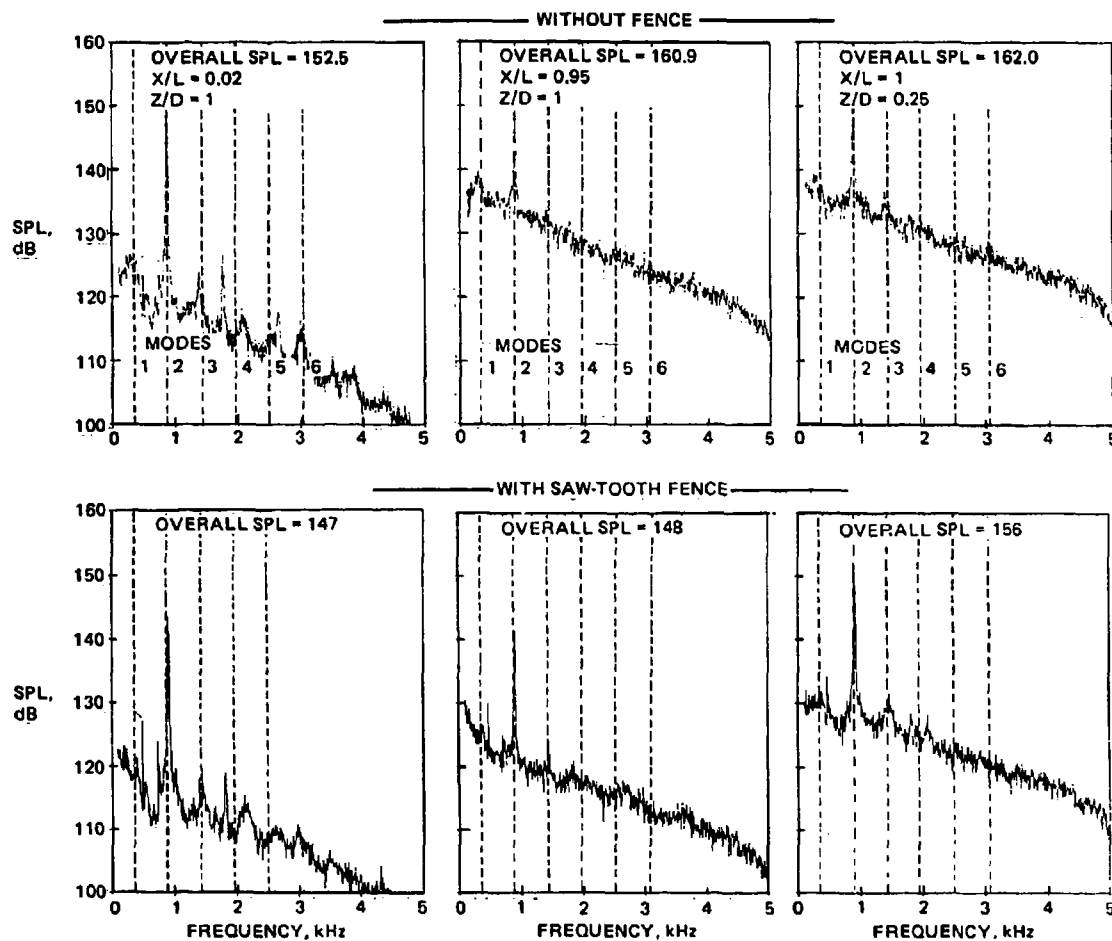
0934-002(T)

Figure 253 Effects of Cavity Oscillation Suppressor Fence on Frequency Spectra at 3 Locations in  $L/D = 5.6$  Cavity at  $M_\infty = 0.6$ . (Theoretically predicted frequencies are indicated by dashed lines.)



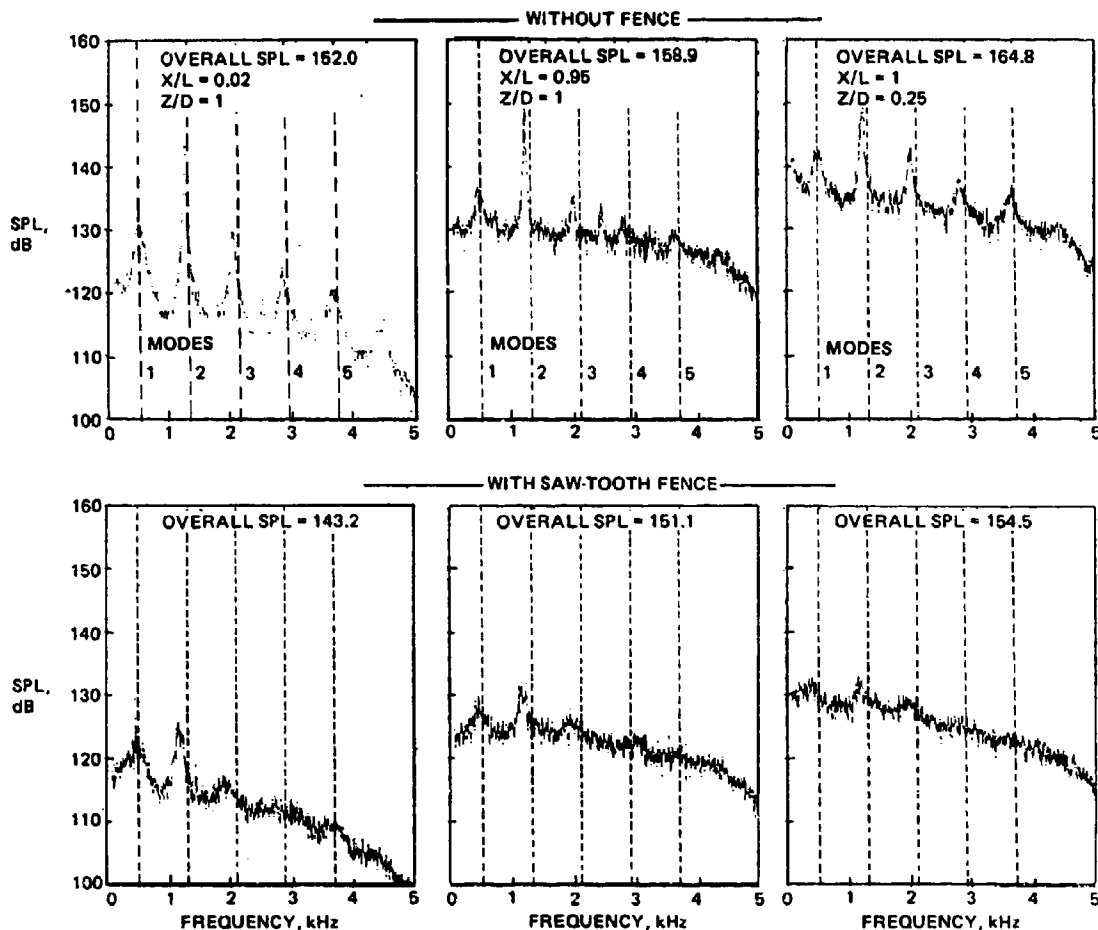
0934-003(T)

Figure 254 Effects of Cavity Oscillation Suppressor Fence on Frequency Spectra at 3 Locations in  $L/D = 5.6$  Cavity at  $M_\infty = 0.7$ . (Theoretically predicted frequencies are indicated by dashed lines.)



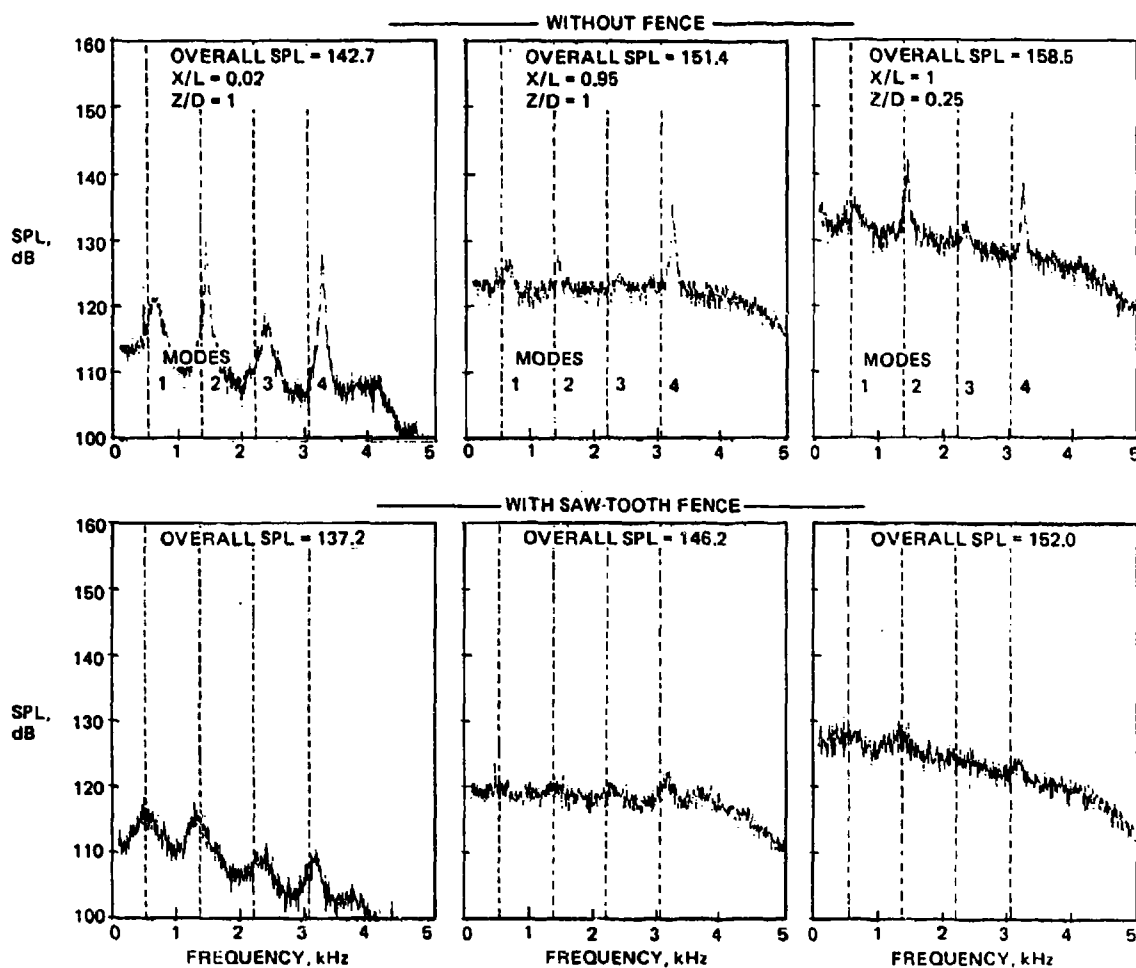
0934-004(T)

Figure 255 Effects of Cavity Oscillation Suppressor Fence on Frequency Spectra at 3 Locations in  $L/D = 5.6$  Cavity at  $M_\infty = 0.74$ . (Theoretically predicted frequencies are indicated by dashed lines.)



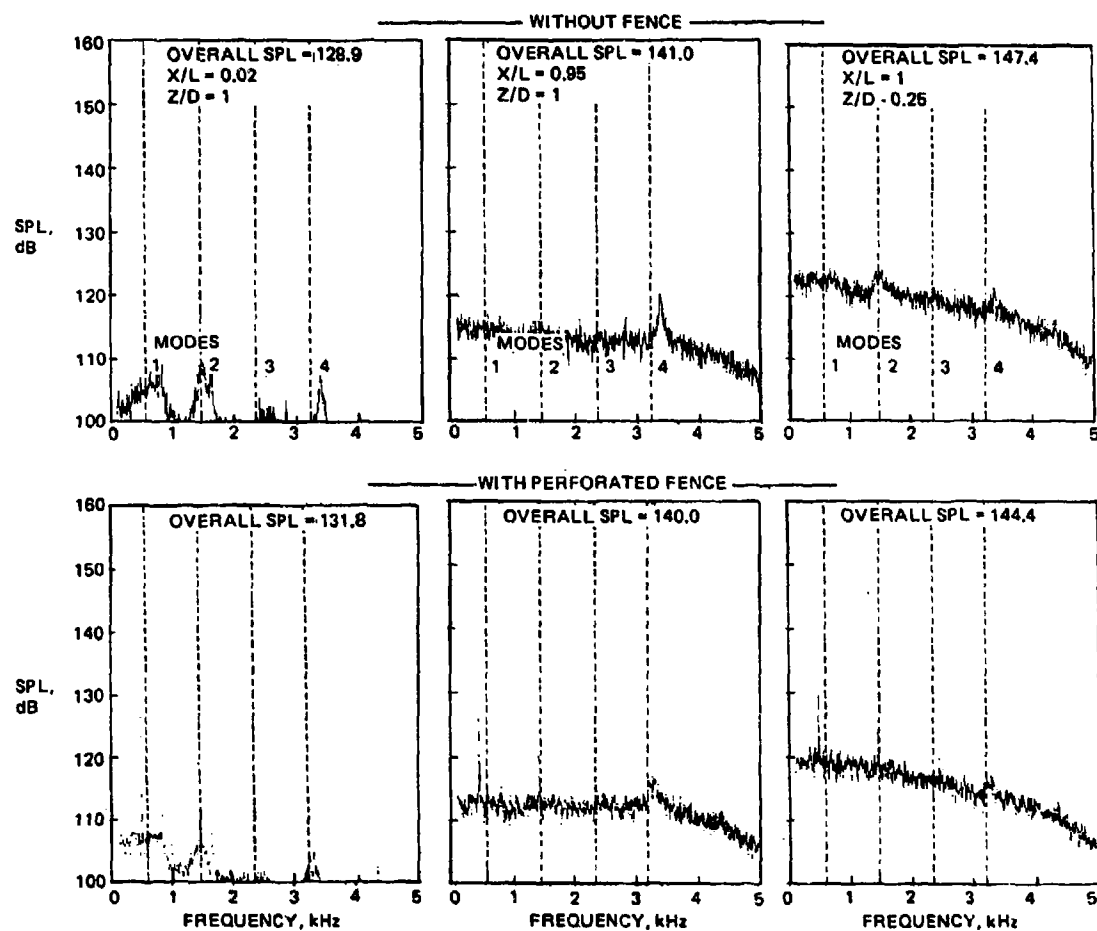
0934-005(T)

Figure 256 Effects of Cavity Oscillation Suppressor Fence on Frequency Spectra at 3 Locations in  $L/D = 5.6$  Cavity at  $M_\infty = 1.5$ . (Theoretically predicted frequencies are indicated by dashed lines.)



0934-006(T)

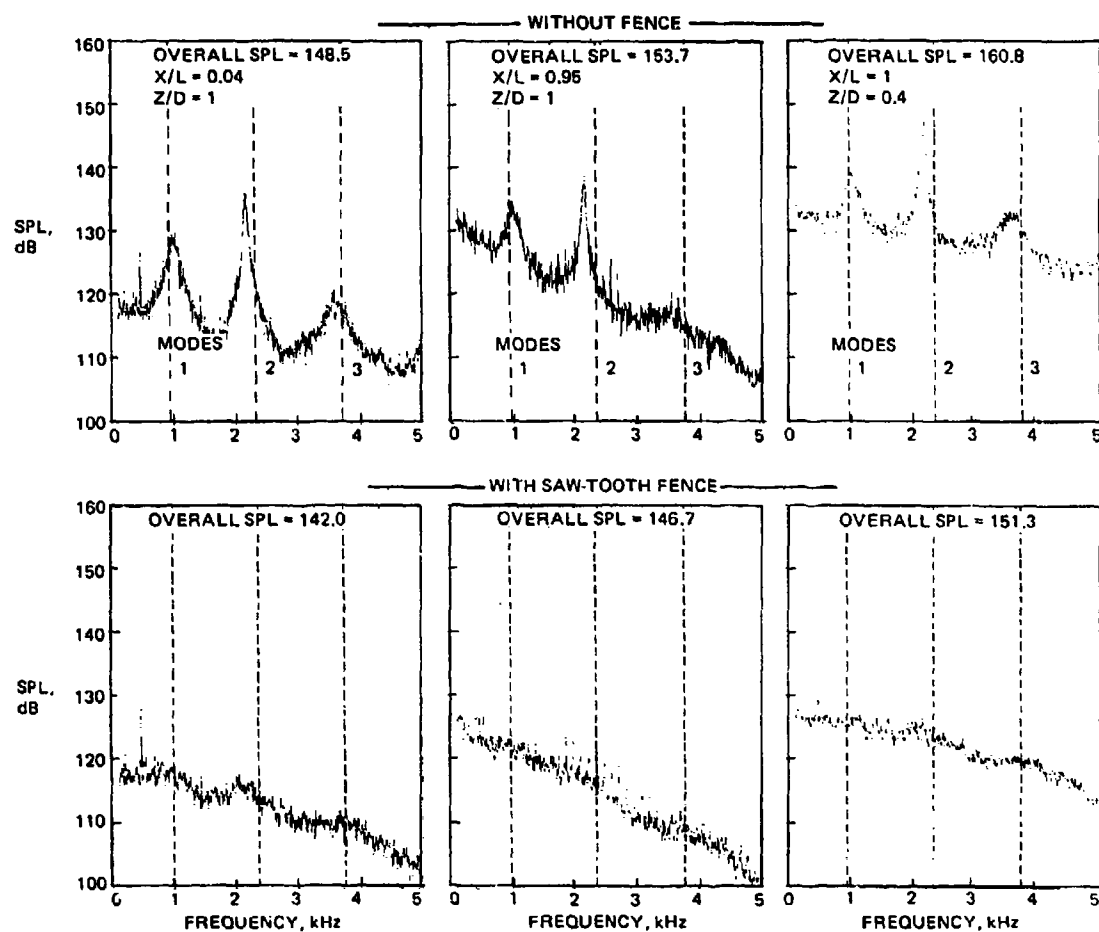
Figure 257 Effects of Cavity Oscillation Suppressor Fence on Frequency Spectra at 3 Locations in  $L/D = 5.6$  Cavity at  $M_\infty = 2.3$ . (Theoretically predicted frequencies are indicated by dashed lines.)



0934-007(T)

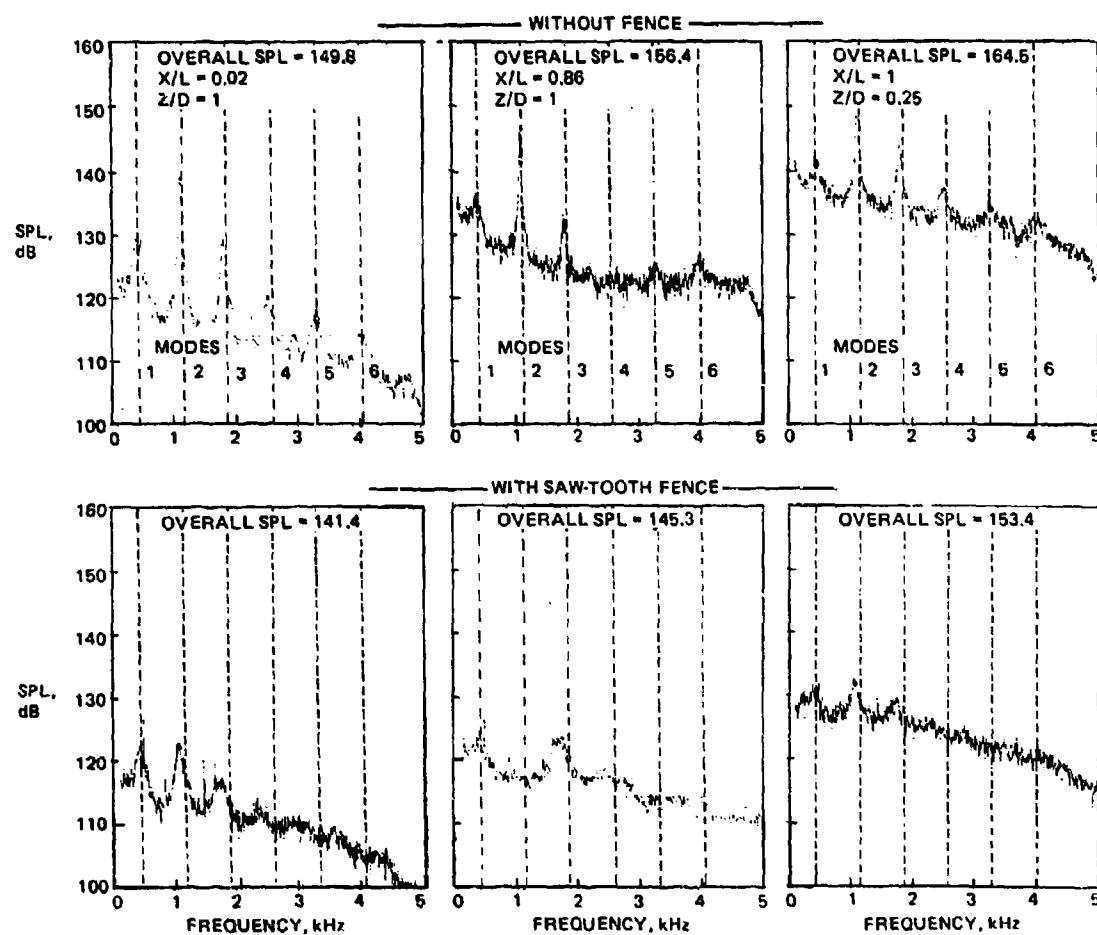
Figure 258 Effects of Cavity Oscillation Suppressor Fence on Frequency Spectra at 3 Locations in  $L/D = 5.6$  Cavity at  $M_\infty = 3.0$ . (Theoretically predicted frequencies are indicated by dashed lines.)





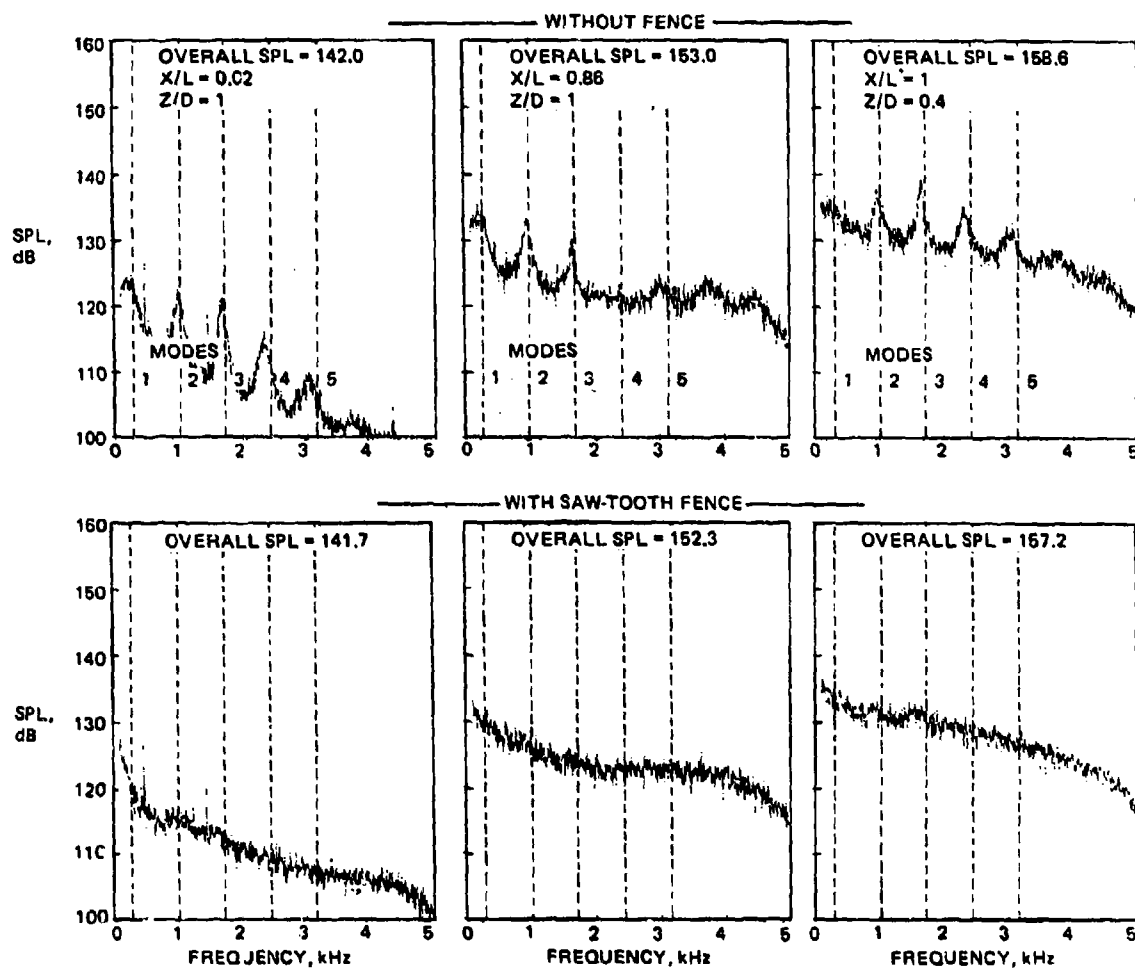
0934-008(T)

Figure 259 Effects of Cavity Oscillation Suppressor Fence on Frequency Spectra at 3 Locations in  $L/D = 5.1$  Cavity at  $M_\infty = 1.5$ . (Theoretically predicted frequencies are indicated by dashed lines.)



0934-009(T)

Figure 260 Effects of Cavity Oscillation Suppressor Fence on Frequency Spectra at 3 Locations in  $L/D = 6.2$  Cavity at  $M_\infty = 1.5$ . (Theoretically predicted frequencies are indicated by dashed lines.)



0934-010(T)

Figure 261 Effects of Cavity Oscillation Suppressor Fence on Frequency Spectra at 3 Locations in  $L/D = 9.9$  Cavity at  $M_\infty = 1.5$ . (Theoretically predicted frequencies are indicated by dashed lines.)

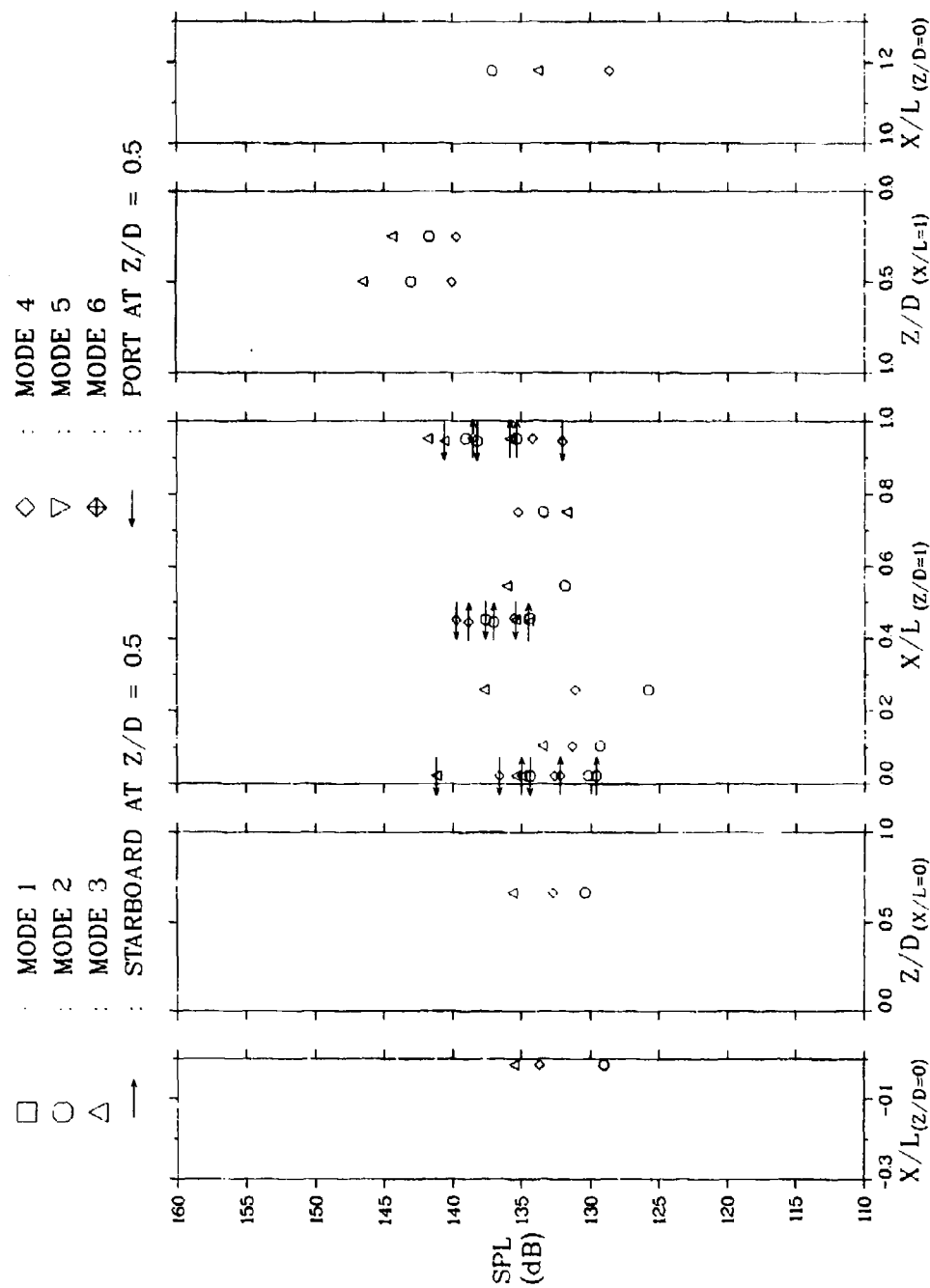


Figure 262 Acoustic Modal Pressure Distributions in the  $L/D = 5.6$  Cavity at  $M_\infty = 0.70$

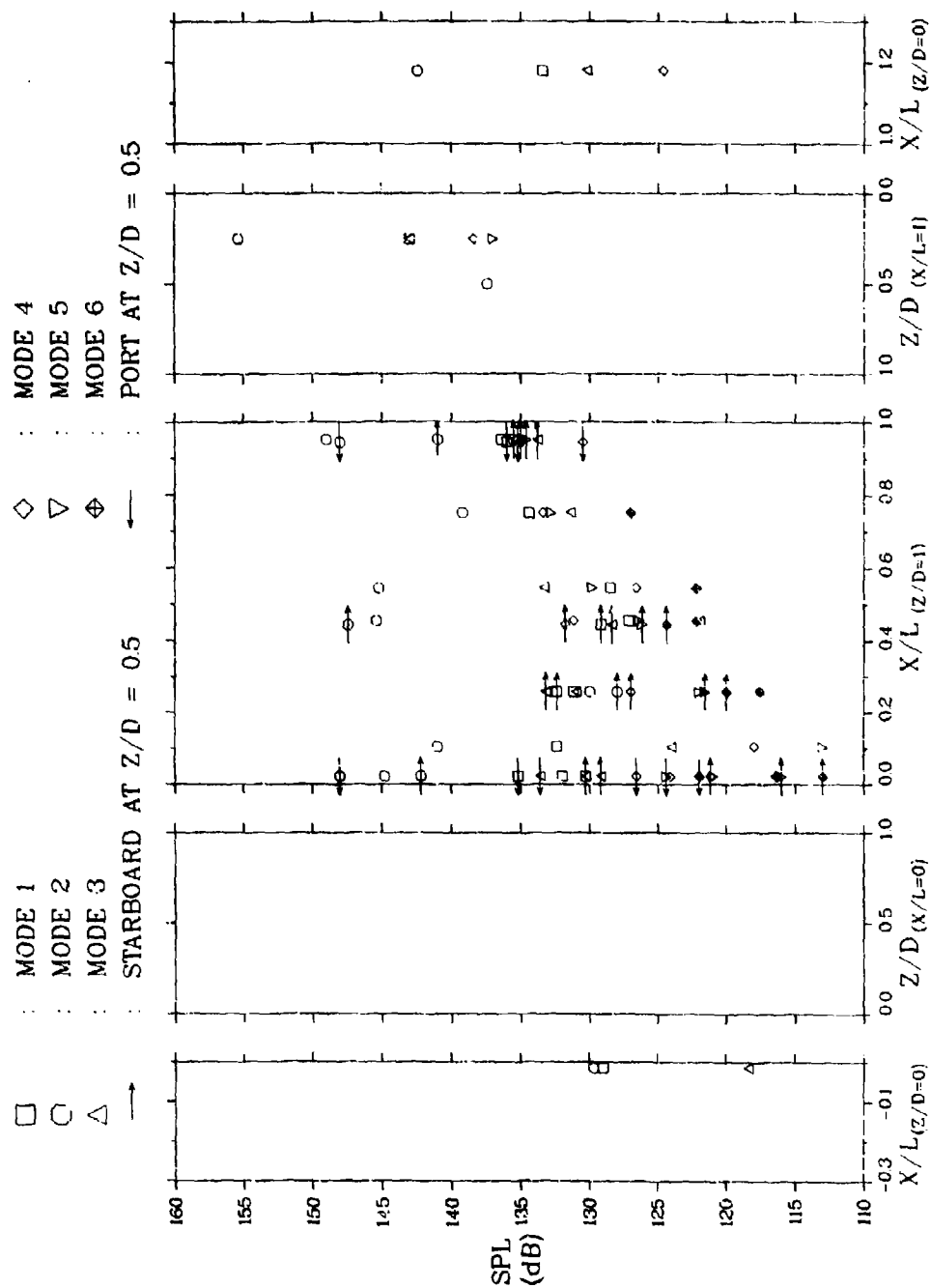


Figure 263 Acoustic Modal Pressure Distributions in the  $l/D = 5.6$  Cavity at  $M_0 = 1.5$

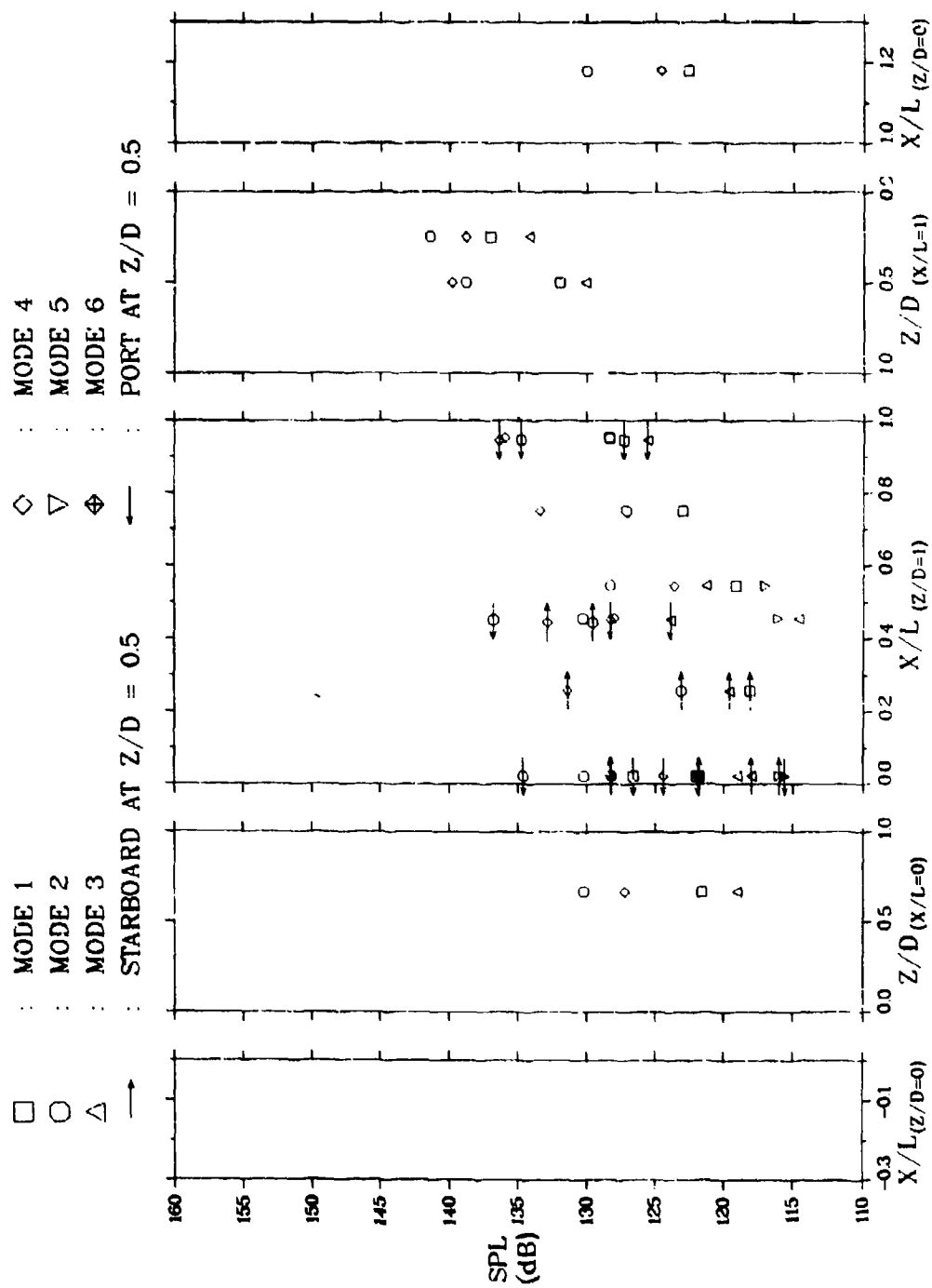


Figure 264 Acoustic Modal Pressure Distributions in the  $L/D = 5.6$  Cavity at  $M_0 = 2.3$

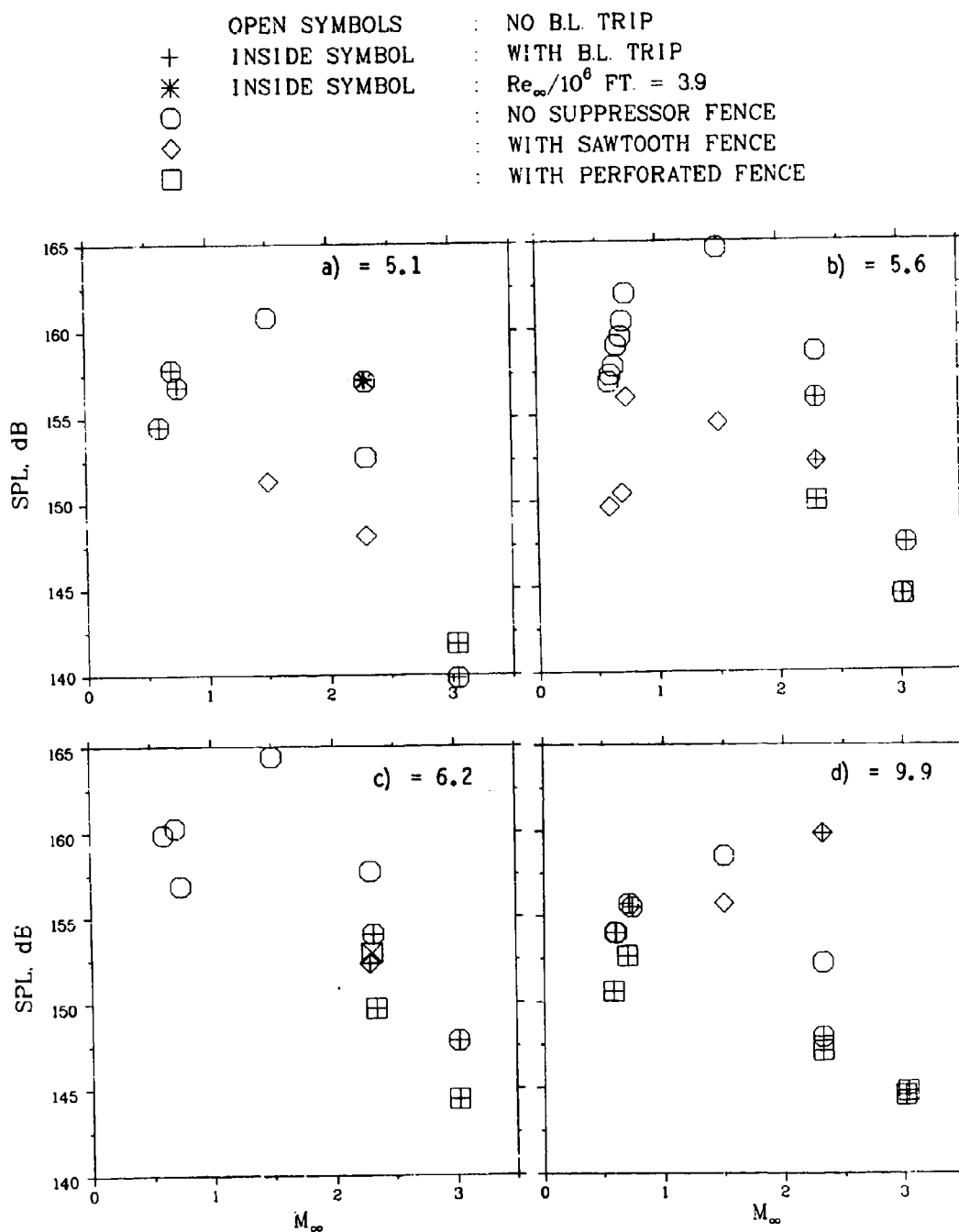


Figure 265 Maximum Acoustic Pressure Variations with Mach Number for Four L/D Values

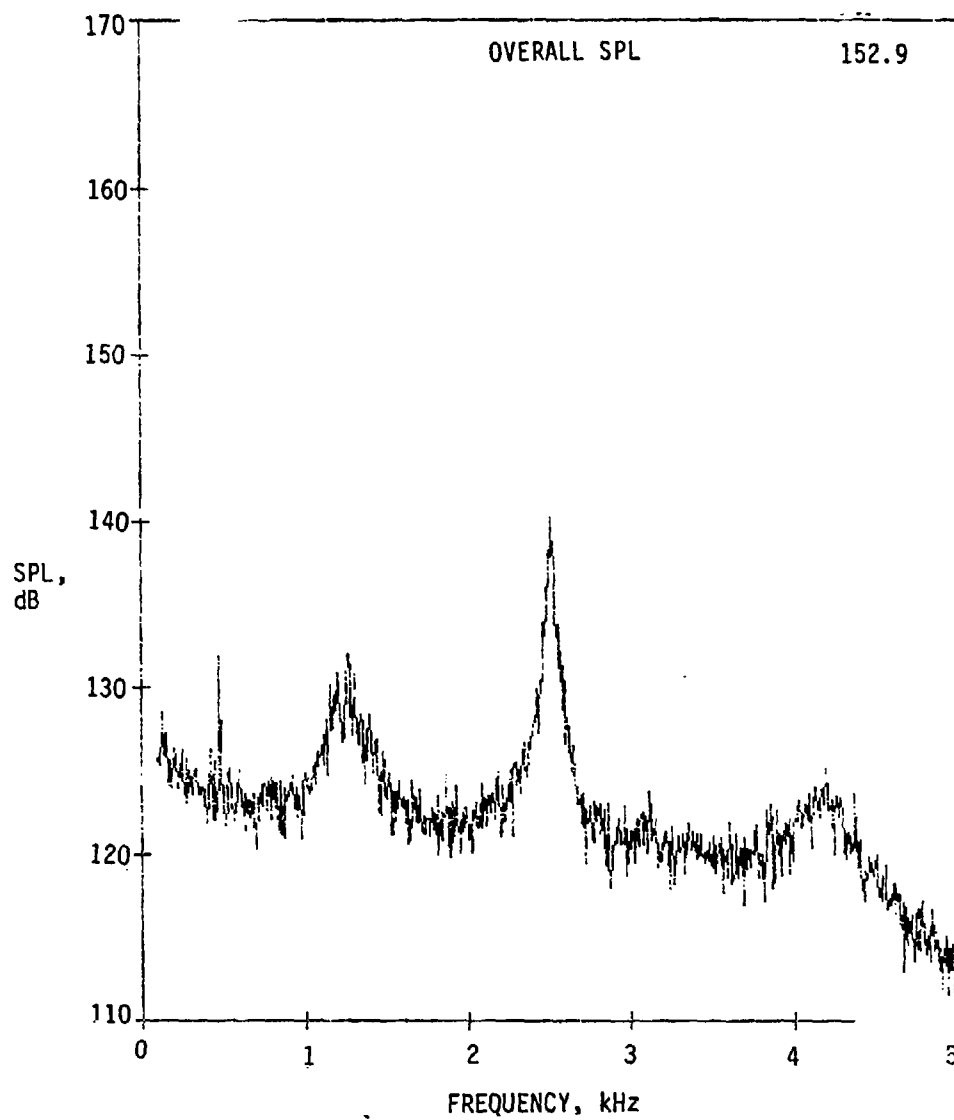


Figure 266 Pressure Spectrum on the Rear Bulkhead of  $L/D = 5.1$   
Cavity for  $M_\infty = 2.3$  at  $Re = 2.9 \times 10^6/ft$



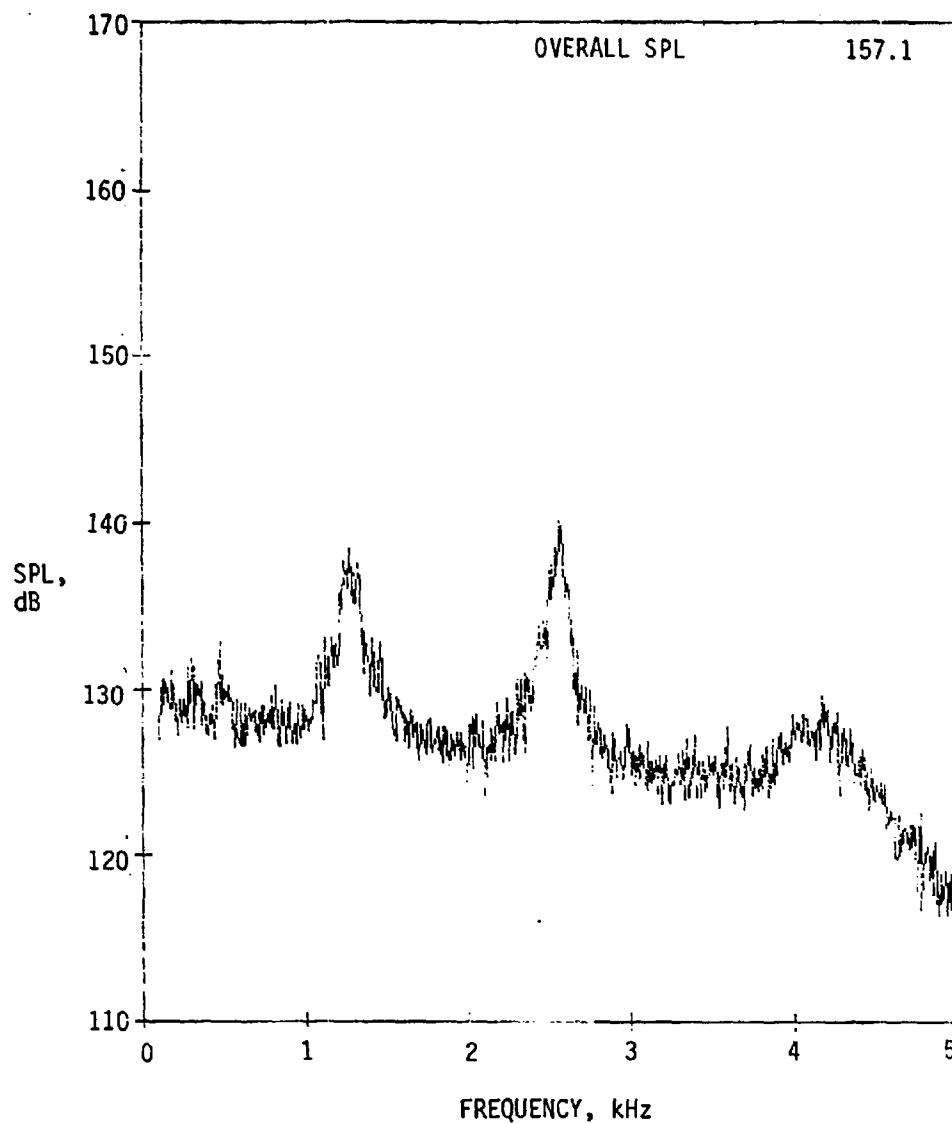


Figure 267 Pressure Spectrum on the Rear Bulkhead of  $L/D = 5.1$   
Cavity for  $M_\infty 2.3$  at  $Re = 3.9 \times 10^6/ft$

+	OPEN SYMBOLS	:	NO B.L. TRIP
*	INSIDE SYMBOL	:	WITH B.L. TRIP
○	INSIDE SYMBOL	:	$Re_{\infty}/10^6$ FT. = 3.9
◇		:	NO SUPPRESSOR FENCE
□		:	WITH SAWTOOTH FENCE
◇		:	WITH PERFORATED FENCE
		:	WITH SAWTOOTH FENCE AND TOTAL HEAD TUBE

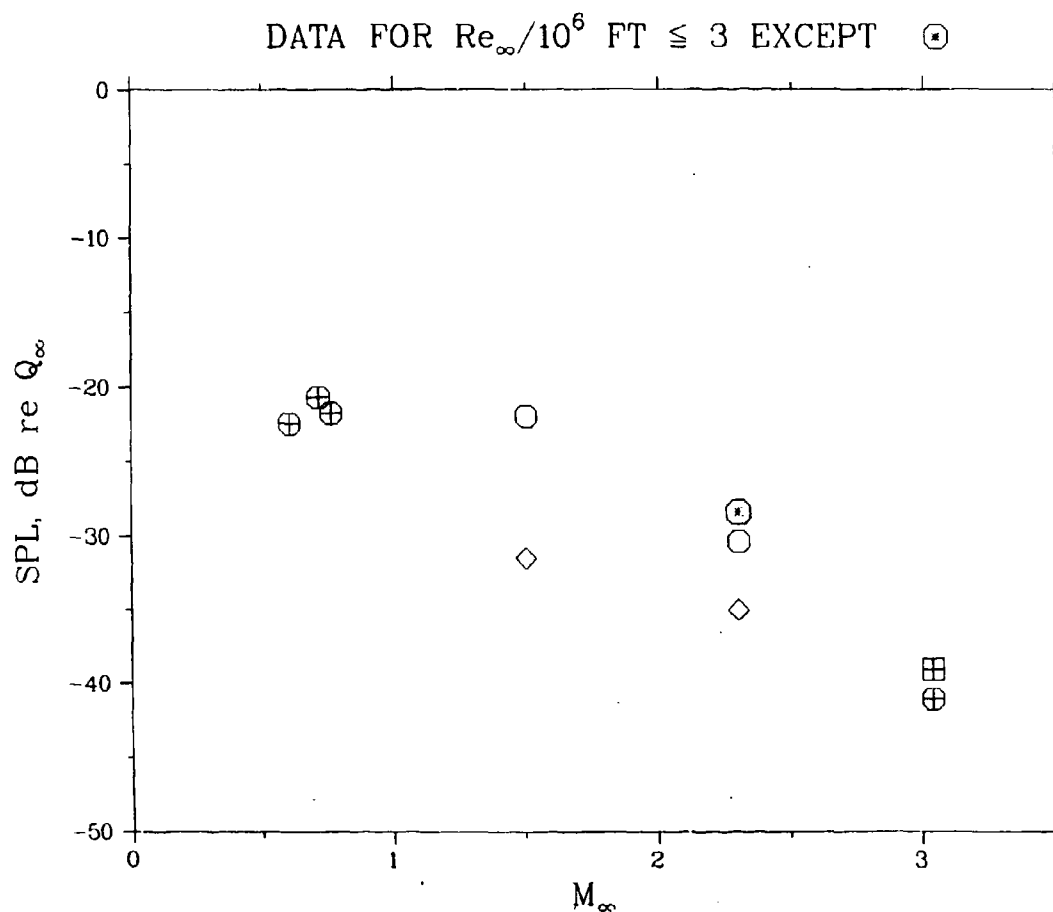


Figure 268 Mach Number Dependence of the Normalized Maximum Acoustic Pressure in the  $L/D = 5.1$  Cavity

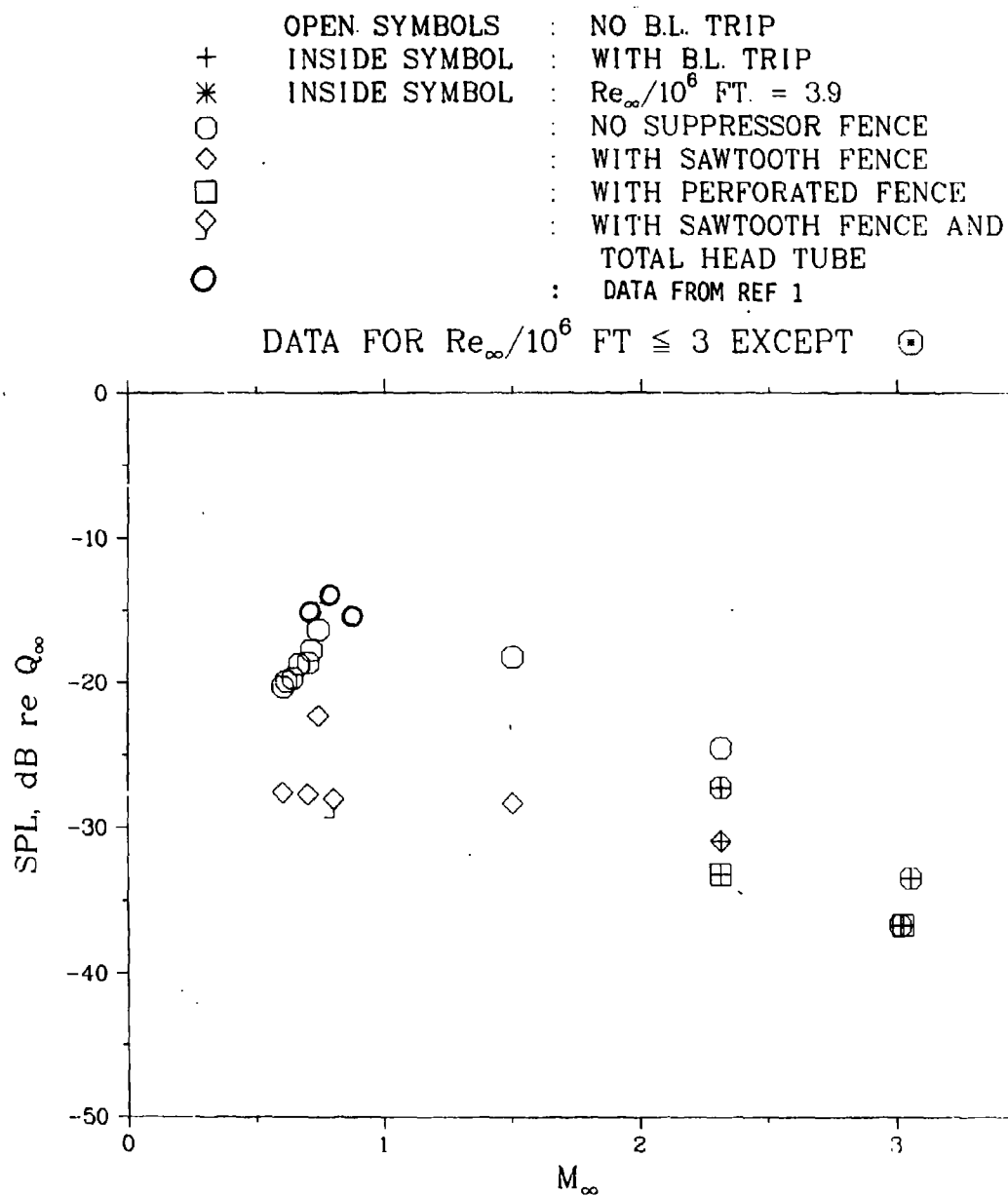


Figure 269 Mach Number Dependence of the Normalized Maximum Acoustic Pressure in the  $L/D = 5.6$  Cavity

+	OPEN SYMBOLS	:	NO B.L. TRIP
*	INSIDE SYMBOL	:	WITH B.L. TRIP
*	INSIDE SYMBOL	:	$Re_{\infty}/10^6 \text{ FT.} = 3.9$
○		:	NO SUPPRESSOR FENCE
◇		:	WITH SAWTOOTH FENCE
□		:	WITH PERFORATED FENCE
◇		:	WITH SAWTOOTH FENCE AND
		:	TOTAL HEAD TUBE

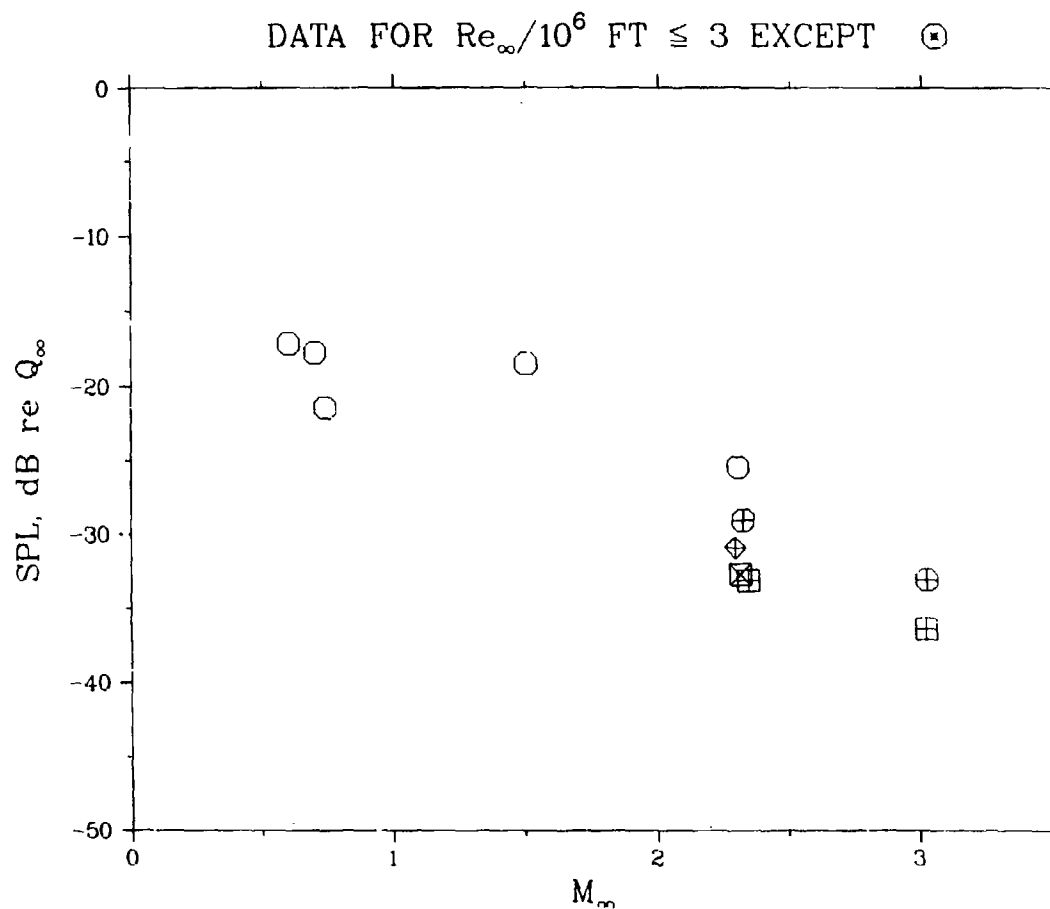


Figure 270 Mach Number Dependence of the Normalized Maximum Acoustic Pressure in the  $L/D = 6.2$  Cavity

	OPEN SYMBOLS	:	NO B.L. TRIP
+	INSIDE SYMBOL	:	WITH B.L. TRIP
*	INSIDE SYMBOL	:	$Re_{\infty}/10^6 \text{ FT.} = 3.9$
○		:	NO SUPPRESSOR FENCE
◇		:	WITH SAWTOOTH FENCE
□		:	WITH PERFORATED FENCE
◇		:	WITH SAWTOOTH FENCE AND TOTAL HEAD TUBE

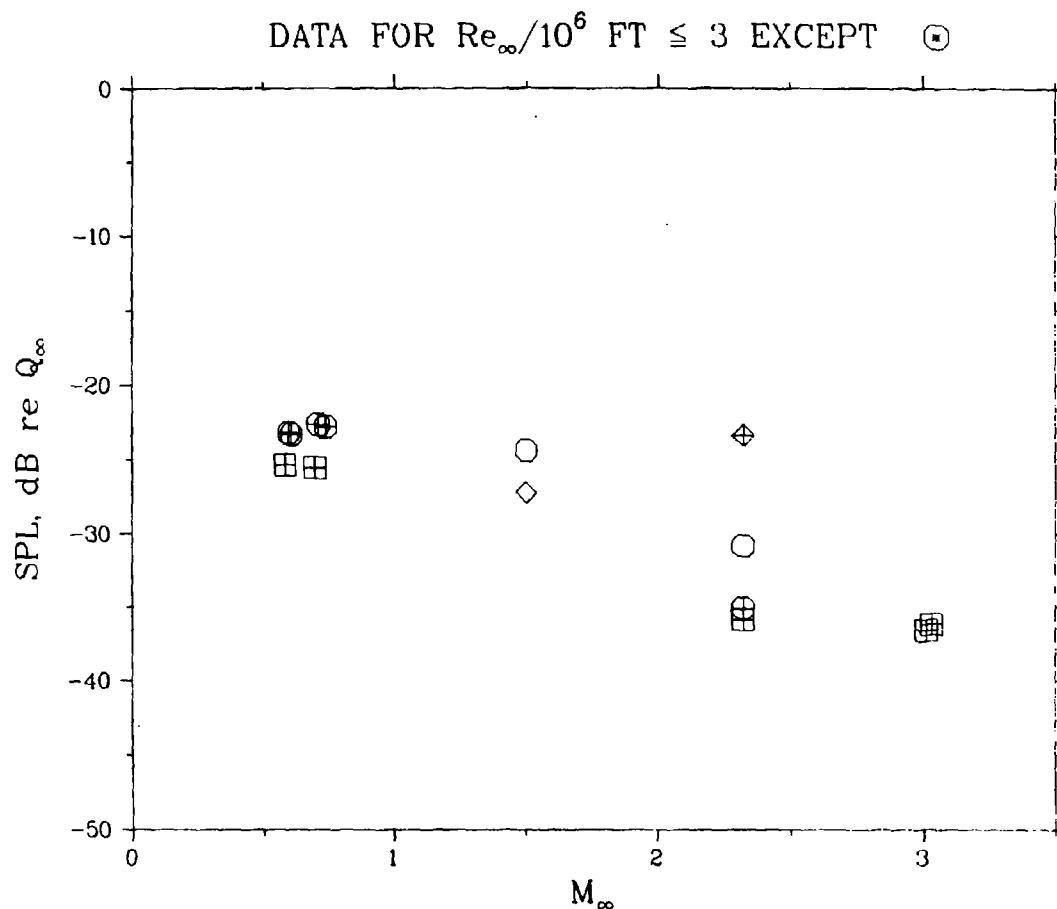


Figure 271 Mach Number Dependence of the Normalized Maximum Acoustic Pressure in the  $L/D = 9.9$  Cavity

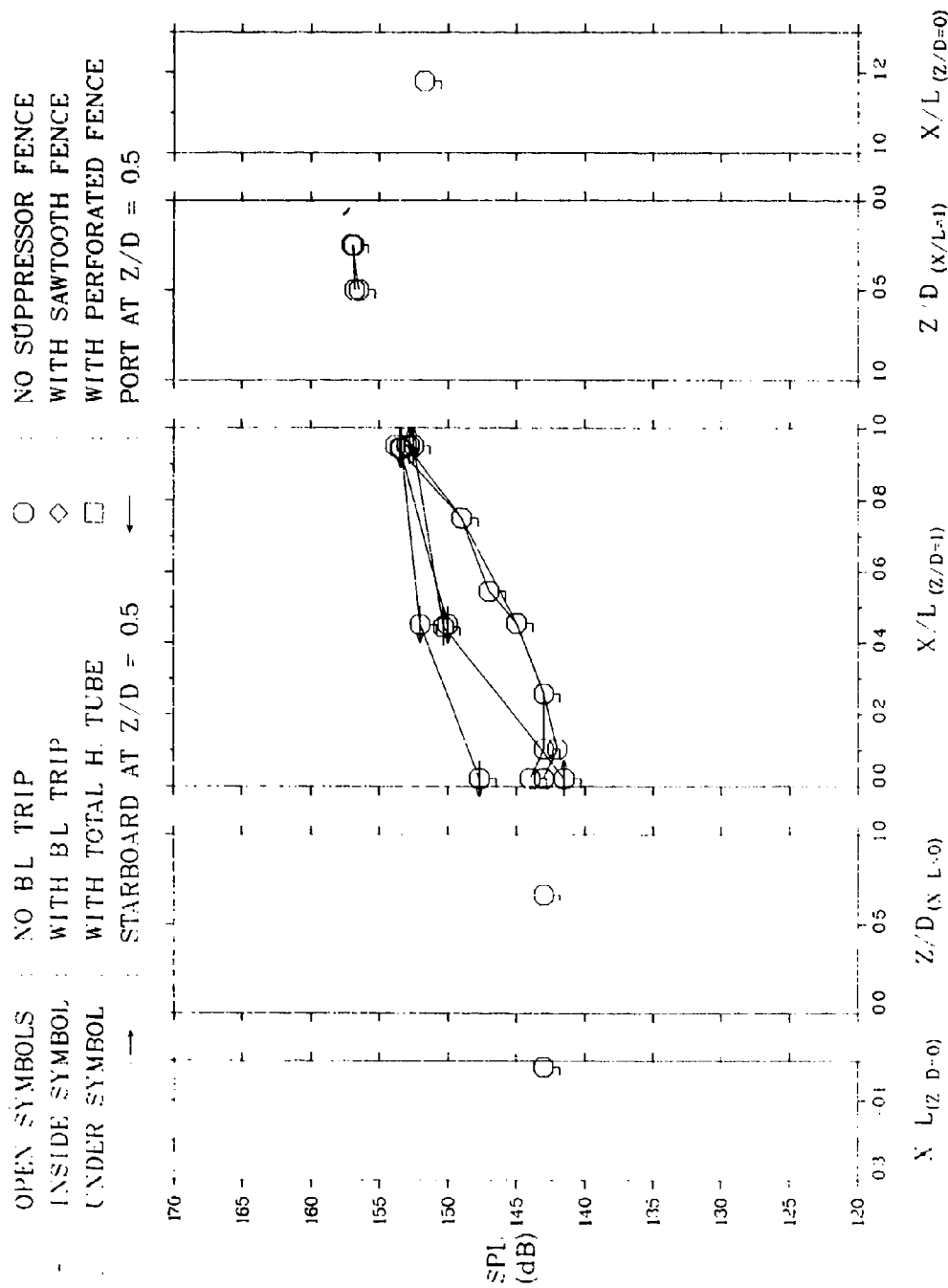


Figure 272 Effect of the Total Head Tube on the Acoustic Pressure Distributions in the  
 L/D = 5.6 Cavity for  $M_\infty = 0.60$ , Without Suppression Fence

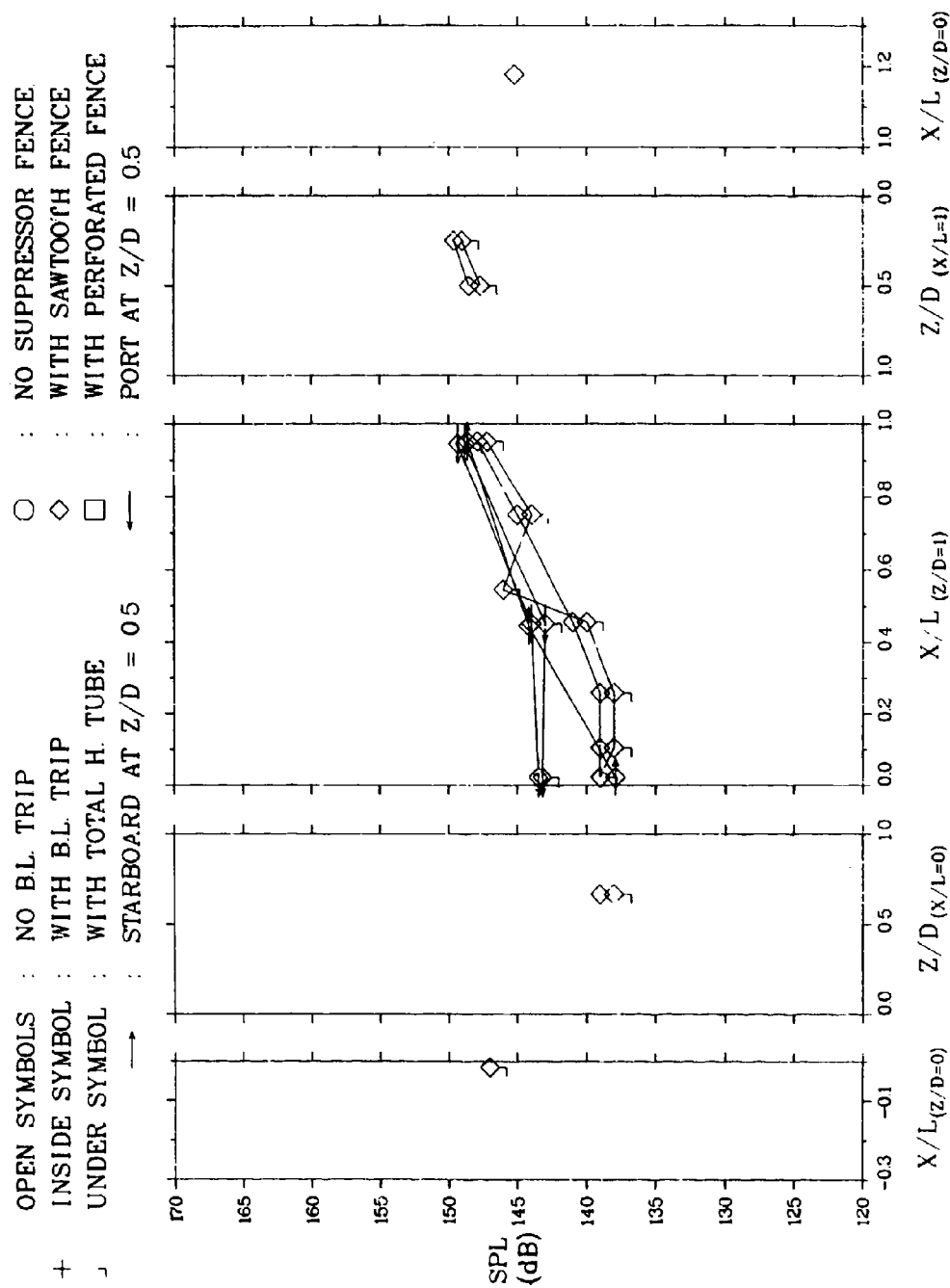


Figure 273 Effect of the Total Head Tube on the Acoustic Pressure Distributions in the  
 $L/D = 5.6$  Cavity for  $M_\infty = 0.60$ , With Suppression Fence

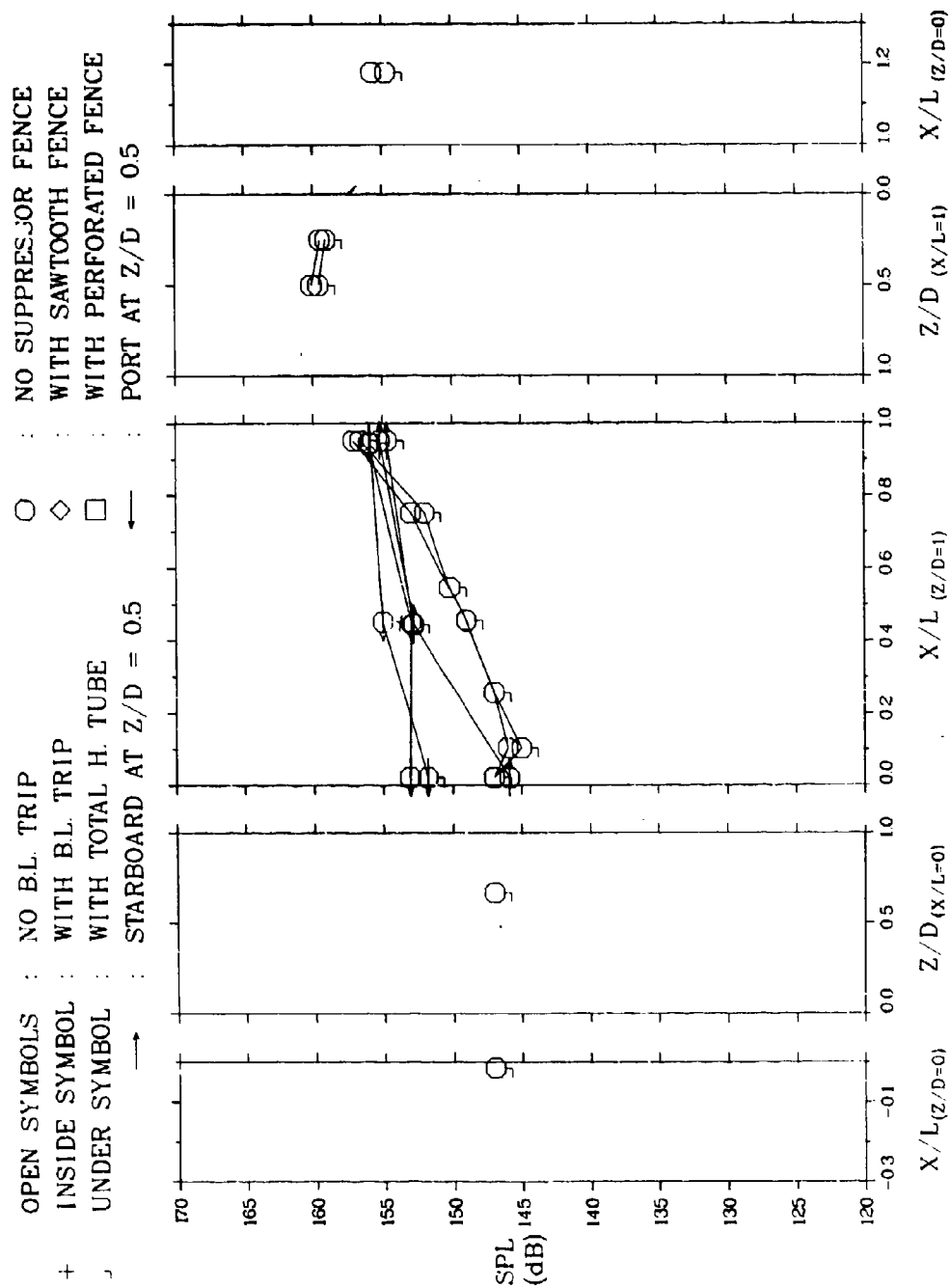


Figure 274 Effect of the Total Head Tube on the Acoustic Pressure Distributions in the  $L/D = 5.6$  Cavity for  $M_\infty = 0.70$ , Without Suppression Fence



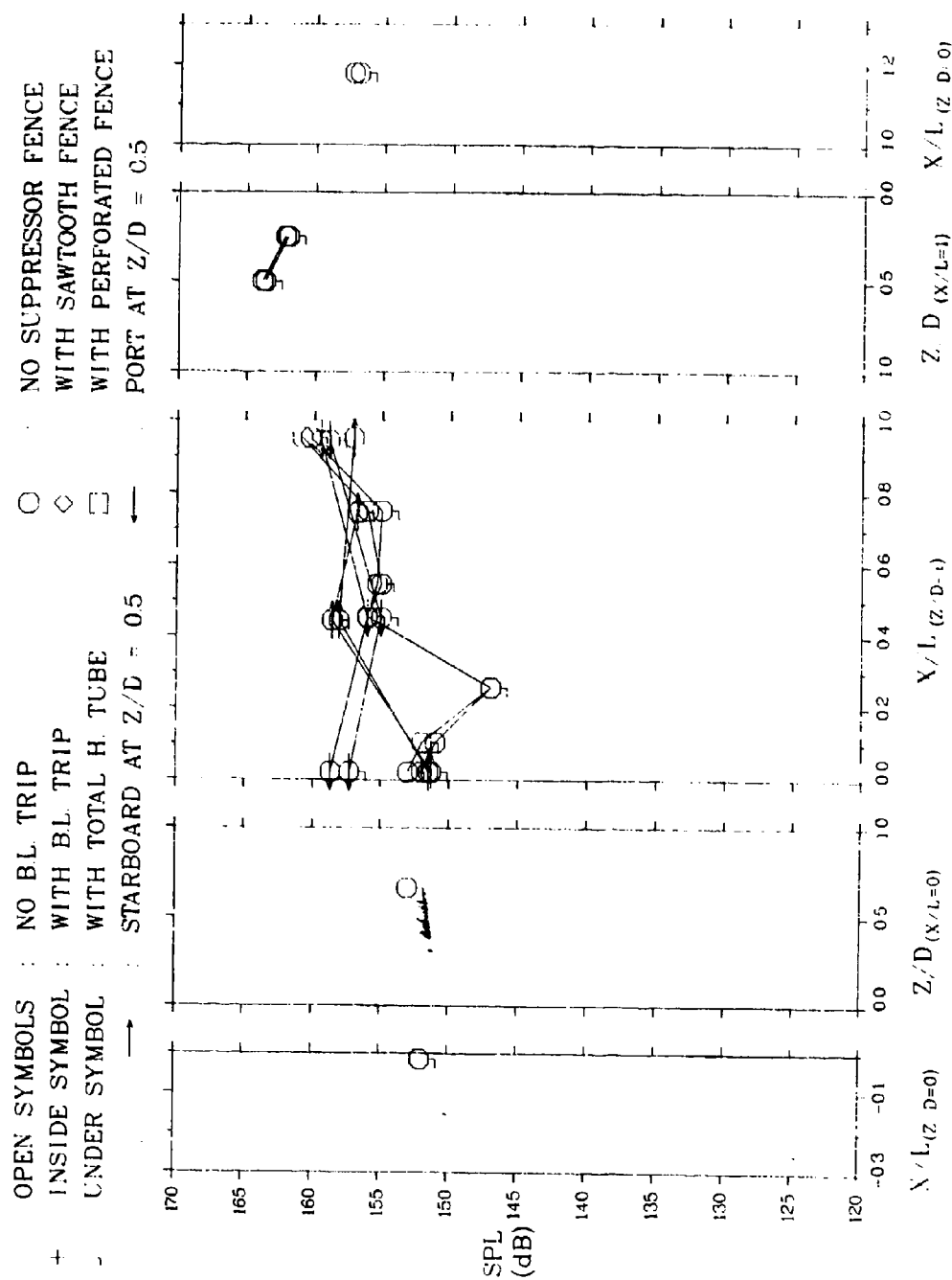


Figure 275 Effect of the Total Head Tube on the Acoustic Pressure Distributions in the  
 $L/D = 5.6$  Cavity for  $M_\infty = 0.74$ , Without Suppression Fence

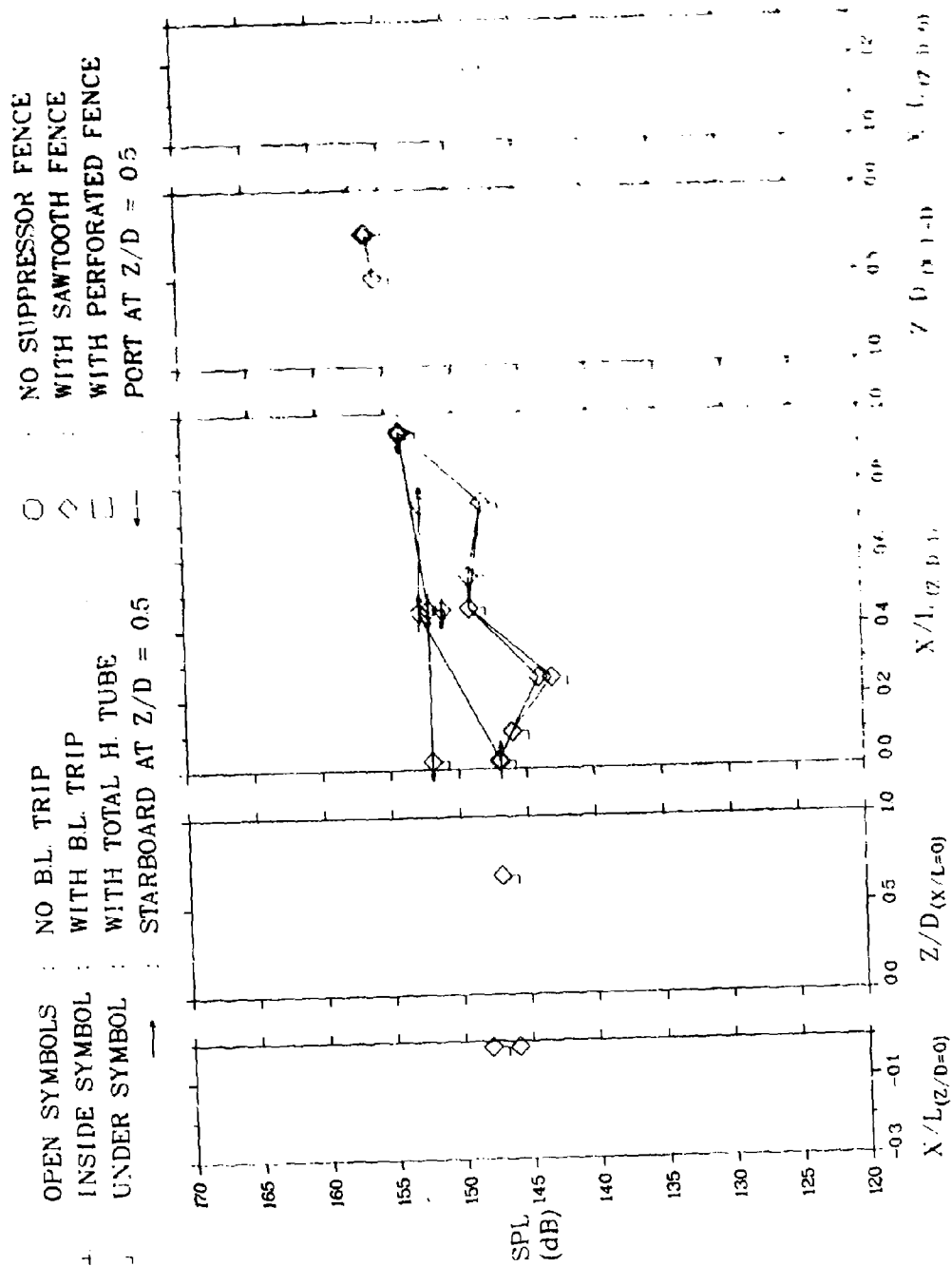


Figure 276 Effect of the Total Head Tube on the Acoustic Pressure Distributions to the  
 $L/D = 5.6$  Cavity for  $M_\infty = 0.74$ , With Suppression Fence

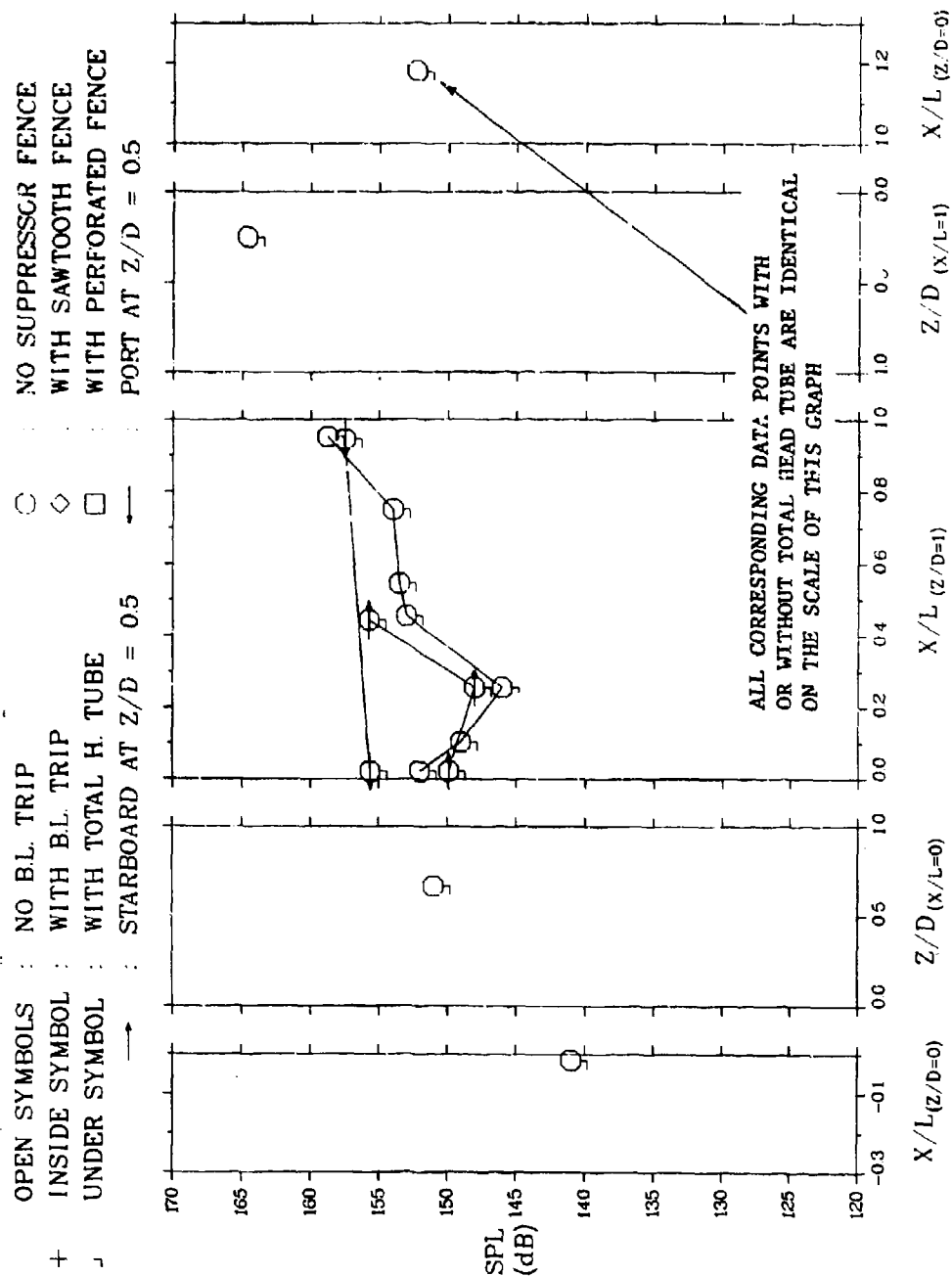


Figure 277 Effect of the Total Head Tube on the Acoustic Pressure Distributions in the  
 $L/D = 5.6$  Cavity for  $M_\infty = 1.5$ , Without Suppression Fence

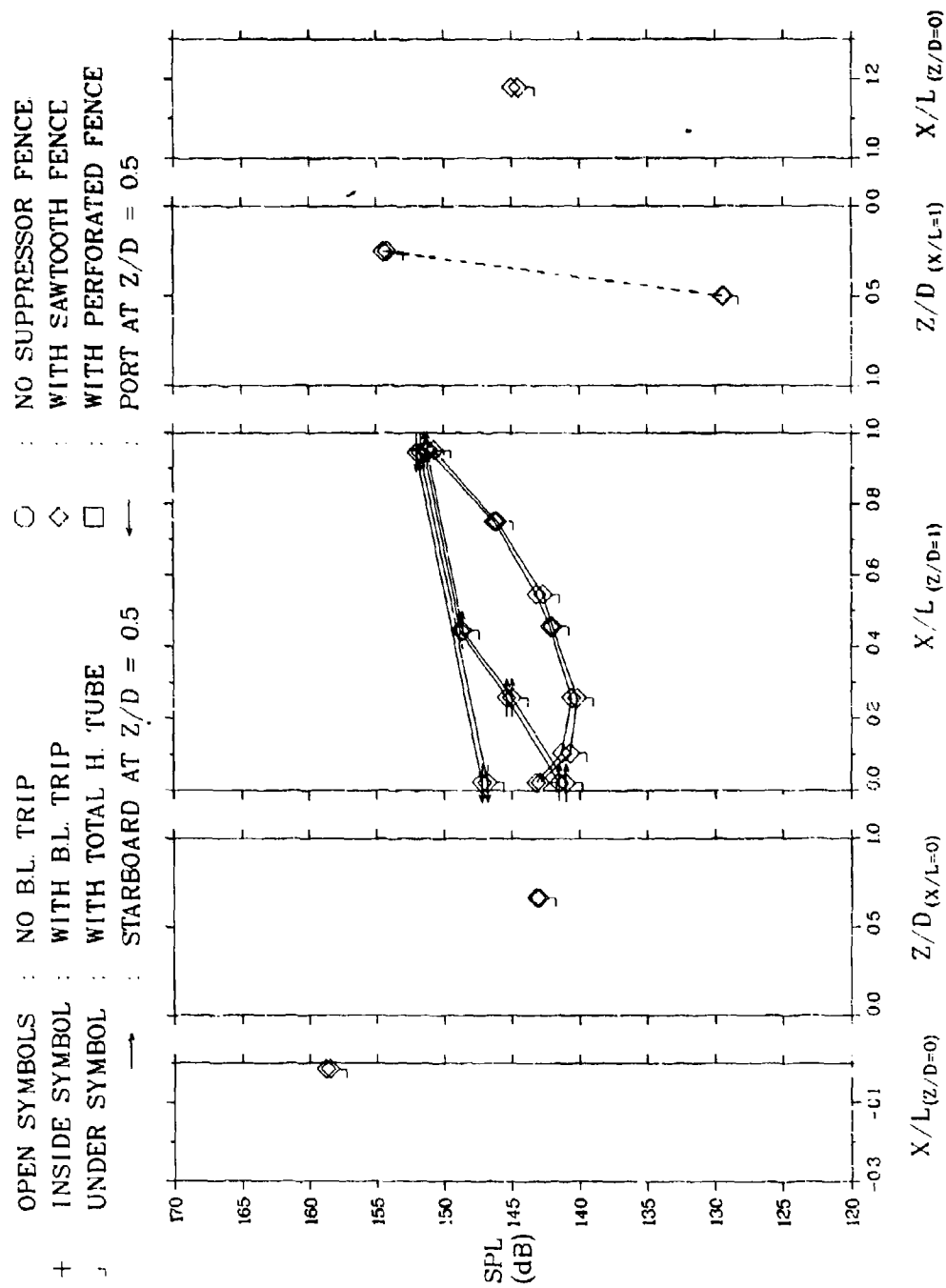


Figure 278 Effect of the Total Head Tube on the Acoustic Pressure Distributions in the  $L/D = 5.6$  Cavity for  $M_\infty = 1.5$ , With Suppression Fence

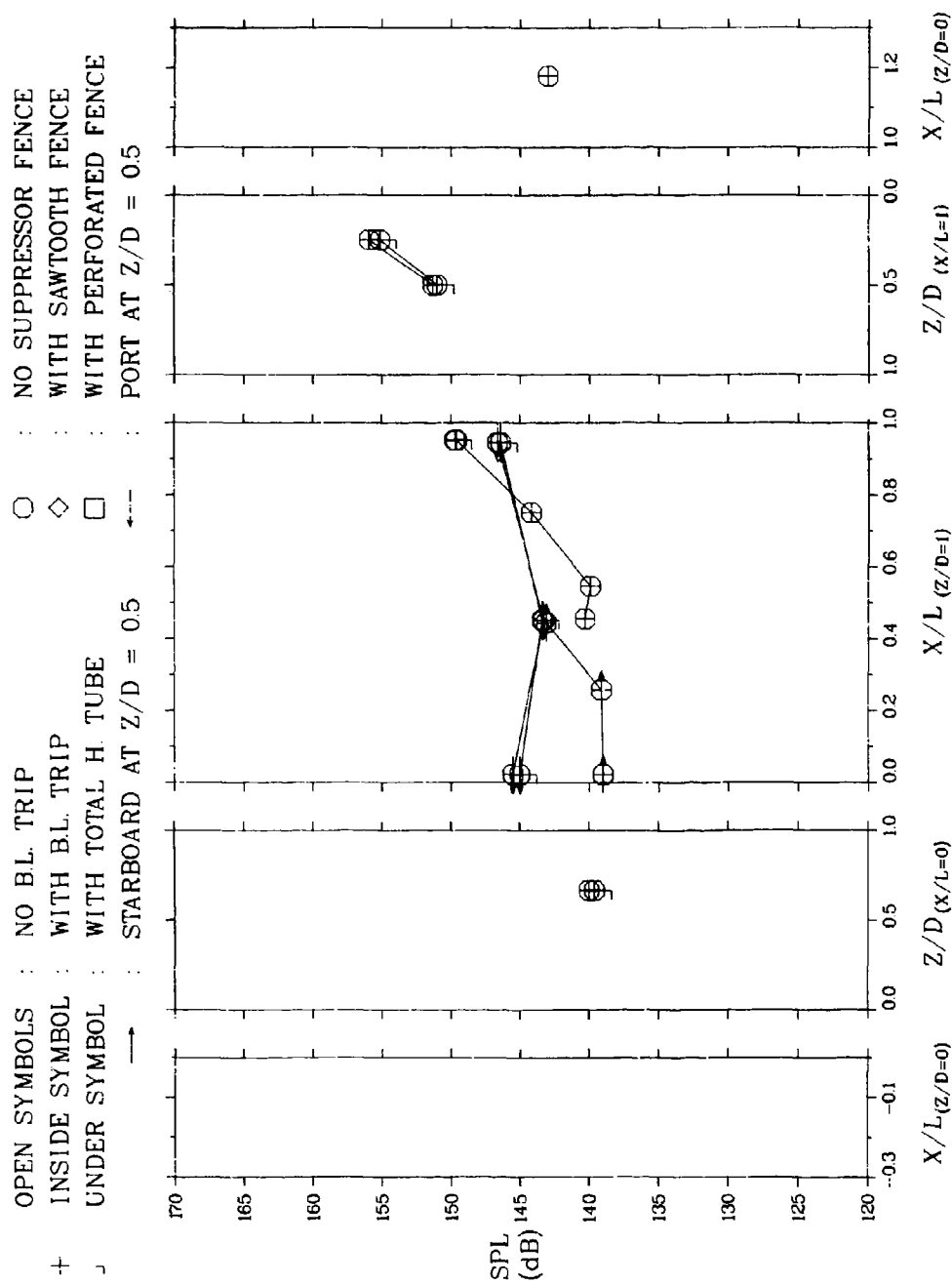
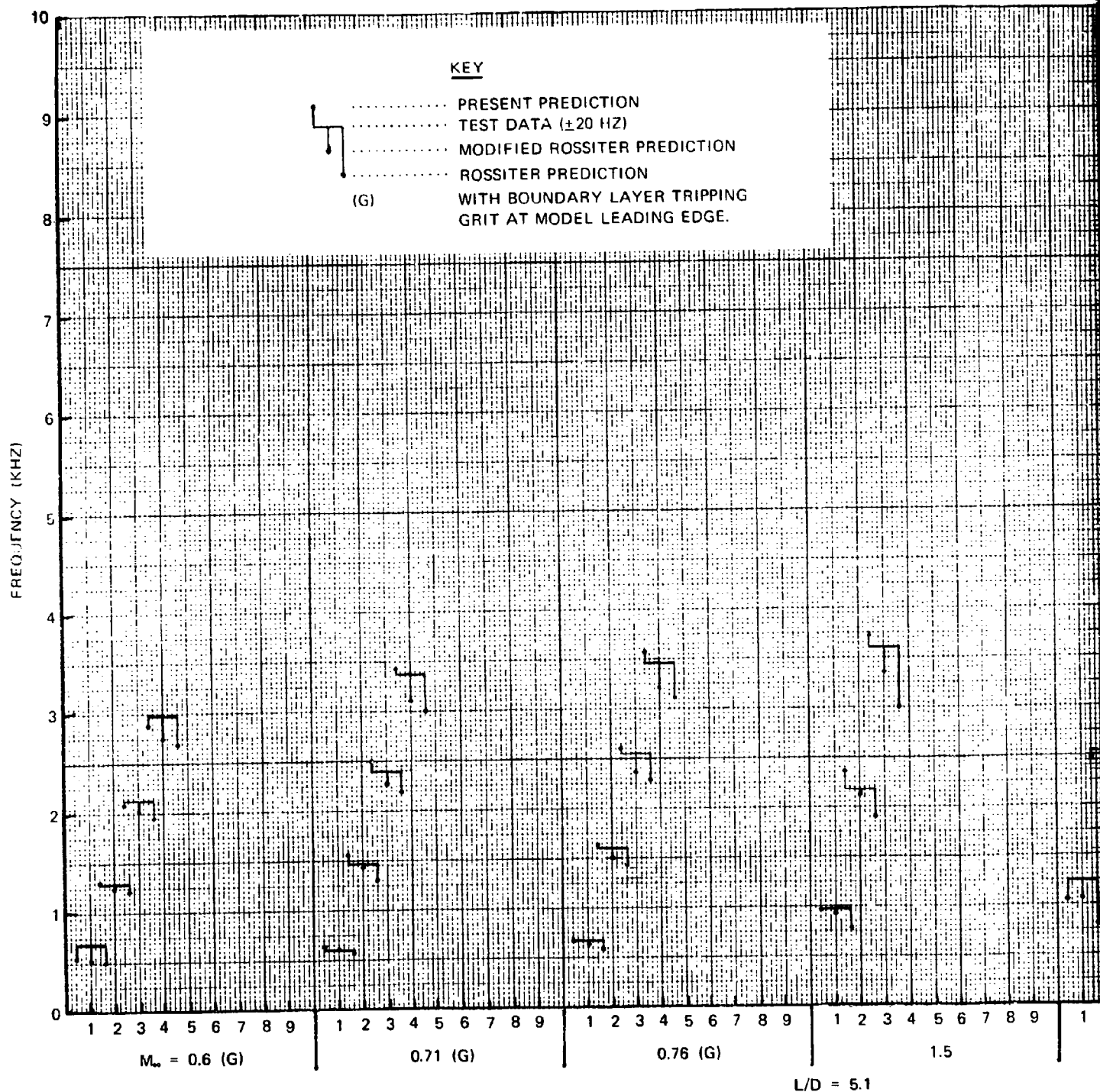


Figure 279 Effect of the Total Head Tube on the Acoustic Pressure Distributions in the  $L/D = 5.6$  Cavity for  $M_\infty = 2.3$ , Without Suppression Fence



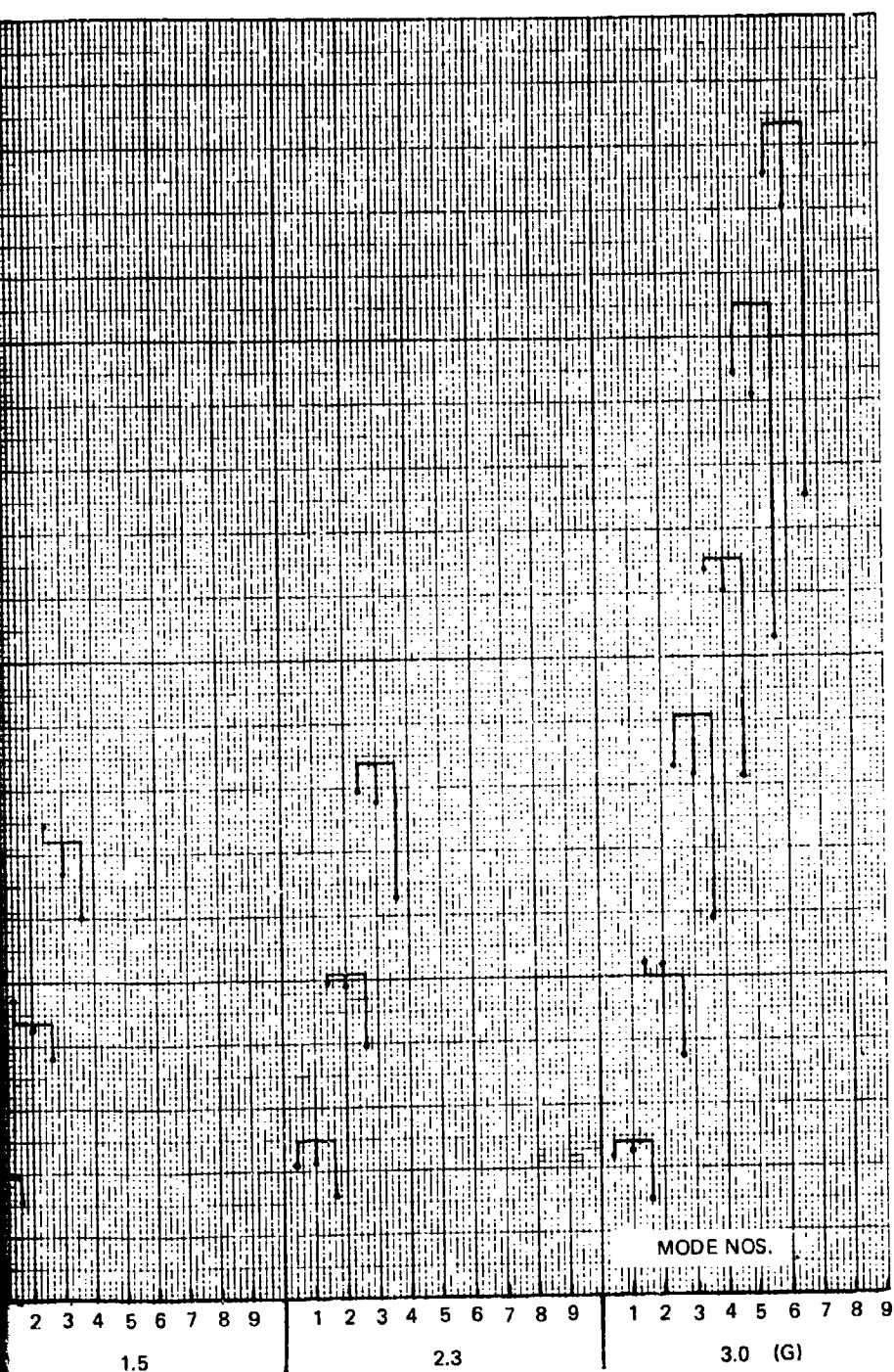
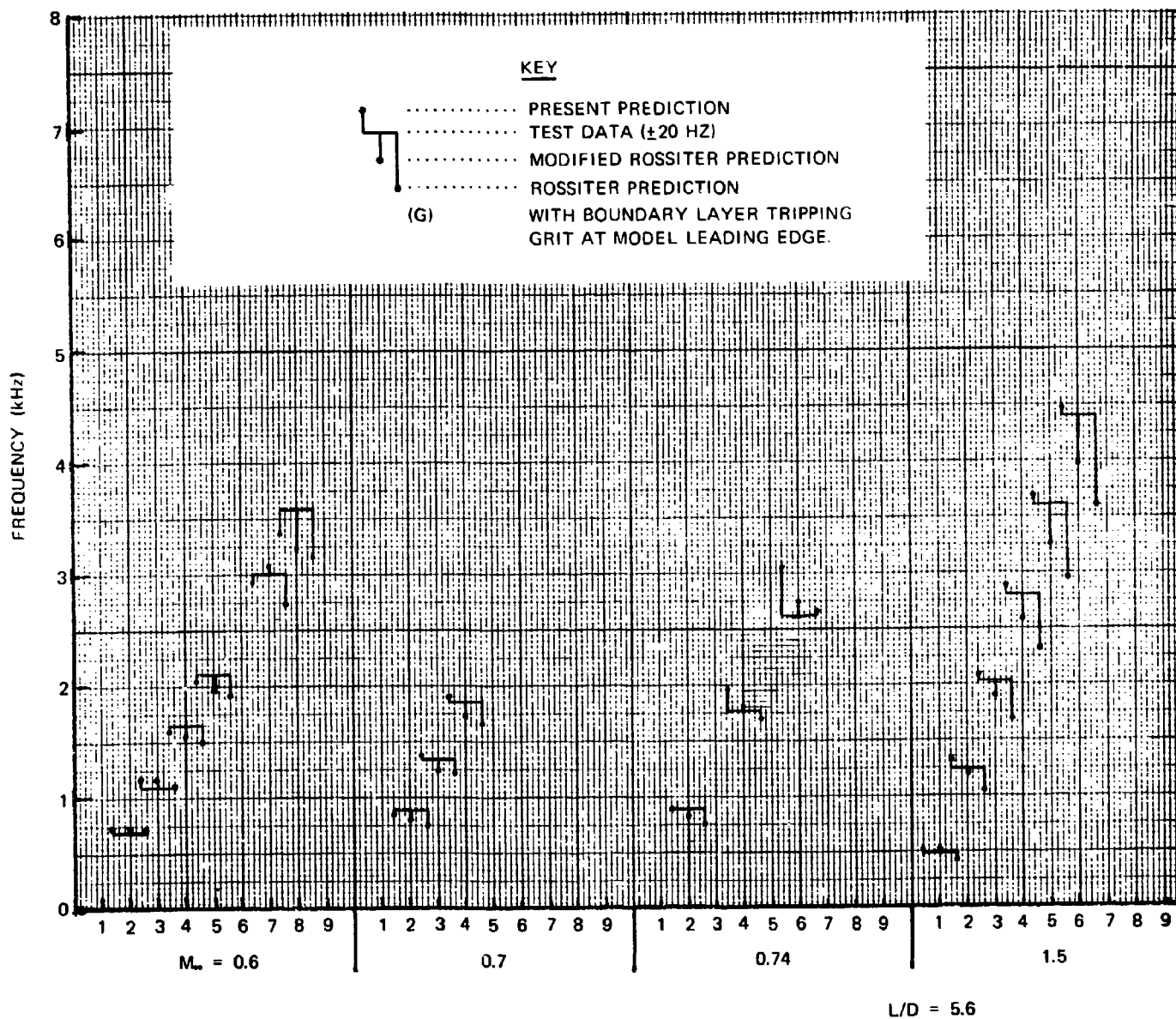


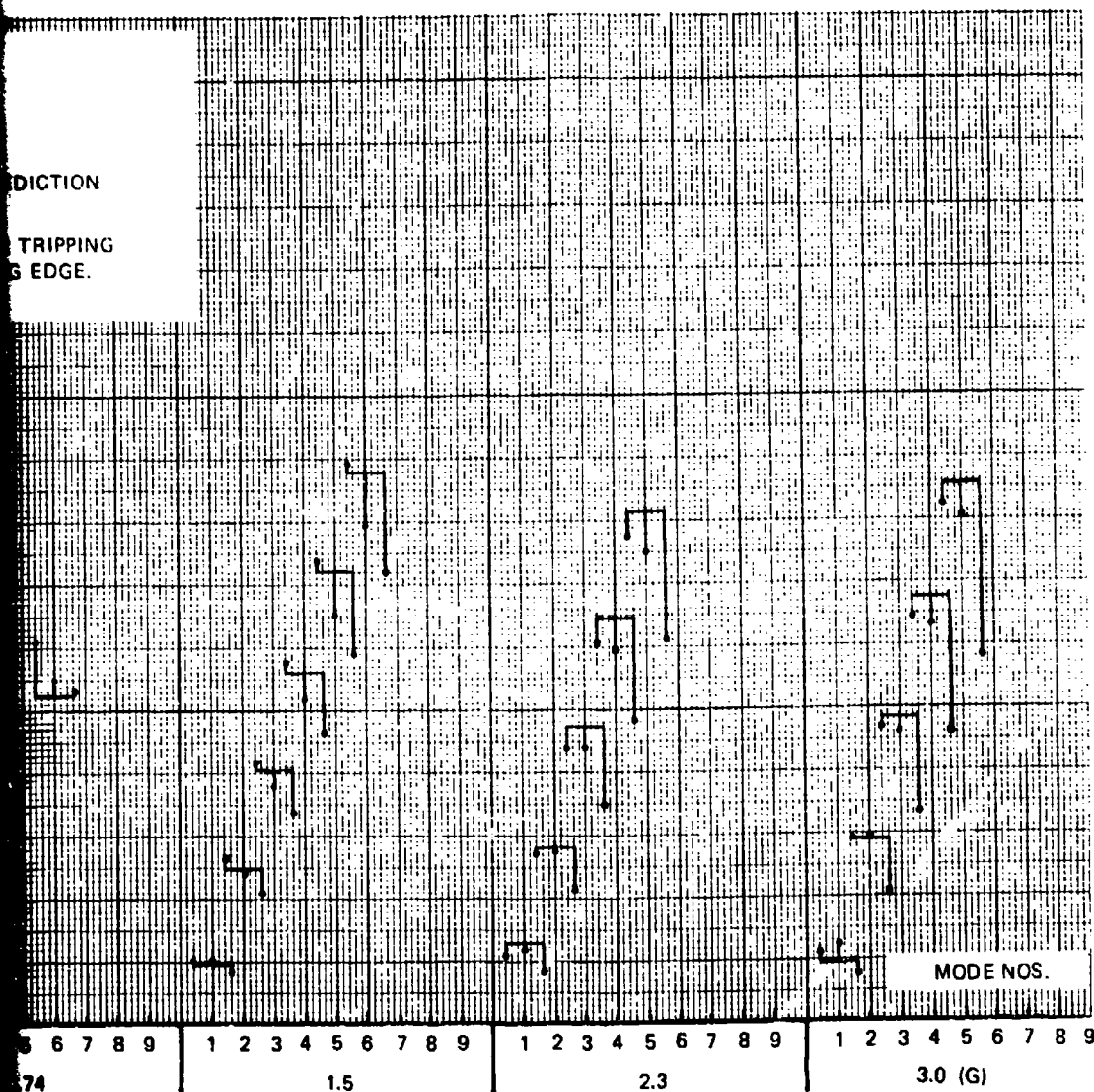
Figure 280 Comparison of Measured vs Predicted Oscillatory Mode Frequencies for Rectangular Cavities,  $L/D = 5.1$





PREDICTION

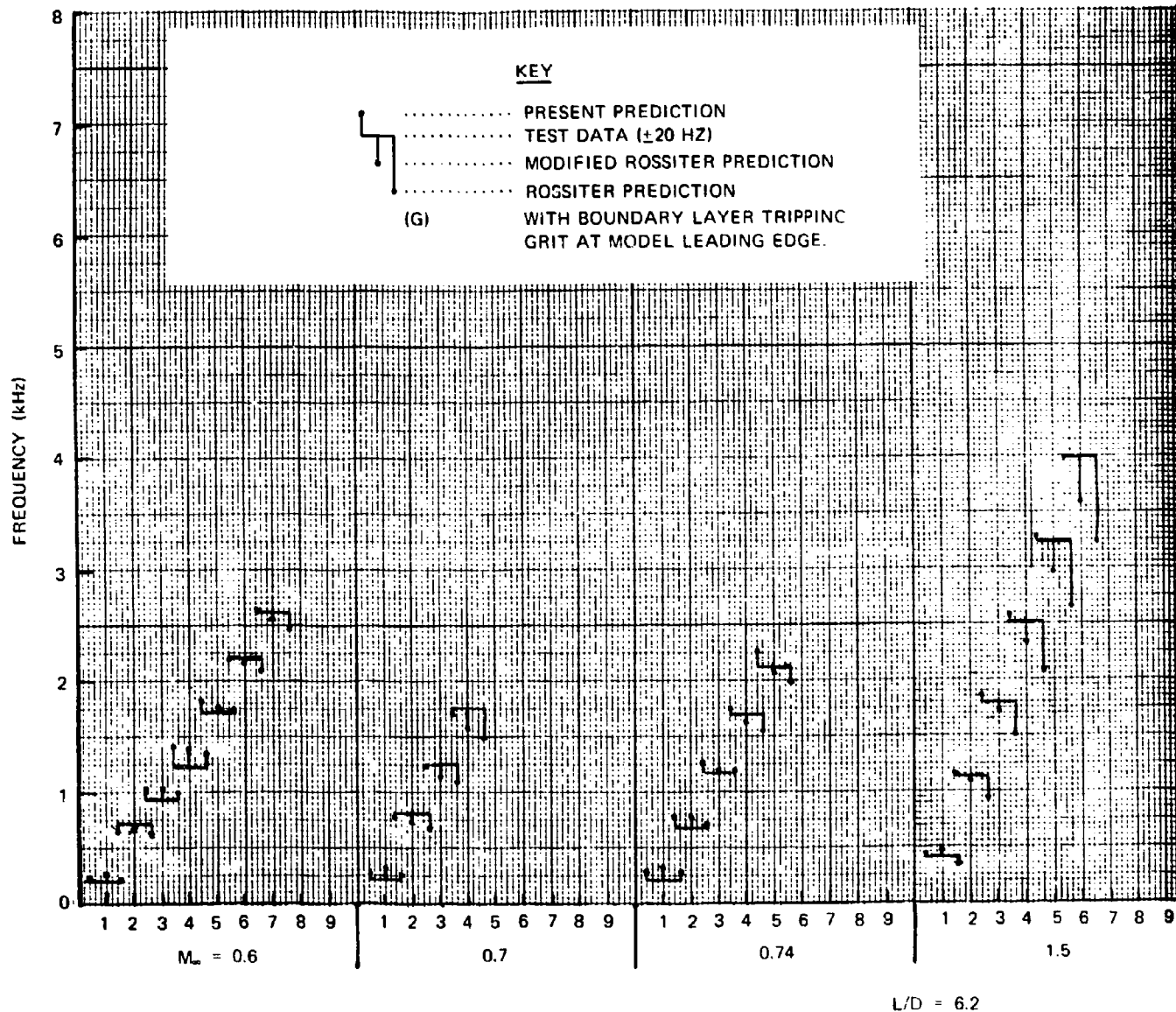
TRIPPING  
EDGE.

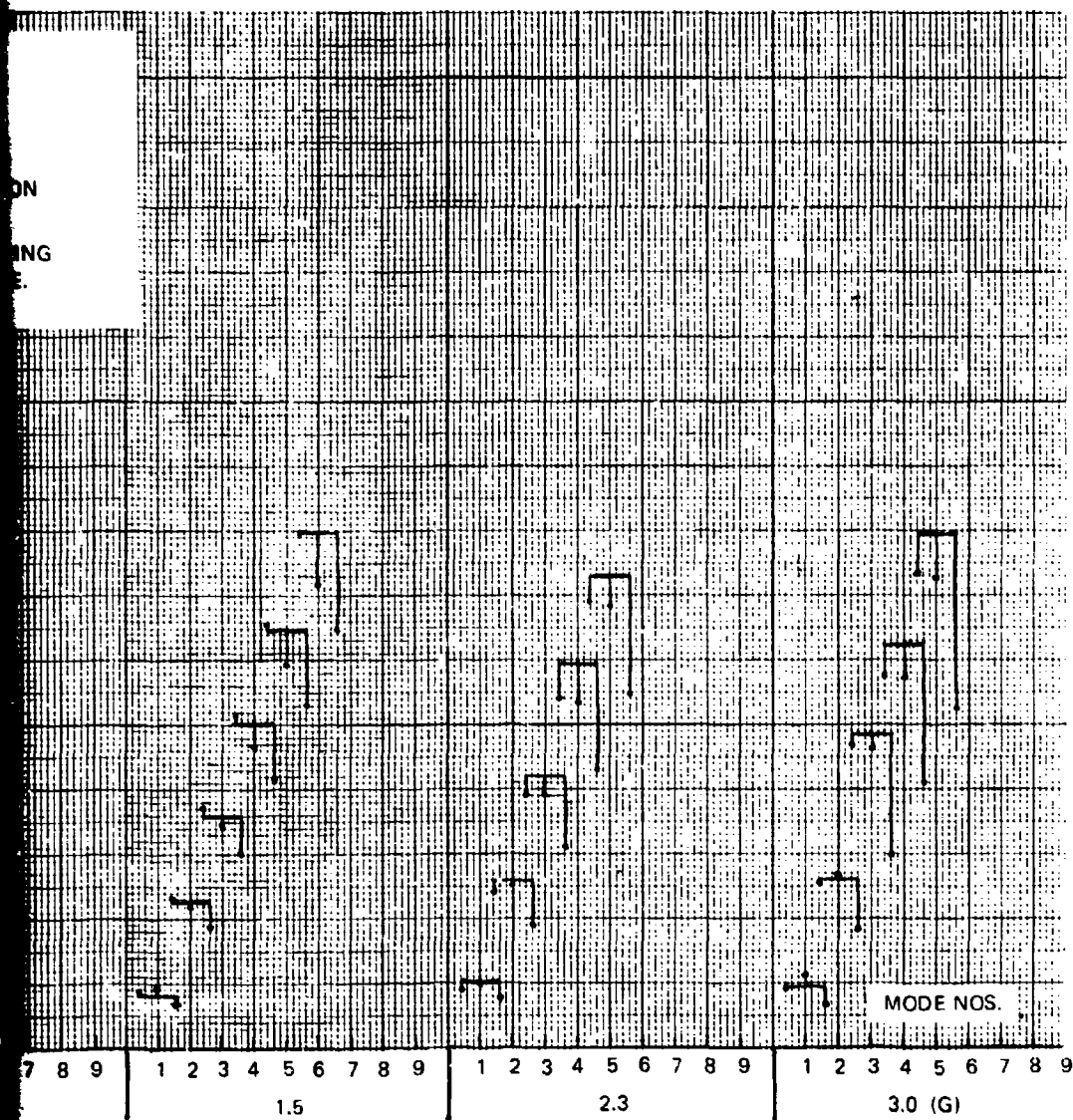


L/D = 5.6

Figure 281 Comparison of Measured vs Predicted Oscillatory Mode Frequencies for Rectangular Cavities, L/D = 5.6

2





$L/D = 6.2$

Figure 282 Comparison of Measured vs  
Predicted Oscillatory Mode  
Frequencies for Rectangular  
Cavities,  $L/D = 6.2$

2

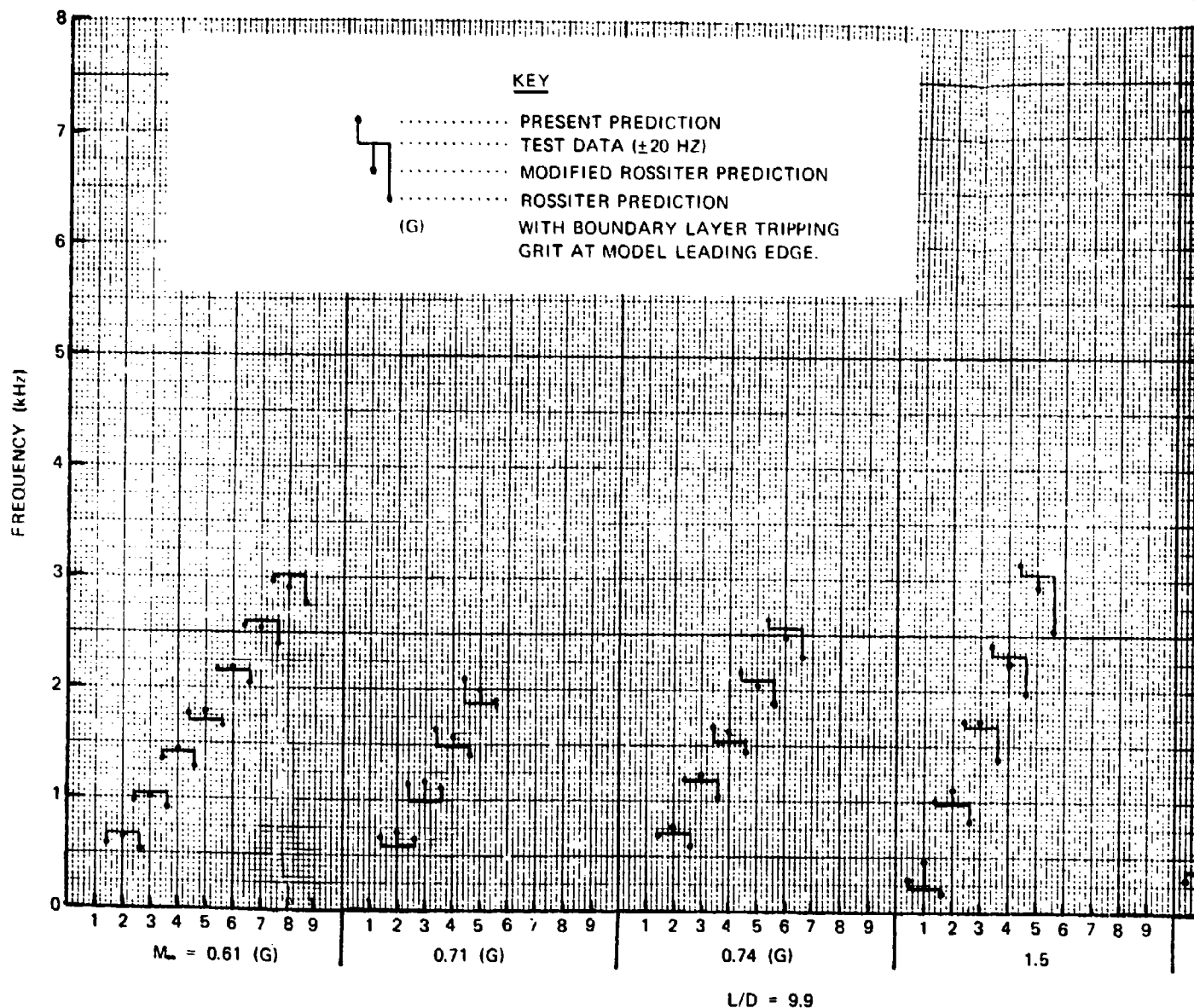


Figure 283 Comparison of Predicted and Measured Frequencies of Cavity Modes

PRESENT PREDICTION  
 TEST DATA ( $\pm 20$  HZ)  
 MODIFIED ROSSITER PREDICTION  
 ROSSITER PREDICTION  
 WITH BOUNDARY LAYER TRIPPING  
 INIT AT MODEL LEADING EDGE.

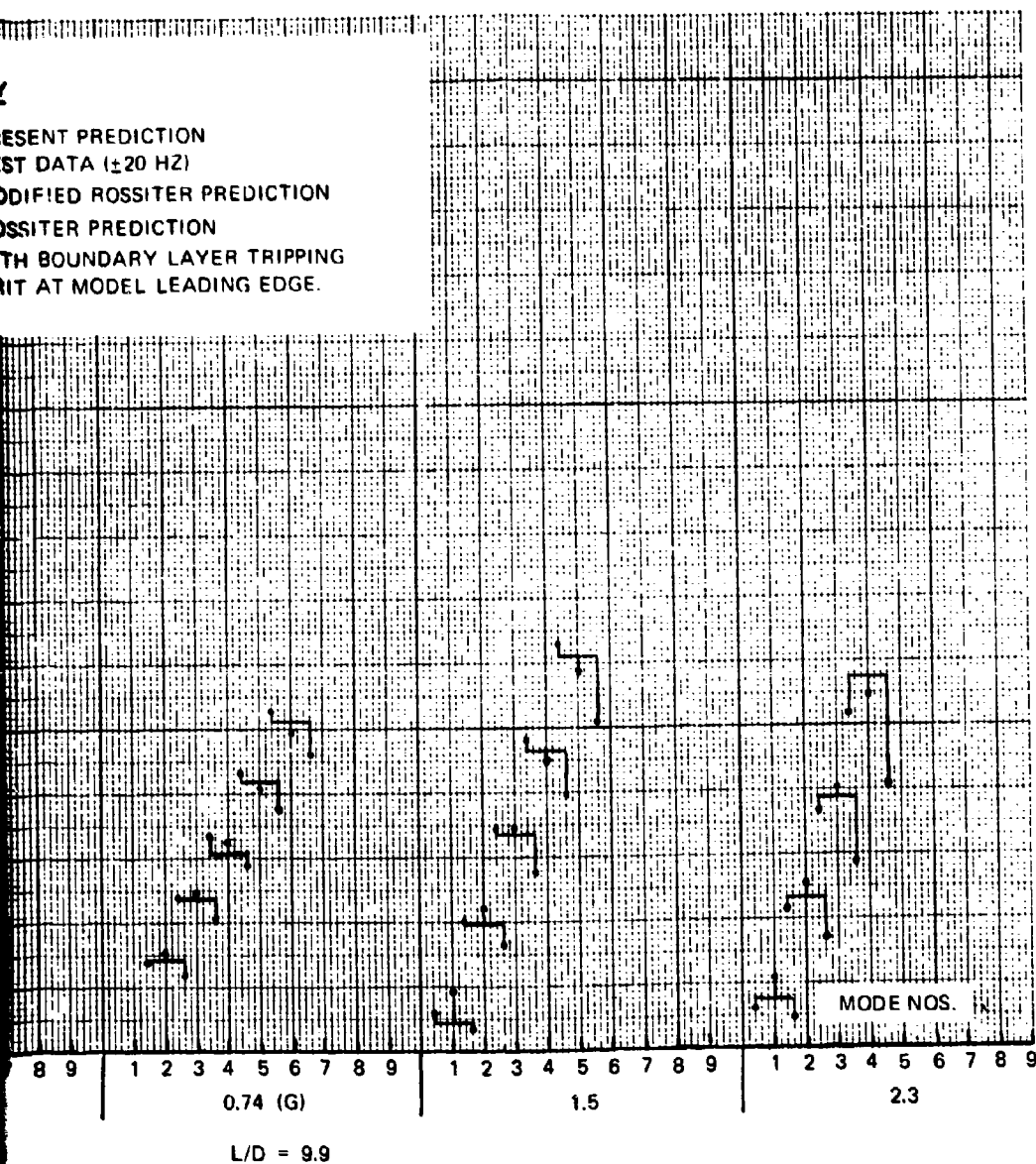


Figure 283 Comparison of Measured vs Predicted Oscillatory Mode Frequencies for Rectangular Cavities,  $L/D = 9.9$